Leg 202 Preliminary Report

Southeast Pacific Paleoceanographic Transects

29 March–30 May 2002

Shipboard Scientific Party

Ocean Drilling Program
Texas A&M University
1000 Discovery Drive
College Station TX 77845-9547
USA

September 2002

PUBLISHER'S NOTES

This report was prepared from shipboard files by scientists who participated in the cruise. The report was assembled under time constraints and does not contain all works and findings that will appear in the *Initial Reports* of the ODP *Proceedings.* Reference to the whole or to part of this report should be made as follows:

Shipboard Scientific Party, 2002. Leg 202 Preliminary Report. *ODP Prelim. Rpt.,* 102 [Online]. Available from World Wide Web: <http://www-odp.tamu.edu/publications/prelim/202_prel/202PREL.PDF>. [Cited YYYY-MM-DD]

Distribution: Electronic copies of this series may be obtained from the Ocean Drilling Program's World Wide Web site at http://www-odp.tamu.edu/publications.

This publication was prepared by the Ocean Drilling Program, Texas A&M University, as an account of work performed under the international Ocean Drilling Program, which is managed by Joint Oceanographic Institutions, Inc., under contract with the National Science Foundation. Funding for the program is provided by the following agencies:

DISCLAIMER

The following scientists and personnel were aboard the *JOIDES Resolution* for Leg 202 of the Ocean Drilling Program:

Shipboard Scientific Party

Alan C. Mix
Co-Chief
College of Oceanic and Atmospheric Sciences
Oregon State University
104 Ocean Administration Building
Corvallis OR 97331-5503
USA
Work: (541) 737-5212
Fax: (541) 737-2064
mix@coas.oregonstate.edu

Ralf Tiedemann
Co-Chief
GEOMAR
Christian-Albrechts-Universität zu Kiel
Wischhofstrasse 1-3
24148 Kiel
Germany
Work: (49) 431-600-2309
Fax: (49) 431-600-2926
rtiedemann@geomar.de

Peter Blum
Staff Scientist
Ocean Drilling Program
Texas A&M University
1000 Discovery Drive
College Station TX 77845-9547
USA
Work: (979) 845-9299
Fax: (979) 845-0876
blum@odpemail.tamu.edu

Fatima F. Abrantes
Paleontologist (diatoms)
Departamento de Geologia Marinha
Instituto Geologico e Mineiro
Estrada da Portela
Zambujal, Aptdo 7586
2720 Alfragide
Portugal
Work: (351) 21 4718922
Fax: (351) 21 4719018
fatima.abrantes@igm.pt

Heather Benway
Sedimentologist
College of Oceanic and Atmospheric Sciences
Oregon State University
104 Ocean Administration Building
Corvallis OR 97331
USA
Work: (541) 737-5227
Fax: (541) 737-2064
hbenway@coas.oregonstate.edu

Isabel Cacho-Lascorz
Sedimentologist
Department of Earth Sciences
University of Cambridge
Godwin Laboratory
New Museums Site, Pembroke Street
Cambridge CB2 2SA
United Kingdom
Work: (44) 1223 334878
Fax: (44) 1223 334871
icac00@esc.cam.ac.uk

Min-Te Chen
Sedimentologist
Institute of Applied Geophysics
National Taiwan Ocean University
2 Pei-Ning Road
Keelung 202
Taiwan
Work: (886) 2-2462-2191, ext 6503
Fax: (886) 2-2462-5038
mtchen@mail.ntou.edu.tw

Margaret L. Delaney
Inorganic Geochemist
Ocean Sciences Department
University of California, Santa Cruz
1156 High Street
Santa Cruz CA 95064
USA
Work: (831) 459-4736
Fax: (831) 459-4882
delaney@cats.ucsc.edu

José-Abel Flores
Paleontologist (nannofossils)
Departamento de Geología
Universidad Salamanca
Facultad De Ciencias
37008 Salamanca
Spain
Work: (34) 23-294-497
Fax: (34) 23-294-514
flores@usal.es

Liviu Giosan
Physical Properties Specialist
Department of Geology and Geophysics
Woods Hole Oceanographic Institution
Woods Hole MA 02543
USA
Work: (508) 289-2257
lgiosan@whoi.edu

Ann E. Holbourn
Paleontologist (foraminifers)
Institut für Geowissenschaften
Christian-Albrechts-Universität zu Kiel
Olhausenstrasse 40

24118 Kiel
Germany
Work: (49) 431-880-2938
Fax: (49) 431-880-4376
ah@gpi.uni-kiel.de

Tomohisa Irino
Sedimentologist
Graduate School of Environmental Earth Science
Hokkaido University
N10-W5, Kitaku
Sapporo 060-0810
Japan
Work: (81) 11-706-2226
Fax: (81) 11-706-2226
irino@ees.hokudai.ac.jp

Masao Iwai
Paleontologist (diatoms)
Department of Natural Environmental Science
Kochi University
2-5-1 Akebono-cho
Kochi 780-8520
Japan
Work: (81) 88-844-8321
Fax: (81) 88-844-8356
iwaim@cc.kochi-u.ac.jp

Leah H. Joseph
Sedimentologist
Geoscience Department
Hobart and William Smith Colleges
4136 Scandling Center
Pulteney Street
Geneva NY 14456
USA
Work: (315) 781-3954
Fax: (315) 781-3860
ljoseph@hws.edu

Helga F. Kleiven
Sedimentologist
Bjerknes Centre for Climate Research and Department
  of Geology
Universitetet i Bergen
Allègaten 41
5007 Bergen
Norway
Work: (47) 55-583535
Fax: (47) 55-584330
kikki@geol.uib.no

Frank Lamy
Sedimentologist
Fachbereich Geowissenschaften
Universität Bremen
Postfach 33 04 40
28334 Bremen
Germany
Work: (49) 421 2188955
Fax: (49) 421 2183116
flamy@uni-bremen.de

Steven P. Lund
Paleomagnetist
Department of Earth Sciences
University of Southern California
University Park
Los Angeles CA 90089-0740
USA
Work: (213) 740-5835
Fax: (213) 740-8801
slund@usc.edu

Philippe Martinez
Organic Geochemist
Département de Géologie et Océanographie
Université de Bordeaux I
Avenue des Facultes
33405 Talence
France
Work: (33) 5 57 96 29 66
Fax: (33) 5 56 84 08 48
p.martinez@geocean.u-bordeaux.fr

Jerry F. McManus
Sedimentologist
Department of Geology and Geophysics
Woods Hole Oceanographic Institution
121 Clark MS #23
Woods Hole MA 02543
USA
Work: (508) 289-3328
Fax: (508) 457-2175
jmcmanus@whoi.edu

Ulysses S. Ninnemann
Logging Staff Scientist
Lamont-Doherty Earth Observatory
Columbia University
Borehole Research Group
Route 9W
Palisades NY 10964
USA
Work: (845) 365-8695
Fax: (845) 365-3182
ulysses@ldeo.columbia.edu

Nicklas G. Pisias
Stratigraphic Correlator
College of Oceanic and Atmospheric Sciences
Oregon State University
104 Ocean Administration Building
Corvallis OR 97331-5503
USA
Work: (541) 737-5213
Fax: (541) 737-2064
pisias@oce.orst.edu

Rebecca S. Robinson
Sedimentologist
Department of Geological Sciences
Princeton University
Guyot Hall
Washington Road
Princeton NJ 08544

USA
Work: (609) 258-7437
rebeccar@princeton.edu

Joseph S. Stoner
Paleomagnetist
Institute of Arctic and Alpine Research
University of Colorado at Boulder
1560 30th Street
450 UCB
Boulder CO 80309-0450
USA
Work: (303) 492-6387
Fax: (303) 492-6388
Joseph.Stoner@colorado.edu

Arne Sturm
Physical Properties Specialist
GEOMAR
Christian-Albrechts-Universität zu Kiel
Wishchhofstrasse 1-3
24148 Kiel
Germany
Work: (49) 431 600 2253
Fax: (49) 431 600 2926
asturm@geomar.de

Michael W. Wara
Stratigraphic Correlator
Ocean Sciences Department
University of California, Santa Cruz
A316 Earth and Marine Sciences
1156 High Street
Santa Cruz CA 95064
USA
Work: (831) 459-5061
Fax: (831) 459-4882
mwara@aphrodite.ucsc.edu

Wuchang Wei
Paleontologist (nannofossils)
Scripps Institution of Oceanography
University of California, San Diego
Geoscience Research Division
La Jolla CA 92093-0244
USA
Work: (858) 534-5844
Fax: (858) 720-8621
wwei@ucsd.edu

OBSERVERS

Pedro Crignola
Oficina Técnica de Puerto Varas
Servicio Nacional de Geologia y Mineria
La Paz #406
Puerto Varas
Chile
Work: (56) 65-233856
Fax: (56) 65-232202
sernageomin@surnet.cl

Robert Marquina Herrera
Instituto Del Mar Del Peru
Esquina Gamarra y General Valle S/N
Chucuito-Callao
Peru
ANEXO 251-242
Work: (01) 42020000; (01) 4297630
Fax: (01) 4201588
rmarquina71@hotmail.com

Flavia Cecilia Valásquez Ruiz
Oficina Técnica de Puerto Varas
Servicio Nacional de Geologia y Mineria
La Paz #406
Puerto Varas
Chile
Work: (56) 65-233856
Fax: (56) 65-232202
geoflavia21@hotmail.com

Juan Carlos Tapia Aldas
Instituto Oceanografico de la Armada (INOCAR)
Avendio 25 de Julio via Puerto Maritimo
PO Box 5940
Guayaquil
Ecuador
Work: (593) 42 481300
Fax: (593) 42 485166
juancar279@hotmail.com
geologia@inocar.mil.ec

TRANSOCEAN OFFICIALS

Peter Mowat
Master of the Drilling Vessel
Overseas Drilling Ltd.
707 Texas Avenue South, Suite 213D
College Station TX 77840-1917
USA

Scott Pederson
Drilling Superintendent
Overseas Drilling Ltd.
707 Texas Avenue South, Suite 213D
College Station TX 77840-1917
USA

ODP SHIPBOARD PERSONNEL AND TECHNICAL REPRESENTATIVES

Tim Bronk
Assistant Laboratory Officer

Shannon Center
Marine Laboratory Specialist (Photographer)

Lisa Crowder
Marine Laboratory Specialist (Core Laboratory)

Sandy Dillard
Marine Laboratory Specialist (Downhole Tools/
  Thin Sections)

John Davis
Marine Computer Specialist

David Fackler
Programmer

Dean Farrel
Drilling Services Technician

Dennis Graham
Marine Laboratory Specialist (Chemistry)

Ron Grout
Operations Manager

Burney Hamlin
Laboratory Officer

Mike Hodge
Marine Computer Specialist

Jessica Huckemeyer
Marine Laboratory Specialist (Curator)

Brian Jones
Marine Laboratory Specialist (Chemistry)

Steven W. Kittredge
Schlumberger Engineer

Jurie Kotze
Marine Electronics Specialist

William Thomas Mefford
Marine Laboratory Specialist (Core Laboratory)

Debbie Partain
Marine Laboratory Specialist (Yeoperson)

Heather Paul
Marine Laboratory Specialist (Core Laboratory)

Pieter Pretorius
Marine Electronics Specialist

Mads Radsted
Marine Laboratory Specialist (Paleomagnetism)

Patrick Riley
Marine Laboratory Specialist (Physical Properties)

Johanna Suhonen
Marine Laboratory Specialist (Underway Geophysics)

Bob Wheatley
Marine Laboratory Specialist (X-Ray)

ABSTRACT

More than 7 km of long and relatively continuous sediment sequences from 11 sites in the southeast and equatorial Pacific were recovered during Leg 202 for the study of the Earth's climate and biogeochemical systems on scales that range from tectonic (millions of years) to orbital (tens to hundreds of thousands of years) and centennial to millennial (hundreds to thousands of years). These materials will be used to test a broad set of hypotheses on (1) the response of the South Pacific Ocean to major tectonic and climatic events, such as the opening of the Drake Passage, uplift of the Andes Mountains, closure of the Isthmus of Panama, and major expansion of polar ice sheets; (2) linkage between climate changes in the high latitudes and the equatorial Pacific, related to rhythmic changes in Earth's orbit, and the relationship of such changes to well-known glacial events of the Northern Hemisphere; and (3) global and regional changes in climate, biota, and ocean chemistry on scales of centuries to millennia.

Three sites (1236, 1237, and 1241) targeted sequences with relatively low sedimentation rates of <30 m/m.y. to obtain long records of climate change representing the Neogene and, in some cases, the late Paleogene that are not subject to severe burial diagenesis. Two sites (1238 and 1239) targeted moderate sedimentation rates of 30–80 m/m.y. to assess orbital-scale climate oscillations at a resolution suitable for the tuning of timescales and examination of changing responses to orbital forcing during the late Neogene. Six sites (1232 through 1235, 1240, and 1242) recovered sediments that accumulated rapidly, at rates of 80–2000 m/m.y., near the equator and in the southern latitudes to assess equator-to-pole climate linkages at both millennial and orbital scales.

Drilling strategy and near real-time stratigraphic correlation played a significant role in the successful recovery of these sequences. Drilling multiple holes at each site and extensive use of overdrilling with the advanced hydraulic piston corer (APC) provided long records with continuous recovery. Innovative use of rapid core logging allowed for real-time optimization of drilling strategies that maximized recovery and minimized redundant coring. Analysis of core expansion, as well as core-log integration and double-extended core barrel (XCB) coring at some sites facilitated the assembly of cores into a depth framework that will improve the quantitative analyses of sediment accumulation rates.

On Nazca Ridge, Site 1237 provides a continuous sediment sequence, recovered in overlapping APC cores, that spans >30 m.y. (modern to middle Oligocene). Exceptional preservation of the flora and fauna in this long, continuous record indicates that this site will provide a much-needed stratigraphic reference in the southeast Pacific. Abrupt changes in the presence of volcanic ash layers here document an increase in tectonic activity during the late Miocene, while at the same time an increase in biogenic components associated with productive upwelling systems, such as diatoms, are associated with late Cenozoic cooling. Site 1236 provides an equally good record from shallower water depths that, when paired with Site 1237, will document variations of deep and surface water masses in the subtropical South Pacific.

Near the equator, Sites 1238–1241 provide evidence for rhythmic oscillations of pelagic and hemipelagic sediments on the scale of Earth's orbital cycles, which will help to test the hypothesis on tropical vs. polar origins of the well-known 100-k.y. climate cycle that characterizes the late Pleistocene, as well as the response of the equatorial Pacific to closure of the Isthmus of Panama. Again, complete recovery of long and well-preserved sediment sequences will provide unprecedented resolution of biotic and environmental changes.

Century- to millennial-scale climate changes can be addressed with the records from rapidly accumulating (40–200 cm/k.y.) sediments recovered at Sites 1233–1235 from the central Chile margin. These sites will provide important data related to the southern westerlies and Antarctic Intermediate Water variability. A detailed record of paleomagnetic intensity and secular variability will link these

records into a global chronological framework. At Site 1232, in the Chile Basin, we also recovered a rapidly accumulating sequence of Pleistocene sediments, which documents terrigenous sediments eroded from the southern Andes and transported to the deep via turbidity currents. Near the equator, Sites 1240 and 1242 have moderately high sedimentation rates (~8–13 cm/k.y.), which will help to test linkages of millennial-scale climate changes between low and high latitudes.

Together, the array of sites recovered during Leg 202 provides a new view of Southern Hemisphere and tropical climate variability and biogeochemical systems across a broad range of spatial and temporal scales in a region of the ocean that has received relatively little study in the past.

INTRODUCTION

Leg Objectives

The primary scientific objectives of Leg 202 are to assess climate and oceanographic changes and to investigate the role of such changes in biogeochemical systems in the southeast Pacific. The drilling experiment contained three major elements that probe the Earth's system on three different but compatible scales: tectonic (millions of years), orbital (tens to hundreds of thousands of years), and centennial to millennial (hundreds to thousands of years). The sediment records obtained during Leg 202 will allow the testing of a broad set of hypotheses on these three timescales:

1. The response of the South Pacific Ocean to major tectonic and climatic events, such as the opening of the Drake Passage (creating a circumpolar current), uplift of the Andes Mountains (modifying wind systems), closure of the Isthmus of Panama (separating the Atlantic and Pacific Oceans), and major expansion of polar ice sheets in the high latitudes of the Southern and Northern Hemispheres at different times;
2. Linkages between climate changes in the high southern latitudes and the equatorial Pacific, related to rhythmic changes in Earth's orbit, and the relationship of such changes to well-known glacial events of the Northern Hemisphere; and
3. Global and regional changes in climate, biota, and ocean chemistry on scales of centuries to millennia. Such features have been detected in selected locations around the world, but how these regions are linked, or whether the driving mechanisms originate in the high or low latitudes, remains unknown.

On each of these scales, we obtained sediment records suitable for the study of upper ocean circulation, subsurface water masses, climate on land as reflected in eolian and fluvial inputs to the ocean, the role of biogeochemical fluxes in a changing system, and processes related to chemical diagenesis.

Our operational goals were to maximize the depth and latitude range of sites to sample different parts of the water column and upper ocean currents from southern Chile to Central America (Fig. F1; Tables T1, T2). We targeted sites with a range of time spans and sedimentation rates appropriate to the scale of questions to be addressed (Fig. F2). Some sites (1236, 1237, and 1241) targeted low sedimentation rates of <30 m/m.y. to obtain long sequences of climate change in the Neogene and, in some cases, the late Paleogene that are not subject to severe burial diagenesis. Other sites (1238 and 1239) targeted moderate sedimentation rates of 30–80 m/m.y. to assess orbital-scale climate oscillations at a resolution suitable for the tuning of timescales and examination of changing responses to orbital forcing during the late Neogene. Sediments that accumulated rapidly, at rates of 80–2000 m/m.y., were recovered from high

southern latitudes (Sites 1232–1235) and near the equator (Sites 1240 and 1242) to assess equator-to-pole climate linkages at both millennial and orbital scales. At all Leg 202 sites we recovered and verified continuous sedimentary sections as long as possible by drilling multiple advanced hydraulic piston corer (APC) holes and assembling composite sections in real time as drilling progressed.

Here, we summarize the shipboard results of Leg 202 and highlight the progress made at sea in each of the three experimental time frames and within a broad range of processes related to changing climate, ocean circulation, and biogeochemical systems.

Oceanographic Setting

Near-surface waters of the eastern Pacific exhibit enormous spatial variability, reflecting the influence of the Humboldt Current, the largest and most continuous eastern boundary current in the global oceans (Fig. F3). Off southern Chile, cool waters of the Antarctic Circumpolar Current impinge on the continent and form a transition zone between the southward-flowing Cape Horn Current and the northward-flowing Humboldt Current. Here, the westerly winds bring heavy rainfall to the coastal mountains and the Andes, resulting in high sediment fluxes to the ocean (Lamy et al., 1998, 2001). Cool and relatively low-salinity waters of the Humboldt Current are advected northward from Chile to offshore reaches of Peru (Strub et al., 1998) (Fig. F4A). Coastal upwelling driven by southerly winds along the coast off of central Chile and Peru helps to maintain this cool flow and brings nutrients to the sea surface (Fig. F4B) to feed productive ecosystems (Toggweiler et al., 1991). These eastern boundary waters merge to feed the westward-flowing South Equatorial Current, which is in turn maintained by equatorial upwelling as the equatorial cold tongue (Fig. F4A) (Wyrtki, 1981; Bryden and Brady, 1985). On scales ranging from decades to tens of thousands of years, changes in the rate of wind-driven advection of cool water off of the eastern boundary contribute to major variations in the cold tongue, with recognizable effects extending to the western Pacific (Liu and Huang, 2000; Pisias and Mix, 1997; Feldberg and Mix, 2002).

Near the equator east of the Galapagos Islands, the Equatorial Front separates the cold, salty waters of the Peru Current from warmer and fresher tropical waters of the Northern Hemisphere. North of the equator, the Panama Basin region is noted for its extreme warmth (often >30°C), exceptionally low salinity (~32 psu) (Fig. F4C), and a strong, shallow pycnocline (typically centered near 20–40 m depth). These features north of the equator reflect high rainfall relative to evaporation (Magaña et al., 1999), which stabilizes the water column and diminishes vertical mixing of heat and other properties. Some of the net freshwater flux to the Panama Basin originates in the Atlantic or Caribbean (Jousaumme et al., 1986), so low salinities here are also associated with the transport of freshwater from the Atlantic to Pacific Basins via the atmosphere. The dynamics of this transport are important because this relatively small transport of freshwater helps to maintain the relatively high salinity of the Atlantic Ocean—a key parameter in maintaining the global thermohaline "conveyor belt" circulation dominated by North Atlantic Deep Water (Zaucker et al., 1994; Rahmstorf, 1995).

Modern subsurface circulation of the southeast Pacific is illustrated in profiles of dissolved oxygen, phosphate, and salinity in a meridional transect of the eastern Pacific (Fig. F5). Bottom water presently enters eastern basins of the South Pacific from the south, below 3 km depth (Lonsdale, 1976; Tsuchiya and Talley, 1998). After transiting north, accumulating nutrients and losing oxygen in the North Pacific, much of the Pacific Deep Water exits as a middepth southward flow between 1 and 3 km. This middepth outflow and its importance to Pacific (and global) distributions of nutrients have been known for nearly 30 yr (Reid, 1973), but how this outflow changes through time remains a mystery. Debate centers on the role of Southern Hemisphere winds in maintaining global thermohaline circulation (Toggweiler and Samuels,

1993). Much of the advective export of phosphate and nitrate from the Pacific occurs in the southward return flow between 1 and 3 km depth in the eastern Pacific, where concentrations of these nutrients are highest (Wunsch et al., 1983). Thus, changes in this flow have the potential to change the budget of nutrients in the Pacific Ocean and the global ocean (Berger et al., 1997).

At intermediate water depths, water mass properties of the Pacific Ocean are highly asymmetric. Antarctic Intermediate Water (AAIW) is relatively depleted in phosphate (and contains abundant oxygen because it forms in substantial contact with the atmosphere). This combination of processes results in relatively high $\delta^{13}C$ in AAIW (Kroopnick, 1985). At present, AAIW is for the most part restricted to the Southern Hemisphere. North Pacific Intermediate Water (NPIW), which forms in the northwest Pacific with relatively little interaction with the atmosphere (Talley, 1993), contains abundant nutrients but is relatively low in oxygen and has low $\delta^{13}C$. An exceptionally steep property gradient between the southern-source and northern-source water masses occurs, at present, near the equator. These intermediate water masses are found in the eastern Pacific, typically at depths of ~500–1000 m.

At a few hundred meters water depth, the classical oxygen minimum zone (OMZ) is driven by the degradation of organic matter sinking out of the euphotic zone and modified by ocean circulation (Wyrtki, 1962). North of the equator, the OMZ is extremely intense (<0.2 ml/l O_2 between 200 and 900 m). The broad depth range of this OMZ reflects the presence of NPIW, which is depleted of oxygen because it exchanges relatively little with the atmosphere in its northern source areas, as well as the exceptionally high export of organic matter from productive upwelling systems along the eastern boundary of the North Pacific (Tsuchiya and Talley, 1998). A relatively shallow and abrupt pycnocline below low-salinity surface waters helps to maintain the shallow oxygen minimum north of the equator.

Near the equator, the OMZ is shallower (300–400 m depth) and oxygen values return to typical deep Pacific values of 1 ml/l by ~700 m depth (Fig. F5). Farther south, off central Chile, a "double" OMZ reflects southward advection of oxygen-depleted waters from the Peru margin at ~200–500 m depth in the poleward-flowing Gunther Undercurrent (GU) above the relatively oxygen-rich AAIW near ~500–1000 m. Pacific Central Water (PCW) of Northern Hemisphere origin comprises the deeper oxygen minimum from ~1500–2000 m depth. Oxygen is slightly higher (and nutrient contents lower) in the deep basin because of the incursion of Circumpolar Deep Water (CPDW) below ~3000 m.

The large pools of oxygen-poor water at intermediate depths in the modern eastern Pacific (Tsuchiya and Talley, 1998), both north and south of the equator, are major sites of denitrification and represent collectively the largest sink for nitrogen in the world's oceans. By acting as governors of the average oceanic nitrate concentration, these regions (along with the Arabian Sea) have the potential to act as climate rheostats by altering the fertility and thus the rate of CO_2 fixation within the sea. Indeed, temporal decreases and increases in export production off of northwestern Mexico, off of Peru, and in the Arabian Sea do appear to have modulated the oxygen content in upper intermediate-depth waters and the consequent intensity of denitrification during the late Quaternary (Codispoti and Christensen, 1985; Ganeshram et al., 1995). Whether or not such variations occurred on a broad scale over long time periods remains an open question. For example, it is unclear whether biological production of the eastern tropical Pacific was higher (Lyle et al., 1988) or lower (Loubere, 2000) than at present during the last ice age.

The equatorial region is highly productive but is significant in the world's oceans for not consuming all nutrients at the sea surface (Fig. F4B). High phosphate concentrations in tropical surface waters here (Levitus et al., 1993) are now thought to reflect biological limitations associated with iron or other so-called micronutrients. This is significant because any change in the net nutrient utilization would also

cause a change in the net flux of CO_2 and other biologically mediated gases from the sea surface (Mix, 1989; Jasper et al., 1994; Farrell et al., 1995a).

Tectonic Setting

Most of the sites drilled during Leg 202 examine sediments overlying oceanic crust formed either at oceanic spreading centers (Sites 1232 and 1240) or on bathymetric ridges formed by hotspot volcanism (Sites 1236–1239, 1241, and 1242). Three sites are located on the continental margin of Chile (Sites 1233–1235). The sites on the margin may have been influenced by local tectonic effects of subduction at the Peru-Chile Trench, but the time spans covered here (a few hundred thousand years at most) are short enough that tectonic movements at these margin sites can be ignored.

The sites off the margin cover longer time spans, and all are subject to plate tectonic movements. These sites can be "backtracked" to estimate their paleogeographic position relative to South America (Fig. F6), using poles of rotation for the Nazca and Cocos plates (Pisias et al., 1995). The sites may also be backtracked in water depth, assuming they have subsided in response to long-term cooling of the underlying crust (Parsons and Sclater, 1977). Such estimates work reasonably well for normal oceanic crust but are more difficult to apply to oceanic ridges and plateaus that may have experienced different thermal, tectonic, and volcanic histories than the regional oceanic spreading centers (Detrick and Crough, 1978).

Age constraints on the volcanic crust are based mostly on seafloor magnetic lineations (Hey et al., 1977; Lonsdale and Klitgord, 1978; Herron et al., 1981; Cande and Leslie, 1986), along with basal sediment ages developed by shipboard biostratigraphy. For quantitative age estimates, we use the magnetic anomaly age model of Cande and Kent (1995), which is in reasonable agreement with orbitally tuned sedimentary age models of the last 5 m.y. and with radiometric dates at older intervals.

The absolute poles for South America were added to the absolute poles for each respective crustal plate to calculate the position of each drill site relative to South America. Movement of South America in the absolute framework is very small compared to the oceanic plate motions, so these backtrack paths approximate real geography. Sites on the Nazca and Cocos plates' backtrack paths for 0 to 19 Ma are based on the analysis of Pisias et al. (1995). Absolute poles of rotation for the Cocos plate (Sites 1241–1242) were calculated using the pole of relative rotation between the Cocos and Pacific plates (36.823°N, 108.629°W; W = 2.09°/m.y. [DeMets et al., 1990]), and absolute poles for the Pacific Plate (0- to 5-Ma pole, 61.6°N, 82.5°W, W 0.97°/m.y.; for 5 to 20 Ma pole, 70.3°N, 74.4°W, W = 0.73°/m.y. [Cox and Engebretson, 1985]). Absolute poles for the Nazca plate (Sites 1232 and 1236–1240) were calculated using relative motions between the Pacific and Nazca plates (pole = 55.58°N, 90.10°W; W = 1.42°/m.y.) and the absolute Pacific poles noted above.

Major tectonic events undoubtedly influenced the environments of the southeast Pacific. Evaluating these effects is a major element of the Leg 202 experiment. Drake Passage likely began to open about 29 Ma, and a deepwater connection between ocean basins was present by ~23–24 Ma (Barker and Burrell, 1977). Numerical models predict a decrease of the Chile-Peru surface current and a distinct decrease in Antarctic deep and bottom water export to the north as water masses are entrained into a growing circumpolar circulation (Mikolajewicz et al., 1993).

Uplift of the Andes would have caused significant changes in atmospheric circulation and wind-driven oceanic surface circulation. Because it is difficult to separate tectonic and climatic influences on sedimentation, regional elements of this uplift history are controversial. Nevertheless, sedimentation in

the tropical Atlantic, as well as hiatuses and paleobotanical evidence on land, suggest major Andean uplift events in the last 10 Ma (Curry, et al., 1995; Gregory-Wodzicki, 2000; Harris and Mix, 2002).

Neogene tectonic closure of the Central American Isthmus from 13.0–2.7 Ma resulted from the subduction of the Pacific Cocos and Nazca plates, and hotspot volcanics of the Cocos and Carnegie Ridges beneath the North and South American plates and later the Caribbean plate (Duque-Caro, 1990; Dengo, 1985; Collins et al., 1996). The final closure has always been an attractive candidate for the ultimate cause of the Pliocene intensification of Northern Hemisphere glaciation since ~3.1 Ma, but the details of the isthmus formation and the climatic mechanisms that govern the response to this remain uncertain.

OPERATIONAL INNOVATIONS

As with previous paleoceanographic sampling missions, the main operational goal of Leg 202 was to recover complete stratigraphic sections at the preselected sites with as little coring disturbance as possible and as efficiently as possible. Preferred use of the APC coring system over rotary systems, coring of multiple holes at a site to ensure a complete record, and shipboard construction of stratigraphic composite sections and sampling splices became standard strategies over the last several ODP drilling legs that addressed paleoceanographic objectives. During Leg 202, we employed techniques and concepts to further optimize these strategies in order to obtain longer APC sections, to correlate data from multiple holes faster for real-time control on coring offsets and thus minimizing redundant coring, and to correlate and integrate data from cores and downhole logs.

Maximizing APC Penetration: Drilling Over

Two coring systems were used during Leg 202: the APC and the XCB. The APC, a "cookie-cutter" type system that cuts cores with minimal coring disturbance, was always the preferred coring system. The drill pipe is pressurized to shear one or two pins that hold the inner barrel attached to the outer barrel. The inner barrel strikes out and cuts the core. The driller can detect a successful cut or "full stroke" on the pressure gauge on the rig floor.

When "APC refusal" occurs in a hole before the target depth is reached, the XCB is generally used to advance the hole. The XCB is a rotary system with a small cutting shoe extending below the large rotary bit. The smaller bit can cut a semi-indurated core with less torque and fluid circulation than the main bit and thus optimizes recovery. XCB coring disturbs the cores, as the torque of the drill rotation shears and breaks the core into segments. In this process, voids fill with drill slurry and short sections of core appear as "biscuits" that range from a few centimeters to decimeters in length. The degree of XCB disturbance depends strongly on the lithology. Disturbance is most severe in partly lithified sediments that are not stiff enough to maintain their integrity under a rotating bit. Given this disturbance, an operational goal during Leg 202 was to continue APC coring as long as possible prior to switching to the XCB.

APC refusal is conventionally defined in two ways: (1) a complete stroke (as determined from the pump pressure reading) is not achieved by the piston because the formation is too hard, and (2) excess force (>60 kilopounds) is required to pull the core barrel out of the formation because the sediment is too cohesive or "sticky." In cases where full stroke can be achieved but excessive force cannot retrieve the barrel, the core barrel can be "drilled over" (i.e., after the inner core barrel is successfully shot into the formation, the rotary bit is advanced to total depth to free the APC barrel).

During Leg 202 we generally accepted only the first APC refusal criterion (incomplete stroke) for the transition to XCB operations. Drilling over stuck APC barrels allowed us to advance many holes

significantly deeper with the APC than if the second criterion (excess pullout force >60 kilopounds) had been applied (Table T3). A total of 101 core barrels were drilled over during Leg 202, which is more than during any previous leg. These drill-over operations consumed time (in some cases >1 hr per core in addition to normal operations), and in a few cases resulted in damaged core barrels. Nevertheless, we found that these investments of time and equipment paid substantial dividends in terms of enhanced APC penetration. At the Leg 202 sites dominated by carbonate-rich lithologies and characterized by low to moderate sedimentation rates (Sites 1237–1241), overdrilling increased the APC penetration by 12–126% (averaged 77%) in those 10 holes that were cored to APC refusal. At two sites, APC penetration was pushed to >300 mbsf, and at another two sites to >200 mbsf. In addition, by reserving XCB coring for sediments that were substantially lithified, we maximized the quality of recovery within these intervals, in most cases resulting in high-quality cores suitable for developing composite depth sections through most of the sedimentary sections at each site.

Stratigraphic Correlation I

Guiding Coring Offsets and Use of a "Fast Track"

During Leg 202, as during several previous Ocean Drilling Program (ODP) legs with paleoceanographic emphasis, multiple APC holes were drilled at each site to ensure recovery of a complete stratigraphic sequence, despite coring gaps that are present in any one hole. A meters composite depth (mcd) scale for each site was constructed through inter-hole correlation using closely spaced core logging measurements. The mcd scale accommodates core expansion and coring gaps and can be used to define a shipboard splice, a stratigraphically continuous sediment sequence consisting of segments from different holes.

The assembly of composite depth sections with an mcd scale, in principle, can be done with two holes, but in most cases three or more holes are needed because the position of coring gaps is not uniform (and is often unpredictable) as drilling advances downhole. Variations in bit depth may be caused by tides, ship heave (which is not compensated for with APC coring), and limited precision in sensing the depth of the drill bit based on the visual sensing of pipe advances. To optimize the depth offsets between holes, it is desirable to control bit position on a core-by-core basis. This requires knowing the position of a core relative to cores in the previously drilled hole(s) in near real time such that the relative offset of the subsequent core can be estimated and communicated to the driller. Rapid core logging that keeps pace with drilling is an essential requirement of this strategy.

To provide information on core depths for real-time adjustments in bit depth, an automated "fast track" magnetic susceptibility core logger was provided by Oregon State University (OSU) for Leg 202. This track was installed in the *JOIDES Resolution* core laboratory near the catwalk so that whole-round cores could be analyzed as soon as they entered the laboratory. The OSU Fast Track employs a Bartington MS2 susceptibility meter that was zeroed before each section scan. The usual sampling interval was 5 cm, although intervals were adjusted as needed to keep pace with drilling. Where possible, a 1-s integration time was used. Using this setting, full cores (seven sections) could be analyzed in ~15 min. However, several of the Leg 202 sites had little terrigenous material and low magnetic susceptibility. At these sites, a 10-s integration time was needed and this increased the logging time to ~40 min per core. Even with this slow setting, core flow was significantly faster than the ODP multisensor track (MST) logging time and fast enough to keep up with drilling under most circumstances.

The availability of the Fast Track magnetic susceptibility data, in many cases, allowed us to verify complete recovery of the APC-cored interval with two holes or with a third hole that was spot cored to cover specific gaps. By minimizing redundant drilling, the Fast Track strategy effectively preserved time

for deeper penetration with the APC by overdrilling and for occupying three alternate sites that added greatly to the overall scientific results of Leg 202. Use of the OSU Fast Track for most composite section development and drilling offset decisions had an additional scientific benefit, as it allowed the ODP MST to be run more slowly to optimize data quality. This strategy allowed us to increase the use of the slower MST sensors, such as the natural gamma counters, which provided a useful data set for core-log integration. Effectiveness of stratigraphic correlation and core logging would have been seriously compromised without the extra core logging track on Leg 202. Based on our experience, we recommend that future operations requiring rapid verification of complete recovery employ a similar Fast Track strategy.

Revised Meters Composite Depth

A revised meters composite depth (rmcd) scale was generated to account for the differential stretching and squeezing observed between correlated cores from each hole drilled at a particular site of Leg 202. The stretching or squeezing between cores from different holes may reflect small-scale differences in sedimentation, but more commonly is denoted by distortion caused by the drilling process.

To map cores to the splice, we developed an rmcd scale at some sites using the inverse correlation method of Martinson et al. (1982). A MATLAB program (N.G. Pisias, pers. comm., 2002) was used to correlate each core from a site to the splice record for that site. For cores already included in the splice, no correlation is necessary. For cores not in the splice, the inverse technique calculates a mapping function that allows for small changes in the mcd depth scale of the core and maximizes the correlation coefficient between the core and splice records. The program allows for exclusion of portions of the core that are not well correlated to the splice or are from intervals that contain coring distortion, such as flow-in. The generation of an rmcd scale for a given core results in a table that contains meters below seafloor (mbsf), mcd, and rmcd values for any sample from that core at a resolution equivalent to the MST data used for the mapping.

Corrected Meters Composite Depth and Mass Accumulation Rates

Composite depth scales typically are expanded by 10%–20% when compared to drilled intervals because of the expansion of cores upon recovery as a result of elastic rebound, expansion of volatile hydrocarbons (mostly biogenic methane), and mechanical stretching during the coring process. This expansion is assumed to occur without significant uptake or loss of interstitial water per unit mass of dry sediment. If this assumption is correct, sediment densities determined by wet and dry mass and volume measurements are most compatible with those measured in situ. Calculations of mass accumulation rate (MAR) require information on both sediment density and linear sedimentation rate (LSR). LSR is typically based on the mcd scale, which suffers from core expansion and must be corrected to be compatible with density measurements.

To facilitate the calculation of MAR, during Leg 202 we established the corrected meters composite depth (cmcd) scale, which adjusts the mcd scale for empirically observed expansion. A cmcd datum is produced by dividing the mcd value by the average expansion of the mcd scale relative to the mbsf scale over a sufficiently long interval so that random variations in drill pipe advance are negligible. The cmcd scale provides a complete stratigraphic sequence that is the same length as the total depth cored. The cmcd scale is a close approximation of actual drilling depths, and unless further corrected by logging data, the cmcd scale should be used when calculating LSR or MAR.

Equivalent Logging Depth

At three sites (1238, 1239, and 1241), logging operations produced data sets that were of sufficient quality to allow for core-log integration. Core-log integration produces yet another depth scale, equivalent log depth (eld). This depth scale has the advantage that it corrects for stretching and squeezing within cores. The disadvantage is that it is rarely a complete data set for correlation of the entire hole. The eld scale typically begins at ~100 mbsf, which is where the drill pipe is positioned during logging operations. Where available and where logging data are of sufficient quality, the eld is the best estimate of in situ depth and is ideal for calculating MAR.

To determine eld, logging and whole-core MST data were imported into the Sagan software package (version 1.2) and culled as necessary to remove extraneous errors associated with voids in cores or with poor sensor contact with the borehole. Because core logging data generally have a higher resolution than downhole logging data, it is necessary to smooth the core logs before comparing them with downhole logs. Sagan allows the correlation of individual cores within different holes with the data series recovered from logging. We found that Formation MicroScanner (FMS) data integrated around the borehole using 64 buttons was particularly useful because its high depth resolution compared well with that of core gamma ray attenuation (GRA) density measurements (Fig. F7). We also found good agreement between some cored intervals, natural gamma data (Fig. F8), and gamma densities measured both in the cores and in the borehole (Fig. F9).

Tidal Effects on Coring Offsets

Because we had near real-time Fast Track magnetic susceptibility data to assess coring depth offsets between holes, we attempted to make adjustments in drilling depth as coring progressed. As we scrutinized the data to make these decisions, we noticed that the differential offsets appeared to vary systematically through a daily cycle. We hypothesized that these variations were due to variations in water depth resulting from the tides.

Site 1240 illustrates variations in drilling depths well because we APC cored the entire recovered section and were able to construct a splice that spans a 2.5-day-long time interval of operations. We obtained a deep-ocean tide prediction for the drill site courtesy of Dr. Gary Egbert at OSU. A comparison of the two (Fig. F10) shows that local tides and differential drilling offsets share a 12-hr period and have a similar magnitude (~2 m) over the period of operations. This similarity suggests that deep-sea tides produce up to a 2-m change in the offset between cores that varies within a 12-hr period. As coring proceeds at a site, tides can either add to or subtract from the depth offsets, depending on the time at which two holes are begun relative to the tidal cycle (i.e., on a rising or falling tide). We imagine that in the future tidal predictions could be used to adjust drill pipe advances as needed to maintain coring overlap in multiple holes. Effective implementation of this strategy, along with the provision for heave compensation during APC coring, would likely provide for complete recovery in two holes at a site, rather than the three to five holes per site that are typically needed in current operations.

Use of Color Reflectance Spectroscopy in Lithostratigraphy

Physical properties are the expression of the lithologic, textural, and structural variations in sediments, and, in many cases, they can be used to empirically infer these primary properties over long intervals at much higher resolution than can be practically measured using traditional laboratory-based direct measurements on discrete samples. During Leg 202, reflectance spectroscopy data were calibrated with

direct geochemical measurements to provide rapid optical estimates of carbonate and total organic carbon (TOC) percentages in sediments as well as relative abundance of oxides, such as hematite and goethite, and organic pigments known as chlorins.

The reflectance spectroscopy data included 31 reflectance values over the visual spectrum (400 to 700 nm) averaged over 10-nm intervals. First derivatives of these data with respect to wavelength are commonly used to emphasize variations in spectral shape. Empirical equations were calibrated based on least-squares multiple regressions fit to discrete chemical data. Regression terms were selected with a stepwise procedure and were retained in the equations only if significant above a 95% level. The advantages of using this technique in real-time during the cruise are that the technique provides us with (1) a better understanding of sediment composition and physical properties and 2) a detection of scales of variability in carbonate and TOC that could not be attained rapidly at sea based on direct measurements with low depth resolution. Variations detected by the detailed optical data set can be targeted rapidly for manual sampling to make sure that extreme events are verified with precise chemical techniques. One example of the successful use of reflectance spectroscopy estimates of lithology during Leg 202 is the detection at Site 1237 of rhythmic variations in estimated TOC at scales of 5 to 10 m (Fig. F11). Based on preliminary shipboard age models, such variations may be associated with known ~400-k.y. cycles of Earth's orbit and suggest a climatic and biogeochemical response to this external forcing.

Digital Imaging of Cores

A new digital imaging system (DIS) implemented by ODP in 2002 and installed on the *JOIDES Resolution* during Leg 200 was used routinely for the first time during Leg 202. Essentially, all cores were imaged with this tool. As would be expected with a new, custom-made measurement system, we encountered some problems and came up with some recommendations for the operation of the system and use of the data, as well as with some recommendations for future improvements that would maximize the benefit of such measurements at sea. Although we found the digital images extremely useful for purposes of basic visual description (especially for postdescription review when the cores were not easily available for viewing), we also found that the digital image calibration was not sufficiently stable or reliable when using the digital data as a measure of quantitative brightness or color.

We found systematic millimeter- and centimeter-scale stripes in the digital images that result from the system's attempt to adjust image exposure based on calibration pixels at the site of the digital array. These pixels were inadvertently aligned with millimeter and centimeter marks on reference rulers along the sides of each core section. This problem can be mitigated by careful alignment of the camera or by using low-contrast markings on reference rulers that will not trigger automatic adjustments in camera calibration.

Significant variations in the brightness of digital images from the top to the bottom of core sections occurred because of variations in ambient lighting in the laboratory. Such ambient lighting effects may be corrected in one of three ways: (1) by enclosing the imaging system in a sealed box that shades the core sections from ambient light, (2) by increasing the brightness of the lamps that illuminate the core sections so that ambient light is overpowered by a constant source, or (3) by modifying the system to move core sections under a fixed camera so that ambient light is effectively constant rather than having the system move the camera over fixed core sections as the system is now designed.

By analyzing standard materials, we also found that small (millimeter scale) variations in camera-to-core distance (which inevitably result from irregularities in cut core surfaces) result in variations in the brightness of core images. Such an effect could be mitigated by increasing the distance between the light source and the camera system relative to the core surfaces so that small variations in the core surface are

negligible relative to the total system geometry. Increases in the core-to-lamp distance, however, work against the goal of increasing light intensity to overpower ambient light, and this effect must also be considered.

Significant temporal drift in the calibration of the digital camera system relative to white standards dictates frequent recalibration of the camera system. Ideally, such calibrations should be done automatically between each run. Calibration standards could include multiple gray levels that would compensate for nonlinear responses of the camera system across its full range of brightness.

Finally, we found it awkward to set the camera's aperture and focus manually in sediment sequences that vary significantly in their reflectance or geometry. Although manual settings are fine for occasional measurements, a greater degree of automation in camera settings and calibrations would be beneficial for ODP operations in which the camera is used continuously for long periods of time by a variety of operators who are working under stressful conditions at sea.

BIOSTRATIGRAPHY, MAGNETOSTRATIGRAPHY, AGE MODELS, AND SEDIMENTATION RATES

At Sites 1232–1235, located in the Chile Basin and on the Chile margin, late Pleistocene sediments were recovered. Because biostratigraphic resolution is limited in this time frame, estimates of sedimentation rates at these sites rely primarily on a correlation of magnetic susceptibility data to previously dated Holocene sequences (Lamy et al., 2001) and to known magnetic excursions, as well as an analysis of paleomagnetic remanence intensity and secular variations in magnetic directions.

Geomagnetic Field Behavior

Paleomagnetic measurements made during Leg 202 on cores from the Chilean margin Sites 1233, 1234, and 1235 document that these sites may provide the highest-resolution long-term record of paleomagnetic secular variation (PSV) and excursional field behavior ever recovered. They also will provide some of the very first records that document high-resolution paleomagnetic field behavior in the Southern Hemisphere. Shipboard measurements indicate that reproducible records of directional PSV have been recovered from four independent holes at Site 1233 (Fig. F12) over the entire 137 mcd, from the uppermost 60 mcd of three independent holes at Site 1234 (Fig. F13), and from the uppermost 30 mcd of three independent holes at Site 1235. The prospect is good that even better final PSV records from these intervals extending to greater depths at Sites 1234 and 1235 will be developed with shore-based paleomagnetic studies.

Shipboard paleomagnetic measurements also clearly suggest that paleomagnetic field paleointensity variations can be determined from these cores. Initial relative paleointensity estimates determined by normalizing the sediment natural remanent magnetization (NRM) to magnetic susceptibility have been developed for all of Site 1233 and the uppermost 60 mcd of Site 1234. The Site 1233 shipboard relative paleointensity and directional PSV records (Fig. F14) suggest that after shore-based paleomagnetic studies we will be able to develop the longest and highest-resolution "total-vector" PSV record ever observed. A close-up of the total-vector PSV record (Fig. F15) from Site 1233 shows that remarkable cyclicity, on the scale of ~3 m (equivalent to ~2 k.y. based on preliminary shipboard age models), exists in both the directional PSV and paleointensity records for more than 30,000 yr of the late Pleistocene. This total-vector PSV record, when finally developed, should provide important new insights into the working of the Earth's outer-core dynamo, which generates the Earth's magnetic field.

The directional PSV data from Sites 1233 and 1234 also document at least two magnetic field excursions. The younger of these excursions probably occurred around 41,000 yr ago, based on an initial timescale (Figs. F14, F15) determined by correlation of the paleointensity data with other sites around the world, and is almost certainly the Laschamp Excursion (Fig. F16). The PSV record of the Laschamp Excursion at Site 1233 is 2.4 m in width (documented in three separate holes) and probably spans a time interval of <1500 yr. That makes this the highest-resolution paleomagnetic record of an excursion ever recovered. Moreover, this excursion is also recorded at Site 1234, more than 400 km away, and the pattern of more normal directional PSV can be correlated between the two sites (Fig. F16). Further shore-based paleomagnetic studies of these Laschamp Excursion records should provide valuable new insight into the workings of the Earth's magnetic field during times of anomalous behavior that may be related to the geomagnetic field reversal process, as well as magnetostratigraphic information in unprecedented detail that will likely provide reference stratigraphic sections for the region and for the world.

Cenozoic Biostratigraphic and Magnetostratigraphic Reference Sections

Shipboard data suggest that two of the sites with long stratigraphic records, Sites 1237 and 1241, have great potential to provide not only a well-constrained chronological framework for studying the long-term tectonic, climatic, and biogeochemical history of the region, but also excellent stratigraphic reference sections in the Pacific Ocean.

Site 1237

The 360.65-mcd-thick pelagic sequence recovered at Site 1237 spans the last ~31 m.y. (the Holocene through the early Oligocene) without any detectable stratigraphic breaks. The composite depth section based on the four holes drilled at the site documents complete recovery for the entire sequence, which is dominated by biogenic components with a minor terrigenous (probably eolian) component that decreases downhole.

Calcareous nannofossils and foraminifers are generally abundant or common and well to moderately well preserved throughout the sequence. Diatoms are abundant and well preserved down to ~60 mcd, but abundance decreases and preservation deteriorates below ~69 mcd, and diatoms are absent below ~174 mcd. Most of the standard nannofossil and planktonic foraminiferal zonal markers, as well as some nonstandard nannofossil markers, can be used to establish a relatively detailed biostratigraphy. Diatoms provide additional biostratigraphic control down to ~137 mcd. All fossil groups examined on board the ship provide relatively consistent age assignments (Fig. F17). On a broad scale, sedimentation rate increases from ~10 m/m.y. prior to ~7 Ma to ~20 m/m.y. after ~7 Ma (Fig. F17). This sharp rise in biogenic accumulation rate is of special significance for regional and global paleoceanographic reconstructions.

The paleomagnetic stratigraphy at Site 1237 includes the clear definition of all chrons and subchrons for the 0- to 5- and 7- to 13-Ma intervals. Some fine-scale features and short polarity subchrons are also apparent, such as "Cobb Mountain" within the Matuyama Chron. The polarity data from the 5- to 7-Ma interval and the lowermost part of the sequence between 13 and 31 Ma appear to be promising, although assignments of chrons and subchrons are not certain yet because of several possible interpretations.

Shore-based biostratigraphic studies will refine biostratigraphic datums and identify additional events and shore-based paleomagnetic studies are expected to provide a detailed magnetostratigraphy for most or all of the sequence. Thus, the long and apparently complete sequence at Site 1237 has excellent potential for developing an orbitally tuned cyclostratigraphy for the last 31 m.y. Site 1237 should provide not only a well-constrained chronological framework for studying the long-term history of Andean uplift and

continental climate, as well as the evolution of upwelling, sea-surface, and intermediate-water properties in the southeast Pacific and the sequence of biotic events, but will also provide an outstanding stratigraphic reference section for improving integrated biostratigraphic, magnetostratigraphic, and cyclostratigraphic timescales.

Site 1241

This site on the Cocos Ridge was triple-APC cored, and a complete Pleistocene to late Miocene sequence (0–360 mcd) that is unaffected by burial diagenesis was recovered. Calcareous nannofossils are abundant and well preserved throughout the sequence. Planktonic foraminifers are abundant to common and reasonably well preserved. Although rare above ~184 mcd, diatoms are consistently present and show better preservation and higher abundance below this depth. Standard nannofossil, planktonic, foraminiferal, and diatom index markers provide tight biostratigraphic age control from the Pleistocene to latest Miocene (~ 8 Ma) (Fig. F17). The Pleistocene–lower Pliocene sequence has a sedimentation rate of ~26 m/m.y. In the lower Pliocene–uppermost Miocene section, the sedimentation rate increases to ~65 m/ m.y. Below this level, a marked decrease in sedimentation rate occurs at ~6–7 Ma and sediments accumulate at an average rate of ~30 m/m.y.

Site 1241 offers an excellent potential to derive an orbitally tuned timescale that can be tied to the biostratigraphy in order to establish a Pleistocene to late Miocene reference section for the equatorial east Pacific. The new timescale will provide integration and intercalibration of datums from both calcareous and siliceous microfossil groups within a single regional chronological framework. It will also provide a useful link between tropical and subtropical biostratigraphic schemes for the Pacific and between timescales from different oceans (such as the Leg 154 orbitally tuned timescale). The timescale will also serve as the basis for high-resolution studies that aim to reconstruct sea-surface and intermediate-water characteristics in the eastern Pacific, to retrace the history of the closure of the Panama seaway, to decipher the interaction between tropical and high-latitude circulation systems, and to delineate the evolution of various groups of marine biota.

Linear Sedimentation Rates

Except for Site 1232, which is heavily affected by turbidites, the 10 other sites of Leg 202 have yielded excellent biostratigraphies. It is expected that postcruise studies will significantly improve these stratigraphies and establish oxygen isotope stratigraphy and orbitally tuned cyclostratigraphy for most of the sites. Starting from our two stratigraphic reference sites (1237 and 1241), we built a unified stratigraphic framework at all of the Leg 202 sites. Age-depth relationships for Sites 1236–1242 are based principally upon biostratigraphic datums, although paleomagnetic age control points provide greater detail when they are available.

Using our shipboard stratigraphic framework, LSRs for Sites 1236–1241 were estimated using corrected cmcds that account for expansion of cores during recovery. The timing of changes in LSRs is partially controlled by the resolution of the age control points, which will be refined based on postcruise work. To first order, LSR estimates are consistent with regional biogenic fluxes. Sedimentation rates at the Nazca Ridge sites (1236 and 1237) and Cocos Ridge site (1241), all of which lie under low-production oligotrophic regimes, are generally low (<30 m/m.y.), whereas sedimentation rates near the highly productive equator (Sites 1238–1240) and on the Central American margin (Site 1242) are much higher (typically 80–140 m/m.y.). Within this basic theme, variations in sedimentation rates through time at the sites respond to both long-term tectonic drift of the sites relative to the continental margin and to

variations in the local environment that drive changes in both the production and preservation of biogenic sediment components.

Nazca Ridge (Sites 1236 and 1237)

Sites 1236 and 1237, currently located near the outer edges of the subtropical gyre and eastern boundary Peru upwelling system, respectively, exhibit relatively low LSRs (<2 cm/k.y.) throughout their records (Figs. F18, F19). Elevated LSRs between 20 and 15 Ma at Site 1236 likely result primarily from an increase in gravity-driven transport to the site rather than from an increase in productivity or preservation. Variations in LSR at these sites are relatively small until an increase at ~7.5 Ma. LSRs decrease at Site 1236 from ~4 Ma to present, whereas sedimentation rates at Site 1237 experience a low only between 2 and 1 Ma. The LSRs from both sites, but especially from Site 1237, are relatively high in the interval from ~7 to ~2 Ma, roughly similar to trends previously observed at Site 848, Leg 138 (Pisias et al., 1995). Tectonic backtrack paths indicate that Sites 1236 and 1237 were located initially within the low-productivity subtropical gyre and have been progressively approaching the eastern boundary Peru Current system where upwelling drives higher production and greater biogenic rain to the seafloor. Although tectonic drift can account for the general increase in LSR at younger ages at these two sites, it cannot account for the peaks and valleys in regional sedimentation, which likely reflect regional or global climate (and biogeochemical) changes.

Carnegie Ridge (Sites 1238 and 1239)

Sites 1238 and 1239 are currently located just south of the equator on the easternmost flanks of Carnegie Ridge. These sites backtrack through time to the west (based on their origin at the Galapagos hotspot), so they have been near the equatorial upwelling throughout their history (Fig. F6).

Although Site 1239 contains an ~8-m.y. hiatus between 14.5 and 6.5 Ma, both sites exhibit similar LSR trends with an initial increase from baseline LSRs at ~6.5 Ma and a further increase ~4 Ma, followed by a decrease after ~2.5 Ma. Site 1239, closer to the equator, exhibits LSR values that are consistently higher than those of Site 1238, with the exception of the hiatus and the youngest part of the record. The increase in sedimentation rates younger than ~6.5 Ma at Sites 1238 and 1239 is roughly similar to changes observed at Site 846, Leg 138 (Pisias et al., 1995), with a broad high in sedimentation rates from ~6.5 to ~2.5 Ma.

Panama Basin and Cocos Rise (Sites 1240, 1241, and 1242)

Site 1240 has relatively high sedimentation rates of ~8–13 cm/k.y., consistent with its position directly under the productive equatorial upwelling system. Although the record is short (~3 Ma basal age), a reduction in the sedimentation rate may have occurred within the past ~2 m.y. Site 1242, on the Costa Rica margin, also displays high sedimentation rates of ~6–14 cm/k.y., but the LSR here appears to increase near ~2 Ma. It remains unclear whether these different sedimentation rate histories at Sites 1240 and 1242 are related and oceanographically meaningful or whether sedimentation rate changes at the two sites simply reflect random variations in tectonics and sedimentation.

Modern and late Pleistocene sedimentation rates at Site 1241, from the Cocos Ridge, are relatively low, similar to those at Sites 1236 and 1237. In the past, however, sedimentation rates increased at Site 1241 to values >5 cm/k.y., which is consistent with the site's tectonic backtrack path toward the equator and the Galapagos hotspot prior to ~6 Ma.

BIOGEOCHEMICAL CONSTRAINTS

The oceanographic and geographic settings of Leg 202 sites influence their biogeochemical environments, as reflected in the volatile hydrocarbon, interstitial water, and sediment geochemistry. The latitudinal range for Leg 202 (from ~41°S to ~7.5°N) is significantly larger than those ranges for ODP legs that focused on the productive regimes of major eastern boundary currents: Leg 167 sites from the California Current region (~30–40°N) and Leg 175 sites from the Benguela Current region (~4°–32°S). Water depths at Leg 202 sites range from 489 to 4072 m, affecting the delivery of organic matter to the sediment/water interface. Linear sedimentation rates range over at least two orders of magnitude, from <1 to >100 cm/k.y. The oxidation of organic matter is the major influence on interstitial water geochemistry, with resulting effects on volatile hydrocarbon geochemistry and on authigenic carbonate mineralization reactions. In addition to the prevailing influence of organic matter degradation, two sites are affected by methane hydrates (Sites 1233 and 1235), and a third site shows the signature of fluid flow in the underlying basement (Site 1240).

Organic Matter Oxidation: Sulfate Reduction, Methanogenesis, and Nutrient Regeneration

Organic matter oxidation in marine sediments proceeds by a sequence of reactions typically observed with increasing depth (aerobic respiration, denitrification, manganese reduction, iron reduction, sulfate reduction, and methane fermentation). The geochemical sampling and analytical strategies employed during Leg 202 are best suited to observing the effects of organic matter oxidation through the depletion of sulfate, an oxidant, and the production of methane, a product of methane fermentation. On the basis of sulfate profiles (Fig. F20), sites can be divided into three categories:

1. Those with no to limited sulfate reduction (Nazca Ridge sites [1236 and 1237], and the deeper Cocos Rise site [1241]);
2. Those with an intermediate degree of sulfate reduction (the deeper Carnegie Ridge site [1238]); and
3. Those with complete sulfate reduction (Chile Basin site [1232], Chile margin sites [1233–1235], and the shallower Carnegie Ridge and Cocos Rise sites [1239 and 1241]).

Previous studies including some Peru margin sites have found a relationship between interstitial sulfate gradients with depth and bulk sedimentation rates, with steeper sulfate decreases (i.e., shallower depth of sulfate disappearance) related to faster sedimentation rates. This relationship appears to be generally true for Leg 202 sites, with deeper sulfate "zero" depths for the shallower of the Carnegie Ridge and Cocos Rise sites relative to the more rapidly accumulating Chile margin and Chile Basin sites (Fig. F20). However, further evaluation of this requires definition of sedimentation rates for the Chile margin and Chile Basin sites, all with relatively shallow sulfate disappearance depths of <30 mcd (Table T4).

The categorization of sites by sulfate profiles is clearly linked to the production of methane at those sites, as the presence of interstitial sulfate is known to inhibit methanogenesis in marine sediments (Claypool and Kvenvolden, 1983). The sites with limited sulfate reduction and thus high sulfate concentrations had very low methane concentrations, whereas the deeper Carnegie Ridge site (1238) with intermediate sulfate concentrations had only low to moderate levels of measured methane (Table T4). In contrast, all the sites with complete sulfate depletion had high measured methane values, with high methane concentrations being reached at depths coincident with or just deeper than the depth of sulfate

disappearance (Table T4). Note that the limited depth resolution of both interstitial water and volatile hydrocarbon sampling makes a more detailed assessment impossible.

Because the oxidation of organic matter is important in the production of alkalinity in interstitial waters, the values of the alkalinity maxima for these sites also follows the division on the basis of the sulfate profiles. Sites with limited sulfate reduction have relatively low peak alkalinity values (2 to >5 mM), the site with intermediate sulfate reduction has a moderately high alkalinity maximum (>17 mM), and the sites with complete sulfate reduction have the largest alkalinity maxima (>25 mM to as high as 60 mM) (Table T4). The regeneration of phosphorus (as dissolved phosphate) and nitrogen (as dissolved ammonium) are also closely linked to organic matter oxidation, and the peak values at the sites follow the same division by redox intensity (Table T4).

Sedimentary Organic Matter: Competing Influences and the Importance of Dilution

In contrast to the wide ranges of sulfate reduction, alkalinity generation, and methane production, the sedimentary organic carbon concentrations have a much narrower range for Leg 202 sites. The average organic carbon concentrations are typically lowest for the three sites with limited degrees of sulfate reduction (Sites 1236, 1237, and 1241), indicating that the supply of labile organic matter to serve as reductant is the limiting factor in setting the redox state of these sediments (Table T4). Many sites show an initial decline of organic carbon concentrations with increasing depth, consistent with organic matter oxidation. However, the competing influences of organic carbon supply from primary productivity, the effects of water depth at a site on organic carbon delivery to sediments, and the importance of dilution by detrital and biogenic sediments based on site location make simple generalizations about site organic carbon concentrations difficult.

Authigenic Mineralization: Calcium and Magnesium Profiles in Interstitial Waters

Alkalinity produced by organic matter oxidation can drive carbonate mineralization reactions, including precipitation and replacement reactions producing calcite and/or dolomite. If precipitation reactions are sufficiently intense, they can result in substantial decreases in interstitial calcium, in contrast to the more typical conservative increases of calcium with depth driven by reactions in basement seen in many marine sediments. Decreases in calcium can drive large increases in magnesium/calcium ratios, and high values of this ratio appear to be necessary to promote authigenic dolomite formation.

At sites with little to no sulfate reduction, interstitial calcium typically is constant or increases with increasing depth (Fig. F21A) and magnesium/calcium ratios are constant or decrease with increasing depth (Fig. F21C). In contrast, the deeper Carnegie Ridge site (1238) with an intermediate degree of sulfate reduction (Table T4) has a calcium minimum ~40% lower than seawater values, and magnesium/calcium ratios increase to nearly 8 just shallower than the sulfate minimum (Fig. F21A, F21C). The depletion of calcium is more pronounced at sites with complete sulfate reduction and with minimum calcium concentrations at least 80% lower than seawater concentrations (Fig. F21B). The depth of the calcium minimum is typically shallower than the alkalinity maximum (Table T4). The large decreases in calcium drive substantial increases in magnesium/calcium ratios to values as high as 40 (Fig. F21D). Higher magnesium/calcium ratios more effectively promote dolomite formation, which acts as a sink for magnesium. Sites with more intense sulfate reduction via organic matter oxidation are likely to be

influenced more heavily by authigenic carbonate mineralization reactions, and this must be considered when evaluating their utility for ocean history reconstructions.

Chloride Profiles: Gas Hydrates in Two Chile Margin Sites

The two shallower Chile margin sites (1233 and 1235) show clear evidence of the influence of methane hydrates in interstitial chloride profiles based on the large decreases in chloride with increasing depth (Fig. F22). These gradients are significantly larger than those observed at the deeper water, midslope Peru margin basin sites drilled during Leg 112 (Sites 682, 683, 685, and 688; site water depths range from 3072 to 5071 m). Decomposition of gas hydrates could explain the observed chloride decreases as a result of dilution, either through in situ decomposition at depth in the sediment column below the hydrate stability zone or as an artifact during sediment recovery. In contrast to Sites 1233 and 1235, the deeper-water Chile margin site (1234) has a more conservative chloride gradient with depth (Fig. F22).

Fluid Flow in Basement: Panama Basin Site 1240

A Panama Basin site (1240) has a relatively thin total sediment cover, and drilling reached basement at 289.2 mcd. Organic matter diagenesis influences the interstitial water chemistry, as indicated by the sulfate profile (Fig. F23). The decline in interstitial sulfate with depth is accompanied by increases in alkalinity, phosphate, and ammonium (Fig. F23). However, sulfate reduction is not complete at this site. The return of sulfate and alkalinity values toward seawater values near the sediment/basalt interface, along with those of other elements, indicates flow of relatively unaltered seawater in the underlying basement. Large-scale horizontal advection of such waters through oceanic crust in the central equatorial Pacific has been inferred from interstitial water geochemistry and is thought to be responsible for the low conductive heat flow (i.e., low thermal gradients) observed in that region. This influence of advective flow at Site 1240 means that any estimates of the influence of processes like authigenic mineralization based on interstitial water geochemistry may tend to underestimate their effects at this site. The incomplete sulfate reduction is not because of lack of oxidizable organic matter, as indeed the middepth sediments at this site are relatively organic carbon rich, but is the result of the effectiveness of the resupply of sulfate from above and below the sediment column, resulting in distinctive interstitial profiles (Fig. F23).

TECTONICS AND CLIMATE

One of the most perplexing questions in climate is why global climate over the past 40 m.y. changed from very warm conditions (the "Greenhouse World") to conditions of unipolar (Southern Hemisphere) and later bipolar glaciation (the "Icehouse World"). Partial answers include plate tectonic processes, elevation and erosion of vast plateaus, opening and closing of oceanic gateways, and changing concentrations of atmospheric greenhouse gases. The southeast Pacific is a key location for examining the Neogene response of climate, oceanography, and biogeochemical systems to the closure of the Isthmus of Panama and the uplift of the Andes.

Andean Uplift, Eolian Dust, Volcanism, Climate Change, and Biogeochemistry

The Neogene uplift of the Andes Mountains is expected to have caused extensive changes in South American climate, wind-driven oceanic surface circulation, and, hence, productivity by reorganizing the pattern of atmospheric circulation and the hydrological cycle. But the timing and consequences for

climate and ocean circulation, possibly responding to critical thresholds in the uplift history, are poorly constrained.

Continued uplift raised the Andes to an altitude of >4000 m by the end of the Neogene, establishing a barrier for southeast trade winds in the subtropics and for westerly winds in the midlatitude regions of South America (Lenters et al., 1995). Today, the blocking of the westerly winds results in enhanced precipitation on the western side of the mountain range (Chilean and Patagonian glaciers) and causes a strong rain shadow on the eastern side (Patagonian desert). A reversed rainfall pattern marks the low-latitude regions, where the barrier leads to enhanced precipitation from the trade winds on the eastern side of the mountain chain. Heavy rainfalls form a major source for the Amazon River, which drains its sediment load into the Atlantic. The western side suffers from a rainshadow effect and drier climate conditions, as expressed in the Atacama Desert. Moreover, the interplay between the uplift of the Andes and the semipermanent subtropical high-pressure cell over the southeast Pacific may have significantly amplified the aridification along the western margin of South America, as suggested by theoretical studies (Hay, 1996). The Andes constrict the counterclockwise flow on the east side of the high-pressure cell and force low-level high-velocity winds to follow the coast line. This results in enhanced coastal upwelling, lower sea-surface temperatures, reduced evaporation, and increased onshore aridity.

Marked changes in the erosion history of the Andes were detected during Leg 154 (Ceara Rise), which drilled the Atlantic side of South America. The increase in the Amazon River's supply of terrigenous sediments and its change in clay mineralogy indicate major uplift phases from 12 to 8 Ma and since ~4.6 Ma (Curry et al., 1995), as well as substantial regional climate changes (Harris and Mix, 2002). Uplift over the past ~10 m.y. is consistent with paleobotanical reconstructions from the central and Colombian Andes (Gregory-Wodzicki, 2000) and from ~4.6 Ma (Hooghiemstra and Ran, 1994; van der Hammen et al., 1973). The early Pliocene phase is paralleled by the subduction of the Cocos Ridge at ~5 Ma, which formed during the passage of the Cocos plate over the Galapagos hotspot and dramatically elevated the Central American volcanic arc and led to the final phase of the closure of the Isthmus of Panama (Dengo, 1985). Unfortunately the land record can not be used to assess the details of Neogene water mass changes that respond to mountain building, as the land record of uplifted marine sediments contains major hiatuses, for example in Chile between 10 and 3.5 Ma (Martinez-Pardo, 1990).

During Leg 202, we recovered a latitudinal transect of sediment records off the Pacific coast of South America that spans the time interval of the last 32 m.y. and offers an opportunity to assess the impact of Andean uplift on long-term changes in volcanic activity, continental aridity, upwelling/productivity, trade winds, and dust transport.

The long-term history of eolian deposition in the subtropical southeastern Pacific is best recorded at Sites 1236 and 1237 (Fig. F24). Today, both sites underlie the path of eolian transport from the Atacama Desert in Chile. The southeast trade winds are the major dust carriers as indicated by the pattern of quartz distribution in southeast Pacific surface sediments (Molina-Cruz, 1977). The presence of terrigenous hematite and goethite, as well as other mainly clay-sized siliciclastics at Sites 1236 and 1237 (Fig. F24), is indicative of a far-field eolian component (Pye, 1987). The combined records of these tracers suggest that eolian dust has accumulated in the subtropical southeast Pacific since at least the late Oligocene. Shipboard data from Site 1236 provide no information about eolian deposition for the sediments older than middle Miocene because the sediment deposition was dominated by supply from a nearby carbonate platform. Conversely, at Site 1237, the iron oxide signal is lost, probably diagenetically, in sediments younger than ~8 Ma.

From ~31 to ~15 Ma, before the major uplift of the Andes, Site 1237 was located nearly parallel to its modern latitudinal position farther westward (a result of plate tectonic movement), ~2200–1500 km away

from the South American coast, and thus received less dust (Fig. F24). Siliciclastic accumulation rates were lower by an order of magnitude than today and indicate no significant trend over this interval. The hematite record, however, indicates a change in the source region of dust, which was significantly enriched in hematite during the Oligocene and depleted during the Miocene. This gradual change between 26 and 22 Ma may indicate a change in weathering conditions that was possibly associated with a major change in global climate, when late Oligocene warming (~25 Ma) reduced the extent of Antarctic ice and led to warmer conditions that prevailed until the middle Miocene (Zachos et al., 2001). The timing of this shift in eolian sedimentation is also roughly coincident with the opening of Drake Passage from 39–22 Ma (Barker and Burrell, 1977), which established a deepwater connection between oceans and the Antarctic Circumpolar Current. The presence of dust far away from the South American coast suggests that arid or semiarid conditions existed in subtropical South America prior to the uplift of the Andes. Aridity in this region could have been the result of loss of humidity by the southeast trade winds along their continental path across South America and the presence of the adjacent cool Peru-Chile Current (Frakes, 1979). Before the major uplift of the Andes, the trade winds probably had a more zonal distribution that allowed deposition of eolian hematite at Site 1237.

For the period between ~15 and ~8 Ma, a hematite record exists at both sites. Higher hematite content at Site 1237 during this interval is consistent with its closer proximity to a potential South American dust source area. A first slight gradual increase in siliciclastic accumulation rates occurred at ~14 Ma. This may reflect the onset of aridity in the Atacama Desert, as suggested by Alpers and Brimhall (1988) to occur sometime between 15 and ~8 Ma, possibly in response to the uplift of the Andes. However, the increase in siliciclastic accumulation rates since ~14 Ma may also result from strengthened trade winds in response to enhanced global cooling during the Miocene from ~14 to 10 Ma, associated with the reestablishment of a major ice sheet on Antarctica (Zachos et al., 2001), or from the eastward migration of Nazca plate, which moves Site 1237 closer to the dust source (Fig. F24).

The abrupt loss of the iron oxide signal at Site 1237 (~8 Ma) appears to result from diagenetic reduction processes due to an increase in productivity and enhanced rain of organic matter to the seafloor rather than to reflect a change in the dust source area. This is corroborated by the fact that the reddish color signal of the iron oxides persists into the Pleistocene sequence at Site 1236, located about 500 km to the southwest of Site 1237 and thus had an even larger distance to the dust source.

Since the late Miocene and Pliocene, eolian iron oxides are complemented by a significant eolian siliciclastic fraction. Since ~8 Ma, steplike increases are evident in both hematite content at Site 1236 and total dust flux at Site 1237, indicating enhanced eolian deposition (Fig. F24). In accordance, recent sedimentological data from middle Miocene upper Pliocene successions in the modern Atacama Desert indicate that desertification commenced since 8 Ma, punctuated by a phase of increased aridity at ca. 6 Ma (Hartley and Chong, 2002). Moreover, the increase in eolian deposition and aridification is paralleled by a pronounced increase in productivity (reading a maximum of ~6 Ma) along the equatorial upwelling belt (Sites 1239 and 1241 and Leg 138 sites) and in the southeast Pacific, in a region outside the major coastal upwelling zone but within the influence of the Peru-Chile Current (Sites 1236 and 1237) (Fig. F25). A change in atmospheric circulation could explain these features. Intensified trade winds would enhance equatorial upwelling/productivity and the northward advection of nutrient-rich waters transported by the Peru-Chile Current. Modern upwelling along the Peruvian continental margin occurs over a broader region than just a very narrow coastal strip (Fig. F25). This may be because the wind stress curl associated with the topographically steered winds (the result of an effective mountain barrier) is positive, creating a broader upwelling zone than a strictly uniform wind with an equatorward component (Pickard and Emery, 1990). Thus, the late Miocene paleoposition of Site 1237 also was possibly influenced by upwelling

features. Enhanced coastal upwelling, in turn, would have led to increased aridification of the Atacama Desert.

The inferred enhancement in wind speed at ~8 Ma is consistent with a coarsening in eolian mass flux at south equatorial Sites 848 and 849 (Hovan, 1995), which were recovered during Leg 138. At about the same time, the first occurrence of discrete ash layers in sediments of the South Pacific record the onset of intense volcanism in the central Andes and possibly a phase of major uplift that led to the deposition of 55 ash layers at Site 1237 over the last 9 Ma (Fig. F26). Taken together, this chain of evidence may indicate a critical threshold in the uplift history at ~8–9 Ma by forming an effective topographic barrier that enhanced the steering of trade winds along the coast, resulting in stronger meridional flow, enhanced eolian transport, coastal upwelling, and biogenic productivity. This event is also recorded in the Atlantic Ocean as a rapid increase in the chlorite:kaolinite ratio off the Amazon, suggesting an abrupt increase physical weathering following uplift (Harris and Mix, 2002).

Paleobotanical evidence as summarized by Gregory-Wodzicki (2000) suggests a different uplift history for the central and northern Andes. These data suggest that the central Andes had attained no more than half of the modern elevation by ~10 Ma and imply surface uplift on the order of 2000–3500 m since the late Miocene. Major uplift of the Colombian Andes has been suggested to occur at a later stage, between 2 and 5 Ma, reaching no more than 40% of its modern elevation by ~4 Ma and a modern height by ~2.7 Ma. The temporal distribution of ash layers along the latitudinal transect of the Leg 202 sediment records might be a useful proxy in tracing the different evolution of the mountain range from Central to South America, if major uplift phases were accompanied by intense volcanism. The sediment records of Leg 202 comprise >200 volcaniclastic horizons that were deposited during the last ~9 m.y. (Fig. F26). Maxima in ash layer frequency occurred at ~8–6 Ma off the coast of southern Peru (~16°S). Farther to the north, between 2°S and 8°N, significant amounts of ash layers did not occur before ~5 Ma. The Miocene occurrence of ash layers at north equatorial Site 1241 is interpreted to reflect the volcanic activity of the Galapagos hotspot based on the presence of black lapilli-sized scoria. The deposition of such ash layers ceased at ~6 Ma, probably due to the northeastward movement of Site 1241 away from the Galapagos hotspot. The interval of the last 5 Ma is marked by ash layers enriched in clear glasses, possibly originating in Central America.

Another maximum in ash layer frequency marks the interval of the last 3 m.y. at all sites along the transect between 16°S and 8°N. The late appearance of ash layers in the northern sediment records during the Pliocene might be indicative of the major uplift phase in the northern Andes between 5 and 2 Ma.

However, it is difficult to conclusively prove a primary teleconnection between the uplift of the Andes and the observed changes in volcanism and atmospheric and oceanic circulation because the inferred uplift rates have limited confidence in absolute paleoelevation and age control. Even if the timing and identification of major changes in the uplift history are known, the sensitivity level for profound changes in climate and ocean circulation may occur at any time during the tectonic process. Furthermore, it is difficult to distinguish the initial climate response in equatorial and southeast Pacific sediment records from effects that may result from the plate tectonic drift of site locations toward the continent. Nevertheless, the sediment records recovered during Leg 202 have an excellent potential to provide detailed insights into the complex tectonics-climate connection.

Additional insights are thought to result from a comparison of sediment records from the southeast Pacific and southeast Atlantic off the coast of Namibia (Legs 175, 208). These regions share strong similarities. Both coasts are bordered by highlands that force the meridional component of the southeast trade winds in connection with the subtropical high-pressure cell to cause enhanced coastal upwelling and desertification (Namib and Atacama Deserts). However, the highlands along the coast of Namibia rise

to an altitude of no more than 2000 m and thus may serve as a modern analog to the late Miocene elevation of the Andes and its impact on atmospheric and oceanic circulation. We mention these thoughts here in the hope of encouraging further research into the tectonic linkages, especially experiments with general circulation models, to test the sensitivity of atmospheric circulation patterns to progressive mountain uplift in the midlatitudes and their effect on oceanic heat transfer via the eastern boundary currents.

Closure of the Isthmus of Panama

The Neogene tectonic closure of the Central American isthmus from 13.0 to 2.7 Ma (Duque-Caro, 1990; Collins et al., 1996) resulted from the subduction of the Pacific Cocos and Nazca plates beneath the North and South American plates and later the Caribbean plate. The early phase of the closure restricted the exchange of deep and intermediate water between the Pacific and the Atlantic and is considered as a potential cause for the "carbonate crash" near the middle/late Miocene boundary (Lyle et al., 1995). This interval is characterized by periods of severe carbonate dissolution and has been documented in sediment records from the eastern equatorial Pacific (~9–11 Ma) and the Caribbean (~10–12 Ma). The dissolution events are more recently interpreted to reflect an intensified influx of corrosive southern source water from the Atlantic into the Caribbean and into the equatorial east Pacific, both in response to a strengthened global thermohaline circulation associated with enhanced production of North Atlantic Deep Water (Roth et al., 2000). However, the major phase of the carbonate crash occurred ~1 Ma earlier in the Caribbean than in the Pacific, leaving behind several questions concerning the timing and mechanisms.

In addition, the closure has always been an attractive candidate for the ultimate cause of the Pliocene intensification of the Northern Hemisphere glaciation since ~3.1 Ma (Mikolajewicz and Crowley, 1997). Closure-induced changes in global thermohaline circulation have been invoked to be the cause either for the onset (Berggren and Hollister, 1974) or for the delay (Berger and Wefer, 1996) or for setting the preconditions of the Northern Hemisphere glaciation (Haug and Tiedemann, 1998; Driscoll and Haug, 1998).

Although the link between the isthmus closure and the Northern Hemisphere glaciation is still a matter of debate, recent studies clearly identify a close link between the formation of the Isthmus of Panama and major oceanographic changes that occurred between 4.6–4.2 Ma, when the Panamanian sill shoaled to a water depth of <100 m (Haug and Tiedemann, 1998). The chain of evidence suggests the development of the modern Pacific-Atlantic salinity contrast of ~1‰ (Haug et al., 2001), a reorganization of the equatorial Pacific surface current system, the intensification of Upper North Atlantic Deep Water formation, and the development of the modern chemical Atlantic-Pacific asymmetry, which is reflected in a strong increase in Caribbean/Atlantic carbonate preservation and a remaining strong carbonate dissolution in the Pacific (Haug and Tiedemann, 1998; Haug et al., 2001; Farrell et al., 1995b; Cannariato and Ravelo, 1997). This major salinity contrast between ocean basins, driven in part by net freshwater transport as vapor across the Isthmus of Panama, is likely responsible for maintaining the global thermohaline "conveyor belt" circulation, which is dominated by North Atlantic Deep Water (Gordon, 1986; Broecker, 1991).

In contrast to Leg 138, the equatorial sediment records from Leg 202 provide only limited evidence for the middle–late Miocene carbonate crash, probably due to the shallower site locations. All information about the Pacific carbonate crash is based on records deeper than 3000 m water depth, a depth level that is highly sensitive to fluctuations in the carbonate compensation depth (CCD) in the eastern equatorial basins (Lyle et al., 1995). However, Site 1241 on the Coccos Ridge was affected by enhanced carbonate

dissolution between ~9 and 12 Ma (Fig. F27), although positioned in a water depth of ~2200 m, well above the modern CCD. The tectonic backtrack moves Site 1241 southwestward, closer to its origin at the Galapagos hotspot into the equatorial high-productivity belt, and into a water depth that was probably several hundred meters shallower during the middle to late Miocene than it is today.

The Miocene interval from ~9 to 12 Ma is marked by low carbonate accumulation rates (Fig. F25) and low carbonate concentrations averaging ~40 wt% (Fig. F27) but relatively high mean sedimentation rates of ~50 m/m.y. Biogenic opal, organic carbon, and siliciclastics became significant contributors to the sediment composition. The preservation of calcareous nannofossils, planktonic foraminifers, and even benthic foraminifers was affected strongly by carbonate dissolution (Fig. F27). The overall increase in biogenic opal (including laminated diatom oozes), organic carbon (up to 1.5wt%), and sedimentation rates is indicative of high surface productivity and enhanced organic carbon rain. Fluctuations in the lysocline depth associated with a change in carbonate vs. biogenic opal productivity ($>C_{org}/CaCO_3$-flux) and supralysoclinal carbonate dissolution in response to organic matter degradation are considered as major contributing factors to the carbonate dissolution events. These findings may revitalize the discussion about the mechanisms that contributed to the carbonate crash. At this stage of results, however, it is difficult to postulate any link to the closure of the Isthmus of Panama.

The most prominent feature of long-term changes in the Leg 202 sediment records is a pronounced late Miocene to early Pliocene maximum in biogenic accumulation rates, suggesting an interval of enhanced oceanic surface productivity between ~8 and ~4 Ma with a maximum at ~6 Ma (Fig. F25). A similar but shorter interval of rapid biogenic accumulation (6.7–4.5 Ma) was found at equatorial east Pacific sites during Leg 138 and is often referred to as the late Miocene to early Pliocene biogenic bloom (Farrell et al., 1995b). Compelling evidence that the biogenic bloom occurred throughout the entire tropical Indo-Pacific is summarized in Farrell et al. (1995b). The ultimate cause of the rise and fall of this bloom is unknown but has been linked to a variety of previous hypotheses including sea level variations, continental weathering, deepwater circulation, trade wind fluctuations, and the closure of the Isthmus of Panama. Sites 1236 and 1237 trace the productivity maximum for the first time farther south and suggest an early onset of this event in the eastern boundary current of the South Pacific. The onset and continuation of the productivity event was probably associated with an increase in trade wind circulation since ~8 Ma as discussed in the context of Andean uplift in the previous section. Whether the wind-driven northward advection of cool and nutrient-rich Southern Ocean waters via the eastern boundary current and its injection into the South Equatorial Current is a possible source for this biogenic bloom will be studied postcruise.

The fall of this event was possibly associated with a decrease in the strength of the southeast trade winds as indicated by grain-size studies on eolian sediments from south equatorial Sites 848 and 849 (Hovan, 1995). The grain-size records, spanning the interval of the last 10 m.y., reveal a pronounced early Pliocene minimum, inferring a decrease in wind speed. Site 1237 underlies the path of eolian transport from the Atacama Desert and is ideally located to verify this hypothesis. In addition to changes in atmospheric circulation, the emergence of the Isthmus of Panama may have played a critical role because the end of the bloom, at ~4.5 Ma, coincides with a critical threshold in the closure history that led to a decrease in equatorial east Pacific sea-surface salinities (Haug et al., 2001) and an eastward shift of maximum biogenic opal productivity (Farrell et al., 1995b). The preliminary results from Leg 202 provide no clear timing for the Pliocene fall of the productivity event (Fig. F25) because the carbonate accumulation rates continued to decrease into the Pleistocene at Sites 1236, 1237, and 1241. At equatorial Site 1238, off the coast of Ecuador, the picture is even more complicated by revealing a bimodal pattern with maxima in carbonate accumulation rates at ~6 and ~3.5 Ma. However, equatorial Sites 1238, 1239,

and 1241 are ideally located to monitor changes in biogeochemical cycles and equatorial oceanography that may result from the closure history of the Isthmus of Panama.

ORBITAL-SCALE CLIMATE VARIABILITY

Sites drilled during Leg 202 will provide an extraordinary opportunity to examine the details of regional climate responses to the onset and amplification of Pleistocene ice age cycles at orbital scales over the last 5 m.y. Evidence from the Southern Ocean (Imbrie et al., 1993) and from the equatorial Pacific (Pisias and Mix, 1997; Lea et al., 2000) suggests that near-surface changes in these areas precede those at high northern latitudes. Thus, climate changes here do not passively respond to Northern Hemisphere glaciation but could be part of the chain of responses that led to Northern Hemisphere glaciation.

Especially important for Leg 202 will be to assess the linkages between changes observed at higher southern latitudes (e.g., Leg 177) with those along the equator (Sites 1238–1240). Site 1237 will provide a useful monitor of the advective link between the high and low latitudes, by monitoring the strength of the cool Humboldt Current at orbital scales of 10^4–10^6 yr. Comparison of benthic water mass tracers from sites at intermediate depths (Sites 1239 and 1242) with those at greater depths (Sites 1238 and 1240) will help to document the role of changing Pacific intermediate waters of northern and southern sources in large-scale climate change (Mix et al., 1991).

Within Pleistocene time, the origin of the large 100-k.y. climate cycle ~ 1 m.y. ago remains puzzling. A number of mechanisms have been proposed, including a threshold response of high-latitude glaciers to gradual long-term cooling associated with uplift of mountain ranges (Ruddiman and Raymo, 1988) or reduction of greenhouse gases (Maasch and Saltzman, 1990); a transition from land-based to marine-based ice sheets (Pisias and Moore, 1981; Berger and Jansen, 1994); erosion of soft sediment below Northern Hemisphere glaciers to expose bedrock, allowing larger glaciers to grow by increasing basal friction (Clark and Pollard, 1998); atmospheric loading of cosmic dust to trigger a response to rhythmic changes in the plane of Earth's orbit (Muller and MacDonald, 1997); and long-term cooling of the deep sea at polar outcrops, which influenced sea ice distributions (Gildor and Tziperman, 2001).

A 100-k.y. cycle of climate may also originate independently of polar climate changes via the responses of tropical climate systems to orbital changes in seasonal insolation (Crowley et al., 1992). Evidence exists for rhythmic 100-k.y. cycles of sedimentation in the eastern tropical Pacific that, if climatically significant, could have provided a "template" for a climate cycle that was later picked up by the global ice sheets (Mix et al., 1995). A range of evidence suggests that tropical climate changes at orbital scales preceded those of the Northern Hemisphere ice sheets and must vary independently from the high northern latitudes (Imbrie et al., 1989; McIntyre et al., 1989; Pisias and Mix, 1997; Harris and Mix, 1999; Lea et al., 2000).

One prediction of climate models that create climate cycles of a 100-k.y. period from a tropical response to orbital precession is that strong cycles of ~400-k.y. duration must also be found. Although shipboard age models are not sufficiently refined to allow interpretation of all the orbital cycles, preliminary data from Leg 202 demonstrate the likely existence of orbital-scale variability in lithologies. Evolutive spectra of the optical lightness parameter L* at Site 1239 (which here tends to mimic calcium carbonate concentrations in the sediment) reveal substantial changes in orbital-scale cycles through time (Fig. F28). Prior to ~1.2 Ma, large variations in sediment L* occurred most strongly within a long period (~400-k.y.). Near ~1.0 Ma, this ~400-k.y. cycle broadens to include variability near the ~100-k.y. period. Rhythmic variations with ~400-k.y. periodicity are also present in reflectance-predicted TOC content at Site 1237.

MILLENNIAL-SCALE CLIMATE CHANGES: POLAR, TROPICAL, OR EXTRATERRESTRIAL CAUSES?

A primary initiative for ODP is to understand the causes and consequences of millennial-scale climate change. Such changes, including the well-known "Heinrich" events at ~5- to 10-k.y. intervals and "Dansgaard-Oeschger" events of ~1- to 3-k.y. periods, are well documented in rapidly accumulating North Atlantic sediments (e.g., Labeyrie and Elliot, 1999; Clark et al., 2000). This regional expression of rapid climate change has led to hypotheses that millennial-scale changes are driven either by instabilities in Northern Hemisphere ice sheets that surround the North Atlantic region (MacAyeal, 1993) or by oscillations in the formation of North Atlantic Deep Water (Broecker et al., 1990) or in some cases perhaps by rhythmic solar forcing that is expressed in the changing climate of the North Atlantic (Bond et al., 1997, 2001). Similar millennial-scale climatic oscillations have been detected in the northeast Pacific (e.g., Hendy and Kennett, 1999, 2000), suggesting the transmission of rapid climate change events from their North Atlantic origins into the Pacific (Mikolajewicz et al., 1997).

An alternative (but perhaps not mutually exclusive) hypothesis to explain the occurrence of millennial-scale climate change is that rapid climate oscillations may emanate from the tropics, where they originate as unstable responses to insolation (McIntyre and Molfino, 1996). A likely tropical source of rapid climate variability may be modulation of interannual-to-decadal climate changes of the eastern tropical Pacific (Cane and Clement, 1999), a region well known for El Niño Southern Oscillation (ENSO) events. The tropical hypothesis is plausible, given lake and ice core records from South America that suggest long-term changes in the mean state of ENSO events (Rodbell et al., 1999; Thompson et al., 1998), glacial–interglacial sea-surface temperature changes that mimic spatial patterns of change associated with modern La Niña events (Pisias and Mix, 1997; Mix et al., 1999b; Beaufort et al., 2001), and model results suggesting the sensitivity of long-term average oceanic condition to changes in El Niño frequency forced by orbital insolation (Clement et al., 1999). It remains unclear how changes in the high latitudes and low latitudes interact, however.

On an interannual to decadal scale, Liu and Huang (2000) argue that based on modern heat budgets, warming in the equatorial Pacific over the past 50 yr is related to reduction of the wind-driven advection of cool water from the eastern boundary current and that such effects that dominate the eastern tropical Pacific extend even to the western Pacific and perhaps elsewhere. On longer (glacial–interglacial) timescales, a similar linkage between the equatorial Pacific and the eastern boundary current seems to be important (Pisias and Mix, 1997; Feldberg and Mix, 2002).

If the tropical hypothesis is true, we expect that millennial-scale climate events will be clearly recorded in sites with high sedimentation rates from the eastern equatorial Pacific, particularly near the Galapagos Islands, a region sampled at Site 1240. If the connection to the eastern boundary current is important in driving such changes, we might also expect to find similar patterns of variability in sites to the south, including Sites 1233, 1234, and 1235.

We already know, based on continental paleoenvironmental records in midlatitude Chile such as glacier advances in the southern Andes correlated to Northern Hemisphere climate events (Lowell et al., 1995; Denton et al., 1999), vegetation changes during both Termination 1 and marine isotope Stage 3 (MIS 3) (Heusser et al., 1999; Moreno et al., 2001), and weathering activity in the Chilean Norte Chico (27°S) (Lamy et al., 2000), that this region is very sensitive to rapid climate change. However, so far it has proven difficult to compare such changes unambiguously to those of the Northern Hemisphere because of limitations in dating.

Short marine cores from the region reveal that surface ocean properties also varied significantly within the southern Peru-Chile Current. Sea-surface temperature reconstructions based on the $U^{k'}_{37}$ method reveal pronounced millennial-scale oscillations during both the late glacial period (Kim et al., in press) and the Holocene (Lamy et al., 2002). Similar variations in sea-surface salinity (SSS) reconstructed for the Holocene at Site 1233 indicate close links to continental climate changes, as SSS within this region is strongly influenced by freshwater input in the southern Chilean fjord region (Lamy et al., 2002).

Recent data, especially from the northeast Pacific (Behl and Kennett, 1996; Mix et al., 1999a; Lund and Mix, 1998) also affirm the importance of understanding Pacific deep and intermediate water circulation on millennial timescales. Broecker (1998) points to the existence of a "bipolar seesaw" effect, in which millennial-scale changes in Antarctic temperature are out of phase with (leading) Northern Hemisphere events. This inference is buttressed by data from the Southern Ocean (Charles et al., 1996) and by comparison of ice core $\delta^{18}O$ or ^2H data from both hemispheres synchronized with the methane record (Blunier et al., 1998). Because the patterns of change are significantly different in the Northern and Southern Hemispheres, we can use the pattern of ventilation events on the millennial scale as a "fingerprint" of their source.

In the Pacific, Northern Hemisphere sites such as Site 893 from the Santa Barbara Basin provide compelling evidence of millennial-scale events of enriched oxygen content (i.e, unvarved sediments containing oxic benthic foraminiferal assemblages), which are approximately correlated with cold events in the North Atlantic (Kennett and Ingram, 1995; Behl and Kennett, 1996; Cannariato et al., 1999). Off Oregon, Site 1019 (980 m water depth) suggests that regional productivity effects could contribute to variations in the oxygen minimum zone off California (Mix et al., 1999a) and that ventilation of intermediate water masses is stronger during warm (e.g., Bølling-Allerød) climate events than it is during cold (e.g., Younger Dryas) climate events. At greater water depths, a possible Southern Hemisphere connection is found, as variations in benthic $\delta^{13}C$ appear linked to the Antarctic Cold Reversal, which precedes Younger Dryas cooling of the Northern Hemisphere (Blunier et al., 1997). With these data alone, the processes responsible for millennial-scale climate changes in the Pacific remain unclear.

Leg 202 sites will contribute to the understanding of millennial-scale climate changes by providing records of high sedimentation rates from sites off central Chile (Sites 1233, 1234, and 1235), within the equatorial cold tongue (Site 1240), and on the Costa Rica margin (Site 1242).

The sites drilled along the Chilean continental margin at 41°S (Site 1233) and ~3°S (Sites 1234 and 1235) (Fig. F29) provide sediment sequences with the potential for unprecedented ultra high resolution records of surface and deep-ocean conditions as well as continental paleoclimates during the last two glacial–interglacial cycles.

Sites 1233–1235 are particularly well located for assessing variations in the strength of AAIW through time (Fig. F30). Site 1235 monitors the boundary between the Gunther Undercurrent (the poleward undercurrent, a relatively low-oxygen water mass), and AAIW (a relatively high-oxygen water mass). Site 1233 is located roughly in the core of AAIW and thus should provide the best available record of AAIW properties relatively close to its source in the Antarctic Subpolar Front. Finally, Site 1234 monitors the deeper boundary of AAIW in its zone of mixing with Pacific Central Water (a relatively low-oxygen water mass).

Together, these records will fill a crucial gap in the paleoceanographic archive because there are no existing high-resolution cores capable of monitoring the intermediate waters that upwell at low latitudes and influence productivity and carbon outgassing to the atmosphere (Broecker and Peng, 1982). The temperature changes deduced from benthic foraminiferal oxygen isotopes at Sites 1233–1235 should provide a sensitive monitor for assessing the effect of intermediate-depth temperature changes on tropical

climate over millennial to decadal timescales. Thus, Sites 1233–1235 afford an excellent opportunity to examine the role of chemical changes in high-latitude surface waters that can be transferred to the tropics via AAIW (e.g., Oppo and Fairbanks, 1989; Ninnemann and Charles, 1997).

Shipboard biostratigraphic data indicate that the bases of Sites 1233–1235 are younger than 260 ka. Additional tentative stratigraphic markers are derived from analyses of paleomagnetic variations, such as the Laschamp Excursion at ~41 ka, which is particularly pronounced at Sites 1233 and 1234 (see "Biostratigraphy, Magnetostratigraphy, Age Models, and Sedimentation Rates," above). These data indicate that sedimentation rates are generally >50 cm/k.y. reaching >1 m/k.y. in major parts of the recovered sequences, particularly at Sites 1233 and 1235. Such high sedimentation rates at key locations provide an outstanding opportunity to explore atmospheric and oceanographic variability in the Southern Hemisphere on the relatively short timescales from millennia to centuries and perhaps even decades.

Sediments at all three sites are dominated by lithologically homogeneous fine-grained terrigenous material with very high magnetic susceptibilities (Fig. F31). Minor amounts of biogenic components, mostly well preserved for paleoceanographic studies, are present throughout nearly the entire recovered sequences. The high sedimentation rates can be explained by extremely high terrigenous sediment supply due to enhanced fluvial discharge in response to heavy continental rainfall (Lamy et al., 2001). Probably in response to northward decreasing precipitation, sedimentation rates appear to be lower at Sites 1234 and 1235 when compared to Site 1233, particularly during MIS 2 to 3. However, this pattern might have been different in the older parts of the records, either indicating a different contribution of syndepositional sediment focused within the local basins or different rainfall patterns during MIS 5 and 6.

The magnetic susceptibility records of all sites document pronounced variability both on Milankovitch and sub-Milankovitch timescales. Higher magnetic susceptibility appears to be characteristic of glacial intervals, which might indicate increased terrigenous sediment input due to higher rainfall during regional cold phases. This is consistent with findings from marine sediment cores off central and northern Chile (Lamy et al., 1998, 1999).

Even as the Leg 202 cores were being analyzed at sea, we were able to develop preliminary age models based on correlation of magnetic susceptibility data at Site 1233 and in a ^{14}C-accelerator mass spectrometry (AMS)-dated gravity core from the site that spans the last ~8000 yr (Lamy et al., 2001). In addition, shipboard paleomagnetic data revealed a major excursion of Earth's magnetic field, which we correlated to the well-known Laschamp Excursion at ~41 ka. The shipboard chronologies do not yet allow us to link specific variations in magnetic susceptibility at Sites 1233–1235 to climate changes recorded in either the Northern Hemisphere or Southern Hemisphere ice sheets. Nevertheless, it is already clear that such linkages are likely to be found. For example, within the interval of the last ~45 k.y., Site 1233 displays strong sub-Milankovitch variability with general patterns similar to those observed in polar ice cores (Fig. F32). By analogy to variations within the Holocene (Lamy et al., 2001) and to longer-period glacial–interglacial variations in the region, we expect that the variations in magnetic susceptibility at Site 1233 are related to changes in continental rainfall, which probably reflect latitudinal shifts of the southern westerly winds.

Shipboard data on diatom abundance and assemblage composition reveal pronounced sub-Milankovitch variability, possibly reflecting changes in upwelling and biological production at Site 1233. Furthermore, significant changes in continental freshwater input seem to be indicated by the abundance of freshwater diatoms.

In the tropics, Site 1240 is ideally located to assess rapid variations in equatorial upwelling, perhaps related to long-term stability of ENSO events (Clement, 1999; Beaufort et al., 2001). Here, sedimentation

rates are near 10 cm/k.y., suggesting that climate changes on the scale of centuries may be well recorded here.

Site 1242 will provide for analyses of sea-surface salinities in the Panama Basin, related to excess precipitation relative to evaporation near the intertropical convergence. This region of the Panama Basin is noted for its extreme warmth (often >30°C), exceptionally low salinity (near 32), and a strong, shallow pycnocline (typically centered near 20–40 m depth). These features all reflect high rainfall relative to evaporation (Magaña et al., 1999), which stabilizes the water column and diminishes vertical mixing of heat and other properties. A portion of the net freshwater flux to the Panama Basin originates in the Atlantic or Caribbean (Jousaumme et al., 1986), so low salinities here partially reflect the transport of freshwater from the Atlantic to Pacific Basins via the atmosphere. The dynamics of this transport are important because this relatively small transport of freshwater helps to maintain the relatively high salinity of the Atlantic Ocean—a key parameter in maintaining the global thermohaline "conveyor belt" circulation dominated by North Atlantic Deep Water production (Zaucker et al., 1994; Rahmstorf, 1995). Thus, a millennial-scale record of sea-surface salinity variation at Site 1242 will help to test the tropical hypotheses of rapid climate change and will evaluate a possible mechanism that would link climate changes of the tropics via the hydrological cycle to those of the high latitudes through the control of oceanic salinity budgets on deepwater formation.

Variations in paleomagnetic secular variation and NRM intensity observed at Sites 1233–1235 and 1240 will likely facilitate synchronization of these important Southern Hemisphere sedimentary records to high-resolution records from the Northern Hemisphere, and this will provide a test of the phasing of millennial-scale climate changes between the two hemispheres.

SUMMARY AND PERSPECTIVES

During Leg 202, we recovered a total of 7081 m of sediment at 11 sites, ranging in age from early Oligocene (~31.5 Ma) to Holocene (Tables T1, T2; Fig. F2). Sites 1232–1242 form an east Pacific latitudinal transect from 41°S–8°N as well as an intermediate to deepwater transect from 490–4070 m water depth. The pelagic and hemipelagic records provide an excellent base for a broad spectrum of detailed studies that aim to reconstruct the evolution of upwelling, biota, biogeochemistry, sea-surface, and intermediate-water characteristics in the southeast and equatorial Pacific, as well as the closure of the Isthmus of Panama, the history of Andean uplift, and continental climate. Moreover, these records permit paleoceanographic studies on a variety of timescales, including centennial to millennial (10^2 to 10^3 yr), orbital (10^4 to 10^5 yr), and tectonic (>10^5 yr) time resolution.

Operational successes during Leg 202 include the ability to make rapid drilling decisions by using a rapid-scanning core logging track, which includes measurements of magnetic susceptibility. Efficient planning, based on the availability of these logging data, made time for extensive overdrilling of APC cores to improve recovery.

One of the most exciting results was the successful recovery of unprecedented ultra high resolution records (Sites 1233, 1334, and 1235) from the Chilean continental margin between 41°S and ~36°S at water depths between 490 and 1115 m. Shipboard stratigraphic data indicate that the base of Sites 1233–1235 is younger than 260 ka. These records are marked by exceptionally high sedimentation rates of 40–200 cm/k.y., apparently driven by extremely high terrigenous sediment supply due to enhanced river discharge in response to heavy continental rainfall. The dominance of siliciclastic sediments here resulted in a high-resolution record of paleomagnetic variations. Among them, the most prominent feature in the late Pleistocene is the Laschamp Event at ~41 ka, which is particularly pronounced at Sites 1233 and 1234

(e.g., covering an interval of 2 m at Site 1233). These extraordinary paleomagnetic records provide opportunities for high-resolution regional and global correlation of marine and terrestrial records using paleomagnetic secular variation and paleointensity variation to test the phasing of climate changes between the Southern and Northern Hemispheres. Together with a rich array of well-preserved biogenic and mineralogic tracers of paleoclimatic utility, these sites provide a unique chance for understanding the role of South Pacific oceanography and Southern Hemisphere climate in a global context on scales from millennia to centuries and perhaps even decades.

In the tropics, climate and oceanographic changes on the scale of centuries and millennia may be well recorded at Site 1240 in the Panama Basin and at Site 1242 on Cocos Ridge. Nannofossils, planktonic foraminifers, and diatoms provided well-constrained biostratigraphic age models and magnetostratigraphic information through the Brunhes and Matuyama Chrons that significantly augmented the age model at Site 1240. Both records comprise a complete stratigraphic sequence of the last ~2.6 m.y., and sedimentation rates vary in the range of 6–20 cm/k.y., with higher rates in the Pliocene sequence. Persistent decimeter- to meter-scale variability in core logging data (bulk density and magnetic susceptibility) are mainly related to changes in the relative supplies of carbonate and biosiliceous and siliciclastic material and are tentatively interpreted to reflect millennial- to orbital-scale changes in equatorial productivity and/or climate.

These records are ideally located to monitor rapid changes in upwelling and productivity in response to variations in nutrients and wind forcing (Site 1240), as well as changes in sea-surface salinities due to fluctuations in precipitation that are linked to the moisture export from the low-latitude Atlantic and to the latitudinal position of the Intertropical Convergence Zone (Site 1242). Paleomagnetic measurements at Site 1242 indicate a great potential for a good record of magnetic paleointensities that will allow high-resolution chronological comparisons to examine linkages and differences in the hydrological cycle between the mid and low latitudes.

On longer timescales, the response of the southeast and equatorial Pacific to orbital and tectonic forcing is recorded at Sites 1238, 1239, and 1241, covering the interval of the last ~11–15 m.y., and at Sites 1236 and 1237, spanning the interval of the last ~28–32 m.y. Thus, the geographic distribution of these sites affords a latitudinal comparison for the last 11 m.y. between ~21°S and ~6°N. The water depth distribution of these sites between ~1320 and ~3210 m will allow for the first time detailed insights into the Neogene evolution of equatorial and South Pacific intermediate water chemistry. Most of the pelagic to hemipelagic sequences, especially from the upper Miocene and early Pliocene with sedimentation rates as high as 50–110 m/m.y. (Sites 1238, 1239, and 1241), reveal clear lithologic changes on meter and decimeter scales that are most likely related to orbitally induced changes in precession and obliquity. If so, these cycles provide a basis for both (1) developing orbitally tuned age models and (2) testing the phase relationships between major climate and oceanographic components to assess the role of South Pacific oceanography and biogeochemistry within the chain of climate forcing mechanisms.

The predominantly good preservation of calcareous microfossils and the prevalent presence of diatoms resulted in a remarkable biostratigraphic framework that offers the opportunity to generate an improved biostratigraphic scheme for the southeast Pacific, as well as correlations with the low-latitude zonations. In addition, the APC-cored record from Site 1237 yielded an outstanding magnetic polarity reversal stratigraphy for the interval of the last 31 m.y. Although the polarity assignments are still preliminary and allow several possible interpretations in the sequence between 13 and 31 Ma, this site offers an excellent potential to derive an orbitally tuned timescale that can be tied to magnetostratigraphy and biostratigraphy to provide a reference section for the South and equatorial Pacific. Low-resolution Site 1236 revealed a magnetic polarity stratigraphy for the last 13 m.y., significantly augmenting the

biostratigraphy and providing a well-constrained chronology. Hiatuses were only registered at Site 1238 from Carnegie Ridge, encompassing the interval from ~7.8 to 13.6 Ma, and at Site 1242 from Cocos Ridge, spanning the interval from ~2.5 to 13 Ma.

On tectonic timescales, significant variability and gradients in the supply of biogenic and siliciclastic sediments, including the abundance of ash layers, are to a large part associated with the history of Andean uplift, closure of the Isthmus of Panama, and the paleodrift of site locations due to tectonic plate motions. Except for Site 1236, no evidence was found for larger changes in paleobathymetry due to the subsidence history of the Cocos, Carnegie, and Nazca Ridges that were formed at hotspots.

The drift of the Cocos plate moved equatorial Sites 1241 and 1242 (Cocos Ridge) from their Miocene paleoposition northeastward away from the equatorial productivity belt closer to the Central American landmass. This resulted in a general decrease in biogenic sediment deposition and may have contributed to the increase in siliciclastics since the Pliocene.

The predominantly eastward migration of the Nazca plate moved South Pacific Sites 1236–1239 from their Oligocene or Miocene pelagic paleopositions closer to the South American continent and thus closer to hemipelagic environments that are influenced by coastal upwelling processes and enhanced terrigenous eolian sediment supply. However, Sites 1238 and 1239 (Carnegie Ridge) drifted eastward within the equatorial upwelling belt and thus experienced little environmental change during their Miocene to Holocene history, as indicated by permanent and relatively high deposition rates of biogenic silica and calcareous sediments. The Pleistocene increase in siliciclastic sediment, as indicated by an increase in magnetic susceptibility values, may result from changes in continental aridity and/or dust transport rather than from the plate tectonic drift.

The late Oligocene to Holocene sediment deposition at Sites 1236 and 1237 is clearly influenced by environmental changes associated with the eastward drift and the subsidence history of Nazca Ridge. The tectonic backtrack path on Nazca plate moves the sites ~20° westward, toward the center of the subtropical gyre. Site 1236 subsided from a few hundred meters of water depth to its modern depth of 1320 m. The deposition of upper Oligocene fine-grained chalk overlying basaltic basement indicates an early phase of pelagic sedimentation. The presence of authigenic glauconite and the relatively high abundance of buliminids and nododariids suggest shallow-water conditions. After the initial pelagic phase, several ash layers suggest a late stage of volcanic activity near 28 Ma that possibly was related to the well-known tectonic reorganization that created the Nazca plate. This phase was followed by the deposition of neritic, grain-rich, calcareous sediment, typical for a supply from carbonate platforms, which may have surrounded volcanic islands in the vicinity of Site 1236. The sediment supply from the carbonate platform persisted until ~17 Ma and is marked by increased sedimentation rates of ~15 m/m.y. The interval of the last 17 m.y. is characterized by the deposition of nannofossil ooze and very low sedimentation rates of ~5 m/m.y., indicating an oligotrophic pelagic environment and possibly winnowing effects at intermediate water depth.

At deepwater Site 1237, the pelagic upper Oligocene to middle Miocene sequence is dominated by nannofossil ooze, carbonate contents >90wt%, and low sedimentation rates of ~10 m/m.y., typical for oligotrophic conditions in the sphere of the subtropical gyre. The general increase in clay, biogenic opal, sedimentation rates, and the occurrence of diatom species indicative of coastal upwelling reflects the paleodrift toward the Peruvian continental margin since the middle Miocene.

Superimposed on such gradual sedimentological changes are long-term variations that result from changes in climate and oceanography, possibly also associated with tectonic processes like the uplift of the Andes and the closure of the Isthmus of Panama. The Neogene uplift of the Andes is expected to have caused an enhanced steering of the southeast trade winds along the Chilean and Peruvian coasts, resulting

in stronger meridional flow, enhanced eolian transport, coastal upwelling, and biogenic productivity. The long-term history of eolian deposition in the southeast Pacific is best recorded at Sites 1236 and 1237, underlying the modern path of eolian transport from the Atacama Desert. There is a stepwise increase in dust flux (Site 1237) and hematite contents (Site 1236) since 8 Ma that may reflect a critical threshold in the uplift history that resulted in a strengthening of trade wind circulation as suggested by enhanced coastal upwelling and productivity. At approximately the same time, discrete ash layers begin to appear at Site 1237, recording the onset of intense volcanism and accompanying the tectonic uplift of the Andes. The sediment records of Leg 202 comprise >200 volcaniclastic horizons that were deposited during the last ~9 m.y. Maxima in ash layer frequency occurred at ~8–6 Ma and during the last 3 m.y.

The most prominent feature of long-term changes in the Leg 202 sediment records is a pronounced late Miocene to early Pliocene maximum in biogenic accumulation rates suggesting an interval of enhanced oceanic surface productivity between ~8 and ~4 Ma, with a maximum at ~6 Ma. A similar but shorter interval of rapid biogenic accumulation (6.7–4.5 Ma) was found at equatorial east Pacific sites during Leg 138 and is often referred to as the late Miocene to early Pliocene biogenic bloom. The ultimate cause of the rise and fall of this bloom is unknown but has been linked to a variety of previous hypotheses, including sea level variations, continental weathering, deepwater circulation, trade-wind fluctuations, and the closure of the Isthmus of Panama. Sites 1236 and 1237 trace the productivity maximum for the first time farther south and suggest an early onset of this event in the eastern boundary current of the South Pacific, which was associated with an increase in trade wind circulation since ~8 Ma. Whether the wind-driven northward advection of cool and nutrient-rich Southern Ocean waters via the eastern boundary current and their injection into the South Equatorial Current is a possible source for this bloom will be studied postcruise.

LEG 202 SITE SUMMARIES

Site 1232

Background

Site 1232 (proposed Site SEPAC-19A) is located in the Chile Basin between the Mocha and Valdivia Fracture Zones, ~50 km westward of the Peru-Chile Trench (Fig. F1). The water depth of 4069 m is ideal for monitoring the influx of CPDW into the Chile Basin and variations in terrigenous sediment transported from southern Chile. On the Nazca plate, the tectonic backtrack path of Site 1232 is roughly parallel to surface-ocean properties, such as sea-surface temperatures in the subpolar transition zone (Figs. F4, F6). Crustal ages are not well defined but are expected to be between 19 and 29 Ma based on the limited study of regional seafloor magnetic lineations. The total thickness of the sedimentary section was estimated at 470 m based on site-survey seismic profiles that revealed well-stratified, moderately reflective layers in a style characteristic of hemipelagic sediments (Fig. F33).

The primary objectives at Site 1232 were to recover a nearly continuous sequence of Neogene hemipelagic sediments for paleoceanographic investigations in order to

1. Assess variations in the character of the Antarctic Circumpolar Deep Water as it enters the Chile Basin from the south, including responses over the Neogene to the opening of the Drake Passage and closing of the Isthmus of Panama and to orbital-scale climate variations;

2. Assess variations in the southernmost reaches of the northward-flowing Peru-Chile (or Humboldt) Current, based on planktonic fauna and flora, including responses of the Southern Hemisphere westerly winds on similar tectonic and orbital scales;

3. Improve biostratigraphic and paleomagnetic stratigraphies in the southeast Pacific and compare them with those of the subtropical and tropical regions to improve magnetobiochronology on a global scale; and

4. Date basal sediments to better constrain the age of oceanic crust between the Valdivia and Mocha Fracture Zones.

The drilling strategy included triple-APC coring until refusal and single-XCB coring to basement, with the expectation that sediments as old as the Miocene and perhaps the Oligocene would be recovered. However, Site 1232 revealed a dramatically different sequence than expected. The upper 382 mcd (362 mbsf) represents an expanded upper Pleistocene section (<1 Ma) of interbedded silty clay (inferred upper parts of turbidites and hemipelagic sediments) with thin beds of sandy silt (basal parts of distal turbidites). Given the apparent uniformity of the seismic section, we infer that all sediments above acoustic basement are similar to that of the cored interval. Given time constraints, development of an appropriate weather window to drill on the margin, and the unlikely prospect of finding pre-Quaternary sediments at Site 1232, we abandoned coring at 382 mcd (362 mbsf). However, we continued APC coring to 98.8 mcd (90.4 mbsf) in Hole 1232B and to 38.9 mcd (33.2 mbsf) in Hole 1232C to improve stratigraphic overlap between sediment sections so that the site objectives related to late Quaternary climate variations may be addressed.

Operations

Leg 202 began at 1200 hr on 29 March 2002 when the *JOIDES Resolution* was tied up in Valparaiso, Chile. We left port at first daylight on 4 April and headed to proposed Site SEPAC-19A on the Chile margin, the southernmost site we planned to drill. After a 515-nmi transit from Valparaiso, which included a brief 3.5-kHz survey of proposed Sites SEPAC-13B and SEPAC-14A, the *JOIDES Resolution* was driven off of Site SEPAC-19A by a force 8 storm and proceeded an additional 94 nm at low speed to occupy Site 1232 (proposed Site SEPAC-09A). Hole 1232A was initiated at 0500 hr on 8 April. Swell continued to be relatively high, and drilling proceeded with 12 APC cores and 27 XBC cores, with a total penetration of 371.3 mbsf. Hole 1232A was not logged. Holes 1232B and 1232C included ten APC cores to 90.1 mbsf and four APC cores to 33.2 mbsf depth, respectively. Operations at this site were concluded at 2200 hr on 11 April and were followed by a 94-nmi (~9 hr) transit back to Site SEPAC-19A under improved weather conditions.

Scientific Results

The 382-m-thick sedimentary sequence recovered at Site 1232 is composed of gray silty clay and clay interbedded with >800 graded layers of dark gray silty sand beds with sharp, sometimes scoured, basal contacts (Fig. F34). Biogenic sediments are present in trace abundance, except in occasional thin layers within the dominant silty clay and clay. The silty sand layers, which we interpret as the basal parts of distal turbidites, have high magnetic susceptibility and GRA bulk density and low chroma (a* and b*) and reflectance (L*) values.

Over the full cored interval, the turbidite layers range from a few millimeters to 118 cm thick (average = 3 cm) and are present throughout the section between silty clay layers that range from a few millimeters to 610 cm thick (average = 27 cm). The sandy silt intervals account for ~9% of the total section. Thickness

and frequency of the turbidites decrease downhole; recognized sandy silt intervals account for ~22% of the section from 0 to 20 mbsf, 15% of the section from 20 to 200 mbsf, and 3% of the section from 200 to 250 mbsf.

Within both interbedded lithologies, clay minerals and feldspar are common, whereas amphiboles, pyroxenes, mica, and quartz are present in minor amounts. Such a mineral assemblage is consistent with a source area in southern Chile that is dominated by andesitic volcanic rocks of the Andes Mountains. A plausible transport path for turbidity currents is via the southernmost extent of the Chile Trench north of the Chile rise, where the trench has relatively little bathymetric expression.

The abundance of calcareous microfossils (nannofossils and foraminifers) at Site 1232 is generally low, and their preservation is generally poor to moderate. Foraminifer species suggest substantial changes in climate, varying between polar (*Neogloboquadrina pachyderma*) and eastern boundary (*Globigerina bulloides* and *Globorotalia inflata*) assemblages. Rare specimens of subtropical foraminifer species with warm-water affinities, such as *Globigerinoides ruber*, were found in a few samples. Diatom abundance and preservation fluctuate significantly and deteriorate noticeably deeper than 202 mcd (185 mbsf; Hole 1232A). Marine diatoms abundance is highest in the upper 100 m of the sediment record, and the assemblage is dominated by coastal upwelling and eastern boundary current forms, such as *Chaetoceros* spp.

Reworking of microfossils is apparent in all of the fossil groups examined. In particular, freshwater and benthic diatoms, such as *Aulacoseira granulata*, and shallow-water benthic species, such as *Eunotia* spp., are especially abundant in the intervals at 43–69 mcd (37–56 mbsf; Hole 1232A) and 193–241 mcd (176–224 mbsf; Hole 1232A) and suggest reworking from continental sources.

Ages of the sediment are inferred from calcareous nannofossils and planktonic foraminifers. The nannofossils suggest an age of 0.26 Ma at 143 ± 5 mcd (126 ± 5 mbsf; Hole 1232A), 0.46 Ma at 259 ± 5 mcd (241 ± 5 mbsf; Hole 1232A), and <1.7 Ma for the deepest core at 382 mcd (362 mbsf; Hole 1232A).

NRM intensities at Site 1232 were extremely high both before (mean = 1.41 A/m) and after alternating-field (AF) demagnetization (0.21 A/m) at peak fields up to 20 mT. The large drop in remanence intensity after demagnetization is due to a strong drill string positive magnetic overprint that is substantially but incompletely removed after shipboard demagnetization. Aside from drilling disturbance and the drill string overprint, the NRM after demagnetization is characterized by negative inclination (normal polarity) throughout the sequence and therefore is interpreted to represent the Brunhes Chron (0–0.78 Ma).

A complete composite section and splice were developed in the interval from 0 to 42.7 mcd (0–37.6; mbsf in Hole 1232B). Father downhole, correlation between cores in different holes form a floating splice to 100.4 mcd (83.94 mbsf; Hole 1232A). We primarily used magnetic susceptibility data acquired with the OSU Fast Track system for the correlation. This track analyzes individual 1.5-m core sections in about 2 min and allows stratigraphic correlation to keep pace with and guide coring operations.

Additional core logging data, including magnetic susceptibility, GRA density, natural gamma radiation, and *P*-wave velocity, were acquired with the ODP MST. Reflectance spectra and point-sensing magnetic susceptibility were measured on the archive-half MST. The Geotek line-scan digital imager was operated on its own track to record red-green-blue color images at a pixel resolution of ~100 μm. These three additional tracks operated at a slower rate than the Fast Track, typically at 5–20 min/s, in order to optimize data quality. These data will be used later to refine hole-to-hole correlation and to interpret lithologic composition in greater detail. Physical property measurements of moisture and density yielded excellent relationships to GRA density, which indicates minimal coring disturbance at this site.

Results from gas, interstitial water, and sedimentary composition measurements at Site 1232 reflect the influences of organic matter diagenesis and the low biogenic content of sediments at this site. The sediments were moderately gassy, with methane first appearing at 27.3 mcd (23.0 mbsf, Hole 1232A) and

dominating the gas composition throughout. The disappearance of dissolved sulfate in interstitial water (<2 mM) at this depth, coupled with high alkalinity concentrations (>30 mM) and elevated phosphate and ammonium concentrations (>50 mM and >2 mM, respectively), is consistent with organic matter degradation being a primary influence on interstitial water and gas composition at this site. Interstitial waters have dissolved silicate concentrations <600 µM, below saturation with respect to biogenic opal. Dissolved calcium concentrations decrease from seawater values at the sediment water interface to <6 mM by 27.2 mcd (23.0 mbsf), with a pronounced minimum of <4 mM at 93.4 mcd (85.0 mbsf; Hole 1232A). The sediments are poor in organic carbon, typically <0.25 wt%. Organic carbon/organic nitrogen ratios indicate dominance of marine organic matter. Calcium carbonate contents are typically low, less than a few weight percent, although isolated peaks were found with values as high as 27 wt%.

The combination of the age constraints from biostratigraphy and magnetostratigraphy suggest siliciclastic-dominated sediment accumulation rates of >450 m/m.y., roughly a factor of 10 to 20 higher than regional pelagic sedimentation. The seismic reflection profile indicates an unconformity between the bottom reflector and the turbidite-dominated Pleistocene sequence. Extrapolation of late Pleistocene sedimentation rates to the unconformity suggests that much of the sediment accumulation here has occurred within the last million years. A similar situation has been described on the Peruvian continental margin, with a change from carbonate to terrigenous deposition in the late Pleistocene (0.93–0.44 Ma). Whether these dramatic secular changes in sedimentation off western South America can be attributed to changes in tectonics or climate remains a question. On the fine scale, inferred sedimentation rates imply that the turbidite layers observed at Site 1232, which have an average depth spacing of ~30 cm, have an average recurrence time on the order of hundreds of years. Great earthquakes associated with active tectonism of southern Chile, as well as century- to millennial-scale climate changes, may serve as possible triggers for large turbidity flows that transport continental sands and silts to Site 1232.

Site 1233

Background

Site 1233 (proposed Site SEPAC-19) is located 38 km offshore (20 km off the continental shelf) at 838 m water depth in a small forearc basin on the upper continental slope (Fig. F1). Here, shoreward of the Peru-Chile Trench, basement is likely continental crust. Predrilling survey data included high-resolution Parasound profiles that imaged the site to a depth of 80 mbsf (Fig. F35) and an 8-m sediment core (GeoB3313-3) that suggested continuous sedimentation at the site at rates of 100 cm/k.y. within the Holocene. The drilling strategy included multiple-APC coring to ensure complete stratigraphic coverage in a composite section.

The intent of drilling at Site 1233 was to recover a very high resolution hemipelagic record of late Quaternary sediments for paleoceanographic investigations to (1) reconstruct millennial- to century-scale changes of climate related to latitudinal shifts of the westerly wind belt, upwelling intensity, and productivity; (2) reconstruct sea-surface salinity anomalies indicative of variations in river runoff or episodes of net glacier retreat in the fjord region of southern Chile (continental climate); and (3) monitor changes in the signature of AAIW (nutrients, temperature, and salinity), which ventilates the Pacific to intermediate depths.

Operations

This was our second attempt to occupy proposed Site SEPAC-19A; our first attempt on 7 April was aborted prior to drilling because of unsuitable weather. Operations at Site 1233 began at 0945 hr on 12 April. On approach to the site, the *JOIDES Resolution* 3.5-kHz precision depth recorder documented seismic reflectors to a depth of 110 mbsf (Fig. F36). A request to drill to that depth was approved by ODP/Texas A&M University (TAMU) headquarters.

The first attempt at a mudline core (Core 202-1233A-1H) resulted in a full core barrel. The bit was raised 7 m, and APC coring in Hole 1233B was initiated with a shot from 844.0 meters below rig floor (mbrf), which obtained a good mudline and advanced to 109.5 mbsf. The vessel was offset 10 m southeast three times to core and drill Holes 1232C, 1232D, and 1232E to depths of 116.3, 112.3, and 101.5 mbsf, respectively. Optimization of coring offsets was guided by real-time correlation of magnetic susceptibility data obtained with the OSU Fast Track. A total of six downhole temperature measurements were taken at Site 1233. The transit to the next site began at 0400 hr on 14 April.

Scientific Results

Five APC holes were drilled at Site 1233 to ensure a complete stratigraphic overlap between cores from different holes (Fig. F37). Detailed comparisons between high-resolution core logging data, including records of magnetic susceptibility, GRA bulk density, natural gamma ray (NGR), and color reflectance demonstrated that the entire recovered sedimentary sequence to 116.4 mbsf (136 mcd) was recovered completely.

The magnetic susceptibility of the uppermost 9 mcd recovered at Site 1233 can be correlated directly to the ^{14}C-dated sediment record of core GeoB 3313-1, implying Holocene sedimentation rates of ~1200 m/m.y. on the mcd scale (which is about 20% more than true depths due to gas expansion and elastic rebound of the sediments after recovery). Anomalous magnetic directions and low remanence intensities over a 2-m interval between 65 and 70 mcd in Holes 1233B, 1233C, and 1233D suggest that a geomagnetic field excursion is recorded, perhaps the Laschamp Excursion (~41 ka). This preliminary evidence suggests sedimentation rates that could be as high as ~1800 m/m.y. during the pre-Holocene, which would imply an age near 70–80 ka at the base of the recovered sediment sequence. With these sedimentation rates, a diverse record of biogenic and terrigenous sediment components promises an unprecedented Southern Hemisphere record of millennial- to century-scale climate variability. Moreover, a shipboard-derived magnetic paleointensity proxy suggests that variations in geomagnetic field strength are recorded that may form the basis for synchronization of the stratigraphy at Site 1233 with other high-resolution climate records from the Northern and Southern Hemispheres.

The recovered sedimentary sequence at Site 1233 consists primarily of clay and silty clay with varying amounts of calcareous nannofossils. Interbedded minor lithologies include thin silt-rich layers, which might represent distal turbidites, and five volcanic ash layers that offer the potential to provide regional stratigraphic markers. High magnetic susceptibility values are consistent with hemipelagic sedimentation with a predominant siliciclastic component. Preliminary predictive relationships between color reflectance and carbonate and TOC, developed via a multiple linear regression (R^2 = 0.7 and 0.9, respectively), indicate substantial millennial-scale variability in these biogenic components.

High mean magnetic susceptibility values below ~10 mcd are consistent with high sedimentation rates and an increased terrigenous sediment supply during the last glacial interval. TOC contents and, to a lesser extent, calcium carbonate contents decrease from the Holocene to the glacial interval, consistent

with either significant terrigenous dilution of the biogenic components or downhole diagenesis of organic matter.

The inferred sedimentation rates of 1200–1800 m/m.y. at Site 1233 (Fig. F38) are high, even for most upper continental slope settings (which commonly have accumulation rates in the range of hundreds of m/m.y.). The southern coast of Chile is marked by high rainfall and a dense drainage system of rivers in a mountainous region, and this combination of forcing factors on sediment supply may plausibly account for high sedimentation rates in this local basin, although local focusing of the regional supply may also occur. The paucity of turbidites in the basin suggests that downslope turbidity flows are mostly channeled away from the basin in the extensive system of canyons that characterizes this portion of the Chile margin.

Mineral assemblages at Site 1233 are consistent with a siliciclastic sediment provenance in both the Andes and the Coastal Ranges. Quartz/feldspar ratios decrease downhole, and this might indicate an increase during the last glacial interval in the supply of basaltic to andesitic Andean source rocks that are rich in feldspar relative to the predominantly metamorphic source rocks of the Coastal Range that are rich in quartz.

Calcareous nannofossils, foraminifers, and diatoms are abundant and well preserved at Site 1233. The continued presence of *Emiliania huxleyi* to the bottom of Hole 1233B documents that the entire sequence is younger than 0.26 Ma. However, the *E. huxleyi* acme zone (base at 0.08 Ma) was not observed because of the generally low abundance of the species.

The planktonic foraminiferal assemblage indicates an age younger than 0.65 Ma for the entire sequence. The observed species are typical of eastern boundary settings in the transition from the subtropical to the subpolar systems. Benthic foraminiferal assemblages represent 15% to 50% of the total foraminifers and indicate an upper to middle bathyal environment with high carbon fluxes to the seafloor. The downhole benthic foraminiferal succession likely reflects changes in bottom-water oxygenation that probably relate either to fluctuations in surface water productivity and/or subsurface circulation, including AAIW.

The diatom flora is dominated by *Chaetoceros* spores, bristles and vegetative cells, and *Thalassiosira* species and reflects intermittent upwelling conditions at Site 1233. Freshwater diatoms, mainly *Aulacoseira granulata*, are present in low abundance throughout the core but appear more consistently between 58 and 97 mcd. This interval is also marked by marine benthic diatoms that suggest sediment redeposition. Silicoflagellates, radiolarians, sponge spicules, and phytoliths are observed in most samples.

NRM intensities at Site 1233 were extremely high before and after AF demagnetization at peak fields up to 25 mT. AF demagnetized inclinations averaged approximately –52°, close to the expected inclination for an axial geocentric dipole (–59°) at this site latitude (~40°S), indicating that the drill string overprint was largely removed. The negative inclinations are consistent with normal polarity, and the entire sequence is interpreted to lie within the Brunhes Chron (0–0.78 Ma). Fine-scale variations in magnetic inclination and declination are consistent from hole to hole, suggesting that a high-fidelity record of geomagnetic secular variation is recorded. Anomalous magnetic directions and low remanence intensities over a 2-m interval between 65 and 70 mcd in Holes 1233B, 1233C, and 1233D suggest that a geomagnetic field excursion is recorded. Based on estimated sedimentation rates, this could be the Laschamp Excursion (~41 ka). Normalization of the demagnetized NRM intensity by MST-derived magnetic susceptibility suggests that these sediments may provide high-resolution records of relative geomagnetic paleointensity. These extraordinary records should provide opportunities for high-resolution regional correlation of marine and terrestrial records using paleomagnetic secular variation and perhaps global correlations through paleointensity variations. Two intervals with exceptionally low remanence

intensity (95–101 and 113–118 mcd) may reflect events of extreme sediment diagenesis, suggesting that the paleomagnetic data from these two intervals should be considered with caution.

Gas, fluid, and sediment geochemical profiles are dominated by the influence of organic matter diagenesis, despite the relatively low organic carbon contents (average = 0.9 wt%; range = 0.4–2.5 wt% TOC). C/N averages 5.9, consistent with a marine origin of the organic matter. Sulfate reduction is complete by 5 mcd, with methane, apparently of biogenic origin, increasing by 20 mcd and remaining at high levels throughout. These findings are consistent with the downhole decrease in organic carbon content from ~2 wt% in the uppermost sediments to <1 wt% by 20 mcd. The zone of sulfate depletion is marked by a maximum in dissolved barium, possibly from barite dissolution. High alkalinity (peak values > 60 mM), high ammonium concentrations (up to 5 mM), and high phosphate concentrations (up to >200 mM) result from organic matter degradation by sulfate reduction and methanogenesis, similar to observations at other continental margin sites. Dissolved calcium concentrations drop rapidly, consistent with the effects of authigenic mineralization reactions driven by the high alkalinity values. Interstitial water chloride concentrations decrease by >10% over ~120 mcd, requiring some source of relatively fresh water at depth. Calcium carbonate content of the sediments averages 5.4 wt%, with a range of 1.24–10.75 wt%.

The combination of continuous recovery in a composite section to ~136 mcd, exceptionally high sedimentation rates apparently driven by input of terrigenous silt and clay in a hemipelagic setting, an extraordinary record of paleomagnetic field variations, clear geochemical signatures of organic matter diagenesis and authigenic mineralization, and a rich array of well-preserved biogenic and mineralogic tracers of paleoclimatic utility suggest that Site 1233 will provide unprecedented opportunities for understanding Southern Hemisphere and global climate changes on scales from millennia to centuries, perhaps even decades, and processes of sediment diagenesis.

Site 1234

Background

Site 1234 (proposed Site SEPAC-13B) is located ~65 km offshore (5 km off the continental shelf) and 60 km shoreward of the Peru-Chile Trench on a relatively flat bench in the middle of the continental slope at 1015 m water depth (Figs. F1, F39). Basement is likely continental crust. Precruise seismic survey data suggested mostly hemipelagic sedimentation at the site. The uppermost part of the seismic profile shows flat-lying reflectors with deformed but continuous layers farther below, possibly reflecting the original relief of the acoustic basement (Fig. F40).

This site was chosen to take advantage of the high sedimentation rates on the continental margin that will allow reconstructions of regional climate and oceanographic variability on millennial to centennial timescales for the late Quaternary. Specific goals were to

1. Assess late Quaternary history of biological production in a coastal upwelling center near Concepción, Chile, which is sensitive to regional winds, with millennial to centennial-scale resolution;
2. Assess variations in terrigenous sedimentation off central Chile to reconstruct climate variability on land;
3. Monitor changes in the boundary between oxygen-rich (nutrient poor) AAIW and oxygen-poor (nutrient-rich) PCW using tracers of paleo-oxygen and paleonutrients; and

4. Assess late Quaternary variations in paleomagnetic intensities in the southeast Pacific as a stratigraphic tool for comparison with similar data from the Northern Hemisphere.

Operations

The vessel was on station by 0650 hr on 15 April, after a 288-nmi, 26-hr transit from the previous site. Hole 1234A was initiated with the recovery of a mudline core and advanced to 100.3 mbsf with 101% recovery, which was followed by XCB coring to the target depth of 205.2 mbsf with 84% recovery. The vessel was moved 10 m to the east, and Hole 1234B was initiated with an offset to target coring gaps in Hole 1234A. Another mudline was recovered, and piston coring advanced to the APC refusal depth at 93.8 mbsf with an average recovery of 104%. The hole was deepened to 182.4 m with the XCB. The vessel was offset 10 m east of Hole 1234B to target remaining coring gaps in Hole 1234C, which was advanced to a depth of 79.1 mbsf. Prior to coring Core 202-1234B-1H, a bottom-water temperature measurement was obtained using the APC temperature tool (APCT). Downhole APCT temperature measurements were attempted with Cores 202-1234A-4H, 7H, and 10H (33.8, 62.3, and 90.8 mbsf, respectively). The vessel left location at 2300 hr on 16 April in dynamic positioning mode because the next site (proposed Site SEPAC-14A) was only 7 nmi away.

Scientific Results

We developed a composite depth section at Site 1234 (0.0–240.4 mcd) and a splice representing a complete stratigraphic section from 0 to 94.4 mcd based primarily on hole-to-hole correlation of magnetic susceptibility data. Expansion of cores because of elastic rebound and degassing after recovery caused the composite depth section to be longer than the cored interval by ~18%.

The 239-mcd-thick sequence (203.8 mbsf) of Quaternary sediments (Fig. F41) is dominated by siliciclastic components, primarily of homogeneous dark olive-gray to dark gray silty clay and clay, with subtle and gradational color changes that mainly reflect small variations in sediment composition. Eight ash layers were recovered. The clastic/biogenic ratio increases and the quartz/feldspar ratio decreases downhole, indicating increased dilution of the biogenic material with detritus from the Andean provenance downcore.

Of the biogenic components, calcareous nannofossils are the most abundant overall, with decreasing concentration downhole. Diatoms are the next most abundant group and show maximum concentration in the middle part of the section. Foraminifer abundance peaks near the top and is low through to the base of the section. Fragments of mollusk shells are common, consistent with downslope transport of material from the continental shelf. Recognizable turbidites are rare; however, a few thin silt-rich layers were found, indicating that major turbidity flows are contained in the extensive channel system that characterizes this steep continental margin.

All fossil groups indicate that the entire sequence is of Quaternary age. The nannofossils suggest that the base of the cored interval is younger than 0.26 Ma. Calcareous nannofossils are generally moderately to well preserved in the samples examined, except for the core catcher samples from the lowermost six cores where recrystallization was significant. Planktonic foraminifers are present in all samples, but abundance and preservation vary markedly. Large fluctuations in the relative abundance of both planktonic foraminiferal and nannofossil taxa indicate large changes in surface water properties through time.

Site 1234 is within the highly productive coastal upwelling area near Concepción, and diatom floras are dominated by the upwelling-related taxa. Despite the dominance of the coastal upwelling forms, warm-

water species are present in higher abundances below 62 mcd, whereas cold-water forms dominate the younger record. Benthic diatoms are present in most of the samples, indicating relatively persistent redeposition from the upper continental margin.

The benthic foraminiferal assemblage is dominated by high carbon flux indicators that are common in continental margin settings. Downhole variations may reflect shifts in bottom-water oxygenation related to either changes in deepwater circulation or changes in surface production and export of organic matter. For example, a distinct peak in the abundance of *Bolivina* spp. at ~175 to 223 mcd (>40% of total benthic foraminifers) points to an intense episode of seafloor dysoxia.

Gas, fluid, and sediment geochemical profiles are dominated by the influence of organic matter diagenesis, despite the relatively low organic carbon contents (average = 1.1 wt%; range = 0.2–3.0 wt% TOC). Sediments from Site 1234 were very gassy. Core liners were perforated after recovery to relieve the pressure and prevent excessive core expansion. High amounts of methane and low amounts of ethane indicate that the gas is biogenic in origin, resulting from in situ methanogenesis of the marine organic matter. Two intervals with high organic carbon concentrations are present at 54.5–90.2 mcd and at a depth of ~220 mcd with values up to 2.95 wt%. TOC/total nitrogen ratios range between 5 and 10, indicating a marine origin of the organic matter. This is consistent with pyrolysis results, which show that sedimentary organic matter is significantly degraded.

Calcium carbonate concentrations are low, ranging from 0.8 to 11.7 wt%, averaging 3.5 wt%, and increasing at depths >115 mcd. The good preservation of carbonate fossils in most samples indicates that the relatively low carbonate contents result mostly from dilution by siliciclastic material carried by intense river runoff rather than from dissolution and recrystallization associated with the degradation of organic matter. Sulfate reduction is complete by 9.7 mcd, with methane, apparently of biogenic origin, increasing rapidly to 9.7 mcd then remaining at high values throughout. High alkalinity (peak values > 63 mM), high ammonium concentrations (up to 11 mM), and high phosphate concentrations (up to >120 mM) result from organic matter degradation by sulfate reduction and methanogenesis, similar to observations at other continental margin sites. Dissolved calcium concentrations drop rapidly, consistent with the effects of authigenic mineralization reactions driven by the high alkalinity values. Magnesium/calcium ratios increasing to >30 from 17.9 to 40.4 mcd are consistent with authigenic precipitation of calcite in shallower sediments. Below that interval, magnesium/calcium ratios decrease with increasing depth to ~12 by 230 mcd, indicating that authigenic mineralization reactions may take up magnesium deeper in the sediments.

NRM intensities at Site 1234 were extremely high before and after AF demagnetization at peak fields up to 25 mT. AF demagnetized inclinations averaged approximately –30°, far from the expected inclination for an axial geocentric dipole (–55°) at this site latitude (~36°S), indicating that the drill string overprint was substantial. The largest apparent overprints occurred when the APCT was used, perhaps due to the extra time the sediment sat in the steel core barrel while temperature measurements were made.

In spite of these difficulties, patterns of paleosecular variation are apparent that include excursional directions in both inclination and declination in three holes from 21 to 23 mcd, which may represent the Laschamp Excursion (~41 ka). If so, average sedimentation rates in the upper 23 mcd are ~50 cm/k.y. Extrapolation of either of these estimates suggests that Site 1234 records at least two, and perhaps up to four, of the late Pleistocene glacial–interglacial cycles at very high resolution.

In summary, the combination of continuous recovery in a composite section to ~94.4 mcd, a rich assemblage of biogenic fossils and terrigenous sediment components, promise of an improved paleomagnetic record after further removal of overprints, and sedimentation rates high enough to record millennial-scale climate variability over at least one full (and perhaps several) glacial cycles makes Site

1234 a perfect complement to Site 1233. Shipboard data provide evidence for substantial variations in biogenic production and suggest that the recovered sediment sequence will provide a detailed record of climate and biogeochemical changes of the late Quaternary.

Site 1235

Background

Site 1235 (proposed Site SEPAC-14A) is located on a gently sloping terrace of the upper continental slope, ~65 km shoreward of the Peru-Chile Trench and ~60 km offshore (Figs. F1, F39). This site was chosen to take advantage of the expected high sedimentation rates to decipher the late Quaternary history of continental climate and southeast Pacific oceanography on millennial to centennial timescales at a water depth appropriate to monitor the boundary between the subsurface Gunther Undercurrent and AAIW. Predrilling surveys, including gravity cores and seismic data, provided evidence for hemipelagic sedimentation at the site. The upper part of the seismic profile documents well-stratified, flat-lying reflectors (Fig. F42). At greater depths, deformed but continuous layers of moderate reflection appear to smooth the original relief of the acoustic basement, which is likely to be continental crust.

Site 1235 is located at a water depth of 489 m, ~526 m shallower than and 10 km to the northeast of Site 1234. We expect that these two sites have been influenced by similar surface water conditions, so major differences in physical, chemical, and paleontological properties can be attributed to depth-related effects.

The primary goals of Site 1235 are to

1. Assess centennial- to millennial-scale changes of biological production through the late Quaternary in a coastal upwelling center off central Chile that is sensitive to regional winds;
2. Assess the late Quaternary history of terrigenous sedimentation off central Chile to reconstruct climate variability on land;
3. Assess variations in the boundary between oxygen-poor Gunther Undercurrent water and oxygen-rich AAIW using tracers of paleo-oxygen and paleonutrients; and
4. Monitor centennial- to millennial-scale variations in paleomagnetic intensities and field directions in the southeast Pacific during the late Quaternary as a stratigraphic tool for comparison with similar data from the Northern Hemisphere.

Operations

The vessel was offset 7.0 nmi from Site 1234 using the dynamic positioning system and with the drill string deployed to 375 m. The transit took 5.5 hr at an average speed of 1.3 kt, and the vessel was on location at 0412 hr on 17 April. Three APC holes were drilled at Site 1235 in an attempt to recover a complete stratigraphic section. Most cores contained numerous voids because of gas expansion during the retrieval process. Holes were drilled into the core liners using nonmagnetic brass drill bits to relieve some of the gas pressure before cores were processed on the catwalk. We were able to reach the maximum authorized penetration at Site 1235 using APC coring, so no XCB coring was attempted. Two bottom-water and six downhole temperature measurements were taken with the APCT in Holes 1235A and 1235B.

A nonmagnetic core barrel, cutting shoe, and flapper valve were deployed here for the first time during Leg 202 (Cores 202-1235C-3H, 5H, 7H, 9H, and 11H) after excessive magnetic overprint was discovered in

cores recovered with standard tools. Cores retrieved with the nonmagnetic barrel had substantially less overprint than those retrieved in the regular steel barrels.

Scientific Results

At Site 1235 we recovered a 215-m-thick hemipelagic sequence of rapidly accumulated upper Pleistocene to Holocene silty clay (Fig. F43). The planktonic foraminiferal assemblage is typical of the late Pleistocene Subzone Pt1b, and the continued presence of the calcareous nannofossil species *E. huxleyi* to the bottom of Hole 1235A documents that the entire sequence is younger than 0.26 Ma (Zone NN21). Sedimentation rates are at least 80 cm/k.y. This allows us to provide materials for reconstruction of Pleistocene and Holocene climate and oceanography with millennial- to centennial-scale resolution and accomplishes one of our primary objectives at this site.

Three APC holes were drilled to ensure a complete recovery of the stratigraphic section. A composite section was constructed on the basis of high-resolution core logging data, and complete recovery was most likely achieved to ~171.45 mcd. Significant ship heave during drilling combined with gas expansion of the sediment after recovery made correlation between holes difficult. For example, precise splicing between holes was problematic in three intervals at ~45–49, 71–73, and 126–128 mcd, and as a result a formal splice was not constructed.

The hemipelagic sequence at Site 1235 is composed primarily of siliciclastic silty clay with little lithologic variability. The silt fraction is dominated by feldspars, with lesser amounts of quartz, pyroxenes, and volcanic glass. These mineral assemblages are consistent with a siliciclastic sediment provenance in both the Andes and the Coastal Range. The large supply of siliciclastic sediment onto the upper continental margin of central Chile mainly results from rivers that drain the mountainous regions of the Andes and the Coastal Range.

Calcareous nannofossils, diatoms, and foraminifers vary from rare to abundant, and the species present are typical of an active upwelling zone on a continental margin. Microfossil preservation is good in the upper section and deteriorates downhole. Reworked benthic diatoms are found frequently. The ubiquitous presence of burrows and benthic faunal assemblages does not reveal any episodes of bottom-water anoxia. As at Site 1234, the benthic foraminiferal assemblage is dominated by species associated with high carbon fluxes in an oxygen minimum zone environment. Marked changes in the relative proportions of benthic foraminiferal species indicate variations in oxygenation or carbon fluxes at the seafloor that are probably related to temporal and spatial fluctuations of the upwelling system and/or shifts in subsurface water masses. A distinct peak in the abundance of *Bolivina* (>40% of total benthic foraminifers) between 78 and 118 mcd points to an intense episode of seafloor dysoxia. This interval comprises a narrower interval (~90–102 mcd) of distinctly decreased magnetic susceptibility and a* values (Fig. F44).

Sediment from Site 1235 contained abundant methane. Low amounts of ethane indicate that the gas is biogenic in origin, resulting from in situ methanogenesis of marine organic matter (TOC/total nitrogen ratios = 5–9). TOC contents are low throughout the core, averaging 0.6 wt% and ranging from 0.4 to 1.5 wt%. Calcium carbonate concentrations average 2.4 wt% and range from 0.3–15.5 wt%. The low organic carbon and carbonate contents relative to other continental margin settings indicate dilution with siliciclastic material. Organic matter degradation and carbonate dissolution also contribute to the observed variations of these components.

Authigenic pyrite and carbonate are present, especially in deeper intervals. Conspicuous carbonate concretions are intermittently present downhole. Intervals of abundant authigenic carbonate underlie zones of intense burrowing in at least three repetitive sequences. Color reflectance data document the

presence of hematite and goethite (corresponding to positive a* values) near the top of these sequences, in each case overlying green sediments (negative a* values). Such systematic variations in mineralogy and color may indicate zones of strong redox contrast, perhaps related to major changes in sedimentation rate, productivity, and organic rain, or bottom-water oxygen content.

Sulfate reduction is complete at Site 1235 by 19.7 mcd. At this depth, the methane concentration increases rapidly to 55,648 ppmv and remains elevated at all greater depths. High alkalinity (peak values > 60 mM), ammonium (>8 mM), and phosphate (>200 mM) concentrations in interstitial waters result from organic matter degradation associated with sulfate reduction and methanogenesis. Dissolved calcium concentrations drop rapidly with depth to values <2 mM, consistent with the effects of authigenic carbonate mineralization driven by the high alkalinity. Magnesium/calcium ratios reach a high value of 41 at 53.6 mcd, consistent with precipitation of authigenic calcite in shallower sediments, but decrease to values as low as 2.4 at 210.3 mcd, indicating dolomite formation in deeper sediments. Calcium, strontium, and boron all increase significantly at depths >140 mcd, implying a source of these elements at depth.

Pore water chlorinity at Site 1235 decreases by >12%, from 553 mM at 1.5 mcd to 483 mM by 210.3 mcd. This change is accompanied by even larger decreases in salinity and sodium concentration. The decrease in chlorinity with depth at Site 1235, similar to that of Site 1233, is more extreme than those observed at the midslope sites on the Peru margin drilled during Leg 112 and indicates the presence of methane hydrates that dissociated either within subsurface sediments or after recovery.

Initial NRM intensities were extremely high, ranging from 0.5 to 2.1 A/m, and were characterized by steep positive inclinations (averaging ±79°) associated with a drill string magnetic overprint. AF demagnetization at peak fields up to 25 mT only partially reduced this overprint. To mitigate these analytical artifacts, a nonmagnetic core barrel, cutting shoe, and flapper valve were alternated with a standard steel core barrel for every other core of Hole 1235C. The nonmagnetic core barrel substantially reduced the viscous magnetic overprint and therefore may prove to be of significant benefit for future paleomagnetic studies in sediment of this type. Paleomagnetic secular variation features may be preserved at Site 1235 within the declination record, and this may provide a means of detailed correlation with Sites 1233 and 1234.

Site 1235 has clearly met our shipboard objectives of providing rapidly accumulating sediment for the study of century- to millennial-scale changes of climate, biogeochemistry, oceanography of surface and subsurface water masses, and paleomagnetic variations. Preliminary data on the fossil biota, geochemical composition of interstitial water and sediment, and terrigenous sediment components lead us to anticipate a rich paleoceanographic and paleoclimatic record, as long as stratigraphic challenges associated with recovery of gassy cores can be overcome.

Site 1236

Background

Site 1236 (proposed Site NAZCA-10A) is located atop Nazca Ridge, a fossil hotspot track with its modern expression at Easter Island (Fig. F1). Based upon a fixed hotspot model and on magnetic anomalies of the surrounding oceanic crust, basement ages are expected to be 30–35 Ma. The ~20-km-wide plateau occupied by Site 1236 is punctuated by small volcanic spires a few hundred meters high that represent eroded remnants of an archipelago of volcanic islands. The plateau and smaller seamounts formed as the site moved eastward over the hotspot. This anomalously shallow section of Nazca Ridge occurs where the

Nazca Fracture Zone, a zone of crustal weakness, intersects the hotspot track. About 20 km to the southwest of Site 1236, a flat-topped guyot, which is presumably younger than the plateau surface, rises to within 350 m of present sea level. The existence of this relatively well preserved shallow bathymetric feature adjacent to the deeper, more eroded plateau surface suggests multiple episodes of volcanism in the region.

A tectonic backtrack path on the Nazca plate moved Site 1236 ~20° westward toward the center of the subtropical gyre by 30 Ma (Fig. F45). Thermal subsidence would predict that the site was at shallower water depths during the early Miocene and perhaps above sea level very early in its history.

The total thickness of sediment at Site 1236 is ~200 m. Seismic data reveal a well-stratified pelagic sequence with strong to moderately reflective layers from the sediment surface to ~120 mbsf (Fig. F46). At depths from ~120 to ~200 mbsf, deformed but almost continuous layers of moderate reflection appear to smooth the relief of the acoustic basement.

Today, Site 1236 is situated near the western edge of the northward-flowing Peru-Chile Current in an oligotrophic region of the subtropical gyre and at depths suitable for monitoring intermediate-water chemistry in the open ocean. Given its tectonic backtrack to the west, toward the center of the gyre, we expected relatively low biogenic sedimentation rates (<10 m/m.y.) and minor amounts of terrigenous sediment, except for volcanics and possible shallow-water sediment early in its history.

The primary objectives at Site 1236 are to provide a continuous sequence of Neogene and Quaternary sediments to

1. Improve on regional Neogene timescales by combining magnetostratigraphy, biostratigraphy, and isotopic stratigraphy in a region midway between the tropical and high-latitude systems;
2. Assess climate changes of the southern subtropical Pacific, focusing on major intervals of changing climate (e.g., the early Miocene intensification of Antarctic glaciation [~24 Ma], the middle Miocene climatic optimum [14–15 Ma], the glaciation of the East Antarctic ice sheet [~13 Ma], and the mid-Pliocene intensification of the Northern Hemisphere glaciation [3.1–2.6 Ma]);
3. Examine the late Miocene to early Pliocene reorganization in South Pacific surface and intermediate-water circulation in response to the closure of the Isthmus of Panama (10–4 Ma); and
4. Reconstruct changes in the boundary between the Pacific Deep Water and AAIW on orbital and tectonic timescales.

Operations

Three APC holes were cored at Site 1236, to a maximum depth of 173.1 mbsf (189.7 mcd) in Hole 1236A. Hole 1236A was advanced with the XCB to a total depth of 207.7 mbsf (223.2 mcd), where basement was reached. Hole 1236B was piston cored to 122.8 mbsf, where mechanical problems were encountered and a pipe trip was required to recover a broken float-valve system. In Hole 1236C, 13 more APC cores were recovered (to a refusal depth of 167.3 mbsf) to span coring gaps that remained from the previous two holes. A total of six downhole and one bottom-water temperature measurements indicated a normal thermal gradient for sediment overlying oceanic crust (38°C/km). Cores were oriented starting with either the third or fourth APC core in each hole. The nonmagnetic core barrel assembly was deployed on every other core in each APC-cored interval, in even-numbered Cores 202-1236A, 2H to 20H; odd-numbered Cores 202-1236B-1H to 13H; and even-numbered Cores 202-1236C-2H to 18H.

Scientific Results

A 223.2-m-thick sedimentary sequence at Site 1236 spans the entire Neogene and the late Oligocene to ~28 Ma (Fig. F47). A composite section was constructed on the basis of high-resolution core logging data (reflectance and magnetic susceptibility), and complete recovery was documented to ~129.7 m (~17–18 Ma). Color reflectance (a*) was the most useful stratigraphic tool for correlation at this site.

Pelagic sedimentation is prevalent at Site 1236, but the impact of volcanic evolution of Nazca Ridge during the late Oligocene is also clearly represented. An early interval of pelagic sedimentation at relatively shallow water depths (hundreds of meters) probably indicates subsidence of the young volcanic plateau prior to 28 Ma. Glassy volcaniclastic sediment, likely air fall ash, suggests a late stage of volcanic activity near 28 Ma. Nevertheless, we cannot exclude the possibility that the volcanic layers may originate from the erosion of older topographic highs. Well-preserved guyots near Site 1236 rising nearly a kilometer above the main plateau of Nazca Ridge may also represent the remnants of an active volcanic phase that followed primary ridge construction. Shipboard stratigraphy suggests an age of this volcanic interval coeval with the well-known tectonic reorganization that created the Nazca plate ~28 m.y. ago. Volcanic sediments were deposited at the earliest stage, and nonpelagic calcareous (carbonate platform) materials were transported to Site 1236 until the middle Miocene (~17 Ma).

Pelagic sediments at Site 1236 are dominated by calcium carbonate, with an average of 95 wt%. Some isolated minima in weight percent $CaCO_3$ correspond to discrete volcanic ash layers and zones of slightly increased siliciclastic contents. The lowest $CaCO_3$ contents are visible at the base of the record where the sediments contain a significant siliciclastic and volcaniclastic component in addition to authigenic glauconite.

Four major lithologic units are defined at Site 1236. Unit I corresponds to the last 17 m.y. and contains primarily pelagic nannofossil ooze. Two isolated layers at depths of ~65 and ~98 mcd consist dominantly of containing neritic grains and represent a waning supply of gravity flows from a nearby carbonate platform to Site 1236 in the late Miocene. A minor siliciclastic fraction corresponding to increased magnetic susceptibilities in the uppermost ~40 mcd may represent eolian material transported from South America during the Pleistocene and Pliocene. Presence of goethite and hematite, detected via reflectance spectrometry, also suggests that an eolian component, originating probably on the South American continent, reached the site via the southeast trade winds.

Unit II (~17 to ~24 Ma) consists mainly of carbonates characterized by high GRA bulk density and reflectance (L* lightness) as well as low magnetic susceptibility. These sediments are comprised primarily of nannofossil ooze (Subunit IIB) and unlithified calcareous mudstone (Subunit IIB), consistent with the presence of a pelagic sedimentary environment at Site 1236 since the late Oligocene. Frequent intercalation of well-sorted nonpelagic calcareous sediments (neritic grains and micrite), which sometimes fine upward, points to gravity current supply of detritus from nearby carbonate platforms. Micrite, which becomes dominant in Subunit IIB, reflects in situ recrystallization of nannofossils.

Allochthonous coarse-grained calcareous sediments in Unit III, including recrystallized larger benthic foraminifers, bryozoan fragments, and some remains and encrustations of red algae, indicate proximity to a carbonate platform. The presence of glauconite within Unit III sediments is consistent with a shallow-water environment below the storm wave base. Volcaniclastic constituents with relatively high magnetic susceptibility are present through the late Oligocene, suggesting proximity to volcanic islands at this time.

Unit IV is a fine-grained chalk with abundant nannofossils and foraminifers overlying basalt (inferred basement), with no evidence for input of nonpelagic material. We infer, based on the presence of

authigenic glauconite, a relatively shallow open-ocean environment, on the order of hundreds of meters below sea level.

Calcareous nannofossil and planktonic foraminifer biostratigraphies indicate that the upper Pleistocene to upper Oligocene succession is essentially complete. Calcareous nannofossils are generally abundant and are moderately to well preserved throughout the interval. Some of the standard nannofossil datums are missing, but alternative events were used to reconstruct the biostratigraphic succession.

Planktonic foraminifers are common to abundant down to ~150 mcd (19–20 Ma). Below this depth, foraminiferal abundance decreases and preservation deteriorates markedly. Benthic foraminiferal assemblages document an oligotrophic, pelagic environment from Pliocene to middle Miocene time. Older intervals of the lower Miocene and upper Oligocene contain higher numbers of buliminids and nodosariids, reflecting shallower water depth and proximity to the oxygen minimum zone. The presence of poorly preserved larger benthic foraminifers, which have modern equivalents that host algal endosymbionts, indicates redeposition from a nearby carbonate platform during the Oligocene and early Miocene.

Diatoms are only found close to the two ash layers and indicate either increased diatom production near the time of ash deposition or anomalous preservation as a result of the presence of ash. A typical low-latitude diatom assemblage with an age of between 13.5 and 12.5 Ma is present at 82.3 mcd. The presence of benthic and neritic diatoms at 82.3 and 206.7 mcd indicates redeposition from shallow-water environments.

Interstitial water chemistry at Site 1236 is consistent with low input of organic matter in an oligotrophic setting. Diagenesis of opal and calcite is minimal, as reflected in silicate, calcium, and magnesium measurements of interstitial waters. Sulfate concentrations are high, >23 mM. Alkalinity, phosphate, and ammonium concentrations are all low. Methane is <2 ppmv, near the detection limit, and organic carbon content is <0.2 wt%. Interstitial water geochemistry varies little with lithologic unit except in the deepest sedimentary unit overlying presumed basement, where alkalinity, silicate, and boron decrease and manganese increases.

The NRM intensities are similar to the magnetic susceptibility profiles and reflect the major lithologic changes at Site 1236. Prior to demagnetization, inclinations are steeply positive, characteristic of a drill string–induced magnetic overprint. Much of the overprint is removed after demagnetization at either 20 or 25 mT, with a clearer polarity record in cores taken with the nonmagnetic core barrel. A preliminary magnetostratigraphy was established for the last 13 m.y. that can be correlated to the geomagnetic polarity timescale, significantly augmenting the biostratigraphy and providing a well-constrained chronology.

A long history of oligotrophic conditions with little input of nonbiogenic sediments at Site 1236 has resulted in low sedimentation rates averaging <10 m/m.y. Winnowing processes may have contributed to the overall low sedimentation rates on this bathymetric rise. Sedimentation rates of ~5 m/m.y. are typical for the middle and late Miocene (~15 to ~6.5 Ma) and for the last ~4 m.y. Higher rates of 10–15 m/m.y. occur from ~6.5 to ~4 Ma and from ~25 to 17 Ma. The late Oligocene and early Miocene maxima in sedimentation rates reflect the influence of nearby carbonate platforms and/or islands, which supplied significant amounts of siliciclastic, volcanic, and nonpelagic calcareous material until ~17 Ma. The late Miocene to early Pliocene peak in sedimentation rates from ~6.5 to ~4 Ma, however, is controlled by changes in pelagic sedimentation. Given no detectable changes in fossil preservation in this interval, high sedimentation rates likely reflect an interval of increased productivity. A similar interval of rapid accumulation was found at Sites 846–850 in the equatorial Pacific (3°S–1°N, 90°–115°W) and is often referred to as the late Miocene to early Pliocene biogenic bloom. All of the sites that contain this bloom

event are influenced by either the Peru-Chile Current or its westward extension into the South Equatorial Current, suggesting that the source of the bloom is in the Southern Hemisphere. The ultimate cause of this extraordinary event, which has been hypothesized to relate to the closure history of the Isthmus of Panama and/or changes in deep-sea circulation, remains a question for postcruise research.

Site 1236 has clearly met our shipboard objectives of providing an essentially complete Neogene to Quaternary sequence relatively unmodified by burial diagenesis and recovered with the APC. The tight framework of biostratigraphic and magnetostratigraphic age controls together with a good preservation of calcareous microfossils extending to the late Oligocene will provide a solid base for detailed studies that aim to reconstruct the long-term history of sea-surface and intermediate-water characteristics in the southeast Pacific.

Site 1237

Background

Site 1237 (proposed Site NAZCA-17A) is located on a relatively flat bench on the easternmost flank of Nazca Ridge, ~140 km off the coast of Peru (Fig. F1). Nazca Ridge, a fossil hotspot track with its modern expression at Easter Island, terminates just outboard of the Peru-Chile Trench, where it is deformed and subducted beneath Peru. Eastern Nazca Ridge is covered by a thick drape of pelagic sediment to its shallowest reaches. The seismic record reveals well-stratified reflective layers, which clearly drape the underlying bathymetry from the sediment surface to acoustic basement (Fig. F48). Prior to drilling, basement ages were expected to be between 40 and 45 Ma, based upon a hotspot model and magnetic anomalies of the surrounding oceanic crust. The oldest material recovered at the site was ~31.5 Ma.

The tectonic backtrack path on the Nazca plate has moved Site 1237 about 20° westward and 7° southward relative to South America over the past 32 m.y. (Fig. F45). Considering the thermal subsidence over this time span, the site may have been within a few hundred meters of sea level in its early history.

Today, Site 1237 is situated near the eastern edge of the northward-flowing Peru-Chile Current, a major conduit of cool-water transport from high to low latitudes. The site's position near the productive upwelling system of Peru suggests that it may record changes in upwelling and biological production during the past few million years. The site underlies the path of eolian dust that originates in the Atacama Desert of Chile, as indicated by the spatial quartz distribution in the southeast Pacific that reflects the pattern of the southeast trade winds. Given the tectonic backtrack to the west toward the center of the oligotrophic gyre and assuming that there were no compensating changes in the environment, we expect that accumulation rates of both biogenic and eolian sediments at Site 1237 were smaller in the past and increased with time.

The modern water depth of Site 1237 reflects the transition zone between the relatively oxygen-rich (nutrient poor) remnants of CPDW, which enter the Peru Basin as bottom water through the Peru-Chile Trench, and the relatively oxygen-poor (nutrient rich) PCW. During its early history, the site may have occupied depths of the modern PCW or its paleoequivalent.

The primary objective at Site 1237 was to provide a continuous and complete sedimentary sequence of the late Cenozoic to

1. Improve on regional chronological frameworks by combining magnetostratigraphy, biostratigraphy, isotopic stratigraphy, and orbital tuning methods;

2. Assess climate and biogeochemical changes of the southern subtropical Pacific, focusing on major intervals of changing global climate, such as the early Miocene intensification of Antarctic glaciation near 24 Ma, the middle Miocene climatic optimum near 14–15 Ma, the glaciation of the East Antarctic ice sheet near 13 Ma, the mid-Pliocene intensification of Northern Hemisphere glaciation from 3.1 to 2.6 Ma, and the transition (~0.9 Ma) from early Pleistocene climate cycles dominated by ~41-k.y. rhythms to those of the late Pleistocene that are dominated by ~100-k.y. rhythms;

3. Examine the impact of tectonic events on regional climate, productivity, biogeochemical cycles, and ocean circulation, including the opening of Drake Passage near 25 Ma, the major uplift of the Andes within the past 15 m.y., and the closure of the Isthmus of Panama from 10 to 4 Ma; and

4. Reconstruct changes in the boundary between PCW and CPDW on orbital and tectonic timescales.

Operations

The 432-nmi voyage from Site 1236 to Site 1237 was accomplished in 39.0 hr at an average speed of 11.1 kt. At 0340 hr on 26 April, the vessel left Chilean waters and entered the territorial waters of Peru.

Four APC holes were drilled. While drilling, permission was granted from ODP/TAMU headquarters to deepen the hole by APC coring as much as 30 m beyond the approved maximum depth of 300 m. Hole 1237A recovered a full core barrel, but the mudline was not recovered, and so the hole was terminated. Hole 1237B recovered the mudline, and piston coring advanced until the wireline parted at the rope socket while attempting to recover Core 202-1237B-13H (110.0–119.5 mbsf). Two extra wireline trips were required to recover the Tensor tool, sinker bars, and barrel containing Core 202-1237B-13H, respectively. APC coring resumed and deepened the hole to refusal at 317.4 mbsf (Core 202-1237B-34H). This represented the deepest penetration with the APC since Leg 162. To our knowledge, only four other piston-cored holes in ODP have exceeded a penetration of 300 m.

The vessel moved 10 m west before Hole 1237C was initiated. The hole was deepened to 315.3 mbsf, where Core 202-1237C-33H failed to achieve a full stroke. After the vessel moved 10 m west, Hole 1237D was initiated with the objective to spot core four intervals to cover coring gaps left in the previous holes.

Cores were oriented starting with the third core in each hole. A total of 15 core barrels in Hole 1237B and 16 core barrels in Hole 1237C were drilled over when a force of 60 kilopounds could not retrieve the cores. The nonmagnetic core barrel was deployed on even-numbered cores up to and including 202-1237B-20H, on odd-numbered cores up to and including 202-1237C-17H, and on Cores 202-1237D-2H, 4H, 6H, and 8H. The nonmagnetic core barrel was not used below these intervals to prevent possible damage to hardware as a consequence of the drilling-over process. One bottom-water and nine sediment temperature measurements were taken with the APCT in Holes 1237B and 1237C, which indicated a thermal gradient of ~33°C/km.

Scientific Results

The 360.65-mcd-thick pelagic sequence recovered at this site spans the interval from the early Oligocene to the Holocene (0 to ~31.5 Ma) without any detectable stratigraphic breaks (Fig. F49). The composite depth section documents complete recovery for the entire sequence. The hole-to-hole correlation was based on high-resolution core logging data, including magnetic susceptibility, reflectance, natural gamma radiation, and GRA bulk density.

The upper 100 mcd of the sequence reflects pelagic sedimentation with a minor terrigenous (probably eolian) component that decreases downhole. Such a gradual trend, likely a consequence of tectonic drift

of the oceanic plate toward the continent, is recorded by a gradual transition from nannofossil-bearing (silty) clay to nannofossil ooze. At greater depths, the sedimentary sequence is dominated by nannofossil ooze. In the interval >150 mcd, calcium carbonate contents are high (>90 wt%), organic carbon values are low (< 0.3 wt%), and sedimentation rates are ~10 m/m.y., typical for oligotrophic settings far from the continents. Micrite increases at depths >148 mcd.

A marked color change from more greenish younger sediment to reddish older sediment containing goethite and hematite is present at ~164 mcd (~9 Ma) (Fig. F50). This oxide component is carried in eolian dust transported to the site via the southeast trade winds from arid regions of South America. The abrupt green to red color change at ~9 Ma appears to result from diagenetic reduction processes rather than a change in the dust source area because the reddish color signal persists into the Pleistocene section at Site 1236, located ~500 km southwest of Site 1237. At ages of <8 Ma, both siliciclastic and biogenic accumulation rates increase at Site 1237, suggesting that eastward drift continues to enhance the eolian dust component, even though the reddish color is gone.

At approximately the same time as the color change, discrete ash layers and dispersed ash begin to appear in the sediment. Fifty-five ash layers were deposited during the last 9 m.y. This transition near 9 Ma may record the onset of intense volcanism and accompanying tectonic uplift of the Andes. If so, the topographic barrier of an early mountain range would have enhanced the steering of westerly and trade winds along the coast, resulting in stronger meridional flow, enhanced eolian transport, coastal upwelling, and biogenic productivity within the eastern boundary current.

The enhanced rain of organic carbon that follows from high productivity would also support the hypothesis of a diagenetic boundary that reduced the reddish oxides. High production continued and expanded into a Miocene to early Pliocene biogenic bloom (~8 to ~4 Ma). A similar but shorter interval of rapid accumulation was found at Site 1236, as well as in the equatorial Pacific (6.7–4.5 Ma). A variety of previous hypotheses have linked the rise and fall of this event to changes in global nutrients associated with erosion and chemical weathering of the rising Tibetan Plateau, reorganizations in deep ocean circulation, and closure of the Isthmus of Panama. Although we are not yet able to identify a unique cause of the biogenic bloom, our shipboard results help to pose new hypotheses by tracing the event into the eastern boundary current of the southeast Pacific and by providing detailed chronological controls based on biostratigraphy and magnetostratigraphy that reveal structure in the bloom event and suggest an early onset in the South Pacific.

Carbonate concentrations decrease from ~90 to ~10 wt% in the interval <4.5 Ma, and Neogene carbonate accumulation rates at Site 1237 reach their lowest level during the last 2 m.y. (0–41 mcd). The Pliocene–Pleistocene interval contains significant amounts of both terrigenous material and siliceous microfossils with various contributions from calcareous microfossils. Siliciclastic accumulation rates increased again at ~3 Ma and may reflect an enhanced eolian supply to Site 1237. This increase was apparently paralleled by the intensification of the Northern Hemisphere glaciation, which was associated with enhanced subtropical aridification and intensified trade wind circulation, partly due to a steeper pole-to-equator temperature gradient.

Calcareous nannofossil and planktonic foraminifer biostratigraphies indicate that a complete upper Pleistocene to upper Oligocene succession was recovered. Most of the standard nannofossil and planktonic foraminiferal zonal markers as well as some nonstandard nannofossil markers can be used to reconstruct the biostratigraphic succession. Calcareous nannofossils at the base of the hole suggest an age younger than 31.5 Ma. Diatoms provide additional biostratigraphic control down to ~136.7 mcd.

Calcareous nannofossils and foraminifers are generally abundant or common and well to moderately well preserved throughout. Diatoms are abundant and well preserved down to ~60 mcd, but abundance decreases and preservation deteriorates below ~69 mcd and diatoms are absent below ~174 mcd.

Marked changes in the relative proportions of benthic foraminiferal species within the Pleistocene–upper Pliocene assemblage indicate variations in carbon fluxes at the seafloor that are probably related to temporal and spatial fluctuations of the coastal upwelling system and/or shifts in subsurface water masses. In contrast, the lower Pliocene to upper Oligocene benthic foraminiferal assemblage characterizes an oligotrophic, pelagic environment. The diatom assemblage down to 59 mcd is typical of a coastal upwelling zone on a continental margin. Below this depth, typical upwelling forms are present only occasionally with some oceanic forms.

The paleomagnetic stratigraphy at Site 1237 is excellent, with clear definitions of all chrons and subchrons over the last 5 m.y. and from 7 to 13 Ma. Even fine-scale features and short polarity subchrons are hinted at, like the "Cobb Mountain" within the Matuyama Chron. The polarity assignments for the interval from 5 to 7 Ma and for the lowermost part of the sequence between 13 and 31 Ma are still preliminary because the polarity sequence allows several possible interpretations. The age interpretations are consistent with the biostratigraphy where clear geomagnetic correlation to the geomagnetic polarity timescale is observed. This site offers an excellent potential to derive an orbitally tuned timescale that can be tied to the magnetostratigraphy and biostratigraphy to provide a reference section for the South Pacific.

Chemical gradients in the uppermost sediments reflect a minor influence of organic matter diagenesis, a limited degree of biogenic opal dissolution, and a minor signature of biogenic calcite diagenesis. Organic matter diagenesis, driven by microbially mediated oxidation reactions, has a relatively minor influence on interstitial water composition. Sulfate undergoes a limited degree of reduction, primarily in the uppermost sediments, by no more than 4 mM from typical seawater values of ~29 mM. Alkalinity has a shallow maximum of >5 mM and declines with depth to ~2.2 mM. Phosphate concentrations are ~9 µM in the shallowest sediments and decline to <2 µM. Ammonium concentrations have peak values of >250 µM. The shallow and relatively minor maxima in alkalinity, phosphate, and ammonium, along with minor sulfate reduction, result from degradation of organic matter in the upper ~70 mcd. Dissolved silicate concentrations have highest values in the depth range where diatoms are reported to have the best preservation and abundance, averaging ~800 µM in the upper ~70 mcd and declining to an average of 325 µM in the deeper interval barren of diatoms. Authigenic mineral precipitation reactions have a limited influence on interstitial water geochemistry at this site, with no indications of calcite precipitation or dolomite formation in the calcium and magnesium profiles. Strontium concentrations increase to a maximum of >200 µM, with the profile similar in character, although with a smaller maximum value, to those in calcium carbonate rich equatorial sites driven by biogenic calcite recrystallization.

Site 1237 clearly surpassed our shipboard objectives by providing a complete upper Paleogene to Neogene sequence relatively unmodified by burial diagenesis and fully recovered with the APC. Good preservation of calcareous microfossils extending to the base of the Oligocene and the tight framework of biostratigraphic and magnetostratigraphic age controls will provide an excellent base for a broad spectrum of detailed studies that aim to reconstruct the long-term history of Andean uplift and continental climate as well as the evolution of upwelling, biota, biogeochemistry, and sea-surface and intermediate-water characteristics in the southeast Pacific.

Site 1238

Background

Site 1238 (proposed Site CAR-2C) is located ~200 km off the coast of Ecuador, on the southern flank of the Carnegie Ridge (Fig. F1). The region is draped with pelagic sediment ~400–500 m thick on a bench that slopes gently to the south (Fig. F51). Sediments consist mainly of diatom nannofossil ooze and nannofossil diatom ooze.

Basement at Site 1238 likely consists of basalt formed at the Galapagos hotspot at ~11–13 Ma. A tectonic backtrack path on the Nazca plate moved Site 1238 about 600 km westward and slightly to the south relative to South America, probably to shallower water depths by 12 Ma (Fig. F52).

Today, Site 1238 is situated under the eastern reaches of the equatorial cool tongue in an open-ocean upwelling system near the equator (Fig. F52). The nutrient-rich Equatorial Undercurrent (EUC) supplies waters that upwell here and along the coasts of Peru and Ecuador, driving high primary productivity. Sediments at the site are likely to record changes in upwelling and biological production, as well as long-term changes in upper ocean temperature and pycnocline depth. The modern water depth is appropriate to monitor the PCW south of Carnegie Ridge, roughly at the sill depth of Panama Basin.

The primary objectives at Site 1238 were to provide a continuous sedimentary sequence of Neogene age to

1. Assess the history of near-surface water masses, including the eastern reaches of the equatorial cold tongue;
2. Assess changes in biogeochemistry and biota that are linked to variations in nutrients, productivity, and fluxes of organic matter and biogenic sediments to the seafloor;
3. Monitor temporal and vertical fluctuations of PCW; and
4. Monitor changes in the occurrence and frequency of volcanic ashes that might be associated with active tectonic phases of the northern Andes.

Operations

After leaving Peruvian waters, the vessel proceeded to a rendezvous point in the Gulf of Guayaquil, Ecuador (south of Salinas; 2.5°S, 81.0°W), to pick up an Ecuadorian observer and an ODP engineer and to drop off a Peruvian observer. The 889-nmi transit required 77.5 hr at an average speed of 11.5 kt. After the helicopter transfer of personnel at 0946 hr, the *JOIDES Resolution* proceeded to proposed Site CAR-2C. The 114-nmi transit required 9.5 hr at an average speed of 12.0 kt.

Three holes offset from each other by 10 m were completed at Site 1238. Hole 1238A was cored with the APC to 204.5 mbsf (Core 202-1238A-22H), followed by the XCB from 204.5 mbsf to refusal at 430.6 mbsf (Core 202-1238A-46X). Hole 1238B was APC cored to 201.0 mbsf, and Hole 1238C was APC cored to 162.5 mbsf to ensure the recovery of a complete stratigraphic section.

Hole 1238A was flushed and displaced with sepiolite mud and then logged with the bit at 99.4 mbsf, first using the triple combination (triple combo) tool string with the Lamont-Doherty Earth Observatory (LDEO) Multisensor Gamma Ray Tool (MGT) on top and then by the FMS-sonic tool string. One pass with the triple combo was conducted from 429 mbsf (total depth) to the mudline, followed by one full pass from 430 mbsf to the bit and one pass from 167 mbsf to the seafloor with the MGT. The two subsequent passes with the FMS-sonic tool string also reached the bottom of the hole. Hole conditions were unusually smooth, and the hole diameter ranged in size from 11.5 to 14.5 in (29–37 cm). The accelerometer (General

Purpose Inclinometer Tool) logs showed increasing deviation vertically in the hole below 170 mbsf, reaching 6.5° at the base.

Cores were oriented starting with the third (Holes 1238A and 1238B) or the fourth (Hole 1238C) core in each hole. The nonmagnetic core barrel was deployed on even-numbered cores to Cores 202-1238A-12H and 202-1238C-14H and on odd-numbered cores to Core 202-1238B-11H. Five downhole temperature measurements were taken with the APCT, yielding a temperature gradient of ~12.5°C/100 m.

Scientific Results

A 424.75-m-thick (467.3 mcd) sediment sequence dating back to the middle Miocene (~11 Ma) was recovered from three holes at Site 1238 (Fig. F53). Correlation of magnetic susceptibility and other core logging data between holes documented complete recovery of the section cored with the APC to a depth of 225.4 mcd. A composite section and a spliced record were constructed over this interval. XCB cores from Hole 1238A were appended onto the mcd scale, using a 10% growth rate of mcd relative to mbsf.

The dominant lithologies at Site 1238, nannofossil diatom ooze and diatom nannofossil ooze, reflect primarily biogenic sedimentation in a moderate- to high-productivity pelagic setting. The sediment sequence is characterized by meter-scale alternations of pale olive nannofossil-rich and dark olive diatom-rich intervals, also reflected by variations in core logging properties such as L*, GRA density, magnetic susceptibility, and NGR. Given average sedimentation rates of ~5 cm/k.y., this lithologic banding falls into the frequency range typical of Earth's orbital cycles (Fig. F54). Although shipboard chronologies are not sufficiently detailed to identify specific cycles unambiguously, these observations indicate the likelihood that the site is sensitive to orbital-scale climate changes that are in turn reflected in the major lithologies.

One lithologic unit, divided into two subunits, was defined at Site 1238. Subunit IA spans the upper 403 mcd of the sequence and contains bioturbated nannofossil ooze, diatom nannofossil ooze, and nannofossil diatom ooze with varying abundance of clay and foraminifers. Variability in magnetic susceptibility decreases gradually from 0 to 100 mcd, perhaps in concert with the known reduction in the amplitude of glacial–interglacial climate oscillations in the early Pleistocene.

The Pliocene to Miocene interval from ~1.8 to 7 Ma is marked by relatively high productivity, as indicated by high concentrations of diatoms, organic carbon, and organic pigments in the sediment, along with high sediment mass accumulation rates. The end of this biogenic bloom (~1.8–2.0 Ma) is associated with an increase in biosiliceous microfossils, organic carbon contents, and minima in bulk density and carbonate concentrations. This change was possibly associated with a change in nutrients or upwelling conditions that favored biosiliceous productivity. Several ash layers are present within the upper ~300 m of Subunit IA, including the regionally correlative ash layer L (~230 ka). Increases in the frequency of ash layers at ~5 Ma and during the past 3 m.y. may represent phases of intensified volcanism in the northern Andes.

Subunit IB occupies the base of the sequence (~400–467 mcd) and is characterized by partially lithified diatom and nannofossil oozes interbedded with chalk and occasional chert horizons. Increasing lithification is documented by increases in bulk density (GRA) and decreases in porosity (moisture and density). The presence of chert and micrite indicates significant opal and carbonate diagenesis, respectively. Magnetic susceptibility increases downhole in Subunit IB toward basaltic basement.

Calcareous nannofossils are generally abundant and planktonic and benthic foraminifers are common to abundant, with good to moderate preservation throughout the section, except in the interval of lower Pleistocene and middle Miocene. Benthic planktonic foraminifer ratios generally increase downhole. Diatoms are common to abundant throughout the Pleistocene, Pliocene, and the upper half of the upper

Miocene sequence (to 430 mcd; 9 ± 0.5 Ma). Sediments below this level are essentially barren of siliceous microfossils, likely due to opal diagenesis resulting in chert formation.

The various microfossil groups provide a well-constrained biostratigraphy. The Pleistocene through Pliocene sequence has a sedimentation rate of ~50 m/m.y. In the lower Pliocene–upper Miocene section, the sedimentation rate is ~60 m/m.y., and this section contains a minor component of reworked older microfossils. A marked change in sedimentation rate occurs at 390–415 mcd (7–8 Ma). Below this level, sediments accumulate at an average rate of ~17 m/m.y. Calcareous nannofossils provide a basal age of 10.4–11.6 Ma. Paleomagnetic measurements were compromised by drill string overprints, as well as diagenesis of magnetic minerals, and thus did not provide useful information for age control.

Moderate amounts of biogenic gas, mostly methane but also traces of ethane, result from the limited effects of methanogenesis at this site. Chemical gradients in the interstitial waters reflect the influence of organic matter oxidation by sulfate reduction, although not to complete sulfate depletion. Sulfate decreases to <10 mM by ~75 mcd, coincident with the top of a relatively organic carbon–rich interval. The sulfate decrease is accompanied by increases in alkalinity (>17 mM), phosphate (>15 mM), and ammonium (3 mM). The shallow part of the calcium profile, with a substantial decrease in calcium by ~55 mcd, is controlled by authigenic calcite precipitation driven by the alkalinity increase. The deeper sequence reflects the diffusive influence of basalt alteration, also affecting magnesium, lithium, and potassium profiles. Silicate increases to >1800 µM by ~350 mcd, indicating temperature variation of the solubility of biogenic opal as a control on interstitial water composition here, with sharp decreases in silicate concentrations and incipient chert formation deeper in the site.

The weight percentage of calcium carbonate ($CaCO_3$) ranges between 17 and 94 wt% and averages 60 wt%. $CaCO_3$ concentrations increase with depth and vary rhythmically with ranges of 10–20 wt% along the profile. TOC contents range between 0.1 and 4.3 wt% and vary inversely with $CaCO_3$. The long-term decrease in carbonate concentration is consistent with the migration of the site toward a more coastal setting with greater production of diatoms and organic matter and delivery of terrigenous material that may both dilute and dissolve the carbonate component.

Downhole logging operations experienced smooth borehole conditions and calm seas (peak heave < 2 m), and as a result the data from the density, porosity, and FMS tools that require good borehole contact were of excellent quality. NGR results were highly reproducible between tools and passes and also closely matched the NGR records developed from shipboard core logging. From the base of the drill pipe (84 mbsf) to 209 mbsf, mean values of velocity, resistivity, and density are relatively low, and porosity is high. At greater depths, velocities and densities increase and porosity decreases associated with sediment lithification.

Similar to the core logging data, the downhole logs document cyclic variations in sediment properties on the scale of meters that reflect alternations between carbonate-rich and opal-rich sediments. For example, NGR logs revealed rhythmic low-amplitude oscillations in thorium and potassium. Higher-amplitude oscillations in uranium appear to be well correlated with shipboard measurements of organic carbon in the cores. This correlation points to changes in organic carbon degradation near the sediment/water interface. Organic matter degradation consumes oxygen and drives suboxic diagenesis that concentrates uranium in organic-rich intervals.

A test of the LDEO high-resolution gamma logger was successful and offers the opportunity for detailed correlation of the cores and logs. Even with preliminary analysis at sea, it appears that stratigraphic gaps between XCB cores can be identified, which suggests that the XCB cores can be placed into the framework of logging depths.

Site 1238 met all of its major objectives. With the combination of a complete composite section and a spliced record through the APC interval, excellent logging data to place XCB cores into a true depth framework, and moderately high sedimentation rates, this site will provide excellent opportunities for high-resolution studies of Neogene climate and biogeochemical change. All major fossil groups are present and reasonably well preserved here, which provides both a well-constrained biostratigraphic age model and great potential for the study of near-surface water masses in the eastern reaches of the equatorial cold tongue, including processes of upwelling and paleoproductivity off Ecuador. A well-preserved benthic fauna will facilitate study of deepwater masses. Volcanic ashes are present, which opens opportunities for tephrochronology and for establishing the history of major volcanic events in the northern Andes.

Site 1239

Background

Site 1239 (proposed Site CAR-1C) is located ~120 km off the coast of Ecuador near the eastern crest of Carnegie Ridge (Fig. F1) in the middle of a bench that slopes gently to the south. Just to the east, Carnegie Ridge slopes downward into the Peru-Chile Trench, where subduction is consuming the volcanic seamounts of the Galapagos hotspot track. Basement at Site 1239 likely consists of basalt formed at the Galapagos hotspot (15–18 Ma). Farther north of Site 1239, a series of partially eroded seamounts rises steeply to water depths of 500–1000 m. These bathymetric highs may have been above sea level early in their history, as part of an archipelago similar to the modern Galapagos Islands. The steep basaltic flanks of Carnegie Ridge are mostly bare rock, so some downslope transport of sediment is possible. The tectonic backtrack path on the Nazca plate moves Site 1239 about 600 km westward and slightly to the south relative to South America (Fig. F52) and probably to shallower depths (and perhaps above sea level, which would account for the possible erosion features on the volcanic highs early in the history of this portion of Carnegie Ridge).

The region of Site 1239 is blanketed by pelagic sediments of variable thickness covering rough basement topography. Seismic profiles reveal stratified reflective sediments that drape the underlying bathymetry and fill basement lows (Fig. F55). The sediments are dominated by nannofossil ooze with varying amounts of foraminifers, diatoms, and clay. Several ash layers are present within the sequence.

Today, Site 1239 is situated under the eastern reaches of the equatorial cold tongue in an open-ocean upwelling system near the equator (Fig. F52). The site is close to the equatorial front that separates cool, relatively high-salinity surface waters south of the equator from the warm, low-salinity waters of the Gulf of Panama. The EUC supplies the nutrient-rich upwelling waters that fuel high surface productivity, although nitrate and phosphate are not fully utilized by the phytoplankton. Here, a limited supply of micronutrients such as iron, for which the EUC is today a major source, may play an important role as a regulator of near-surface productivity.

Site 1239 is likely to record changes in upwelling and biological production, as well as long-term changes in upper ocean temperature and pycnocline depth. The surface-ocean properties of the eastern equatorial Pacific are sensitive to interannual to decadal oscillations, such as those of the well-known ENSO, and to longer-term climate changes, such as those of the Pleistocene ice ages. The Site 1239 tectonic backtrack to the west is almost parallel to the equator, so it is likely that the site resided within the highly productive and climatically sensitive region south of the equator throughout its history.

The modern water depth of Site 1239 is within the range of PCW south of Carnegie Ridge but shallow enough that some mixing with remnants of AAIW can be detected here, especially by its relatively low

salinity. NPIW is limited to the Northern Hemisphere and is not detected in the modern water column at Site 1239.

The primary objectives at Site 1239 are to provide a continuous sedimentary sequence of Neogene age (as old as 11–12 Ma) to

1. Assess the history of near-surface water masses, including the eastern reaches of the equatorial cold tongue, upwelling, and paleoproductivity off Ecuador;
2. Monitor temporal and vertical fluctuations of intermediate water masses near 1400 m water depth; and
3. Monitor changes in the occurrence and frequency of volcanic ashes, which might be associated with active tectonic phases of the northern Andes.

Operations

Three APC holes were drilled at Site 1239. Hole 1239A was deepened with the XCB and logged. APC cores in Hole 1239A extend to 174.4 mbsf, and XCB cores cover the interval to 515.4 mbsf, where the last core (202-1239A-55X) contacted acoustic basement.

Hole 1239A was flushed and displaced with sepiolite mud, and the bit was placed at 95.5 mbsf in preparation for downhole logging. One pass with the triple combo was conducted from total depth (517 mbsf) to the mudline, followed by one full pass from 517 mbsf to the bit and one repeat pass from 155 mbsf to the bit with the MGT. Two subsequent passes with the FMS-sonic tool string also reached the bottom of the hole. The hole diameter ranged from ~11.5 to 15 in, allowing good pad contact. Hole 1239A was another unusually smooth hole for logging, resulting in excellent quality of logging data. As in Hole 1238A, hole deviation increased with depth, reaching 7.5° at the bottom.

The vessel was offset 20 m west, and Hole 1239B was drilled with the APC to 171.3 mbsf and extended to 398.7 mbsf with the XCB. The vessel was offset again 20 m west to core Hole 1239C with the objective to fill stratigraphic gaps left in the first two holes.

The nonmagnetic core barrel was deployed on either even- or odd-numbered cores in each APC hole; it was not used for cores that had to be drilled over to avoid damage to hardware as a consequence of the drilling-over process. The piston cores were oriented starting with the third or fourth core in each hole. One bottom-water and four downhole temperature measurements taken with the APCT indicated a thermal gradient of ~88°C/km. The total cored interval at Site 1239 was 1026.1 m, with 1042.2 m recovered, representing an average recovery of 101.6%.

Scientific Results

A 512.3-m-thick (557.5 mcd) sediment sequence extending into the middle Miocene (~14.6 Ma) was recovered (F56). The biostratigraphic sequence is similar to that at Site 1238, except that a major hiatus was identified, encompassing the interval from ~7.8 to 13.6 Ma.

A composite section was constructed using magnetic susceptibility and other core logging data from three holes. All APC cores were correlated, and the splice documents complete recovery of the upper 188.9 mcd. Most of the XCB cores from Hole 1239B were not measured during Leg 202 because of expected depletion of the D-tube supply later in the leg, which prevented the extension of the splice. However, these cores will be measured postcruise, and based on the signal that allowed correlation of XCB cores from Hole 1239A to the downhole logs in the same hole, we expect that a complete splice to basement can be constructed later. Density and NGR records from borehole and core logging data (including the

XCB-cored interval of Hole 1239A) exhibit strong correlation of meter-scale variability. An eld scale was transferred to the XCB cored intervals based on core-log data correlation. This analysis accounts for core expansion, identifies the extent of gaps between cores, and better approximates the "true" depth of the sediment below the seafloor by accounting for small errors in the mbsf scale.

The lithology, as well as the fossil assemblages and abundances at Site 1239, reflect a moderate- to high-productivity pelagic environment, similar to that at Site 1238. The recovered sediments are dominated by foraminifer and nannofossil ooze with varying amounts of diatoms, clay, and micrite. Siliciclastic components include clay minerals and lesser amounts of feldspars and biotite. Almost the entire sequence is characterized by meter-scale cyclic changes in color reflectance (particularly L*) and bulk density that likely reflect changes in relative proportions of biogenic opal and carbonate. Preliminary evaluation suggests that these features are related to the Earth's orbital cycles on the scale of 10^4 to 10^5 yr.

Volcanic ash deposition began in the late Miocene to early Pliocene (~5–4 Ma), increasing in frequency over the last 3 m.y. An ash layer observed at 13.3 mcd can tentatively be correlated to the regional ash layer L (~230 ka), consistent with sedimentation rates of 60 m/m.y. inferred from the shipboard biostratigraphic age model. The magnetic susceptibility signal increases in both mean values and amplitude of high-frequency fluctuations within the interval representing the last ~2.5 m.y. (0–120 mcd). This may reflect the previously documented increase in amplitude of orbital-scale climate variability associated with the Pliocene–Pleistocene intensification of Northern Hemisphere glaciation.

Calcareous nannofossils are abundant and well preserved within the top ~100 mcd, but both abundance and preservation decline slightly below this interval. Planktonic foraminifers are common within the top ~100 mcd but decrease in abundance rapidly at greater depths. Diatoms are also present throughout the sedimentary section, although their abundance is relatively low in the Holocene to middle Pleistocene and lower Pliocene to uppermost Miocene intervals in comparison to Site 1238.

High concentrations of diatoms and nannofossils, increased sedimentation rates (averaging 110 m/m.y.), and enhanced accumulation rates of organic carbon and carbonate characterize the Pliocene interval from ~4.5 to 1.8 Ma, suggesting a period of relatively high productivity. The final phase of this period from ~2 to 1.8 Ma (~85–115 mcd) is associated with a drop in carbonate concentrations, a minimum in L* reflectance, and low bulk density. These significant changes point to an environmental change within the upwelling region that favored biosiliceous productivity, possibly associated with a change in nutrient availability and/or upwelling conditions.

The timing of the onset of this Pliocene productivity maximum remains speculative and relies on interpretations of the biostratigraphic age model between ~4 Ma and the top of a hiatus detected between 519.3 and 527.7 mcd (7.8–13.6 Ma, based on calcareous nannofossils). The current age model suggests sedimentation rates of ~60 m/m.y. for the interval from ~7.8 to 4.5 Ma and higher sedimentation rates of ~110 m/m.y for the interval from ~4.5 to 1.8 Ma. Such a change in sedimentation rates would imply a substantial increase in accumulation rates of organic matter and opal and thus would place the onset of this biogenic bloom at ~4.5 Ma. However, the biostratigraphic framework of diatoms and planktonic foraminifers may indicate that the top of the hiatus occurs later, near 6.5 Ma. This alternative age model would imply high sedimentation rates of ~100 m/m.y. (and attendant high mass accumulation rates of biogenic components) immediately above the hiatus and would place the onset of the biogenic bloom just after or perhaps within the hiatus (i.e., >6.5 Ma). Below the hiatus, sedimentation rates from 13.6 Ma to basal sediments dated at 14.6–14.9 Ma are distinctly lower than those above the hiatus.

Steep positive magnetic inclinations of the sediment at this equatorial location indicate that NRM was affected by a drill string magnetic overprint even after AF demagnetization. Although a detailed magnetic

stratigraphy could not be resolved shipboard, declination data suggest that postcruise work may be able to resolve at least a few polarity transitions of the Matuyama Chron.

Chemical gradients within interstitial water reflect the influence of organic matter oxidation, the dissolution of biogenic silica and its reprecipitation in authigenic phases, the effects of authigenic calcite precipitation, and the diffusive influence of basalt alteration processes. Sulfate is completely consumed by ~71 mcd, coincident with an increase in methane and approaching an interval of higher organic carbon contents that marks the final phase of the late Pliocene biogenic bloom. Within this interval, alkalinity reaches maximum values from ~92 to ~123 mcd and then declines downhole. Alkalinity consumption is associated with carbonate mineral precipitation and also with the diffusive influence of basalt alteration reactions. Authigenic mineral precipitation is reflected by increased amounts of micrite within the sediments at depths >100 mcd and a decrease in calcium concentrations to minimum values by ~75 mcd.

As at Site 1238, the increase in dissolved silicate with increasing depth reflects enhanced dissolution of biogenic opal that is controlled by an anomalously high temperature gradient. Peak silicate values are reached at temperatures of ~45°C (~510 mcd at this site). The subsequent decrease in dissolved silicate values at greater depth is consistent with diagenetic reprecipitation of silicate in chert and its precursors.

The weight percentage of calcium carbonate ranges between 16 and 87 wt%. The upper 200 mcd of the sediment sequence is marked by high-amplitude variations in carbonate concentrations around an average value of 52 wt%. At greater depths, $CaCO_3$ concentrations increase to ~80 wt%. These long-term changes are consistent with the migration of the site toward more coastal conditions with greater production of diatoms and organic matter and an enhanced supply of siliciclastics. TOC concentrations average 1.3 wt% in the Pleistocene interval, then increase to 2 wt% in the interval of inferred high productivity from 1.8 to 4.5 Ma, and decrease again to values <1.5 wt% in the sequence older than 4.5 Ma. Enhanced input of terrigenous organic matter may have occurred during the Miocene (>5.5 Ma) as indicated by high organic carbon/nitrogen ratios.

The downhole logging provided excellent data from the NGR, bulk density, porosity, and FMS tools. The most striking feature of the logs is the high-frequency variability in density and resistivity throughout the sequence from 110 to 517 mbsf. High sedimentation rates and meter-scale rhythmic changes in density and resistivity are encountered in the upper Miocene to Pliocene interval that are interpreted to reflect orbital-scale changes in carbonate vs. biogenic opal in the sediment. Color banding on the FMS images is present on the same scale, which clearly documents the potential for developing an orbitally tuned timescale for this site.

Site 1239 met all of its major objectives. The site combines a complete composite section through the APC interval of 189 mcd, double-XCB coring that may document complete recovery to basement, and excellent logging data to place the deeper APC cores and the XCB cores into a true depth framework. Moderately high sedimentation rates of 50–100 m/m.y., combined with observations of rhythmic shifts in sediment composition that probably represent orbital-scale variability, confirm that this site will provide excellent opportunities for high-resolution studies of late Neogene climate change and for the study of biogeochemical cycles in the ocean. The interval from 7.8 (or 6.5) to 13.6 Ma is represented by a hiatus. All major fossil groups are present at Site 1239 and are moderately to well preserved. This rich fossil record will provide a solid base for the study of near-surface water masses in the eastern reaches of the equatorial Pacific cold tongue, including processes of upwelling, nutrient utilization, and paleoproductivity of the coast of Ecuador. A well-preserved benthic fauna will facilitate study of deepwater masses. Volcanic ashes present an opportunity for tephrochronology and for establishing the history of major volcanic events in the northern Andes.

Site 1240

Background

Site 1240 (proposed Site PAN-2A) is located midway between mainland Ecuador and the Galapagos Islands, north of Carnegie Ridge at 2921 m water depth in the Panama Basin (Fig. F1). The site is in a small east-west–trending trough of basaltic crust formed at the Cocos-Nazca spreading center about 3 m.y. ago (Fig. F57). Tectonic movements over the past 3 m.y. are small; the site backtracks from its current position (~2 km north of the equator) ~40 km to the south and 200 km to the west over the past 3 m.y.

The pelagic sediment cover at Site 1240 drapes the abyssal hills, with a slight thickening of the section within the valleys. Total sediment thickness was estimated at 250–280 m based on seismic survey data (Fig. F58). Dominant sediments are (diatom) nannofossil ooze, with some intervals of nannofossil diatom ooze and occasional ash layers.

Equatorial upwelling driven by southeasterly trade winds is strong over Site 1240, especially in the Southern Hemisphere winter. Nutrient-rich waters of the EUC serve as primary source waters for the modern upwelling. The surface-ocean properties of the eastern equatorial Pacific are sensitive to interannual to decadal variability, such as those of the well-known ENSO events, as well as to longer-term changes associated with the Pleistocene ice ages. Site 1240 is likely to record changes in upwelling and biological production, long-term changes in upper ocean temperature and pycnocline depth, and carbonate dissolution within the Panama Basin.

The primary objectives at Site 1240 are to provide a continuous sedimentary sequence of late Neogene sediment to assess variability of upper ocean processes, including equatorial upwelling, at millennial to orbital timescales.

Operations

At Site 1240, four APC holes, offset by ~10 m, were cored to 253.0, 248.2, 80.2, and 31.7 mbsf, with the objective to recover a complete stratigraphic sequence. Some intervals were drilled without coring to achieve the appropriate stratigraphic overlap. The nonmagnetic core barrel was deployed to ~150–200 mbsf in each hole, either on even-numbered or odd-numbered cores. Below this depth interval, the core barrels had to be drilled over in order to retrieve them, and the risk to the nonmagnetic core barrel was considered too great. The piston cores were oriented starting with the third or fourth core in each hole. Fourteen downhole and one bottom-water temperature measurements were collected with the APCT, yielding a low average thermal gradient of 2.56°C/100 m.

Scientific Results

Site 1240 cored a 282.9-mcd-thick sedimentary sequence that provides a continuous record dating back to the late Pliocene (Fig. F59). Sediments consist mostly of nannofossil ooze with varying amounts of diatoms. Siliciclastic components, primarily clay, are rare. A composite depth scale extends to the bottom of the sequence, and a splice documents complete recovery for the upper 278.28 mcd.

Sedimentation rates are ~80 m/m.y. in the uppermost ~140 mcd of the section (0–1.7 Ma) and 120–160 m/m.y. at greater depths, to a basal age of ~2.6 Ma (based on nannofossil datum) or 2.9 Ma (extrapolated from planktonic foraminifer datums).

A single lithostratigraphic unit was defined and subdivided into three subunits. Subunit IA (0–142.2 mcd; 0–1.7 Ma) is composed of extensively bioturbated nannofossil ooze. Subunit IB (142.2–206.4 mcd; ~1.7–2.2 Ma) is enriched in diatoms, siliciclastic components, TOC, and chlorophyll-related pigments

relative to the other two subunits. Color banding is frequently present throughout Subunit IB. Darker colors are associated with the presence of pennate diatoms. Subunit IB is also characterized by relatively low values in grain density associated with higher biogenic silica content and high values of TOC (1.1–3.1 wt%), chlorins, and NGR. Physical properties in Subunit IB are distinct and separated by sharp transitions from Subunits IA and IC. Relatively high porosity associated with high abundance of diatoms results in low bulk density and higher *P*-wave velocity. The color is characterized by high reddish hue (a* > 0) values. Magnetic susceptibility and lightness (L*) are low. Sediments and physical properties in Subunit IC (206.4–282.9 mcd, ~2.2–2.6 Ma) are very similar to those in Subunit IA.

Characteristics of Subunit IB may indicate increased primary productivity between ~1.7 and 2.2 Ma, perhaps associated with enhanced equatorial upwelling and intensified atmospheric and oceanic circulation. Increased siliciclastic content in this interval also suggests effective eolian transport toward Site 1240, supporting a potential intensification of atmospheric circulation.

Eight ash layers were recorded at Site 1240. Grain compositions of most of the ash layers can be associated with volcanism from northern South America. However, some ash layers containing brown volcanic glass indicate that Central America is a possible source region. In addition, the occurrence of an ash layer fully composed of brown glass (~268 mcd) may indicate a hotspot source such as Galapagos.

Calcareous nannofossils are generally abundant and well preserved at Site 1240, but preservation declines between 20 and 46 mcd and below 120 mcd. Foraminifers are common, with moderate to good preservation, except between 163 and 194 mcd, where the percentage of benthic foraminifers relative to total foraminifers also increases. Diatoms are common throughout the section. They are very abundant but severely fragmented in the upper portions of Subunit IB. Persistent reworking of late Miocene microfossils is noted throughout the sequence; however, the three microfossil groups provide a well-constrained biostratigraphic model.

NRM intensities are consistent throughout the sediment column, suggesting that reduction diagenesis plays a minor role in the magnetic properties of this record. Though still apparently affected by a drill string magnetic overprint after AF demagnetization, declinations corrected by the Tensor tool provide polarity information through the Gauss/Matuyama boundary. The magnetic record from Site 1240 provides an interpretable magnetic stratigraphy that is consistent with the biostratigraphic age model.

Methane was first detected in a headspace gas sample at 19.5 mcd. Below this depth, methane increased to a maximum of 57.4 ppmv at 146.5 mcd, followed by a downhole decrease to concentrations <10 ppmv in basal sediments. Very small amounts of ethane were also detected. These gases originate from in situ fermentation of organic matter.

Pore water chemical gradients reflect the influence of organic matter oxidation in sulfate reduction to values about one-half that of seawater. Fluid flows of relatively unaltered seawater in the underlying basement affect pore waters in the deeper section (e.g., with a return to relatively high concentrations of sulfate and calcium). Fluid flow also results in a thermal gradient of ~2.2°C/100 m, about half the normal gradient for sediments above oceanic crust. Pore water silicate increases to generally high values of >1000 mM, but never reaches the values observed at Sites 1238 and 1239, where downhole temperatures were significantly higher.

Site 1240 met its primary goal of providing a continuous sedimentary sequence of upper Neogene sediment to assess variability of upper ocean processes, including equatorial upwelling, at millennial to orbital timescales. Sedimentation rates at this site are clearly high enough to record millennial-scale variability, and the record is continuous as far back as 2.6 Ma, encompassing the Pliocene–Pleistocene interval associated with Northern Hemisphere glaciation. The major changes in lithology at this setting of equatorial divergence are between sediments rich in calcareous nannofossils and those rich in diatoms

and organic carbon. Although the influence of preservation may not be entirely ruled out, the evidence is consistent with control by variations in upwelling and production.

Site 1241

Background

Site 1241 (proposed Site COC-2A) is located on a gently sloping sediment-covered ramp on the north flank of Cocos Ridge at 2027 m water depth in the Guatemala Basin. The crust underlying the site formed at the Galapagos hotspot ~11–13 m.y. ago. A tectonic backtrack path on the Cocos plate moves Site 1241 southward and slightly to the west relative to South America (Fig. F6). The site was probably located close to the equator and at shallower depths early in its history.

The pelagic sediment drape is ~400 m thick (Fig. F60). Dominant sediments are nannofossil ooze, lithifying at depth, and occasional ash layers that may record the history of volcanism in Central America, northern South America, and the Galapagos Island chain.

Site 1241 is under the warm, relatively low-salinity waters of the Panama Basin. Nutrients at the sea surface are low, and biological productivity is substantially lower than at the equator.

Site 1241 is likely to record changes in upwelling and biological productivity, from higher values early in its history (when it was close to the equator) to relatively low values at present. Furthermore, the site is expected to provide a record of surface-water salinity reduction that occurred in response to the closure of the Isthmus of Panama during the late Miocene, along with a record of volcanism in Central America based on the accumulation rates of ash. On shorter timescales within the Pleistocene, Site 1241 has the potential to record oscillations of ice age climate in changing sea-surface salinity and pycnocline depth, both of which are associated with heavy rainfall under the Intertropical Convergence Zone.

Deep waters of the Guatemala Basin derive from middepth waters of the North Pacific that enter through fracture zones in the East Pacific Rise. Waters of North Pacific origin are relatively depleted in oxygen and enriched in nutrients. The region is an important site of denitrification. The relatively shallow depth of Site 1241 will facilitate the study of changes in the upper reaches of the lysocline in the Guatemala Basin.

The primary objective at Site 1241 is to provide a continuous sedimentary sequence over the Miocene–Pliocene to assess variability of upper ocean processes, including the development of Atlantic to Pacific salinity associated with the closure of the Isthmus of Panama and other late Neogene climate changes. In its recent history, the site is well positioned to monitor the location of the intertropical convergence in the eastern Pacific. Its water depth is suitable for monitoring Pleistocene changes in carbonate dissolution within the Guatemala Basin. Given the tectonic backtrack to the south and to shallower water depths in the past, it also is likely to be suitable for monitoring intermediate waters during late Miocene time.

Operations

At Site 1241, three holes offset by 20 m, were cored with the APC to 314.2, 259.4, and 143.5 mbsf. Holes 1241A and 1241B were advanced with the XCB to 394.4 and 307.6 mbsf, respectively. Several short intervals were drilled without coring in Holes 1241B and 1241C to adjust the coring depth and optimize stratigraphic overlap.

A total of 20 core barrels that could not be pulled with a force of 60 kilopounds were drilled over. The nonmagnetic core barrel was deployed on even- or odd-numbered cores until the first barrel had to be drilled over in each hole. The piston cores in Hole 1241A were oriented starting with the fourth core.

Cores from the subsequent holes were not oriented because one Tensor tool failed and the remaining one was spared so that it could be used at the last site.

Seven downhole and one bottom-water temperature measurements were taken with the APCT, and the results indicated a low thermal gradient of ~2.6°C/100 m.

After the completion of coring operations in Hole 1241B, the hole was flushed and displaced with sepiolite mud. The bit was placed at depths between 97.5 and 82 mbsf for downhole logging. The triple combo tool string with the MGT on top was deployed first, followed by the FMS-sonic tool string. One pass with the triple combo was conducted from total depth (395 mbsf) to the mudline, followed by one full pass from 395 mbsf to the bit with the MGT. One subsequent pass with the FMS-sonic tool string also reached the bottom of the hole. The diameter of the hole ranged from 10 ½–14 ½ in, providing for good log quality.

A supply vessel from Panama (*Viveros*) arrived at the *JOIDES Resolution* in the early morning hours of 25 May, just when operations at Site 1241 were completed. Both vessels waited for daylight for the *Viveros* to come alongside the *JOIDES Resolution* and transfer 150 boxes of D-tubes to replenish the nearly depleted stock. The *Viveros* departed at 0730 hr that morning.

Scientific Results

A 446-m-thick (mcd) sediment sequence was recovered at Site 1241 that spans the interval from the late Miocene (~11.2–11.6 Ma.) to the Pleistocene (Fig. F61). Magnetic susceptibility and GRA bulk density data were the primary parameters used to determine the overlaps of cores between three holes and to construct a composite depth. Complete recovery was documented for the upper 303.14 mcd. XCB cores from Hole 1241A and 1241B were appended onto the mcd scale using a 13% growth rate of mcd relative to mbsf, resulting in a composite section of 446.46 mcd. The splice was not continued below 303.14 m due to a lack of representative signals from these cores. However, density and NGR records from borehole and core logging data (XCB-cored interval of Hole 1241A) exhibit strong correlation of meter-scale variability and may help to generate a spliced section for the XCB-cored intervals of Holes 1241A and 1241B.

Lithology as well as fossil assemblages and abundances at Site 1241 reflect the influence of the equatorial high productivity belt, the Miocene to Holocene path of the site away from the equator toward its modern more northeasterly position at ~6°N, and the vicinity of volcanic islands in the early history of the site. The recovered pelagic sediments are dominated by nannofossil ooze with varying amounts of foraminifers, diatoms, clay, micrite, and volcanic glass. Increases in biogenic silica are reflected by decreases in bulk density. Color reflectance data (lightness L*) correlate well with changes in carbonate contents ($R^2 = 0.8$), and increases in magnetic susceptibility data are associated with increases in clay. Almost the entire sequence is characterized by meter-scale cyclic changes in color reflectance (particularly L*) and bulk density that are interpreted to reflect orbital-scale changes in carbonate vs. biogenic opal. One lithologic unit is defined and divided into three subunits on the basis of changes in sediment composition and associated changes in core logging data (color reflectance, NGR, GRA bulk density, magnetic susceptibility).

The Pleistocene interval of Subunit 1A (0 to ~52 mcd) is marked by moderate carbonate concentrations of 55–75 wt%, including high amounts of foraminifers. Low amounts of biogenic opal and a low mean sedimentation rate of 26 m/m.y. suggest a low productive environment outside of the equatorial upwelling zone. Clay content and magnetic susceptibility values are higher in the upper 15 mcd, probably as a result of less carbonate rather than enhanced eolian supply.

The Pliocene interval from ~2 to 4.5 Ma is characterized by an increase in sedimentation rates from ~36 to ~67 m/m.y and an increase in carbonate contents to ~85 wt% associated with a decrease in the abundance of foraminifers. Considering the backtracking of Site 1241 toward the equator, this may reflect the enhanced influence of the equatorial high-productivity belt. Magnetic susceptibility decreases slightly, probably in response to an increasing carbonate/clay ratio.

The upper Miocene to lower Pliocene sequence (~4.5–9 Ma) of Unit 1B is remarkably homogenous and characterized by high carbonate concentrations ranging between ~70 and 90 wt%, low amounts of foraminifers, moderate amounts of biogenic opal, and high amounts of calcareous nannofossils. Overall, siliciclastics are a minor component. The mean sedimentation rate is high (67 m/m.y) in the interval between ~4.5 and 6.5 Ma, suggesting a period of relatively high productivity. Although changes in lithology are small over the entire upper Miocene sequence, sedimentation rates decrease to a lower level (~34 m/m.y) in the early lower upper Miocene interval (6.5 to 9 Ma).

The period of high carbonate accumulation reflects the vicinity of Site 1241 to the equatorial upwelling/high productivity zone during the late Miocene to early Pliocene interval. A similar interval of rapid accumulation (~4.5–6.5 Ma) was found at the more southern Sites 1236 (~21°S) and 1237 (16°S), as well as in the equatorial Pacific at Sites 846–850 (3°S–1°N, 90°–115°W) and is often referred to as the late Miocene to early Pliocene biogenic bloom. Whether this bloom is related to the influence of the Peru-Chile Current and its westward extension into the South Equatorial Current, to the closure history of the Isthmus of Panama, and/or to changes in deep-sea circulation, remains a question for postcruise research.

The early late Miocene interval (~9 to ~11.2–11.6 Ma; Subunit IC) is marked by low carbonate concentrations averaging ~40 wt% and relatively high mean sedimentation rates of ~50 m/m.y. Biogenic opal, organic carbon, and siliciclastics become significant contributors to the sediment composition. This sequence corresponds to the interval of the carbonate crash (~8.6–11.2 Ma), characterized by low carbonate accumulation rates and poor preservation of calcareous microfossils. The carbonate crash has been documented in sediment records from the eastern equatorial Pacific and the Caribbean and was more recently interpreted to reflect periods of enhanced carbonate dissolution in response to changes in global thermohaline circulation associated with an intensified influx of corrosive southern-source intermediate waters. Although Site 1241 was located well above the lysocline during the middle Miocene, the preservation of calcareous nannofossils, planktonic foraminifers, and even benthic foraminifers was strongly affected by carbonate dissolution. The increase in carbonate dissolution at Site 1241 may, however, result from the degradation of organic carbon. The overall increase in biogenic opal (including laminated diatom oozes), organic carbon, and sedimentation rates is indicative of high surface productivity and enhanced organic carbon rain. To what extent the decrease in carbonate concentration is due to carbonate dissolution or dilution caused by enhanced flux of biosiliceous material and siliciclastics remains a question for postcruise studies.

The increase in clay and volcanic glass during the early late Miocene interval points to an enhanced supply of siliciclastics, possibly from a former island of the Cocos Ridge. The early history of Site 1241 is marked by several ash layers enriched in brown glass and mafic minerals. These ashes and the presence of black lapilli-sized scoria may reflect the volcanic activity of the Galapagos hotspot and its vicinity to Site 1241. The deposition of such ash layers decreased during the late Miocene and ceased at ~6 Ma, probably due to the northeastward movement of Site 1241 away from the Galapagos hotspot. The interval of the last 6 m.y. is marked by ash layers enriched in clear glasses, possibly originating from Central America. The increasing number of such ash layers during the last 2.5 m.y may have resulted from enhanced volcanic activity or from the vicinity of Site 1241 to Central America.

Calcareous nannofossils are abundant and generally well to moderately well preserved throughout the sequence. Planktonic foraminifers are abundant to common in the interval from 0 to 217 mcd and generally rare at depths >217 mcd. The percentage of benthic foraminifers relative to total foraminifers is low (~1%) in the upper interval but high (~99%) in the lower interval. Diatoms are rare to few and are poorly preserved in the upper 184 mcd of the sequence. Diatom abundance increases and preservation improves below ~195 mcd.

Of taxonomic interest is the new observation of a transitional calcareous nannofossil form between *Discoaster bellus* and *Discoaster berggrenii* at the site. This fills in the missing link between the two species and has implications for biostratigraphy and evolutionary studies. The biostratigraphies of the three planktonic microfossil groups document a continuous sequence of the lower upper Miocene through the upper Pleistocene. The good preservation of all groups here suggests that this site will form an important reference section of the eastern tropical Pacific. Calcareous nannofossils and planktonic foraminifers constrain the basal age of the site at ~11.2–11.6 Ma. The uppermost part of the sequence might be affected by a hiatus spanning the interval from 0 to 0.26–0.46 ma as indicated by the absence of the calcareous nannofossils *E. huxleyi* and *Pseudoemiliania lacunosa*. The last occurrence datum of the planktonic foraminifer *G. ruber* (pink) between 2.35 and 3.86 mcd, however, indicates an age younger than 0.12 Ma for the overlying interval, suggesting a continuous sedimentation at least for the late Pleistocene and possibly to the Holocene.

NRM intensities both before and after demagnetization were relatively strong at the top of Site 1241, preserving a stable remanence with demagnetized inclination values close to those expected. Intensities drop dramatically over the upper 15 mcd and parallel a decrease in magnetic susceptibility. Little magnetic remanence is left below this level, with no interpretable paleomagnetic signal. Magnetic polarity, therefore, provides a magnetic stratigraphy for the upper 15 mcd. Correlation with the geomagnetic polarity timescale indicates that the Brunhes/Matuyama boundary and the upper and lower Jaramillo boundaries are clearly recognizable from both inclination and declination records.

Chemical gradients in interstitial water at Site 1241 reflect the limited influence of organic matter oxidation, the dissolution of biogenic silica driven by the relatively low thermal gradient, and biogenic calcite recrystallization. Many of the profiles are consistent with a flow of relatively unaltered seawater in the underlying oceanic crust, but the lack of major change in composition makes this more difficult to assess than at Site 1240. Sulfate reduction lowers sulfate concentrations by no more than 4–5 mM relative to seawater and is associated with relatively small increases in alkalinity, phosphate, and ammonium. Methanogenesis at this site is limited by the persistence of dissolved sulfate and the low organic carbon contents ranging between 0.1 and 1.4 wt%.

Downhole logging provided excellent NGR, bulk density, porosity, and FMS data. The most striking feature of the logs is the high-frequency variability in density and resistivity throughout the sequence from 82 to 395 mbsf. Meter-scale rhythmic changes in density and resistivity are encountered in the upper Miocene to Pliocene interval and are interpreted to reflect orbital-scale changes in carbonate vs. biogenic opal in the sediment. Color banding on the FMS images occurs on the same scale and clearly documents the potential for developing an orbitally tuned timescale for this site.

Site 1241 met all of its major objectives. We recovered a complete 303-m-long composite section through the APC interval and a double-XCB cored interval that may be correlated and spliced later to a set of excellent logging data. These cores will provide unique opportunities to study changes in biogeochemical cycles and equatorial oceanography associated with the Miocene to Pliocene closure history of the Isthmus of Panama and the Miocene carbonate crash. Moderately high sedimentation rates of 30–50 m/m.y., combined with observations of rhythmic shifts in sediment composition that probably

represent orbital-scale variability, offer the opportunity to integrate the excellent framework of biostratigraphy into an orbitally tuned isotope stratigraphy. Volcanic ashes present an opportunity for tephrochronology and the study of linkages between major ash layers from the Caribbean and Pacific to establish the history of major volcanic events in Central America.

Site 1242

Background

Site 1242 (proposed Site COC-4A) is located at 1364 m water depth in a shallow graben within the structurally complex intersection between Cocos Ridge and the Mesoamerican Trench. The crust underlying the site was probably formed at the Galapagos hotspot ~15–16 m.y. ago. A tectonic backtrack path on the Cocos plate moves Site 1242 southward and to the west, placing it close to the equator and near the ancestral Galapagos hotspot early in its history (Fig. F6).

Sediments at Site 1242 are predominantly hemipelagic clay that fill a subsiding basin, ~460 m thick. The basin geometry is complex, however, and is clearly affected by faulting (Fig. F62). Occasional ash layers are present and may record the history of volcanism in Central America.

At its present location, Site 1242 is under the warm, relatively low salinity waters of the intertropical convergence in the Panama Basin. Nutrients at the sea surface are low, and biological productivity is relatively low for a continental margin setting. Site 1242 is likely to record changes in the pool of warm and relatively low salinity surface waters north of the Panama Basin. In the Pleistocene, it will also provide evidence for variations in upwelling and biological production on the Costa Rica margin. Older sediments here may provide a record of the tectonic and oceanographic responses to Isthmus of Panama closure during the late Miocene and Pliocene, along with a record of volcanism in Central America based on the accumulation rates of ash.

The bottom-water mass at the seafloor is associated with the lower reaches of an anomalously thick oxygen minimum zone between North Pacific Deep Water and remnants of NPIW. These waters of North Pacific origin are relatively depleted in oxygen and enriched in nutrients. The region has one of the deepest and strongest oxygen minimum zones in the world and is thus an important site for denitrification.

Given the relatively shallow depth of Site 1242 above the regional lysocline, variations in carbonate dissolution here should be controlled by the relative rates of carbonate rain from surface waters and organic carbon degradation within the sediments.

The primary objective at Site 1242 is to provide a continuous sedimentary sequence of Pliocene to modern sediment in order to assess variability of upper ocean processes at high resolution, including variations in the Atlantic to Pacific salinity contrast and dynamics of the intertropical convergence associated with late Neogene climate changes. The site is well located to study long-term changes associated with denitrification in low-oxygen subsurface water masses.

Operations

We drilled four APC holes at Site 1142, offset by 20 m, with penetration depths of 176.0, 169.9, 166.5, and 91.5 mbsf. Several short intervals were drilled without coring to optimize overlap of cores in adjacent holes. Holes 1242A and 1242B were advanced with the XCB to 250.8 and 256.0 mbsf, respectively. APC cores were oriented, starting with the third or fourth core. The nonmagnetic core barrel was deployed on

even- or odd-numbered APC cores in each hole. A total of seven downhole and one bottom-water temperature measurements indicated a high thermal gradient of ~20°C/100 m.

Scientific Results

A composite sediment sequence of 287.74 mcd was recovered at Site 1242, spanning the interval from the middle Miocene to Holocene (Fig. F63). A splice documents complete recovery for the upper 196.37 mcd. All APC cores and one XCB core can be correlated to the splice. Below the splice, two cores from the two XCB intervals are correlated to each other, and a floating splice is defined to the bottom of the drilled interval.

The upper 280.6 mcd at Site 1242 consists of fine-grained, homogeneous, hemipelagic sediments that represent the past ~2.5 m.y. Based on shipboard stratigraphy, sedimentation rates range from ~60 to 200 m/m.y. Relatively high $CaCO_3$ and low siliciclastic content characterize the upper Pliocene interval. Carbonate content decreases gradually, and siliciclastic content increases in the Pleistocene and Holocene intervals. This sedimentary record may be influenced by the tectonic movements of Site 1242 toward the continental margin, the uplift of the Central American cordillera following closure of the Isthmus of Panama, the focusing of terrigenous material, and the long-term environmental changes affecting both continental rainfall and marine productivity. The upper Pleistocene interval is characterized by relatively low sedimentation rates of ~60 m/m.y and low carbonate content. The early Pleistocene to Pliocene increase in mean sedimentation rate is paralleled by a gradual increase in carbonate concentrations. Magnetic susceptibility varies significantly on decimeter to meter scales throughout this sequence, suggesting changes in the relative supplies of terrigenous and biogenic material to Site 1242. These changes may in part reflect millennial- to orbital-scale changes in productivity and/or climate.

Increased ash layer frequency between ~30 and 120 mcd and ~160 and 210 mcd indicates increased volcanic activity from ~0.4 to 1.1 Ma and ~1.3 to 1.6 Ma, respectively. Clear platy and vesicular glass and intermediate accessory mineral compositions suggest an andesitic volcanic source, most likely in Central America.

Calcareous nannofossils and foraminifers document a relatively continuous sequence that accumulated rapidly (~110 m/m.y.) over the past ~2.5 m.y. A hiatus spanning the time interval of ~2.5–13 Ma is detected. This interval coincides with the closure of the Isthmus of Panama. Middle Miocene sediments are found below the hiatus, from 280.6 mcd to the base of the sequence at 287.7 mcd, representing pelagic conditions with a relatively high abundance of siliceous microfossils. We infer higher Miocene productivity that may be related to the southward tectonic backtrack of Site 1242 on the Cocos plate toward the equatorial upwelling zone.

Calcareous nannofossils are relatively rare at Site 1242, largely due to dilution by clay and some silt-sized detrital grains. Preservation is moderate. Planktonic foraminifers are abundant to common in the upper ~70 m, but abundance decreases markedly downhole. Planktonic foraminifers are rare from 269 to 277 mcd, just below the major unconformity. Preservation is moderate to good in the upper 99 mcd but deteriorates markedly below this depth. The percentage of benthic foraminifers relative to total foraminifers is initially relatively low (<10%) in the upper 109 mcd, but increases markedly downhole, reaching ~99% between 234 and 257 mcd. Benthic foraminifers are better preserved than planktonic foraminifers, but in both groups preservation deteriorates downhole, particularly from 215 to 269 mcd. Diatoms are rare at Site 1242, with the exception of abundant *Ethmodiscus* fragments from ~208 to 215 mcd, representing thin diatom ooze layers. A thin layer at 281 mcd contains a middle–late Miocene diatom assemblage dominated by *Thalassiothrix*.

Paleomagnetic measurements can not yet constrain age models at Site 1241 but offer the potential for a good record of magnetic paleointensities through time.

Chemical gradients in the interstitial waters at Site 1242 reflect the influence of organic matter oxidation by sulfate reduction, authigenic mineralization, the dissolution of biogenic silica, and the diffusive influence of basalt alteration reactions at greater depth. Sulfate decreases to nondetectable levels by 34.4 mcd, coincident with the rise in methane in the gas samples. The disappearance of sulfate coincides with an increase in barium, apparently driven by dissolution of barite. Organic matter oxidation by sulfate reduction and methanogenesis results in significant increases in alkalinity, phosphate, and ammonium. The alkalinity increase drives authigenic mineral precipitation, resulting in minimum calcium concentrations of 2.5 mM at 34.4 mcd. The deeper part of the calcium profile is dominated by a large increase with depth, linearly correlated to a decrease in magnesium. Dissolved silicate increases with increasing depth to >1400 mM from the dissolution of biogenic opal. Calcium carbonate contents range between 5.7 and 51.2 wt%, averaging 24.4 wt%. The calcium carbonate profile shows a long-term increase downhole. TOC contents range between 0.9 and 3.5 wt%, averaging 1.6 wt%, with a large decrease in the uppermost ~10 mcd. TOC/total nitrogen ratios average 7.2, indicating that the organic matter is dominated by material of marine origin.

Site 1242 has clearly met the shipboard objectives of providing a continuous sedimentary sequence of Pliocene to modern sediments to assess the variability of upper ocean and subsurface water mass processes at high resolution. The relatively high sedimentation rates of 60–200 m/m.y. and the abundant fossil record suggest that this site will provide an excellent history of climate and geochemical changes near the Intertropical Convergence Zone.

REFERENCES

Alpers, C., and Brimhall, G., 1988. Middle Miocene climate change in the Atacama Desert, northern Chile: evidence from supergene mineralization at La Escondida. *Geol. Soc. Am. Bull.,* 100:1640–1656.

Barker, P.F., and Burrell, J., 1977. The opening of Drake Passage. *Mar. Geol.,* 25:15–24.

Beaufort, L., Garidel-Thoron, T., Mix, A.C., and Pisias, N.G., 2001. ENSO-like forcing on oceanic primary production during the late Pleistocene. *Science,* 293:2440–2444.

Behl, R.J., and Kennett, J.P., 1996. Brief interstadial events in the Santa Barbara Basin, NE Pacific, during the last 60 kyr. *Nature,* 379:243–246.

Bender, M.L., Malize, B., Orchardo, J., Sowers, T., and Jouzel, J., 1999. High precision correlations of Greenland and Antarctic ice core records over the last 100 kyr, in mechanisms of millennial scale global climate change. *In* Clark, P.U., Webb, R.S., and Keigwin, L.D. (Eds.), *Mechanisms of Global Climate Change at Millennial Time Scales*. Geophys. Monogr., Am. Geophys. Union, 112:149–164.

Berger, W.H., and Jansen, E., 1994. Mid-Pleistocene climate shift: the Nansen connection. *In* Johannessen, O.M., Muensch, R.D., and Overland, J.E. (Eds.), *The Role of the Polar Oceans in Shaping the Global Environment.* Geophys. Monogr., Am. Geophys. Union, 85:295–311.

Berger, W.H., Lange, C.B., and Weinheimer, A., 1997. Silica depletion of the thermocline in the eastern North Pacific during glacial conditions: clues from Ocean Drilling Program Site 893, Santa Barbara Basin, California. *Geology,* 25:619–622.

Berger, W.H., and Wefer, G., 1996. Central themes of South Atlantic circulation. *In* Wefer, G., Berger, W.H., Siedler, G., Webb, D.J. (Eds.), *The South Atlantic: Present and Past Circulation:* Berlin (Springer-Verlag), 1–11.

Berggren, W.A., and Hollister, C.D., 1974. Paleogeography, paleobiogeography, and the history of circulation of the Atlantic Ocean. *In* Hay, W.W. (Ed.), *Studies in Paleo-oceanography.* Spec. Publ.—Soc. Econ. Paleontol. Mineral., 20:126–186.

Blunier, T., Chappellaz, J., Schwander, J., Dällenbach, A., Stauffer, B., Stocker, T.F., Raynaud, D., Jouzel, J., Clausen, H.B., Hammer, C.U., and Johnson, S.J., 1998. Asynchrony of Antarctic and Greenland climate change during the last glacial period. *Nature,* 394:739–743.

Blunier, T., Schwander, J., Stauffer, B., Stocker, T., Dällenbach, A., Indermühle, A., Tschumi, J., Chappellaz, J., Raynaud, D., and Barnola, J.M., 1997. Timing of the Antarctic Cold Reversal and the atmospheric CO_2 increase with respect to the Younger Dryas event. *Geophys. Res. Lett.,* 24:2683–2686.

Bond, G., Kromer, B., Beer, J., Muscheler, R., Evans, M.N., Showers, W., Hoffmann, S., Lotti-Bond, R. Hajdas, I., Bonani, G., 2001. Persistent solar influence on North Atlantic climate during the Holocene. *Science,* 294:2130–2136.

Bond, G., Showers, W., Cheseby, M., Lotti, R., Almasi, P., deMenocal, P., Priore, P., Cullen, H., Hajda, I., and Bonani, G., 1997. A pervasive millennial-scale cycle in North Atlantic Holocene and glacial climates. *Science,* 278:1257–1266.

Brewster, N.A., 1980. Cenozoic biogenic silica sedimentation in the Antarctic Ocean. *Geol. Soc. Am. Bull.,* 91:337–347.

Broecker, W.S. 1998. Paleocean circulation during the last deglaciation: a bipolar seesaw? *Paleoceanography,* 13:119–121.

————, 1991. The great ocean conveyor. *Oceanography,* 4:79–89.

Broecker, W.S., Bond, G., Klas, M., Bonani, G., and Wolfli, W., 1990. A salt oscillator in the glacial Atlantic? 1. The concept. *Paleoceanography,* 5:469–477.

Broecker, W.S., and Peng, T.-H., 1982. *Tracers in the Sea:* Palisades, New York (Lamont-Doherty Geol. Observ.).

Bryden, H.L., and Brady, E.C., 1985. Diagnostic model of the three-dimensional circulation in the upper Equatorial Pacific Ocean. *J. Phys. Oceanogr.,* 15:1255–1273.

Cande, S.C., and Kent, D.V., 1995. Revised calibration of the geomagnetic polarity timescale for the Late Cretaceous and Cenozoic. *J. Geophys. Res.,* 100:6093–6095.

Cande, S.C., Leslie, R.B., Parra, J.C., and Hobart, M., 1987. Interaction between the Chile Ridge and Chile Trench: geophysical and geothermal evidence. *J. Geophys. Res.,* 92:495–520.

Cane, M., and Clement, A.C., 1999. A role for the tropical Pacific coupled ocean-atmosphere system on Milankovitch and millennial timescales, Part II: global impacts. *In* Clark, P.U., Webb, R.S., and Keigwin, L.D. (Eds.), *Mechanisms of Global Climate Change at Millennial Time Scales.* Geophys. Monogr., Am. Geophys. Union, 112:373–383.

Cannariato, K.G., Kennett, J.P., and Behl, R.J., 1999. Biotic response to late Quaternary rapid climate switches in Santa Barbara Basin: ecological and evolutionary implications. *Geology,* 27:63–66.

Cannariato, K.G., and Ravelo, A.C., 1997. Pliocene–Pleistocene evolution of the eastern Pacific surface water circulation and thermocline depth. *Paleoceanography,* 12:805–820.

Charles, C.D., Lynch-Stieglitz, J., Ninnemann, U.S., and Fairbanks, R.G., 1996. Climate connections between the hemispheres revealed by deep sea sediment core/ice core correlations. *Earth Planet. Sci. Lett.,* 142:19–27.

Clark, C.D., Knight, J.K., Gray, J.T., 2000. Geomorphological reconstruction of the Labrador sector of the Laurentide ice sheet. *Quat. Sci. Rev.,* 19:1343–1366.

Clark, P.U., and Pollard, D., 1998. Origin of the middle Pleistocene transition by ice sheet erosion of regolith. *Paleoceanography,* 13:1–9.

Claypool, G.E., and Kvenvolden, K.A., 1983. Methane and other hydrocarbon gases in marine sediment. *Annu. Rev. Earth Planet. Sci.,* 11:299–327.

Clement, A.C., Seager, R., and Cane, M.A., 1999. Orbital controls on the El Niño/Southern Oscillation and the tropical climate. *Paleoceanography,* 14:441–456.

Codispoti, L.A., and Christensen, J.P., 1985. Nitrification, denitrification and nitrous oxide cycling in the eastern tropical South Pacific Ocean. *Mar. Chem.,* 16:277–300.

Collins, L.S., Coates, A.G., Berggren, W.A., Aubry, M.-P., and Zhang, J., 1996. The late Miocene Panama isthmian strait. *Geology,* 24:687–690.

Cox, A., and Engebretson, D., 1985. Changes in motion of the Pacific plate at 5 Myr BP. *Nature,* 313:472–474.

Crowley, T.J., Kim, K.-Y., Mengel, J.G., and Short, D.A., 1992. Modeling 100,000-year climate fluctuations in pre-Pleistocene time series. *Science,* 255:705–707.

Curry, W.B., Shackleton, N.J., Richter, C., et al., 1995. *Proc. ODP, Init. Repts.,* 154: College Station, TX (Ocean Drilling Program).

DeMets, C., Gordon, R.G., Argus, D.F., and Stein, S., 1990. Current plate motions. *Geophys. J. Int.,* 101:425–478.

Dengo, G., 1985. Tectonic setting for the Pacific margin from southern Mexico to northwestern Columbia. *In* Naim, A.E., Stehli, F.G., and Uyeda, S. (Eds.), *The Pacific Ocean: The Ocean Basins and Margins, 7A:* New York (Plenum Press), 123–180.

Denton, G.H., Heusser, C.J., Lowell, T.V., Moreno, P.J., Andersen, B.G., Heusser, L.E., Schlüchter, C., and Marchant, D.R., 1999. Interhemispheric linkage of paleoclimate during the last glaciation. *Geografiska Annaler,* 81A:107–153.

Detrick, R.S., and Crough, S.T., 1978. Island subsidence, hot spots, and lithospheric thinning. *J. Geophys. Res.,* 83:1236–1244.

Driscoll, N.W., and Haug, G.H., 1998. A short circuit in thermohaline circulation: a cause for northern hemisphere glaciation? *Science,* 282:436–438.

Duque-Caro, H., 1990. Neogene stratigraphy, paleoceanography and paleobiogeography in northwest South America and the evolution of the Panama Seaway. *Palaeogeogr., Palaeoclimatol., Palaeoecol.,* 77:203–234.

Farrell, J.W., Pedersen, T.F., Calvert, S.E., Nielsen, B., 1995a. Glacial-interglacial changes in nutrient utilization in the equatorial Pacific Ocean. *Nature,* 377:515–517.

Farrell, J.W., Raffi, I., Janecek, T.C., Murray, D.W., Levitan, M., Dadey, K.A., Emeis, K.-C., Lyle, M., Flores, J.-A., and Hovan, S., 1995b. Late Neogene sedimentation patterns in the eastern equatorial Pacific. *In* Pisias, N.G., Mayer, L.A., Janecek, T.R., Palmer-Julson, A., and van Andel, T.H. (Eds.), *Proc. ODP, Sci. Results,* 138: College Station, TX (Ocean Drilling Program), 717–756.

Feldberg, M.J., and Mix, A.C., 2002. Sea-surface temperature estimates in the Southeast Pacific based on planktonic foraminiferal species: modern calibration and last glacial maximum. *Mar. Micropaleontol.,* 44:1–29.

Frakes, L.A., 1979. *Climate Throughout Geological Time:* New York (Elsevier).

Ganeshram, R.S., Pedersen, T.F., Calvert, S.E., and Murray, J.W., 1995. Large changes in oceanic nutrient inventories from glacial to interglacial periods. *Nature,* 376:755–758.

Gildor, H., and Tziperman, E., 2001. Sea ice as the glacial cycles' climate switch: role of seasonal and orbital forcing. *Paleoceanography,* 15:605–615.

Gordon, A.I., 1986. Interocean exchange of thermocline water. *J. Geophys. Res.,* 91:5037–5046.

Gregory-Wodzicki, K.M., 2000. Uplift history of the central and northern Andes: a review. *Geol. Soc. Am. Bull.,* 112:1091–1105.

Grootes, P.M., Stuvier, M., White, J.W.C., Johnsen, S., and Jouzel, J., 1993. Comparison of oxygen isotope records from the GISP2 and GRIP Greenland ice cores. *Nature,* 366:552–554.

Harris, S.E., and Mix, A.C., 1999. Pleistocene precipitation balance in the Amazon Basin recorded in deep-sea sediments. *Quat. Res.,* 51:14-26.

————, 2002. Climate and tectonic influences on continental erosion in tropical South America, 0–13 Ma. *Geology,* 30:447–450.

Hartley, A., and Chong, G., 2002. Late Pliocene age for the Atacama Desert: implications for the desertification of western South America. *Geology,* 30:43–46.

Haug, G.H., and Tiedemann, R., 1998. Effect of the formation of the Isthmus of Panama on Atlantic Ocean thermohaline circulation. *Nature,* 393:673–676.

Haug, G.H., Tiedemann, R., Zahn, R., and Ravelo, A.C., 2001. Role of Panama uplift on oceanic freshwater balance. *Geology,* 29:207–210.

Hay, W.W., 1996. Tectonics and climate. *Geol. Rundsch.,* 85:409–437.

Hebbeln, D., Wefer, G., Baltazar, M., Beese, D., Bendtsen, J., Butzin, M., Daneri, G., Dellarossa, V., Diekamp, V., Dittert, N., Donner, B., Giese, M., Glud, R., Gundersen, J., Haese, R., and Hensen, C, 1995. Report and preliminary results of SONNE-Cruise SO 102, Valparaiso–Valparaiso, 95. *Berichte aus dem Fachbereich Geowissenschaften der Universität Bremen,* 68: Bremen, Germany (Geowissenschaften der Universität Bremen), 1–134.

Hendy, I.L., and Kennett, J.P., 1999. Latest Quaternary North Pacific surface water responses imply atmosphere-driven climate instability. *Geology,* 27:291–294.

————, 2000a. Dansgaard-Oeschger cycles and the California current system: planktonic foraminiferal response to rapid climate change in Santa Barbara Basin, Ocean Drilling Program Hole 893A. *Paleoceanography,* 15:30–42.

————, 2000b. Stable isotope stratigraphy and paleoceanography of the last 170 k.y.: Site 1014, Tanner Basin, California. *In* Lyle, M., Koizumi, I., Richter, C., and Moore, T.C. (Eds.), *Proc. ODP, Sci. Results,* 167: College Station, TX (Ocean Drilling Program), 129–140.

Herron, E.M., Cande, S.C., and Hall, B.R., 1981. An active spreading center collides with a subduction zone: a geophysical survey of the Chile margin triple junction. *Mem.—Geol. Soc. Am.,* 154:683–701.

Heusser, L.E., Heusser, C.J., Kleczkowski, A., and Crowhurst, S., 1999. A 50,000-yr pollen record from Chile of South American millennial-scale climate instability during the last glaciation. *Quat. Res.,* 52:154–158.

Hey, R., Johnson, G.L., and Lowrie, A., 1977. Recent plate motions in the Galapagos area. *Geol. Soc. Am. Bull.,* 88:1385–1403.

Hooghiemstra, H., and Ran, E.T.H., 1994. Late Pliocene–Pleistocene high resolution pollen sequence of Colombia: an overview of climate change. *Quat. Intern.,* 21:63–80.

Hovan, S.A., 1995. Late Cenozoic atmospheric circulation intensity and climatic history recorded by eolian deposition in the eastern equatorial Pacific Ocean, Leg 138. *In* Pisias, N.G., Mayer, L.A., Janecek, T.R., Palmer-Julson, A., and van Andel, T.H. (Eds.), *Proc. ODP, Sci. Results,* 138: College Station, TX (Ocean Drilling Program), 615–625.

Imbrie, J., Boyle, E.A., Clemens, S.C., Duffy, A., Howard, W.R., Kukla, G., Kutzbach, J., Martinson, D.G., McIntyre, A., Mix, A.C., Molfino, B., Morley, J.J., Peterson, L.C., Pisias, N.G., Prell, W.L., Raymo, M.E., Shackleton, N.J., and Toggweiler, J.R., 1993. On the structure and origin of major glaciation cycles, 2. The 100,000-year cycle. *Paleoceanography,* 8:698–736.

Imbrie, J., McIntyre, A., and Mix, A., 1989. Oceanic response to orbital forcing in the late Quaternary: observational and experimental strategies. *In* Berger, A., Schneider, S., and Duplessy, J.C. (Eds.), *Climate and Geo-Sciences:* Dordrecht (Kluwer Academic), 121–164.

Jousaumme, S., Sadourny, R., and Vignal, C., 1986. Origin of precipitating water in a numerical simulation of the July climate. *Ocean-Air Interact.,* 1:43–56.

Kennett, J.P., and Ingram, B.L., 1995. A 20,000-year record of ocean circulation and climate change from the Santa Barbara Basin. *Nature,* 377:510–513.

Kim, J., Schneider, R.R., Hebbeln, D., Müller, P.J., and Wefer, G., in press. Alkenone-derived high-resolution sea surface temperature reconstruction in the eastern South Pacific off mid-latitude Chile over the past 33 kyr. *Quat. Sci. Rev.*

Kroopnick, P., 1985. The distribution of ^{13}C of SCO_2 in the world oceans. *Deep-Sea Res. Part A,* 32:57–84.

Labeyrie, L., and Elliot, M., 1999. Abrupt climatic changes—causes and consequences: an introduction. *In* Abrantes, F., and Mix, A. (Eds.), *Reconstructing Ocean History, a Window into the Future:* New York (Kluwer), 73–82.

Lamy, F., Hebbeln, D., Röhl, U., and Wefer, G., 2001. Holocene rainfall variability in southern Chile: a marine record of latitudinal shifts of the southern Westerlies. *Earth Planet. Sci. Lett.,* 185:369–382.

Lamy, F., Hebbeln, D., and Wefer, G., 1998. Terrigenous sediment supply along the Chilean continental margin: modern regional patterns of texture and composition. *Geol. Rundsch.,* 87:477–494.

————, 1999. High-resolution marine record of climatic change in mid-latitude Chile during the last 28,000 years based on terrigenous sediment parameters. *Quat. Res.,* 51:83–93.

Lamy, F., Klump, J., Hebbeln, D., and Wefer, G., 2000. Late Quaternary rapid climate change in northern Chile. *Terra Nova,* 12:8–13.

Lamy, F., Rühlemann, C., Hebbeln, D., and Wefer, G., 2002. High- and low-latitude control on the position of the southern Peru-Chile current during the Holocene. *Paleoceanography,* 17(2).

Lea, D.W., Pak, D.K., and Spero, H.J., 2000. Climate impact of late Quaternary equatorial Pacific sea surface temperature variations. *Science,* 289:1719–1724.

Lenters, J.D., Cook, K.H.,and Ringler, T.D., 1995. Comments on "On the influence of the Andes on the general circulation of the Southern Hemisphere." *J. Clim.,* 8:2113–2115.

Levitus, S., Conkright, M.E., Reid, J.L., Najjar, R.G., and Mantyla, N.A., 1993. Distribution of nitrate, phosphate, and silicate in the world oceans. *Prog. Oceanogr.,* 31:245–273.

Liu, Z., and Huang, B., 2000. Cause of tropical Pacific warming trend. *Geophys. Res. Lett.,* 27:1935–1938.

Lonsdale, P., 1976. Abyssal circulation of the southeastern Pacific and some geological implications. *J. Geophys. Res.,* 81:1163–1176.

Lonsdale, P., and Klitgord, K.D., 1978. Structure and tectonic history of the eastern Panama Basin. *Geol. Soc. Am. Bull.,* 89:981–999.

Loubere, P., 2000. Marine control of biological production in the eastern equatorial Pacific Ocean. *Nature,* 406:497–500.

Lowell, T.V., Heusser, C.J., Andersen, B.G., Moreno, P.I., Hauser, A., Heusser, L.E., Schlüchter, C., Marchant, D.R., Denton, G.H., 1995. Interhemispheric correlation of late Pleistocene glacial events. *Science,* 269:1541–1549.

Lyle, M., Dadey, K.A., and Farrell, J.W., 1995. The late Miocene (11–8 Ma) eastern Pacific carbonate crash: evidence for reorganization of deep-water circulation by the closure of the Panama Gateway. *In* Pisias, N.G., Mayer, L.A., Janecek, T.R., Palmer-Julson, A., and van Andel, T.H. (Eds.), *Proc. ODP, Sci. Results,* 138: College Station, TX (Ocean Drilling Program), 821–838.

Lyle, M., Murray, D.W., Finney, B.P., Dymond, J., Robbins, J.M., and Brooksforce, K., 1988. The record of Late Pleistocene biogenic sedimentation in the eastern tropical Pacific Ocean. *Paleoceanography,* 3:39–59.

Maasch, K.A., and Saltzman, B., 1990. A low-order dynamical model of global climatic variability over the full Pleistocene. *J. Geophys. Res.,* 95:1955–1963.

MacAyeal, D., 1993. Binge/purge oscillations of the Laurentide ice sheet as a cause of the North Atlantic's Heinrich events. *Paleoceanography,* 8:775–784.

Magaña, V., Amador, J.A., and Medina, S., 1999. The midsummer drought over Mexico and Central America. *J. Clim.,* 12:1577–1588.

Martinez-Pardo, R., 1990. Major Neogene events of the southeastern Pacific: the Chilean and Peruvian Record. *Palaeogeogr., Palaeoclimatol., Palaeoecol.,* 77:263–278.

Martinson, D.G., Menke, W., and Stoffa, P.L., 1982. An inverse approach to signal correlation. *J. Geophys. Res.,* 87:4807–4818.

McIntyre, A., and Molfino, B., 1996. Forcing of Atlantic equatorial and subpolar millennial cycles by precession. *Science,* 274:1867–1870.

McIntyre, A., Ruddiman, W.F., Karlin, K., and Mix, A.C., 1989. Surface water response of the equatorial Atlantic Ocean to orbital forcing. *Paleoceanography,* 4:19–55.

Mikolajewicz, U., and Crowley, T.J., 1997. Response of a coupled ocean/energy balance model to restricted flow through the Central American isthmus. *Paleoceanography,* 12:429–441.

Mikolajewicz, U., Crowley, T.J., Schiller, A., and Voss, R., 1997. Modelling teleconnections between the North Atlantic and North Pacific during the Younger Dryas. *Nature,* 387:384–387.

Mikolajewicz, U., Maier-Reimer, E., Crowley, T.J., and Kim, K.-Y., 1993. Effect of Drakeand Panamanian gateways on the circulation of an ocean model. *Paleoceanography,* 8:409–426.

Mix, A.C., 1989. Influence of productivity variations on long-term atmospheric CO_2. *Nature,* 337:541–544.

Mix, A.C., Le, J., and Shackleton, N.J., 1995. Benthic foraminiferal stable isotope stratigraphy of Site 846: 0–1.8 Ma. *In* Pisias, N.G., Mayer, L.A., Janecek, T.R., Palmer-Julson, A., and van Andel, T.H. (Eds.), *Proc. ODP, Sci. Results,* 138: College Station, TX (Ocean Drilling Program), 839–854.

Mix, A.C., Lund, D.C., Pisias, N.G., Bodén, P., Bornmalm, L., Lyle, M., and Pike, J., 1999a. Rapid climate oscillations in the Northeast Pacific during the last deglaciation reflect Northern and Southern Hemisphere sources. *In* Webb, R.S.,

Clark, P.U., and Keigwin, L. (Eds.), *Mechanisms of Millennial-scale Global Climate Change.* Geophys. Monogr., Am. Geophys. Union, 112:127–148.

Mix, A.C., Mayer, L.A., Bloomer, S.F., and Pisias, N.G., 1996. *Southeast Pacific Paleoceanographic Depth Transects—Site Survey Data Package 1: Site Tables, Bathymetry, Seismic Constraints:* Corvalis (Oregon State Univ.).

Mix, A.C., Morey, A.E., Pisias, N.G., and Hostetler, S., 1999b. Foraminiferal faunal estimates of paleotemperatures: circumventing the no-analog problems yields cool ice-age tropics. *Paleoceanography,* 14:350–359.

Mix, A.C, Pisias, N.G., Goldfinger, C., Lyle, M., Liberty, L., Janik, A., Hebbeln, D., Wefer, G., and Lamy, F., 2000. *Southeast Pacific Paleoceanographic Transects, Site Survey Data Package 4: NEMO Expedition, Leg III,* R/V Melville, *May–June 2000:* Corvallis (Oregon State Univ.).

Mix, A.C., Pisias, N.G., Goldfinger, C., West, B., Mayer, L.A., and Bloomer, S.F., 1997. *Southeast Pacific Paleoceanographic Transects, Site Survey Data Package 2: Genesis Leg III,* R/V Roger Revelle, *Feb.–Apr. 1997.* Corvallis (Oregon State Univ.).

Mix, A.C., Pisias, N.G., Zahn, R., Rugh, W., Lopez, C., and Nelson, K., 1991. Carbon 13 in Pacific deep and intermediate waters, 0–370 Ka: implications for ocean circulation and Pleistocene CO_2. *Paleoceanography,* 6:205–226.

Molina-Cruz, A., 1977. The relation of the southern trade winds to upwelling processes during the last 75,000 years. *Quat. Res.,* 8:324–339.

Moreno, P.I., Jacobson, G.L., Lowell, T.V., and Denton, G.H., 2001. Interhemispheric climate links revealed by a late-glacial cooling episode in southern Chile. *Nature,* 409:804–808.

Muller R.A., and MacDonald, G.J., 1997. Glacial cycles and astronomical forcing. *Science,* 277:215–218.

Ninkovich, D., and Shackleton, N.J., 1975. Distribution, stratigraphic position and age of ash layer "L," in the Panama Basin region. *Earth Planet. Sci. Lett.,* 27:20–34.

Ninnemann, U.S., and Charles, C.D., 1997. Regional differences in Quaternary subantarctic nutrient cycling: link to intermediate and deep water ventilation. *Paleoceanography,* 12:560–567.

Oberhänsli, H., Heinze, P., Diester-Haass, L., and Wefer, G., 1990. Upwelling off Peru during the last 430,000 yr and its relationship to the bottom-water environment, as deduced from coarse grain-size distributions and analyses of benthic foraminifers at holes 679D, 680B, and 681B, Leg 112. *In* Suess, E., von Huene, R., et al., *Proc. ODP, Sci. Results,* 112: College Station, TX (Ocean Drilling Program), 369–390.

Oppo, D.W., and Fairbanks, R.G., 1989. Carbon isotope composition of tropical surface water during the past 22,000 years. Paleoceanography, 4:333–351.

Parsons, B., and Sclater, J.G., 1977. An analysis of the variation of ocean floor bathymetry and heat flow with age. *J. Geophys. Res.,* 82:803–827.

Pickard, G.L., and Emery, W.J., 1990. *Descriptive Physical Oceanography: An Introduction* (5th ed.): New York (Pergamon).

Pisias, N.G., Mayer, L.A., and Mix, A.C., 1995. Paleoceanography of the eastern equatorial Pacific during the Neogene: synthesis of Leg 138 drilling results. *In* Pisias, N.G., Mayer, L.A., Janecek, T.R., Palmer-Julson, A., and van Andel, T.H.

(Eds.), *Proc. ODP, Sci. Results,* 138: College Station, TX (Ocean Drilling Program), 5–21.

Pisias, N.G., and Mix, A.C., 1997. Spatial and temporal oceanographic variability of the eastern equatorial Pacific during the late Pleistocene: evidence from radiolaria microfossils. *Paleoceanography,* 12:381–393.

Pisias, N.G., and Moore, T.C., Jr., 1981. The evolution of Pleistocene climate: a time series approach. *Earth Planet. Sci. Lett.,* 52:450–458.

Pye, K., 1987. Aeolian Dust and Dust Deposits: London (Academic Press).

Rahmstorf, S., 1995. Bifurcations of the Atlantic thermohaline circulation in response to changes in the hydrological cycle. *Nature,* 378:145–150.

Reid, J.L., 1973. Transpacific hydrographic sections at lats. 43 degrees S and 28 degrees S: the SCORPIO Expedition III. Upper water and a note on southward flow at mid depth. *Deep-Sea Res.,* 20:39–50.

Rodbell, D.T., Seltzer, G.O., Andreson, D.M., Abbott, M.A., Enfield, D.B., and Newman J.H., 1999. An ~15,000 year record of El Niño-driven alluviation in southwestern Ecuador. *Science,* 283:516–520.

Roth, J.M., Droxler, A.W., and Kameo, K., 2000. The Caribbean carbonate crash at the middle to late Miocene transition: linkage to the establishment of the modern global ocean conveyor. *In* Leckie, R.M., Sigurdsson, H., Acton, G.D., and Draper, G. (Eds.), *Proc. ODP, Sci. Results,* 165: College Station, TX (Ocean Drilling Program), 249–273.

Ruddiman, W.F., and Raymo, M.E., 1988. Northern hemisphere climatic regimes during the past 3 Ma: possible tectonic connections. *Philos. Trans. R. Soc. London B,* 318:411–430.

Strub, P.T., Mesias, J.M., Montecino, V., Rutllant, J., and Salinas, S., 1998. Coastal ocean circulation off western South America. *In* Robinson, A.R., and Brink, K.H. (Eds.), *The Sea* (Vol. 11): *Coastal Oceans:* New York (Wiley), 273–313.

Talley, L.D., 1993. Distribution and formation of North Pacific intermediate water. *J. Phys. Oceanogr.,* 23:517–537.

Tans, P.P., Fung, I.Y., and Takahashi, T., 1990. Observational constraints on the global atmospheric CO_2 budget. *Science,* 247:1431–1436.

Thompson, L.G., Davis, M.E., Mosley-Thompson, E., Sowers, T.A., Henderson, K.A., Zagorodnov, V.S., Lin, P.N., Mikhalenko, V.N., Campen, R.K., Bolzan, J.F., Cole-Dai, J., and Francou, B., 1998. A 25,000-year tropical climate history from Bolivian ice cores. *Science,* 282:1858–1864.

Toggweiler, J.R., Dixon, K., and Broecker, W.S., 1991. The Peru upwelling and the ventilation of the south Pacific thermocline. *J. Geophys. Res.,* 96:20467–20497.

Toggweiler, J.R., and Samuels, B., 1993. Is the magnitude of the deep outflow from the Atlantic Ocean actually governed by southern hemisphere winds? *In* Heimann, M. (Ed.), *The Global Carbon Cycle:* Berlin (Springer-Verlag), 303–331.

Tsuchiya, M., and Talley, L.D., 1998. A Pacific hydrographic section at 88°W: water-property distribution. *J. Geophys. Res.,* 103:12899–12918.

van der Hammen, T., Werner, J.H., and Van Dommelen, H., 1973. Palynological record of the upheaval of the Northern Andes: a study of the Pliocene and Lower

Quaternary of the Colombian Eastern Cordillera and the early evolution of its High-Andean biota. *Rev. Palaeobot. Palynol.,* 16:1–122.

Wunsch, C., Hu, D.X., and Grant, B., 1983. Mass, heat, salt, and nutrient fluxes in the South Pacific Ocean. *J. Phys. Oceanogr.,* 13:725–753.

Wyrtki, K., 1962. The oxygen minimum in relation to ocean circulation. *Deep-Sea Res.,* 9:11–23.

————, 1981. An estimate of equatorial upwelling in the Pacific. *J. Phys. Oceanogr.,* 11:1205–1214.

Zachos, J.C., Pagani, M., Sloan, L., Thomas, E., and Billups, K., 2001. Trends, rhythms, and aberrations in global climate 65 Ma to present. *Science,* 292:686–693.

Zaucker, F., Stocker, T.F., and Broecker, W.S., 1994. Atmospheric freshwater fluxes and their effect on the global thermohaline circulation. *J. Geophys. Res.,* 99:12443–12457.

TABLE CAPTIONS

Table T1. Coring summary by site, Leg 202.

Table T2. Coring summary by hole, Leg 202.

Table T3. Summary of advanced hydraulic piston corer (APC) overdrilling.

Table T4. Summary of Leg 202 geochemistry.

FIGURE CAPTIONS

Figure F1. Leg 202 drill sites span a broad latitudinal range from southern Chile to Central America. Site 1232 is in the Chile Basin; Sites 1233–1235 are on the Chile margin; Sites 1236 and 1237 are on Nazca Ridge; Sites 1238 and 1239 are on the Carnegie Ridge; Site 1240 is in the Panama Basin; and Sites 1241 and 1242 are on Cocos Ridge.

Figure F2. Summary stratigraphic columns document cored and drilled intervals, ages, and water depths at Sites 1232–1242. B = Basin.

Figure F3. Upper-ocean currents off the west coast of South America. NECC = North Equatorial Countercurrent, EUC = Equatorial Undercurrent, PCC = Peru-Chile Current, GU = Gunther Undercurrent.

Figure F4. Site locations on modern annual average values of **(A)** sea-surface temperature (°C), **(B)** sea-surface phosphate (μM), and **(C)** sea-surface salinity (PSU).

Figure F5. Cross section of subsurface water masses in a transect through the drilling sites, characterized by **(A)** dissolved oxygen (mM), **(B)** dissolved phosphate (μM), and **(C)** salinity. AAIW = Antarctic Intermediate Water, NPIW = North Pacific Intermediate Water, PCW = Pacific Central Water, GU = Gunther Undercurrent, CPDW = Circumpolar Deep Water.

Figure F6. Plate tectonic backtrack of Leg 202 drill sites. Large circles = the modern location, and successive circles = the backtrack position relative to South America at 1-m.y. intervals. Number at the end of each backtrack path = oldest age of recovered sediment at each site.

Figure F7. Core-log integration. Pervasive meter-scale rhythmic variations were observed in borehole resistivity and core density logs at Sites 1238, 1239, and 1241. Such variability is likely associated with fluctuations in the fractions of carbonate and biogenic opal in the sediments. The Formation MicroScanner (FMS) image of the borehole at Site 1241 is shown to the right of the 64-button average (5-point smoothing) in red. The similarity of the smoothed FMS and the lower-resolution gamma ray attenuation (GRA) bulk density record (blue) in cores from Hole 1241B suggests that borehole logs will provide a relatively continuous proxy record of lithologic variability and will provide for detailed integration of depth scales between the borehole and core logs. Eld = equivalent logging depth.

Figure F8. Comparison of natural gamma radiation data from core logging and downhole logging. Note that the data from two downhole tools (HSGR and MGT) and the MST-NGR correlated very well at meter scale throughout and at submeter scale over most intervals.

Figure F9. Comparison of gamma ray attenuation (GRA) bulk density data from core logging and downhole logging. Note the excellent correlation of variations in magnitude and depth at meter scale. Minor discrepancies at submeter scale may be the result of core disturbance or borehole irregularities.

Figure F10. Relative changes in apparent depth offsets (in the mcd scale) of sequential cores vs. time of coring operation compare well with predictions of tidal sea level oscillations at Site 1240.

Figure F11. Reflectance spectroscopy-derived calcium carbonate and total organic carbon (TOC) contents compared to directly measured quantities at Site 1237.

Figure F12. PSVs at Site 1233, illustrating replication of declination variability in different holes and the assembly of a spliced PSV record with named events from 0 to 30 mcd.

Figure F13. PSVs at Site 1234, illustrating replication of declination variability in different holes, and the assembly of a spliced PSV record, with named events from 0 to 15 mcd.

Figure F14. Variations in paleomagnetic declination (psu) (top), inclination (middle), and normalized relative paleointensity (bottom) at Chile margin, Site 1233, from 0–136 mcd (inferred ~0–140 ka). Note the inferred Laschamp Excursion (~41 ka) near 68 mcd, which implies an average sedimentation rate of nearly 170 m/k.y. from the core top to this level. PSV = paleomagnetic secular variation, BP = before present.

Figure F15. Variations in paleomagnetic declination (top), inclination (middle), and renormalized relative paleointensity (bottom) at Chile margin, Site 1233, from 15–65 mcd (inferred ~11–40 ka). Note the well-defined rhythmic variations in all parameters. PSV = paleomagnetic secular variation, BP = before present.

Figure F16. Comparison of paleomagnetic inclination, declination, and renormalized relative paleointensity at Sites 1233 and 1234. PSV = paleomagnetic secular variation.

Figure F17. Age-depth plot for Sites 1237 and 1241 based on calcareous nannofossil, planktonic foraminifer, and diatom datums. Results for Site 1236, which has similar science objectives and is also located on Nazca Ridge as Site 1237, are shown for comparison.

Figure F18. Leg 202 linear sedimentation rates for Sites 1236–1242, 0–30 Ma.

Figure F19. Linear sedimentation rates since 15 Ma for **(A)** Leg 202, Sites 1236–1242, and **(B)** Leg 138, Sites 844, 846, and 848.

Figure F20. Interstitial sulfate concentrations vs. depth. **A.** All sites. **B.** Sites with complete sulfate reduction, upper 100 mcd. Values below detection limits (typically 1 mM) are plotted at zero.

Figure F21. Interstitial calcium and magnesium/calcium profiles vs. depth. **A, C.** Calcium and magnesium/calcium profiles for sites with limited to moderate sulfate reduction. **B, D.** Calcium and magnesium/calcium profiles for sites with complete sulfate reduction. Note vertical scale changes from C to D.

Figure F22. Interstitial chloride vs. depth for Chile margin sites (1233, 1234, and 1235).

Figure F23. Interstitial profiles of sulfate, alkalinity, phosphate, and ammonium vs. depth for Panama Basin site (1240).

Figure F24. A. Quartz distribution in surface sediments of the subtropical southeast Pacific, expressed as weight percentage (carbonate- and opal-free basis, reproduced from Molina-Cruz, 1977). Gray arrows indicate trade winds. Sites 1236, 1237, 1238, and 1239 are shown with their plate tectonic backtrack. **B.** Siliciclastic accumulation rates and hematite peak height at Sites 1236 (red line) and 1237 (blue line). The accumulation rates of siliciclastics were estimated as (100% – wt% $CaCO_3$ – wt% organic matter) × sedimentation rate × dry bulk density. The shipboard magnetostratigraphy and biostratigraphy were used to calculate sedimentation rates that were smoothed to avoid overinterpretations of the preliminary age model. Note that the siliciclastic accumulation rates at Site 1237 include biogenic silica in the interval of the last ~8 m.y. Based on smear slide data (that overestimate weight percent biogenic opal), biogenic opal values increased from ~1 to 10 vol% over the last 8 m.y. This, however, will not change the general trends observed in the siliciclastic accumulation rate record that is used as a proxy for dust flux. The hematite peak height is derived from color reflectance spectra and serves as a proxy for changing concentrations of hematite.

Figure F25. A. Carbonate accumulation rates at Sites 1236–1238 and 1241, calculated as the product of weight percent $CaCO_3$, sedimentation rate, and dry bulk density. The shipboard magnetostratigraphy and biostratigraphy were used to calculate sedimentation rates that were smoothed to avoid overinterpretations of the preliminary age model. **B.** Annual chlorophyll-a concentrations (mg/m³; http://seawifs.gsfc.nasa.gov), site locations, and tectonic backtrack. Red dots = paleoposition of sites from ~4 to 8 Ma.

Figure F26. Ash frequency was calculated as first derivative of the cumulative number of ash horizons plotted vs. age. Red lines = volcanic ash frequency (number/m.y.), and green bars = thickness of each ash layer (cm) at Sites 1237–1242.

Figure F27. Weight percentage carbonate, weight percentage organic carbon, foraminifer abundance (R = rare, F = few, C = common, A = abundant) and preservation (P = poor, M = moderate, G = good), and the percentage benthic foraminifers at Site 1241. The orange box indicates the time interval of the Miocene carbonate crash observed in the eastern equatorial Pacific.

Figure F28. Evolutive spectra of the lightness parameter L* at Site 1239 (which tends to mimic carbonate content of the sediments) using preliminary shipboard age models. Warm colors indicate greater concentrations of variance within a frequency band.

Figure F29. Sites 1232–1235 are located at the southernmost reaches of the Peru-Chile Current system, in the transition between the subtropical and subpolar gyres. **A.** Contours of annual mean surface water temperatures. Arrows indicate surface water currents. ACC = Antarctic Circumpolar Current, PCC = Peru-Chile Current, PCCC = Peru-Chile Countercurrent, CFW = Chilean Fjord Water, CCC = Coastal Countercurrent. **B.** Salinity contours showing influx of Chilean Fjord Water (CFW). Site 1233 is best located to monitor low-salinity surface waters that advect northward, a measure of the strength or location of the westerly winds. Sites 1234 and 1235 are located to the north, within the eastern boundary current setting, in an upwelling center off of Concepción.

Figure F30. Locations of Sites 1233–1235 on subsurface oxygen. Circles mark the current site locations relative to the oxygen-poor Gunther Undercurrent (GU) and the relatively oxygen-rich Antarctic Intermediate Water (AAIW). Vertical bars on the sites indicate the likely effect of last glacial maximum sea level fall of ~130 m on the position of the sites relative to the sea surface. PCW = Pacific Central Water.

Figure F31. Shipboard correlation of Sites 1233, 1234, and 1235 based on biostratigraphic (<260 ka for all sites) and magnetostratigraphic (e.g., location of Laschamp Event at ~41 k.y.) evidence as well as long-term patterns in magnetic susceptibility, organic carbon, and calcium carbonate concentrations. These data suggest that all three sites will contain viable records of century- to millennial-scale climate change. IU = instrument units.

Figure F32. Millennial-scale variability at Site 1233. Magnetic susceptibility and diatom abundance plotted on a preliminary age scale for the interval 0 to 45 k.y. The age scale is based on Holocene age control points derived from a correlation of the magnetic susceptibility records between Site 1233 and AMS-^{14}C dated core GeoB 3313-1 (Lamy et al., 2001) and the location of the Laschamp Event. All ages are calendar years are BP and are linearly interpolated between the dates. The data are compared to the GISP2 ice core in Greenland (Grootes et al., 1993) and the Byrd ice core in Antarctica (Bender et al., 1999). SMOW = oxygen isotopic composition of standard mean ocean water.

Figure F33. Seismic profile across Site 1232 (proposed Site SEPAC-9A), shotpoint 686 (survey CBA-3A, line 3, shot within 0504–0720 UTC, 08 March 1997). (Mix et al., 1997).

Figure F34. Core recovery, lithology, age, and physical and chemical data summary, Site 1232.

Figure F35. Digital parasound profile, Site 1233 (Hebbeln et al., 1995).

Figure F36. Analog 3.5-kHz profile acquired with the JOIDES Resolution during the approach to Site 1233, 12 April 2002. Depths are represented at 1500 m/s. Reflector numbers appear in boxes.

Figure F37. Core recovery, lithology, age, and physical and chemical data summary, Site 1233.

Figure F38. Age-depth tie points and sedimentation rates, Site 1233. For the top 9 mcd, the points were obtained by direct correlation of Site 1233 magnetic susceptibility data to those of an accelerator mass spectrometry (AMS) 14C-dated sediment core (GeoB3313-3; Lamy et al., 2002). The other points were obtained by correlating a preliminary paleomagnetic intensity record with that published by Stoner et al., in press.

Figure F39. Swath bathymetry of Chilean margin segment, including Sites 1234 and 1235.

Figure F40. Seismic profile across Site 1234 (proposed Site SEPAC-13B), shotpoint 585 (survey CBA-3D, line 4, shot within 2100–0018 UTC, 12 March 1997) (Mix et al., 1997).

Figure F41. Core recovery, lithology, age, and physical and chemical data summary, Site 1234.

Figure F42. Seismic profile across Site 1235 (proposed Site SEPAC-14A), shotpoint 268 (survey CBA-3D, line 15, shot within 0948–1051 UTC, 14 March 1997) (Mix et al., 1997). Note the preferred site at shotpoint 295.

Figure F43. Core recovery, lithology, age, and physical and chemical data summary, Site 1235.

Figure F44. Magnetic susceptibility and chroma (a*) records from the three holes drilled at Site 1235. Green bars = locations of greenish intervals, yellow bars = positions of associated bioturbated intervals, green diamonds = depth of carbonate nodules. The intervals of abrupt change in the physical properties may represent episodes of seafloor dysoxia.

Figure F45. Tectonic backtrack paths for Sites 1236 and 1237. Contours are mean annual sea-surface temperatures. PCC = Peru-Chile Current, SEC = South Equatorial Current.

Figure F46. Seismic profile across Site 1236, shotpoint 366 (survey NAZ-1B, line 5, shot within 2100–2250 UTC, 22 March 1997) (Mix et al., 1997).

Figure F47. Core recovery, lithology, age, and physical and chemical data summary, Site 1236.

Figure F48. Seismic profile across Site 1237, shotpoint 589 (survey NAZ-3B, line 4, shot within 1234–1529 UTC, 29 March 1997) (Mix et al., 1997).

Figure F49. Core recovery, lithology, age, and physical and chemical data summary, Site 1237.

Figure F50. Color measurements at Site 1237 (spliced record) plotted in the a*-b* plane (upper left) and close ups of the L*-a* (upper right), L*-b* (lower left), and a*-b* (lower right) color planes. Measurements plot in two main regions in the a*-b* color plane: the generally greenish sediments of Unit I and Subunit IIA group in the second quadrant, whereas the reddish sediments of Subunit IIB cluster more tightly in the first quadrant. Three populations (IIB1, IIB2, and IIB3) can be distinguished within the red part of the color space.

Figure F51. Seismic profile across Site 1238 (Lyle et al., 2000).

Figure F52. Tectonic backtrack paths for Sites 1238 and 1239. Contours are mean annual sea-surface temperatures.

Figure F53. Core recovery, lithology, age, and physical and chemical data summary, Site 1238.

Figure F54. Preliminary time series analysis results from Site 1238 based on shipboard biostratigraphic age model. Time series and corresponding spectra from 0 to 1 Ma (assuming a linear sedimentation rate between 0.0 and 58.2 mcd, as inferred from one biostratigraphic datum in this interval) of (**A**, **B**) magnetic susceptibility; (**C**, **D**) GRA bulk density; and (**E**, **F**) lightness. Orbital frequencies are denoted by gray bands. The concentration of variance near the known orbital frequencies suggests that meter-scale lithologic banding is associated with orbital-scale climate variability.

Figure F55. Seismic profile across Site 1239.

Figure F56. Core recovery, lithology, age, and physical and chemical data summary, Site 1239 (Lyle et al., 2000).

Figure F57. Swath bathymetry of Panama Basin segment, including Site 1240.

Figure F58. Seismic profile across Site 1240 (Mix et al., 2000).

Figure F59. Core recovery, lithology, age, and physical and chemical data summary, Site 1240 (Lyle et al., 2000).

Figure F60. Seismic profile across Site 1241.

Figure F61. Core recovery, lithology, age, and physical and chemical data summary, Site 1241 (Lyle et al., 2000).

Figure F62. Seismic profile across Site 1242.

Figure F63. Core recovery, lithology, age, and physical and chemical data summary, Site 1242 (Lyle et al., 2000).

Table T1. Coring summary by site, Leg 202.

Site	Number of holes	Average latitude	Average longitude	Average water depth (m)	Maximum penetration (mbsf)	Sum of interval cored (m)	Sum of core recovered (m)	Core recovered (%)	Sum of interval drilled (m)	Time on site (d)
1232	3	39°53.45'S	75°54.08'W	4072	371.3	494.6	416.75	84	0	4.52
1233	5	41°0.01'S	74°26.99'W	838	116.3	411.0	422.23	103	40.6	1.76
1234	3	36°13.15'S	73°40.90'W	1015	205.2	461.6	435.15	94	5.1	1.67
1235	3	36°9.59'S	73°33.98'W	489	181.3	509.5	513.42	101	0.5	1.80
1236	3	21°21.54'S	81°26.17'W	1323	207.7	495.0	490.07	99	2.8	2.64
1237	4	16°0.42'S	76°22.69'W	3212	317.4	744.7	771.05	104	151.5	5.28
1238	3	1°52.31'S	82°46.93'W	2203	430.6	791.1	787.12	99	8.0	4.67
1239	3	0°40.32'S	82°4.86'W	1414	515.4	1026.1	1042.07	102	5.3	4.27
1240	4	0°01.31'N	86°27.76'W	2921	253.0	603.7	622.54	103	9.4	3.34
1241	3	5°50.57'N	86°26.68'W	2027	395.0	799.0	810.14	101	133.9	4.67
1242	4	7°51.35'N	83°36.42'W	1364	256.0	743.8	770.45	104	26.5	2.83
Total:						7080.1	7080.99	100		

Table T2. Leg 202 coring summary by hole.

Site	Hole	Latitude	Longitude	Water depth (m)	Penetration (mbsf)	Interval cored (m)	Core recovered (m)	Core recovered (%)	Interval drilled (m)	APC cores	XCB cores	Time on site (d)
1232	A	39°53.470'S	75°54.082'W	4078.6	371.3	371.3	288.77	78		12	27	
	B	39°53.453'S	75°54.079'W	4069.5	90.1	90.1	96.30	107		10		
	C	39°53.440'S	75°54.082'W	4068.9	33.2	33.2	31.68	95		4		
1232 totals:	3 holes	39°53.45'S	75°54.08'W	4072.3	371.3	494.6	416.75	84		26	27	4.52
1233	A	41°0.001'S	74°26.998'W	837.5	12.0	9.5	9.94	105	2.5	1		
	B	41°0.001'S	74°26.998'W	837.5	109.5	100.0	102.01	102	9.5	11		
	C	41°0.003'S	74°26.992'W	837.7	116.3	116.3	121.75	105		13		
	D	41°0.009'S	74°26.991'W	839.2	112.3	110.3	114.88	104	2.0	13		
	E	41°0.013'S	74°26.983'W	838.1	101.5	74.9	73.65	98	26.6	8		
1233 totals:	5 holes	41° 0.01'S	74°26.99'W	838.0	116.3	411.0	422.23	103	40.6	46	0	1.76
1234	A	36°13.153'S	73°40.909'W	1015.6	205.2	205.2	189.02	92		11	11	
	B	36°13.150'S	73°40.904'W	1014.0	182.4	180.4	169.71	94	2.0	10	9	
	C	36°13.156'S	73°40.894'W	1014.4	79.1	76.0	76.42	101	3.1	8		
1234 totals:	3 holes	36° 13.15'S	73°40.90'W	1014.7	205.2	461.6	435.15	94	5.1	29	20	1.67
1235	A	36°09.591'S	73°33.990'W	489.7	181.3	181.3	182.78	101		20		
	B	36°09.592'S	73°33.983'W	488.5	176.2	176.2	178.81	101		19		
	C	36°09.599'S	73°33.976'W	488.5	152.5	152.0	151.83	100	0.5	16		
1235 totals:	3 holes	36° 9.59'S	73°33.98'W	488.9	181.3	509.5	513.42	101	0.5	55	0	1.80
1236	A	21°21.539'S	81°26.160'W	1323.7	207.7	207.7	197.23	95		20	4	
	B	21°21.541'S	81°26.165'W	1322.5	122.8	122.8	125.10	102		13		
	C	21°21.538'S	81°26.170'W	1322.5	167.3	164.5	167.74	102	2.8	18		
1236 totals:	3 holes	21°21.54'S	81°26.17'W	1322.9	207.7	495.0	490.07	99	2.8	51	4	2.64
1237	A	16°0.420'S	76°22.680'W	3212.7	10.5	9.5	9.95	105	1.0	1		
	B	16°0.421'S	76°22.681'W	3212.7	317.4	317.4	331.35	104		34		
	C	16°0.422'S	76°22.685'W	3211.9	315.3	313.3	323.70	103	2.0	33		
	D	16°0.421'S	76°22.693'W	3211.9	253.0	104.5	106.05	101	148.5	11		
1237 totals:	4 holes	16°0.42'S	76°22.69'W	3212.3	317.4	744.7	771.05	104	151.5	79	0	5.28
1238	A	1°52.310'S	82°46.939'W	2202.2	430.6	430.6	409.77	95		22	24	
	B	1°52.310'S	82°46.934'W	2202.2	201.0	198.0	209.50	106	3.0	21		
	C	1°52.310'S	82°46.928'W	2203.2	167.5	162.5	167.85	103	5.0	18		
1238 totals:	3 holes	1°52.31'S	82°46.93'W	2202.5	430.6	791.1	787.12	99	8.0	61	24	4.67
1239	A	0°40.320'S	82°04.850'W	1414.7	515.4	515.4	515.10	100		19	36	
	B	0°40.321'S	82°04.860'W	1413.3	398.7	396.7	407.32	103	2.0	18	24	
	C	0°40.320'S	82°04.870'W	1413.3	117.3	114.0	119.65	105	3.3	12		
1239 totals:	3 holes	0°40.32'S	82°4.86'W	1413.8	515.4	1026.1	1042.07	102	5.3	49	60	4.27
1240	A	0°01.311'N	82°27.750'W	2922.4	253.0	253.0	264.03	104		28		
	B	0°01.311'N	82°27.756'W	2920.2	248.2	246.2	254.80	103	2.0	26		
	C	0°01.311'N	82°27.760'W	2920.2	80.2	76.0	75.30	99	4.2	8		
	D	0°01.311'N	82°27.766'W	2920.2	31.7	28.5	28.41	100	3.2	3		
1240 totals:	4 holes	0°01.31'N	86°27.76'W	2920.7	253.0	603.7	622.54	103	9.40	65	0	3.34
1241	A	5°50.570'N	86°26.670'W	2027.3	394.4	394.4	404.86	103		34	9	
	B	5°50.570'N	86°26.681'W	2025.8	395.0	303.6	302.23	100	91.4	27	5	
	C	5°50.570'N	86°26.692'W	2027.3	143.5	101.0	103.05	102	42.5	11		
1241 totals:	3 holes	5°50.57'N	86°26.68'W	2026.8	395.0	799.0	810.14	101	133.9	72	14	4.67
1242	A	7°51.352'N	83°36.402'W	1363.4	250.8	250.8	260.11	104		19	8	
	B	7°51.353'N	83°36.413'W	1365.2	256.0	250.5	259.24	103	5.5	18	9	
	C	7°51.352'N	83°36.424'W	1363.1	172.0	166.5	170.95	103	5.5	18		
	D	7°51.353'N	83°36.435'W	1363.1	91.5	76.0	80.15	105	15.5	8		
1242 totals:	4 holes	7°51.35'N	83°36.42'W	1363.7	256.0	743.8	770.45	104	26.5	63	17	2.83

Table T3. Summary of APC overdrilling.

Hole	Depth of first excess force (mbsf)	Maximum APC penetration (mbsf)	Added APC penetration by overdrilling (%)	Reason for APC termination	Number of overdrilled APC barrels	APC cores	XCB cores	Total penetration (mbsf)
1232A	103	112.5	9	B2	2	12	27	371.3
1232B				A2		10		90.1
1232C				A2		4		33.2
1233A				A1		1		12.0
1233B				A1		11		109.5
1233C				A1		13		116.3
1233D				A1		13		112.3
1233E				A1		8		101.5
1234A				B1		11	11	205.2
1234B				B1		10	9	182.4
1234C				A2		8		79.1
1235A				B1		20		181.3
1235B				B1		19		176.2
1235C				A2		16		152.5
1236A				A2		20	4	207.7
1236B				C		13		122.8
1236C	154.8	167.3	8	A2	1	18		167.3
1237A				A2		1		10.5
1237B	148	317.4	114	B1	16	34		317.4
1237C	163.3	315.3	93	B1	15	33		315.3
1237D	234	253	8	A2	3	11		253.0
1238A	90.5	204.5	126	B1	10	22	24	430.6
1238B	87	201	131	B1	8	21		201.0
1238C	139	167.5	21	A2	3	18		167.5
1239A	88.9	174.4	96	B2	6	19	36	515.4
1239B	152.3	171.3	12	B2	3	18	24	398.7
1239C				A2		12		117.3
1240A	174.5	253	45	B1	6	28		253.0
1240B	162.7	248.2	53	B1	8	26		248.2
1240C				A2		8		80.2
1240D				A2		3		31.7
1241A	184.4	314.2	70	B1	13	34	9	394.4
1241B	200.4	259.4	29	B2	7	27	5	395.0
1241C				A2		11		143.5
1242A				B1		19	8	250.8
1242B				B1		18	9	256.0
1242C				A2		18		172.0
1242D				A2		8		91.5
Average* (%):			77					

Notes: APC = advanced hydraulic piston corer. Reason for APC termination: A1 = Pollution Prevention and Safety Panel approved depth is reached, A2 = mission accomplished, B1 = incomplete stroke is indicated, B2 = excessive pull out force >100 klb, C = mechanical. * = average from holes with APC refusal.

Table T4. Summary of Leg 202 geochemistry.

Region	Site	Water depth (m)	Sulfate concentration minimum (mM)	Depth (mcd)	Alkalinity concentration maximum (mM)	Depth (mcd)	Phosphate concentration maximum (M)	Depth (mcd)	Ammonium concentration maximum (mM)	Depth (mcd)	Methane concentration maximum (mM)	Shallowest Depth (mcd)	Calcium concentration minimum (mM)	Depth (mcd)
Limited to no sulfate reduction														
Nazca Ridge	1236	1323	<26	170–191	2.2	—	2	3	<0.005	—	none detected		increases with depth	
	1237	3212	<26	5–63	>5	9–20	9	5	>0.25	9–33	8	42–63	increases with depth	
Cocos Rise	1241	2027	little depletion	—	>5	63–95	5	3	>0.4	53–106	13	189	increases with depth	
Intermediate sulfate reduction														
Carnegie Ridge	1238	2203	<10	75	>17	83–93	>15	10–64	3	82–386	<100		6.1	54
Panama Basin*	1240	2921	<15	135–200	>17	147–190	>30	147–190	>2	147–200	57	147	<3.5	104–179
Complete sulfate reduction														
Chile Basin	1232	4072	<2	26	>30	26–159	>50	throughout	>2	37	>10,000	>60	<6	27
													<4	93–105
Chile Margin	1233	838	BDL	21	>60	21–44	>210	11–55	>5	11–77	High	23	<2	5–11
	1234	1015	BDL	10	>63	18–52	>120	10–52	>11	40–88	High	9	<2	10–112
	1235	489	BDL	20	>60	31–42	>200	20–42	>8	31–42	High	20	<2	20–109
Carnegie Ridge	1239	1414	BDL	71	>28	92–123	>20	61–113	>6	133–378	Moderate–high	100	5.5	71–82
Cocos Rise	1242	1364	BDL	23	>25	23–94	60	34	>7.5	94–170	High	35	2.5	34

Notes: * = Site 1240 is influenced by fluid flow in the underlying basalt, and its geochemistry is discussed separately in the text as a consequence. BDL = below detection limit. Sulfate detection limit was typically 1 mM or lower.
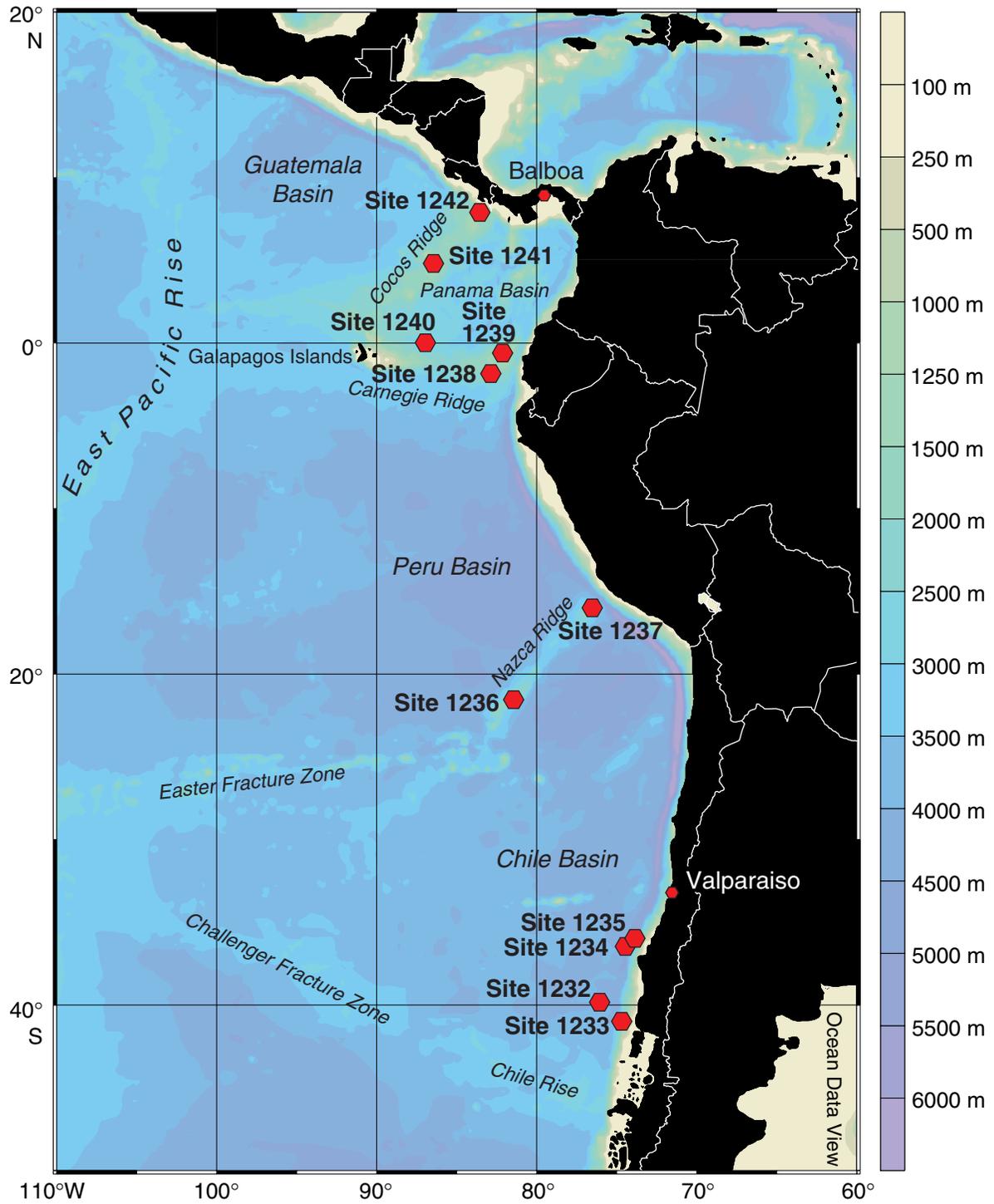
Figure F1
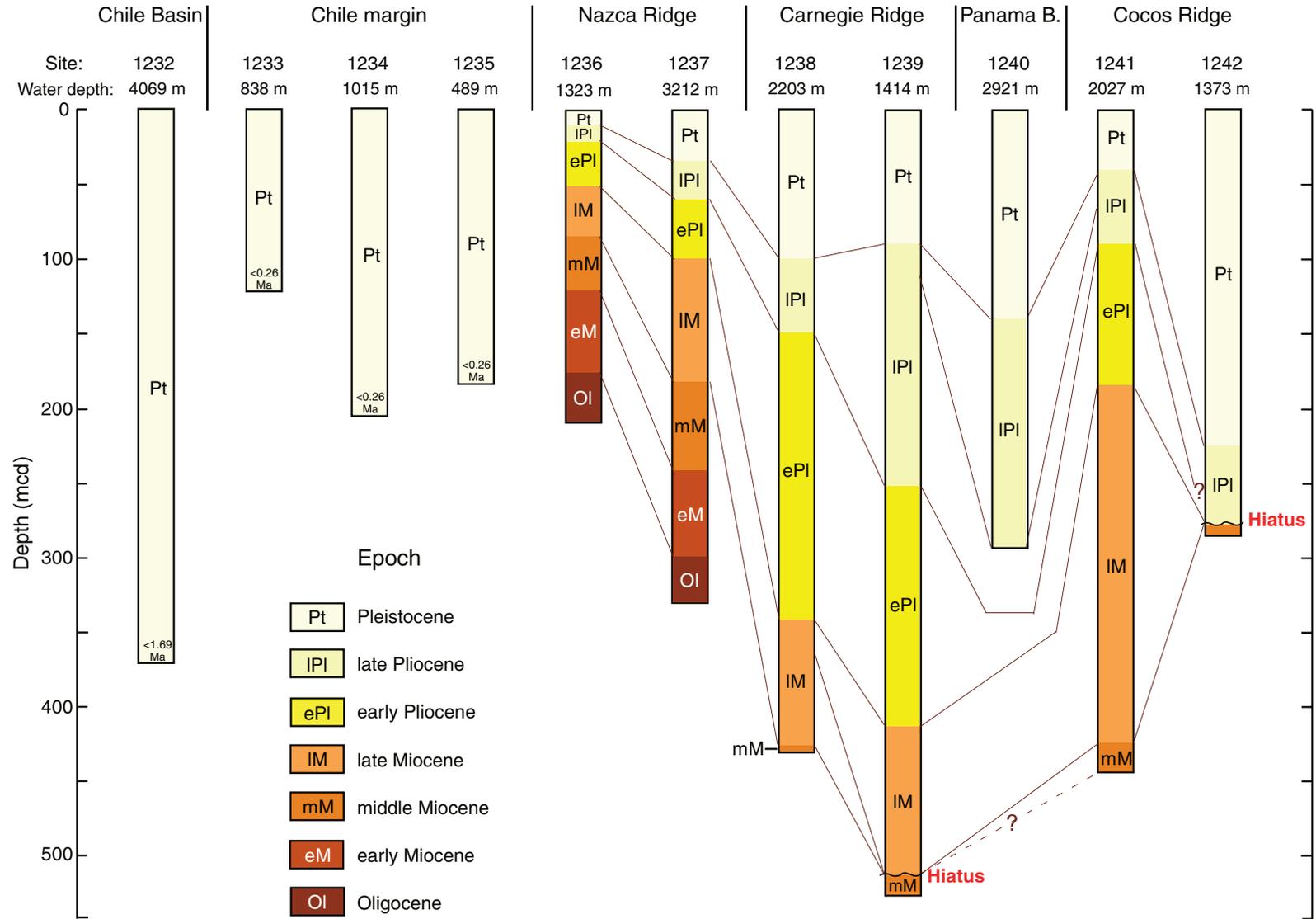
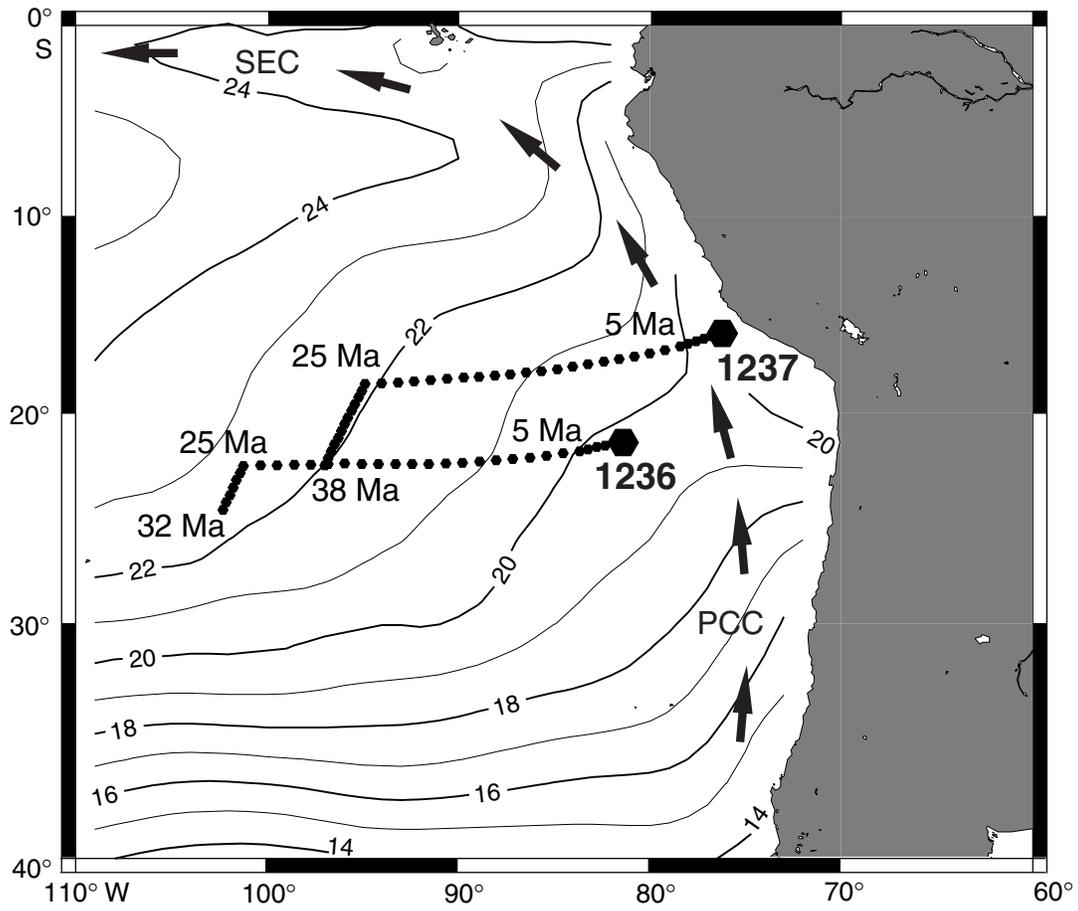Figure F2
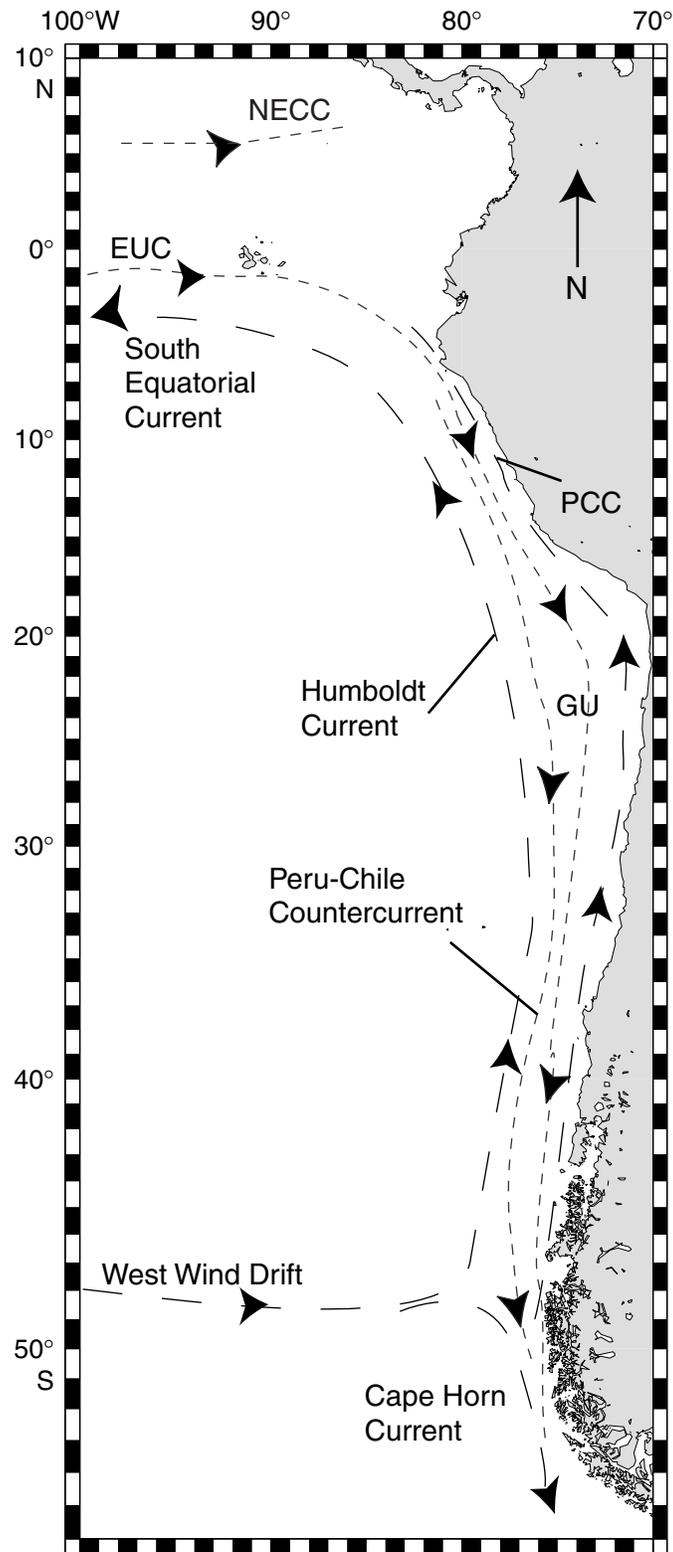
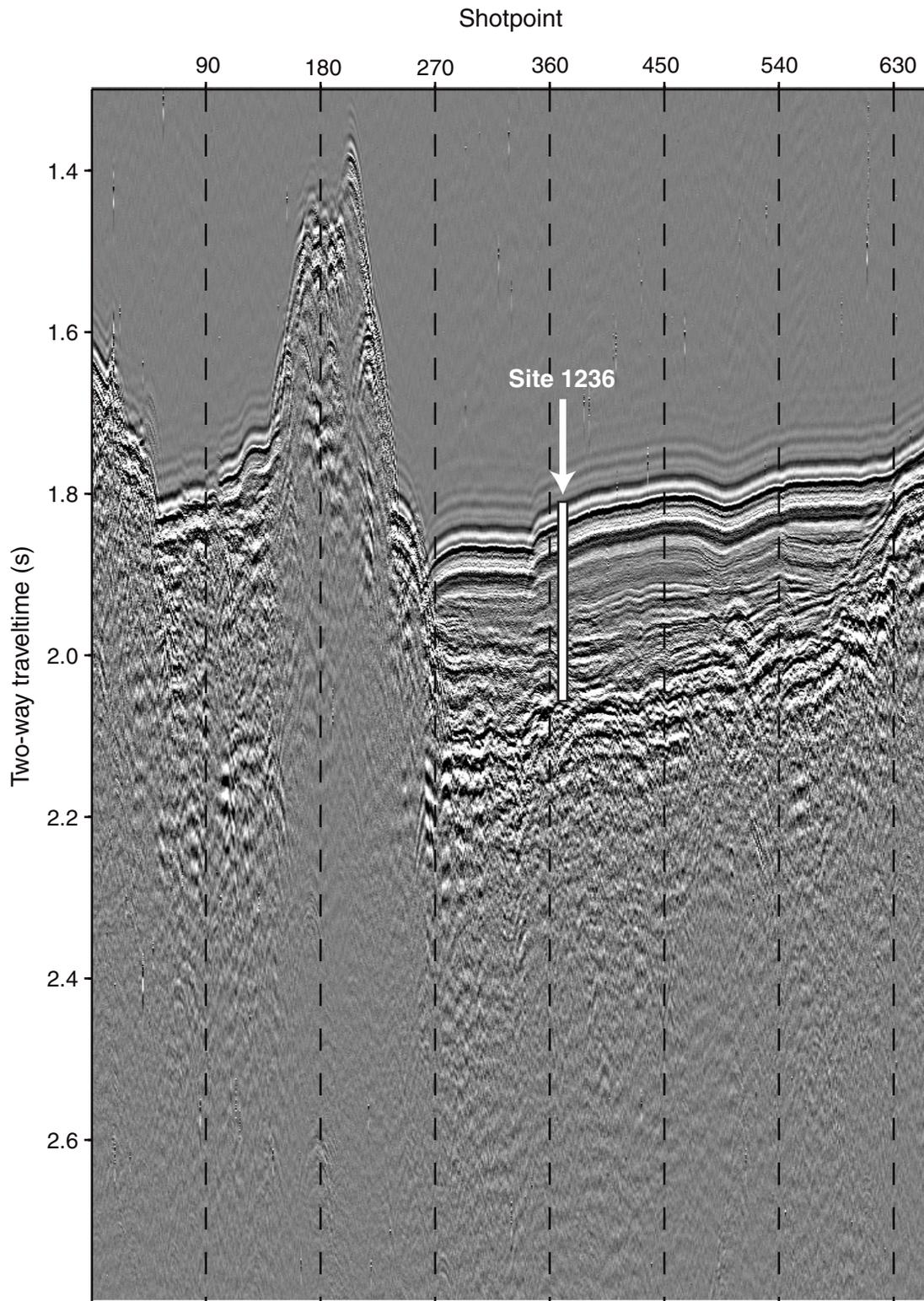Figure F3

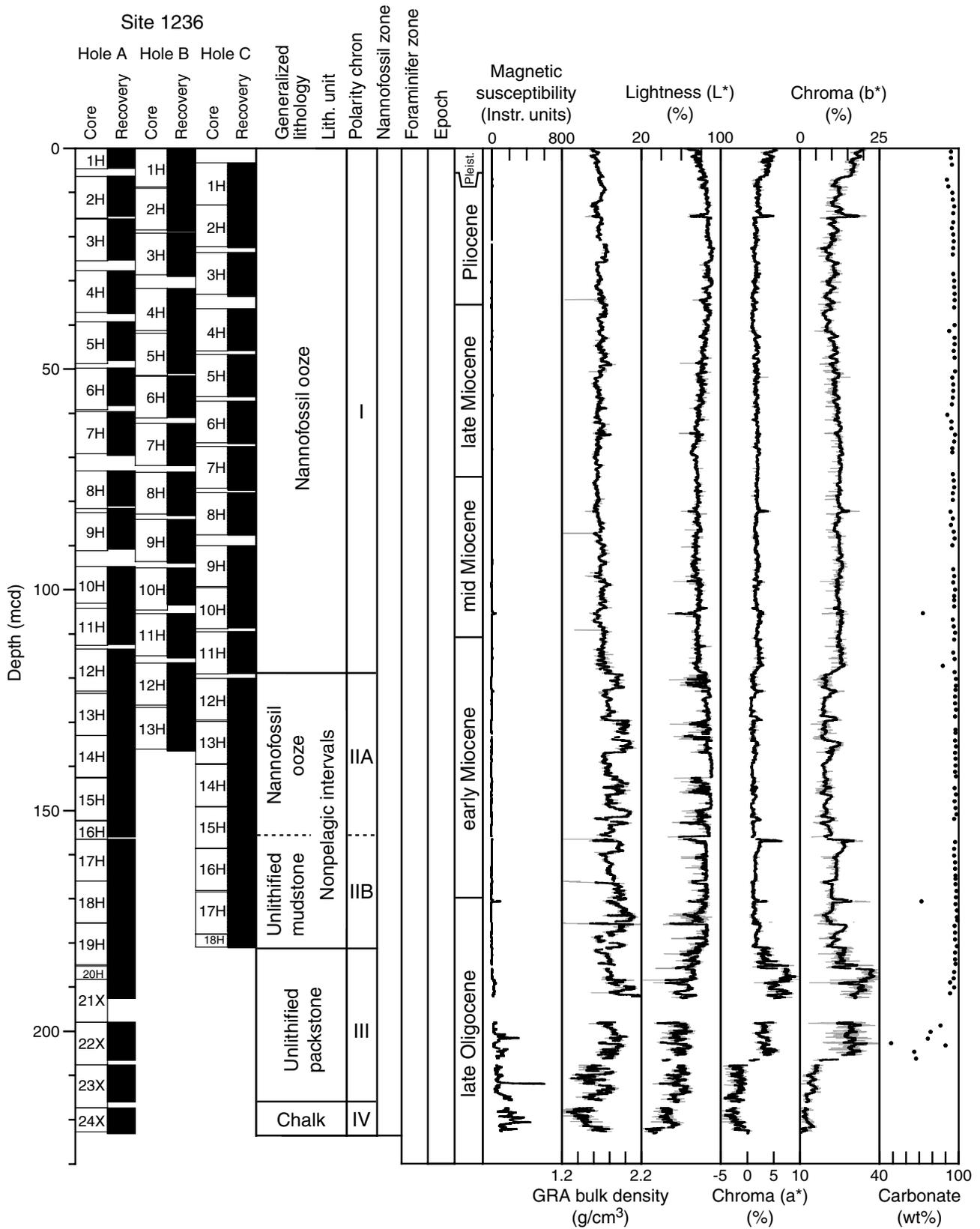Figure F4

**B**

Figure F4 (continued)

C
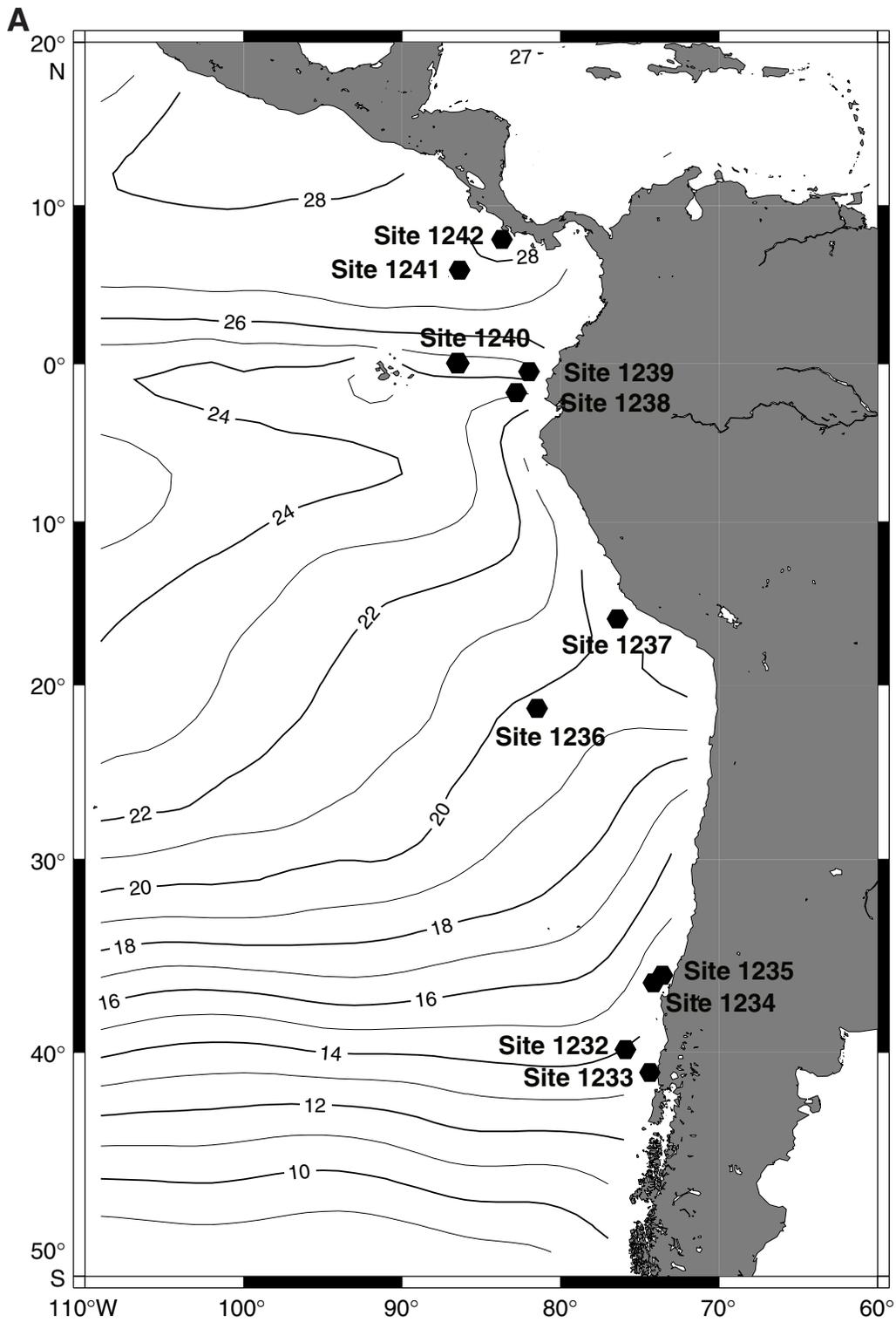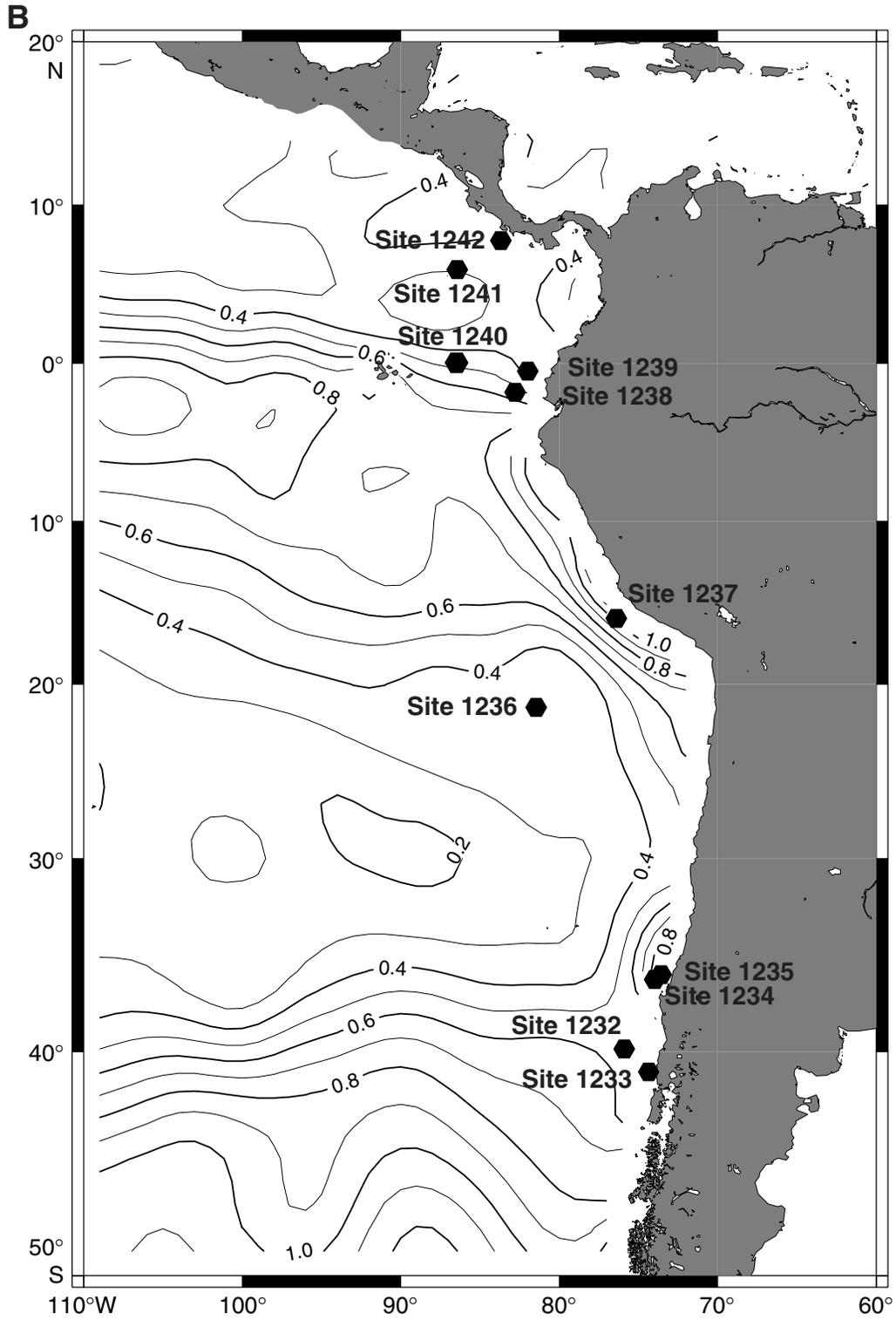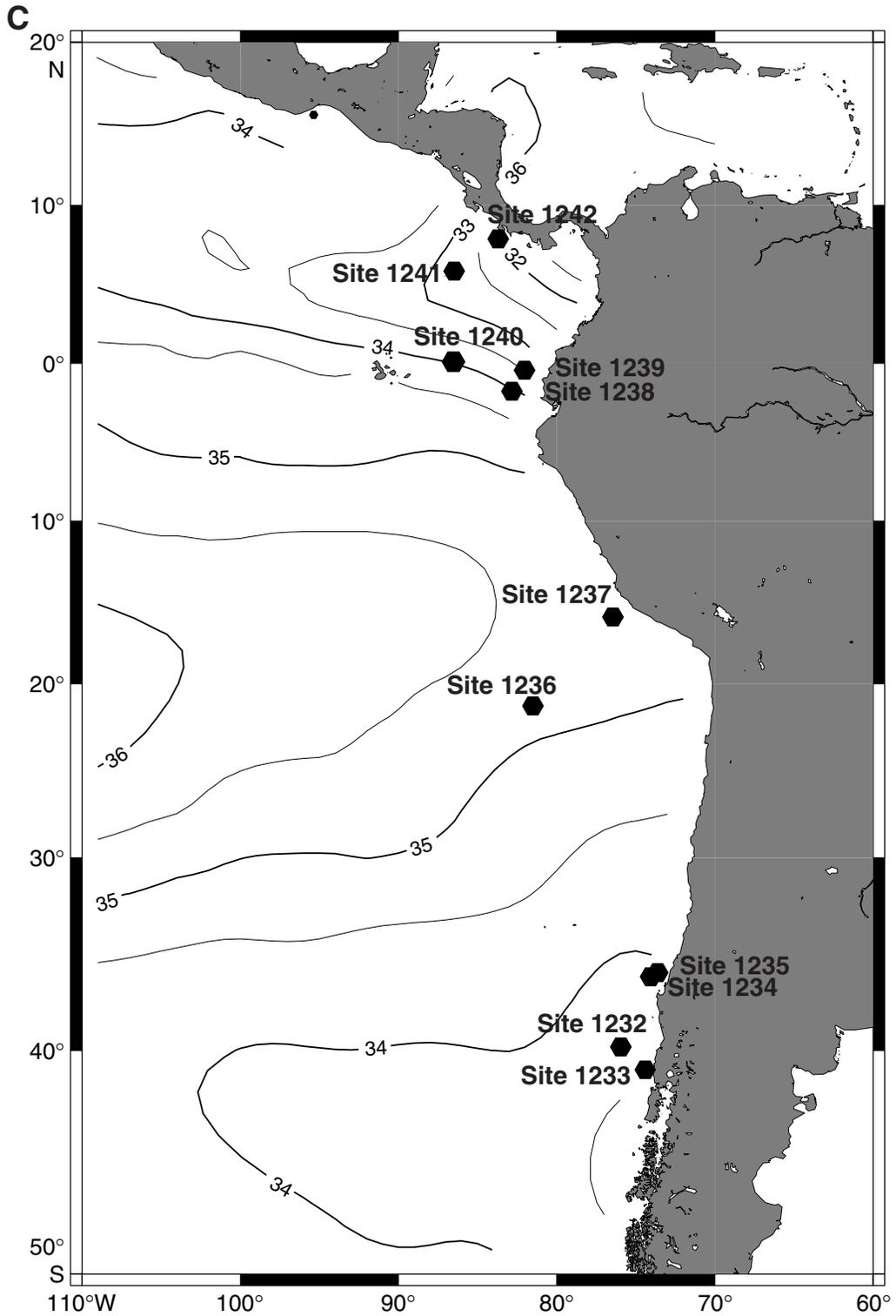
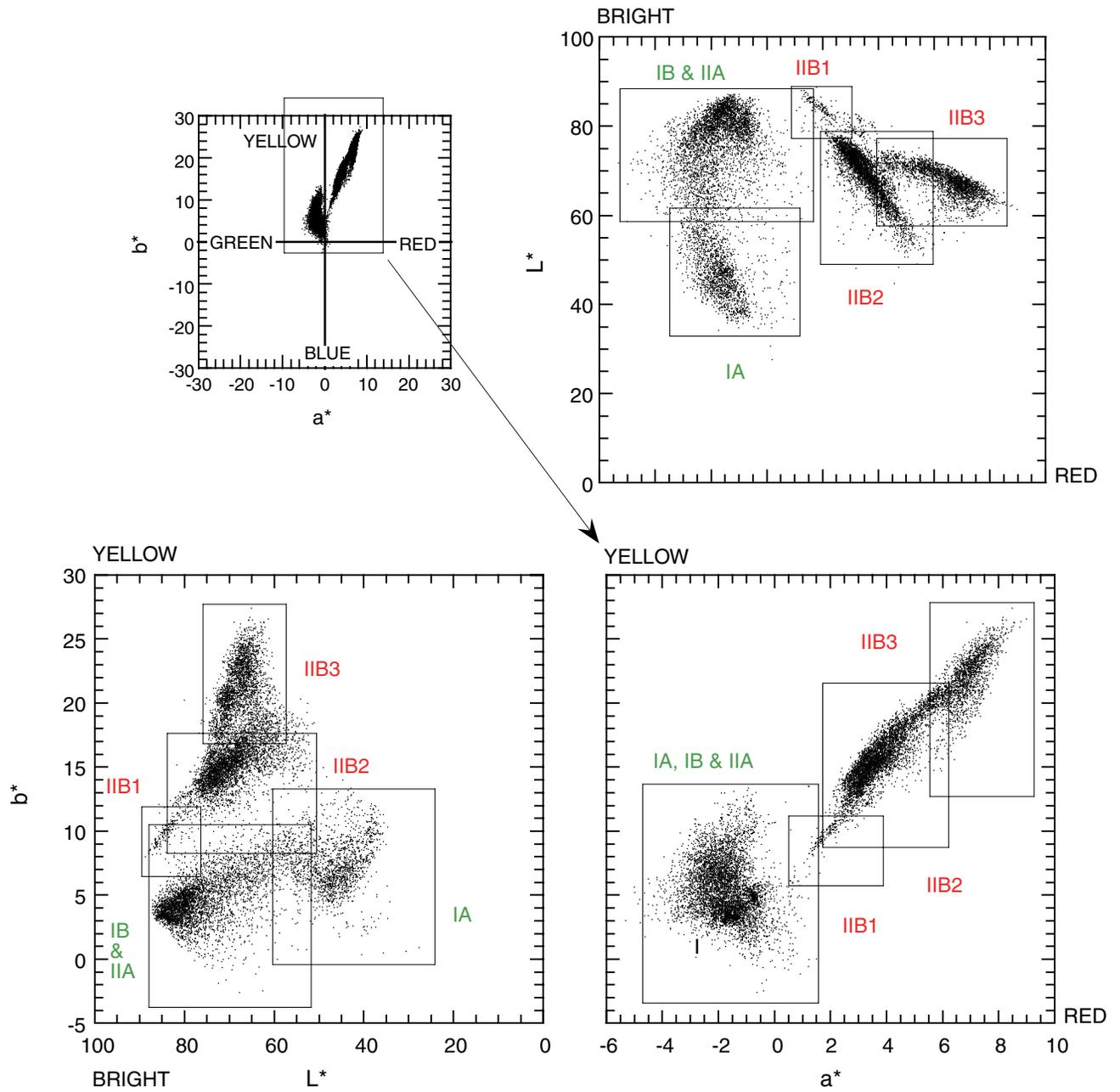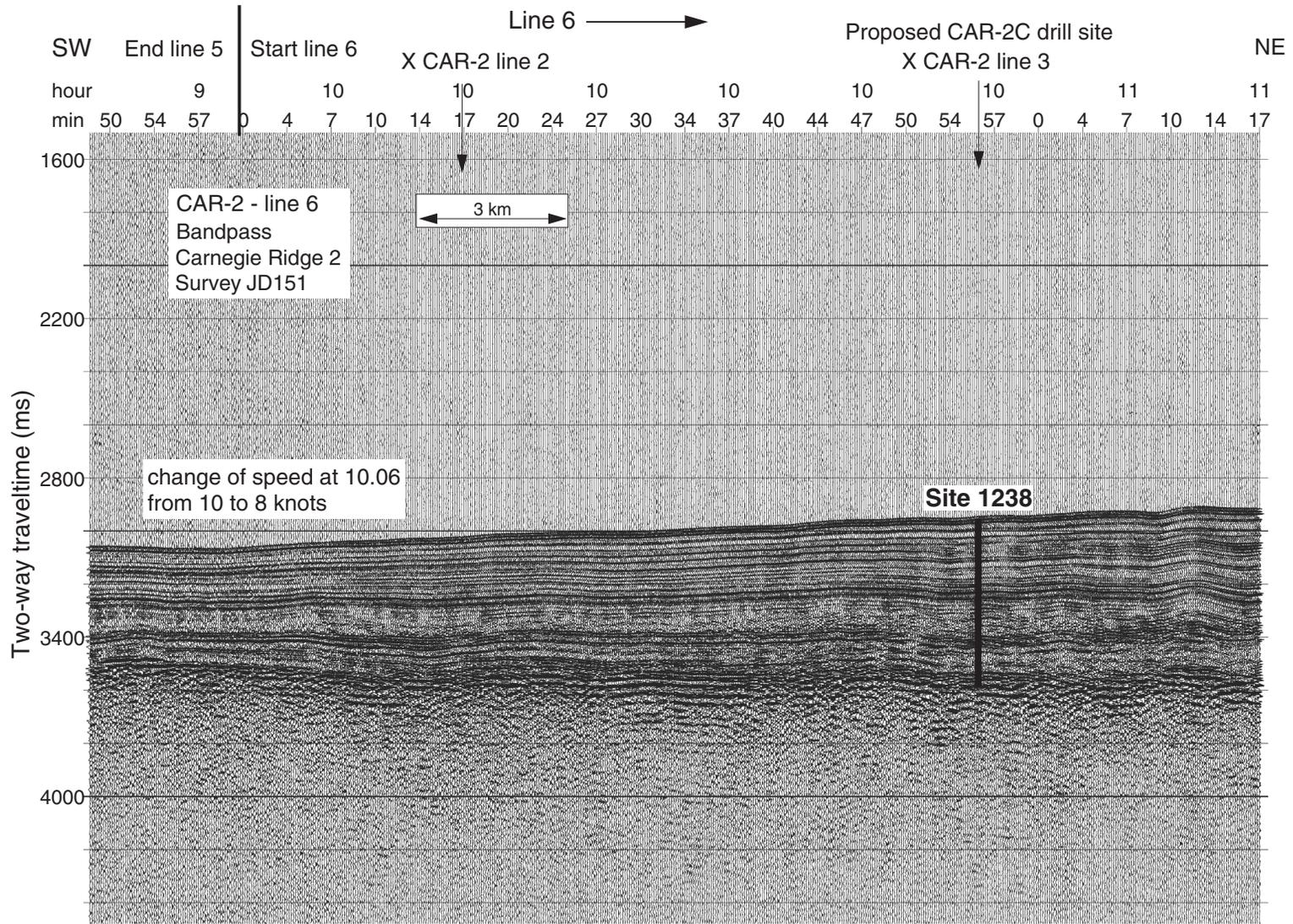Figure F4 (continued)
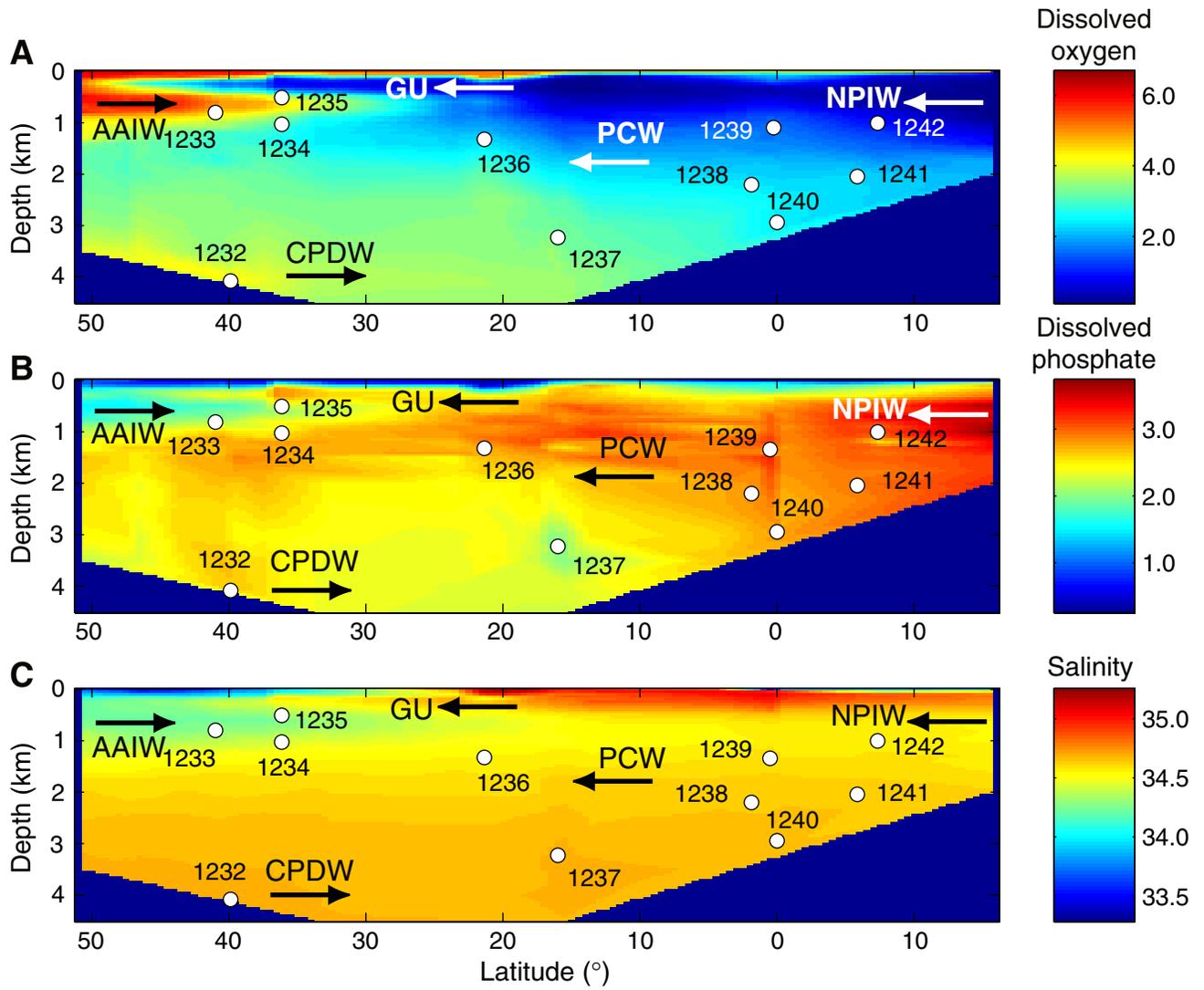
Figure F5
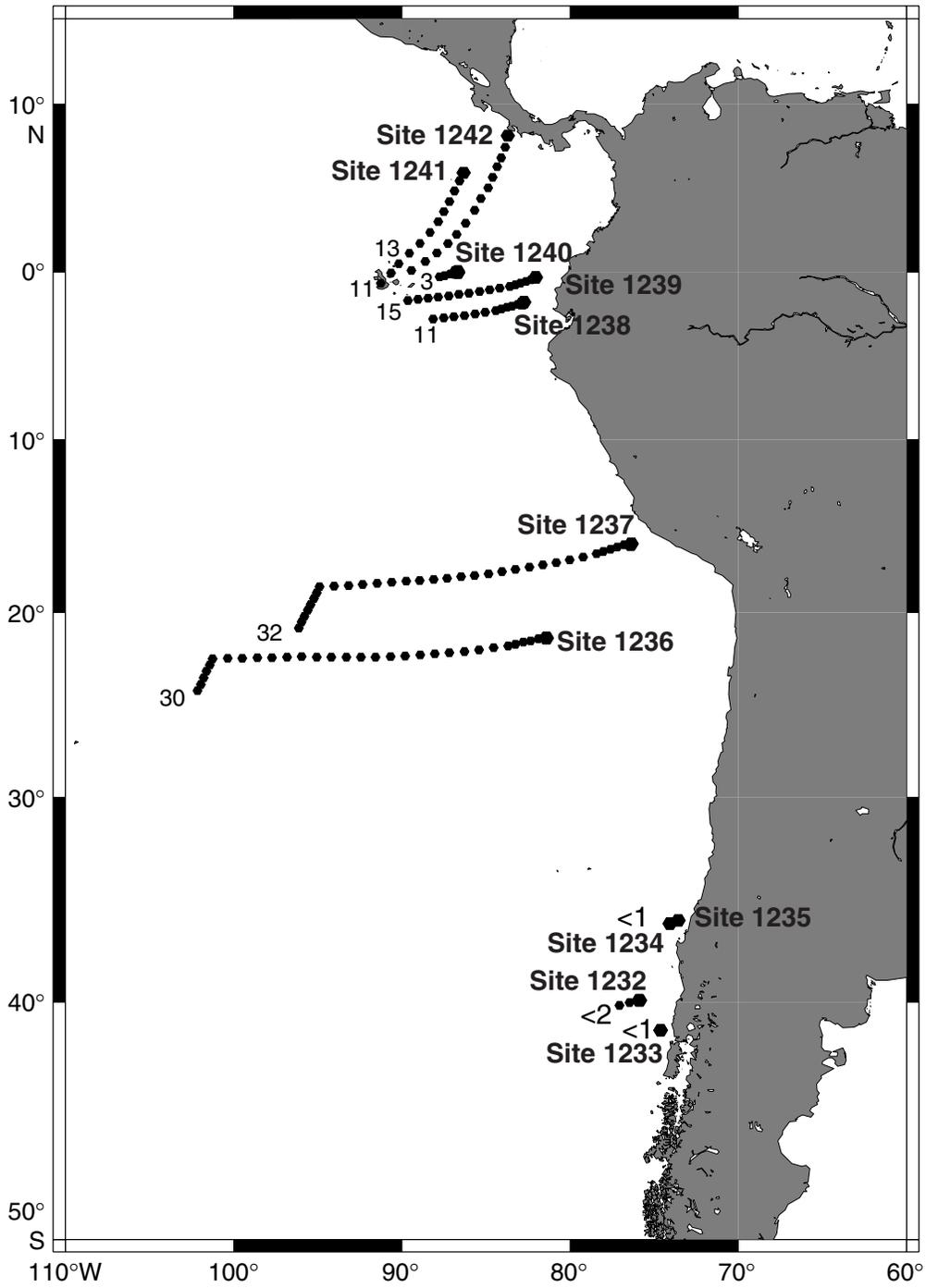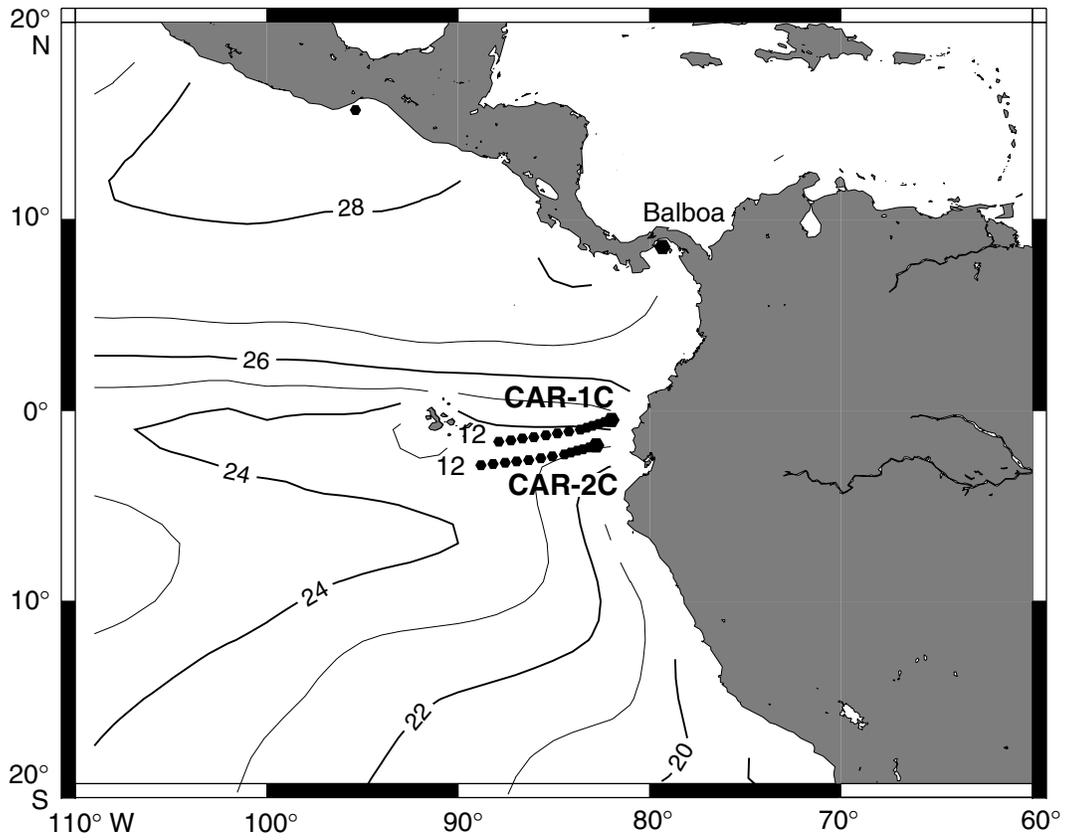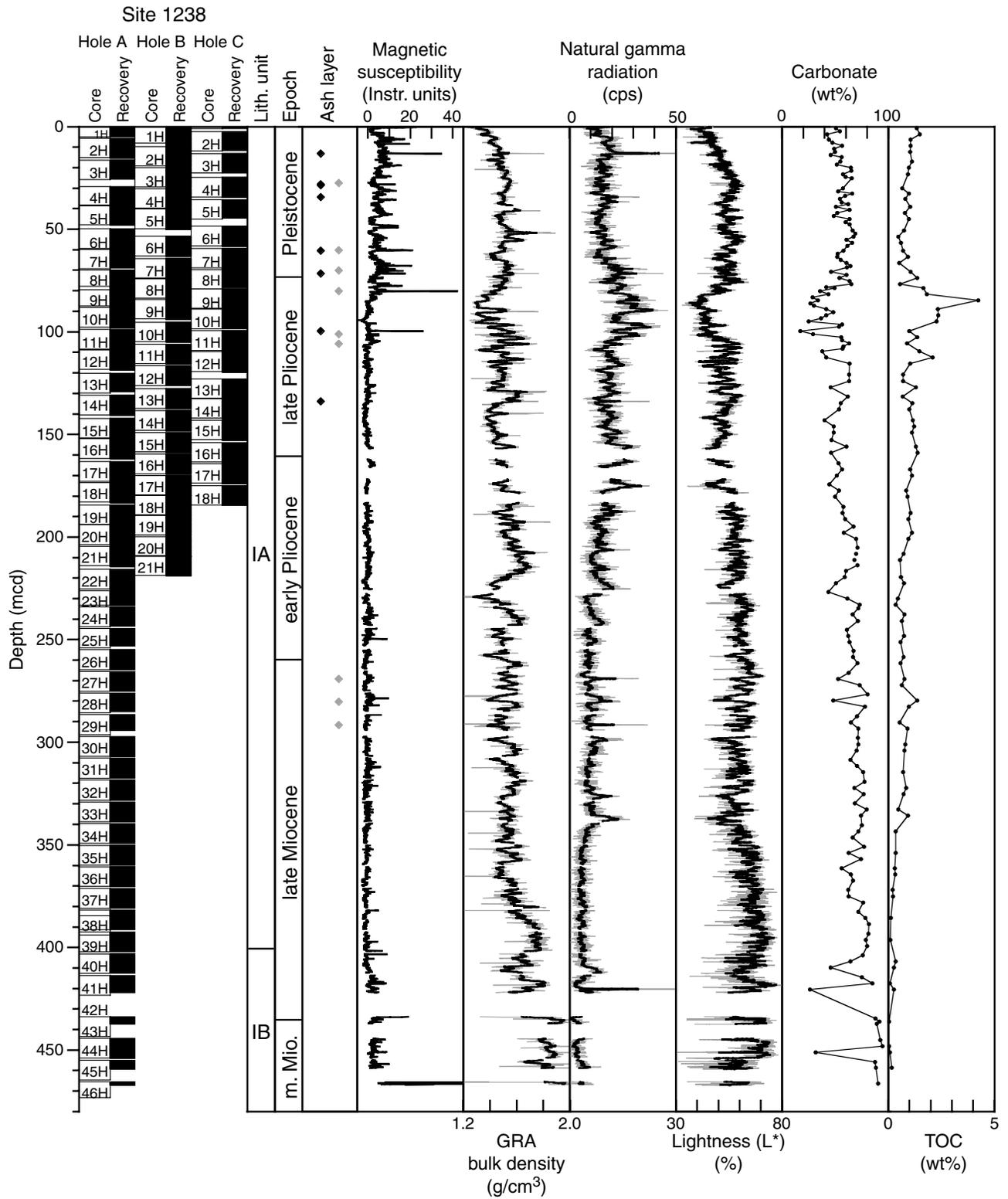
Figure F6
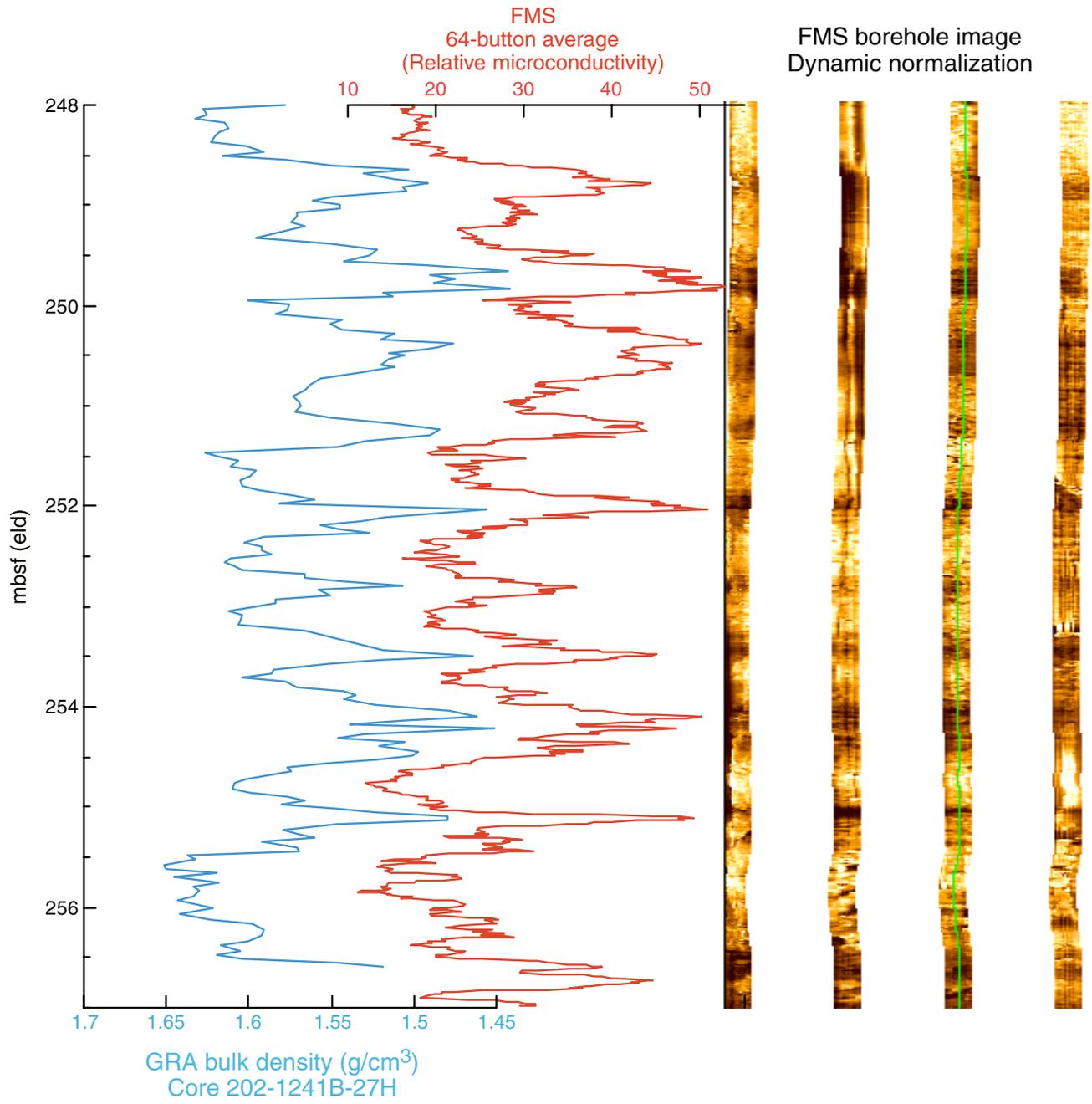
Figure F7
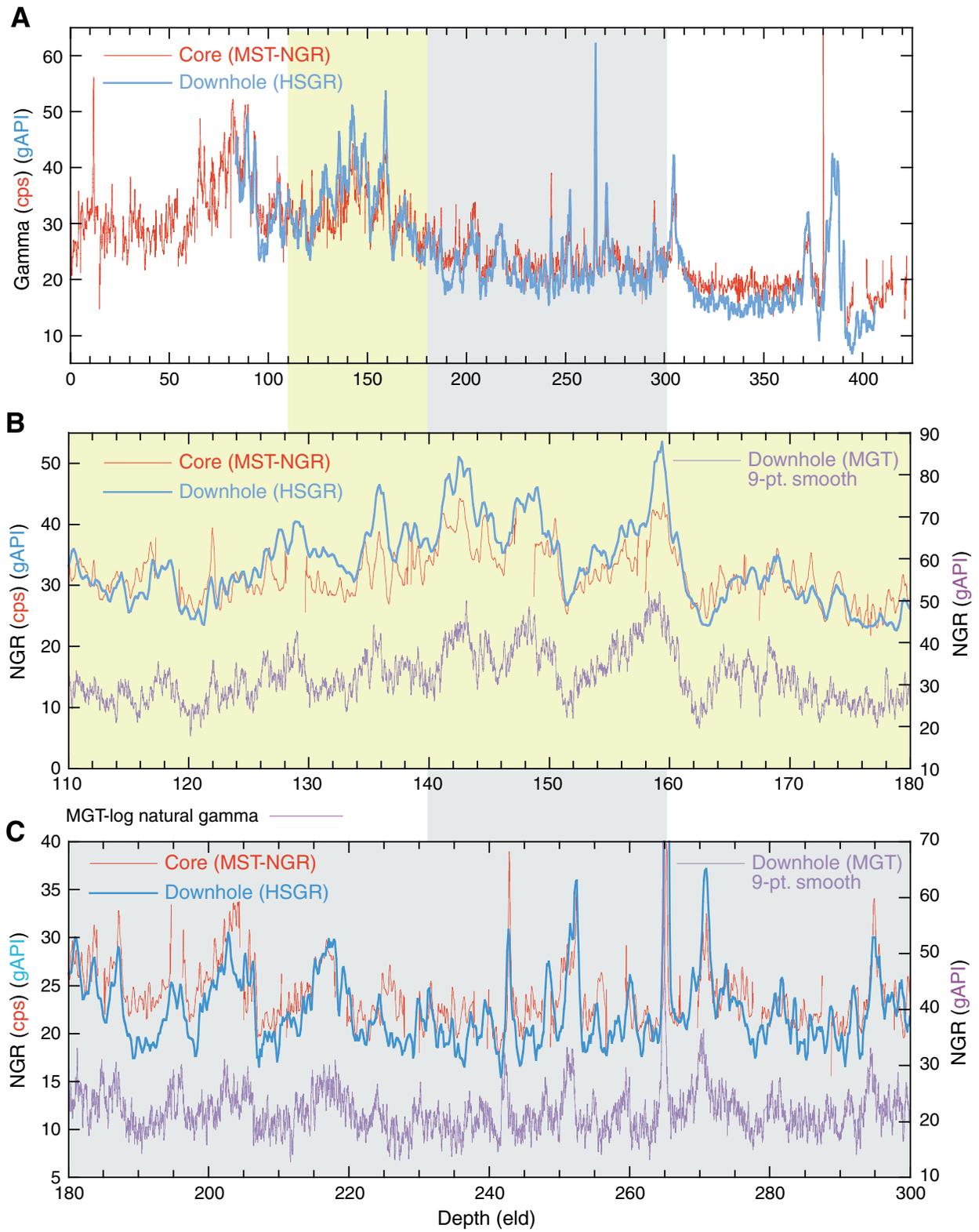
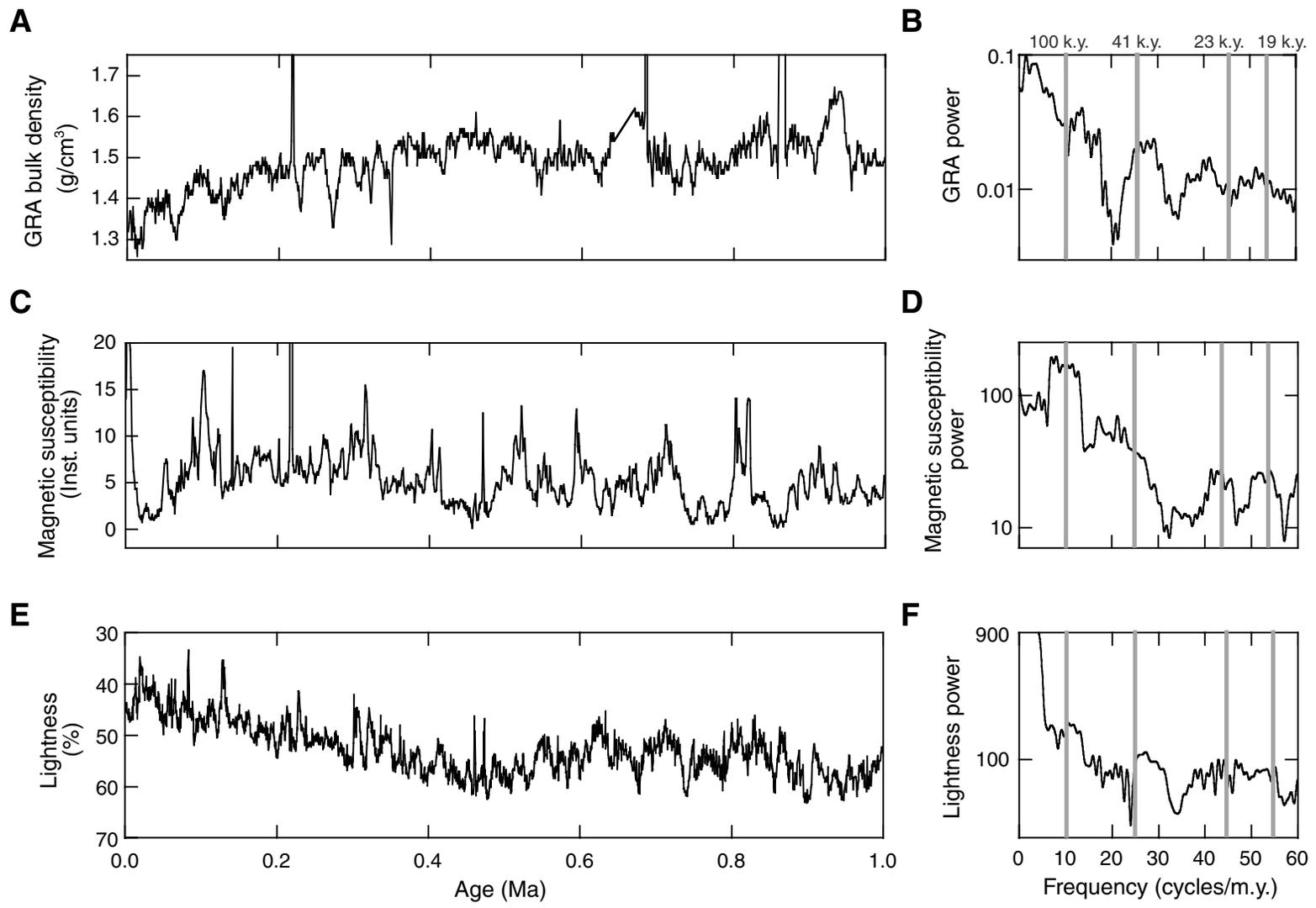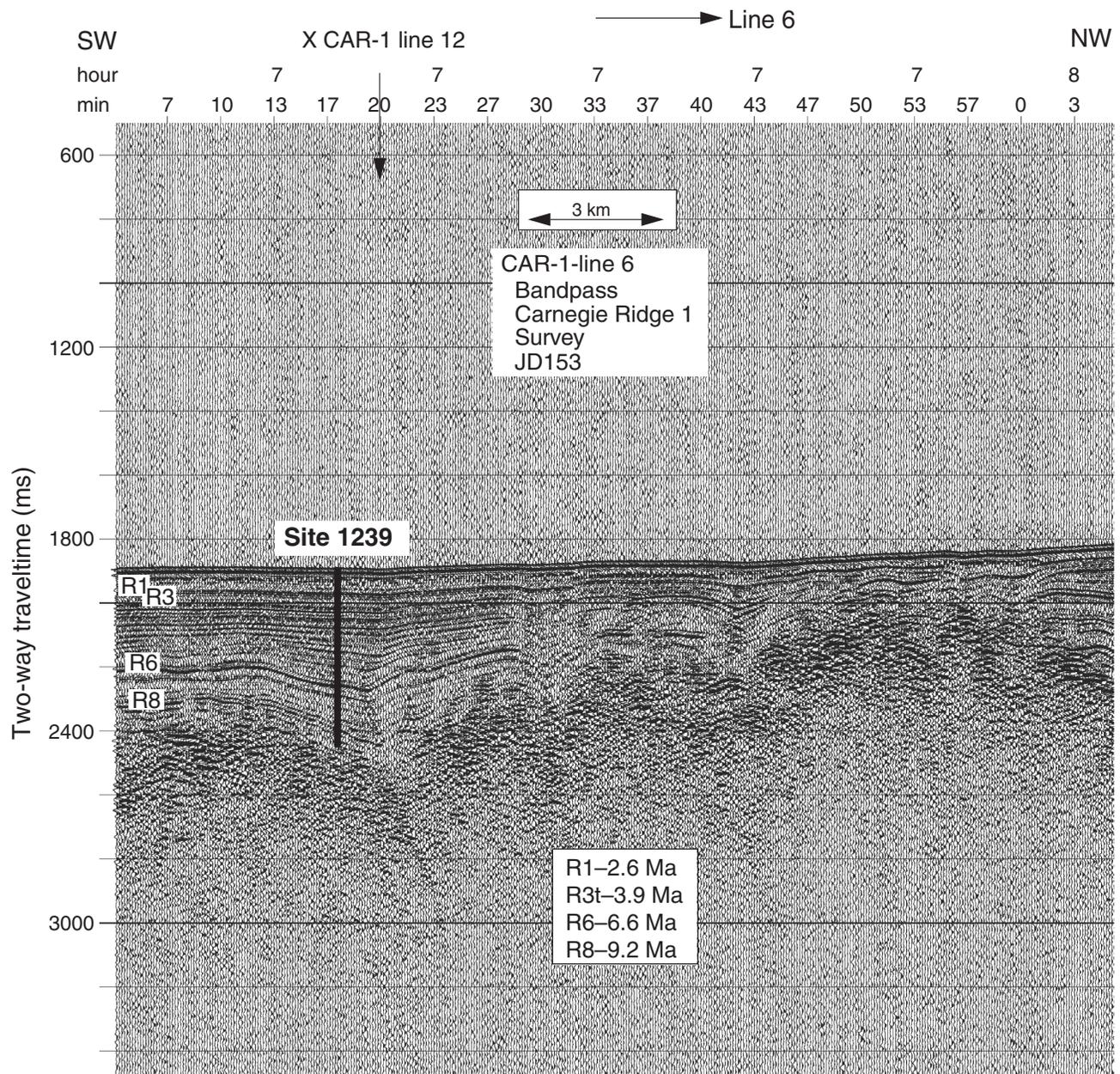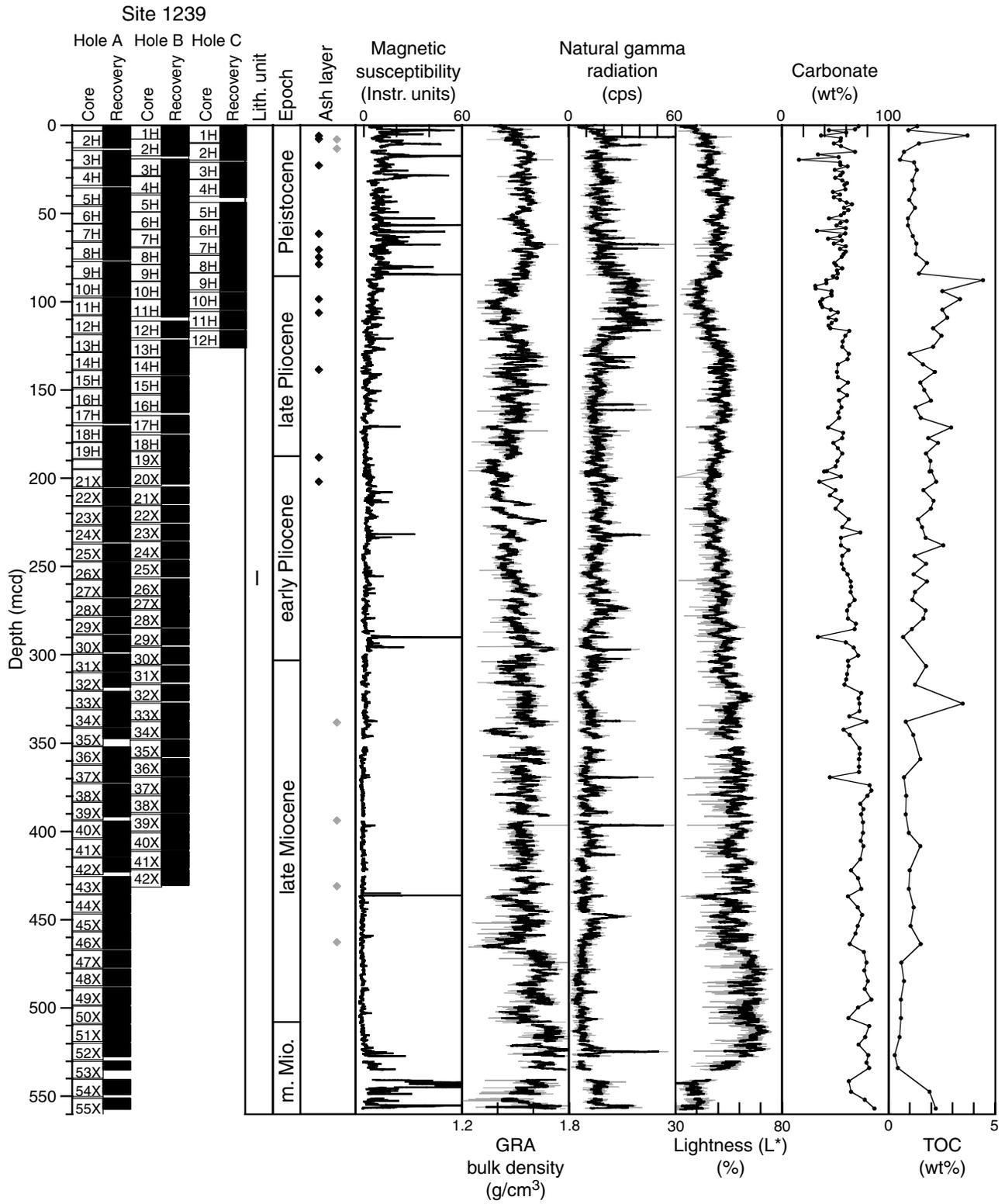Figure F8
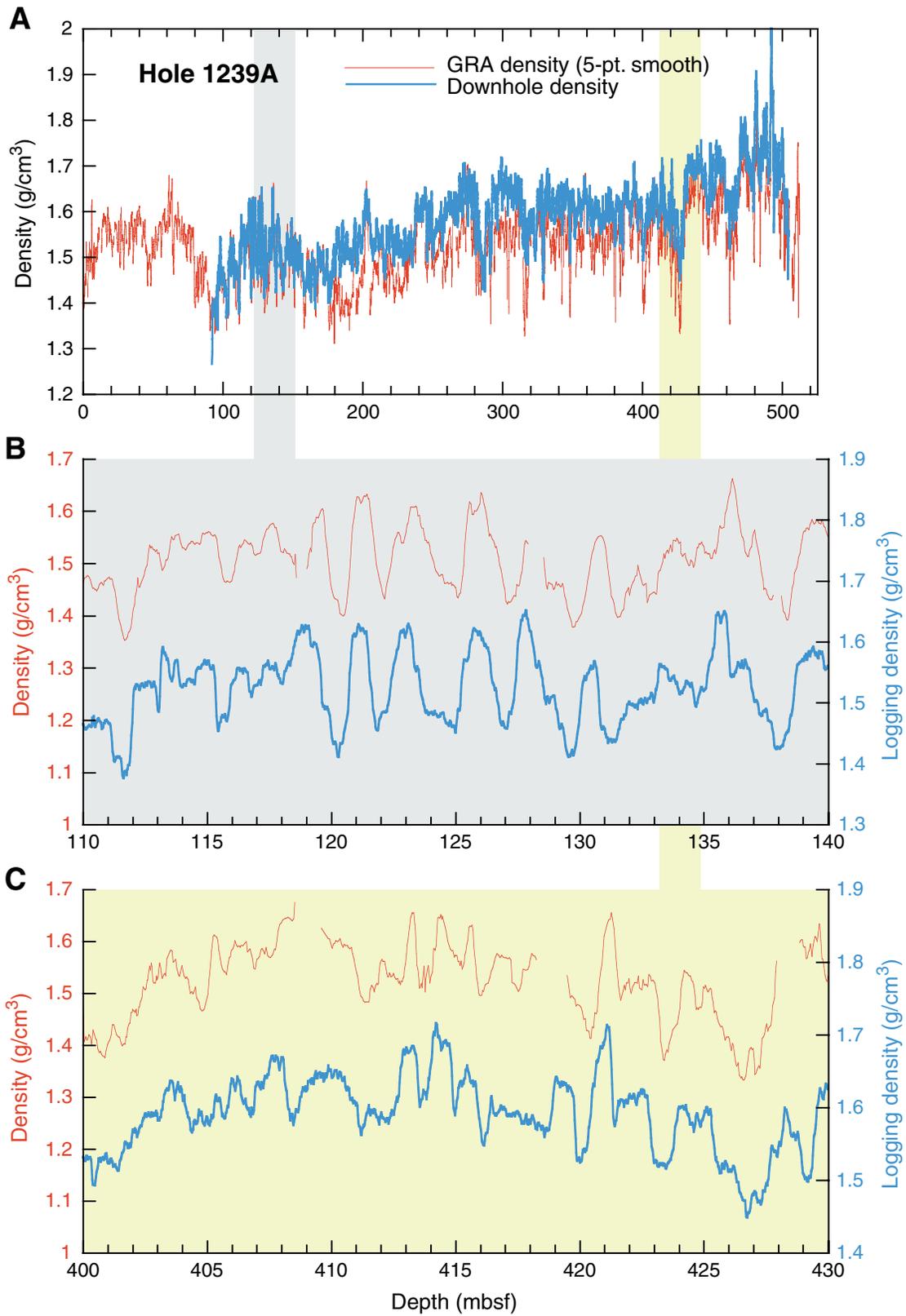
Figure F9
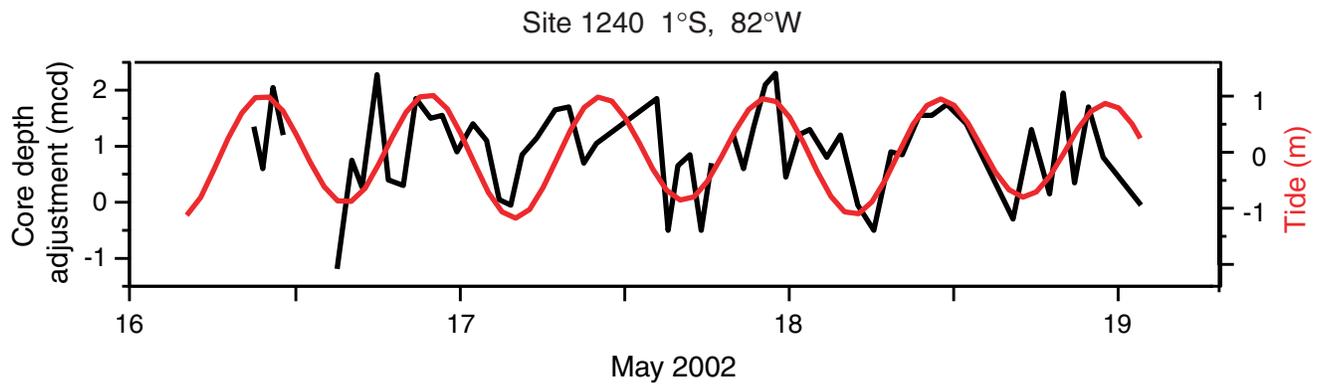
Figure F10
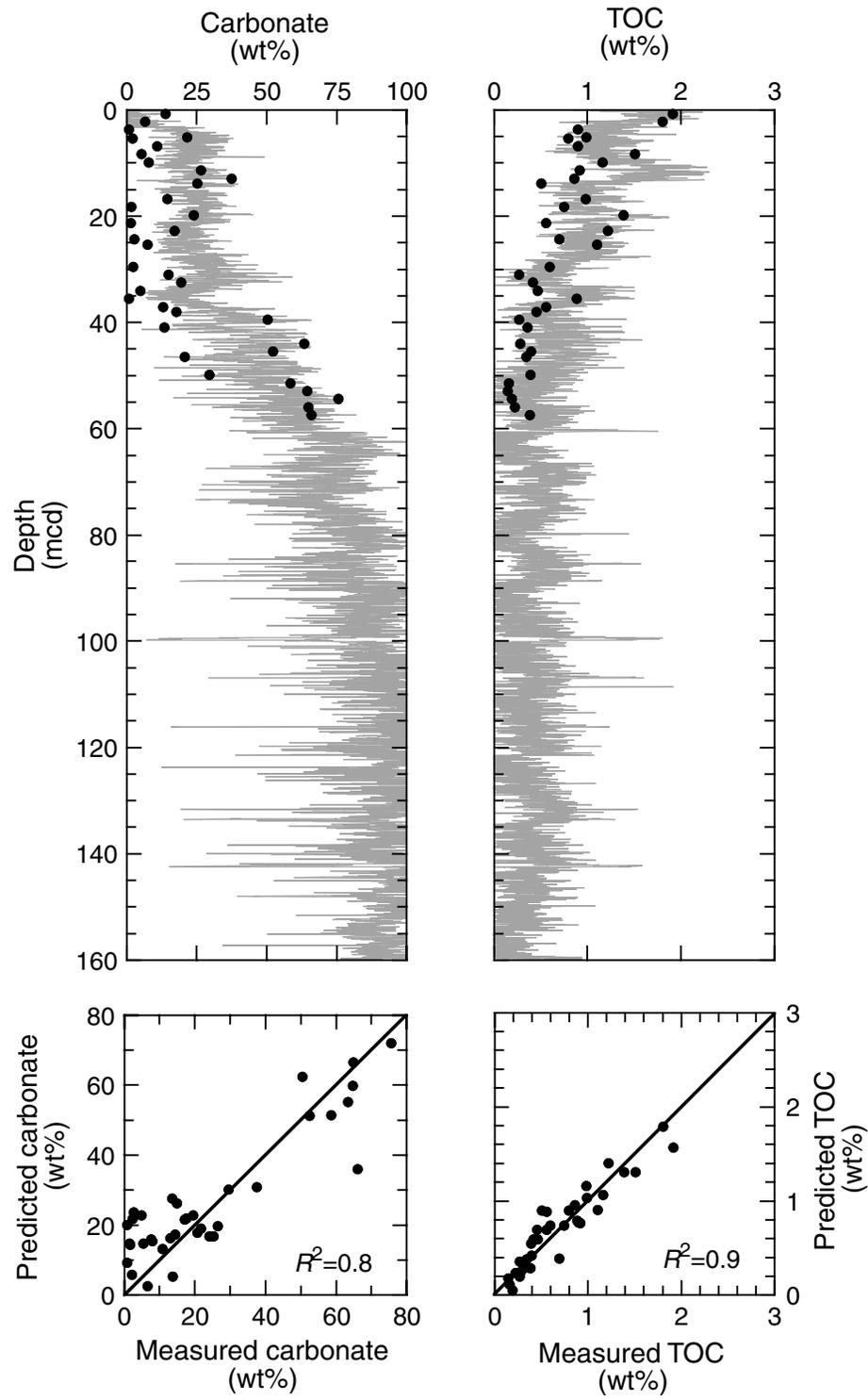
Figure F11
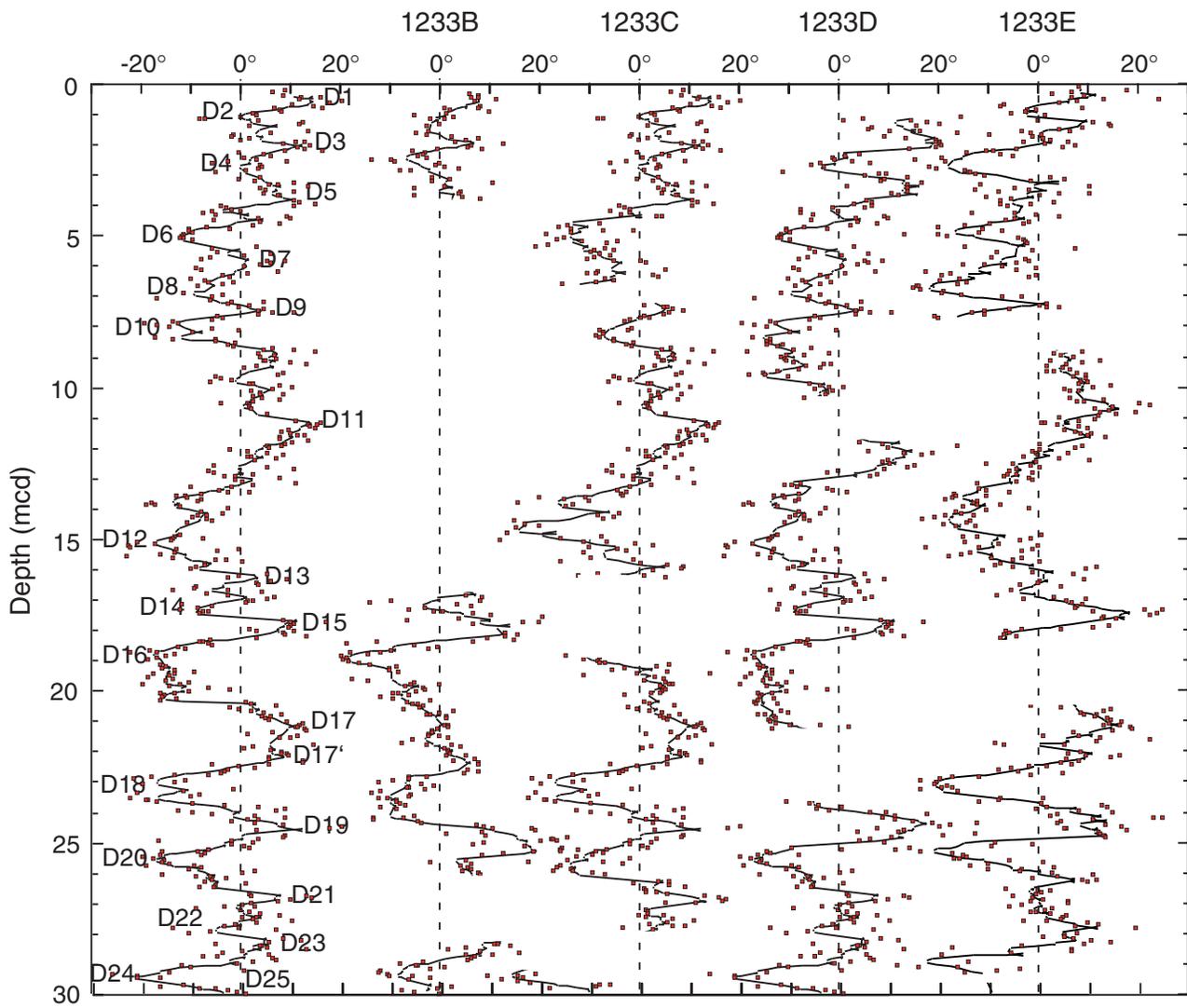
Figure F12
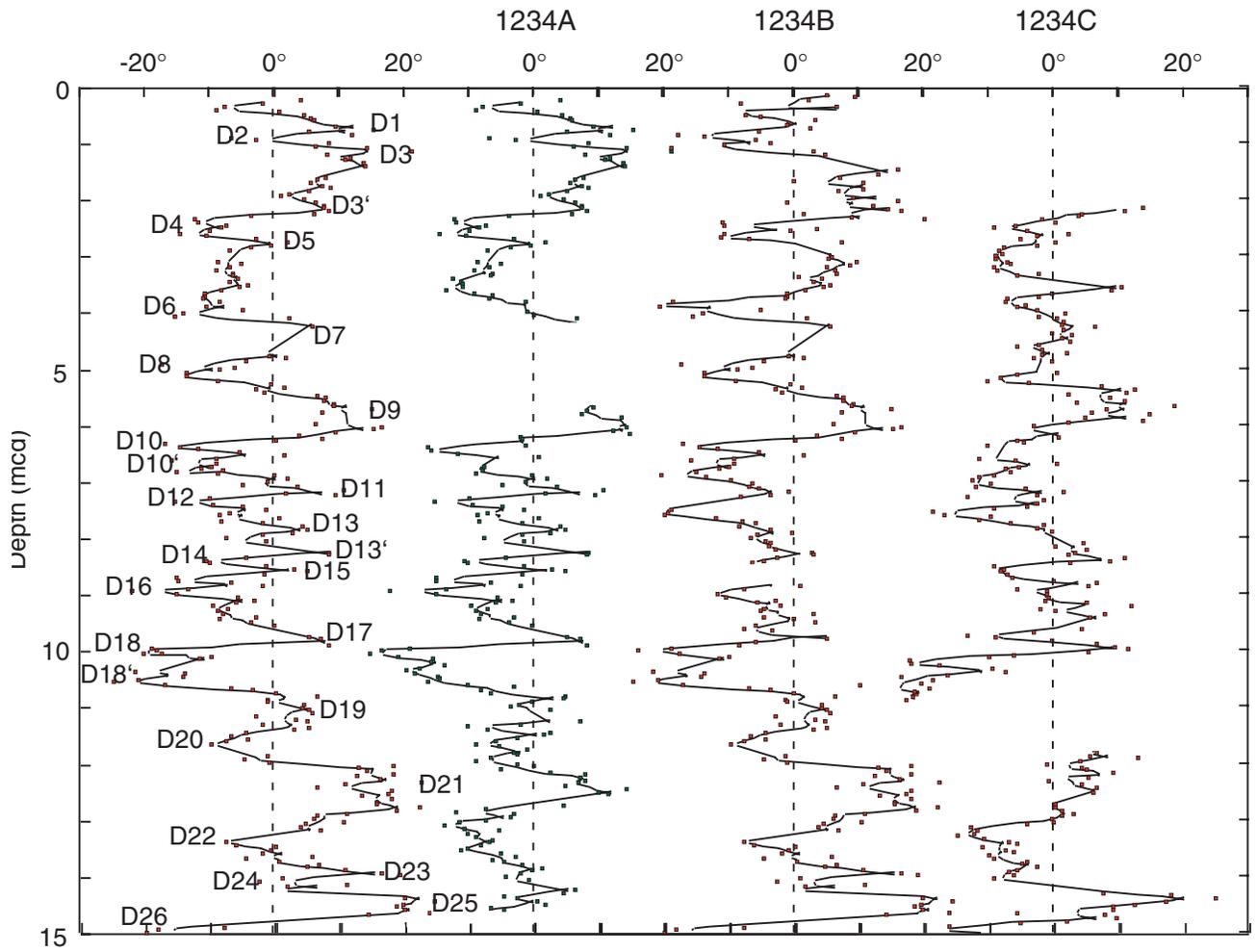
Figure F13
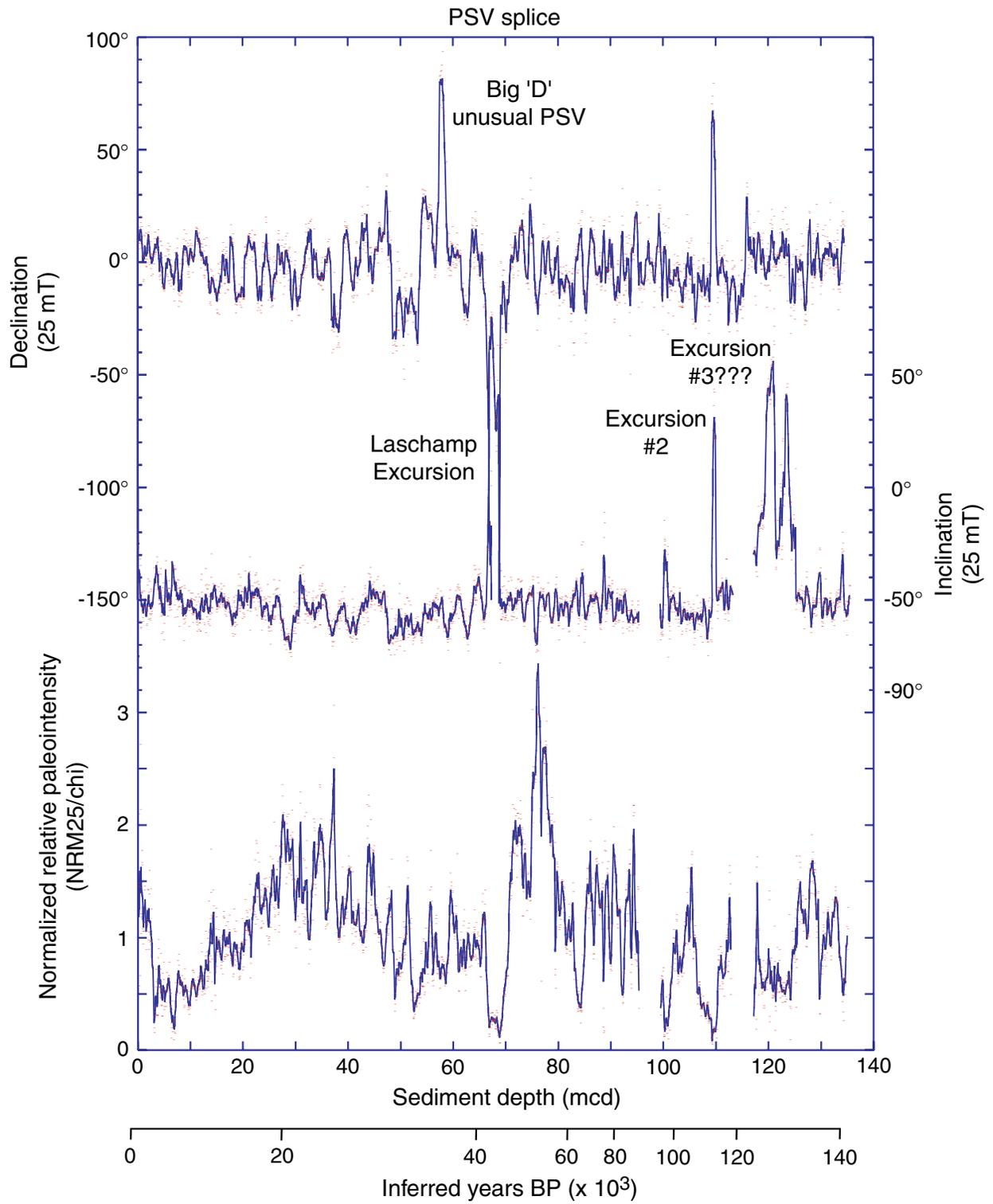
Figure F14
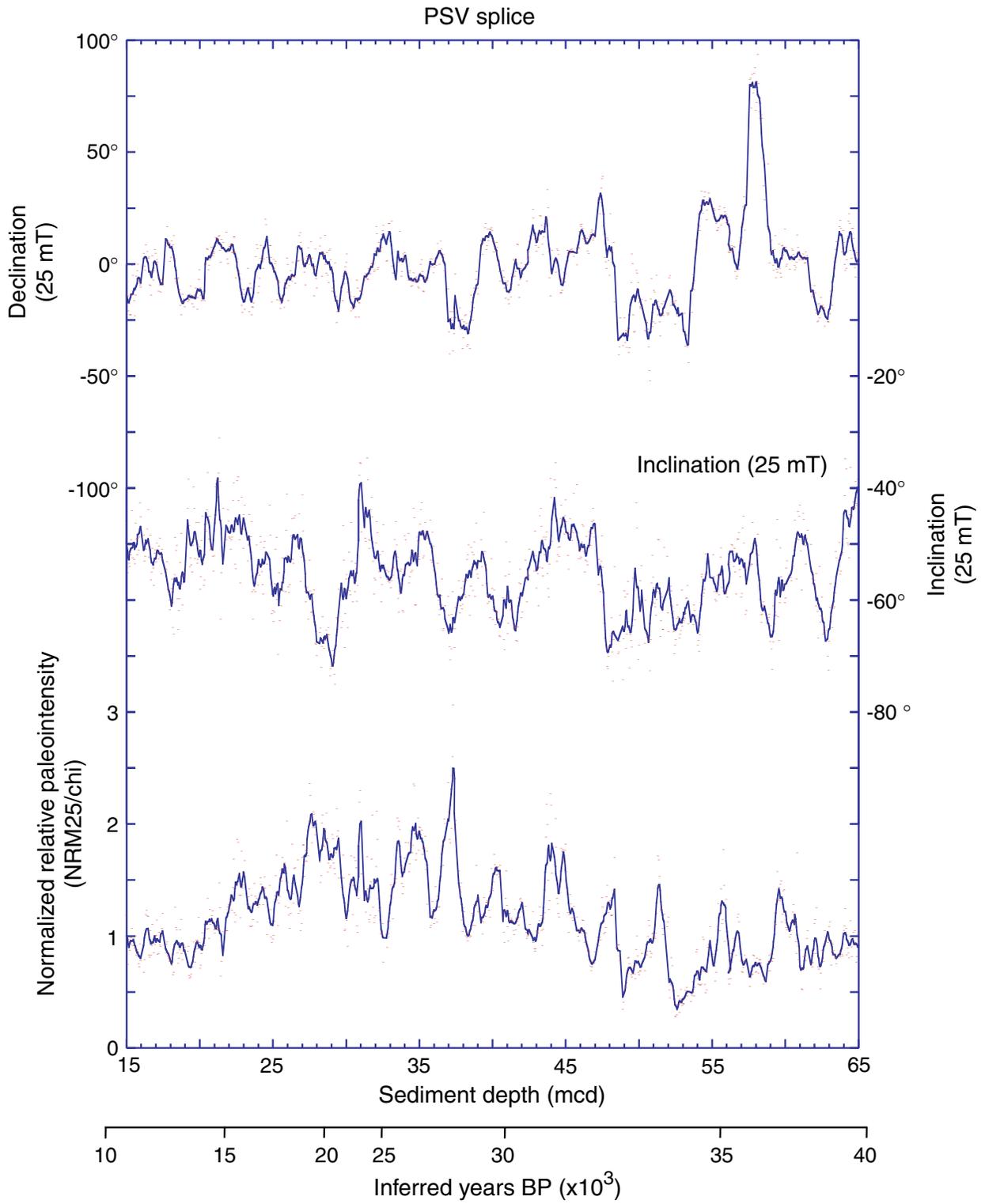
Figure F15
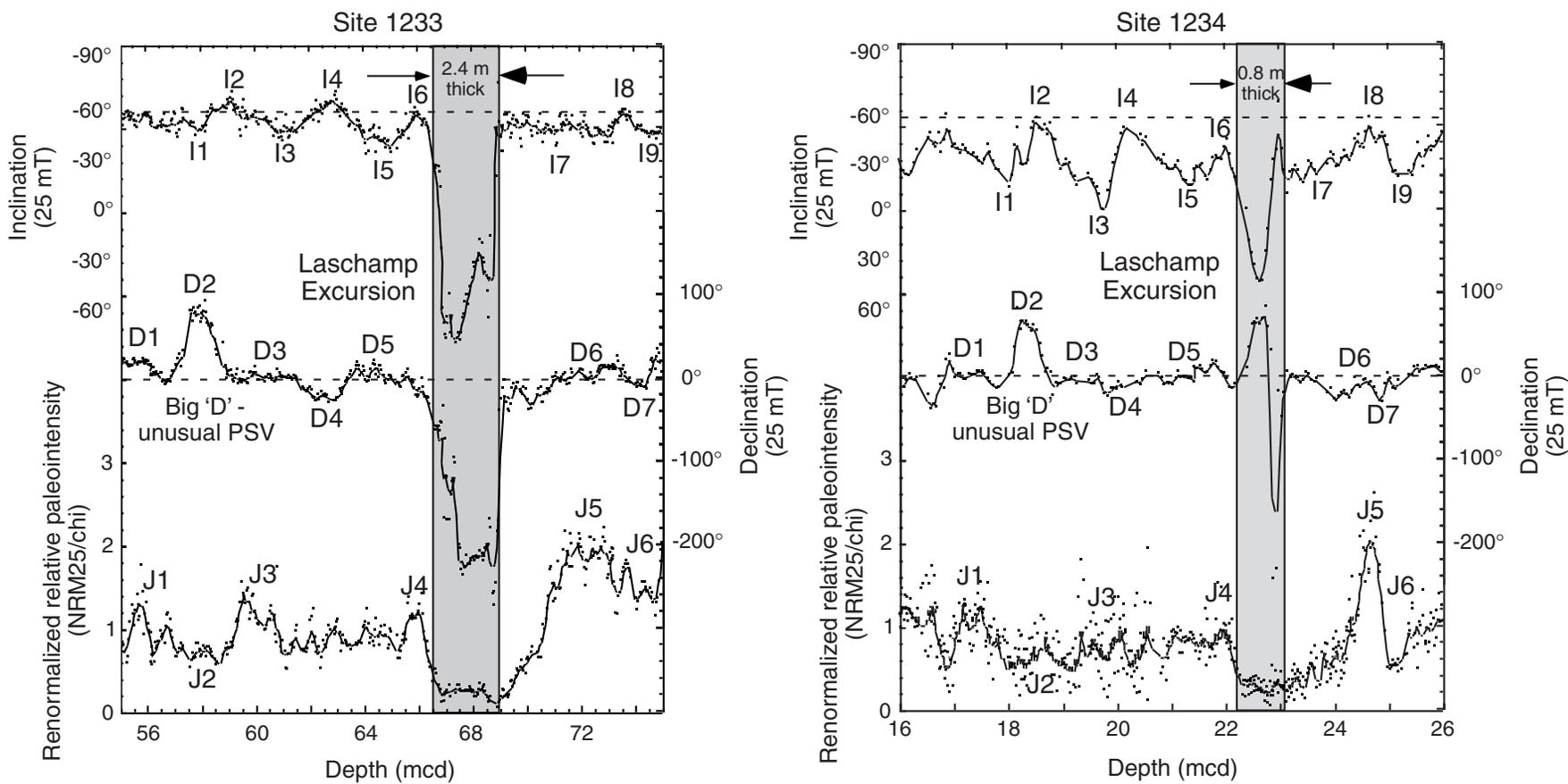
Figure F16
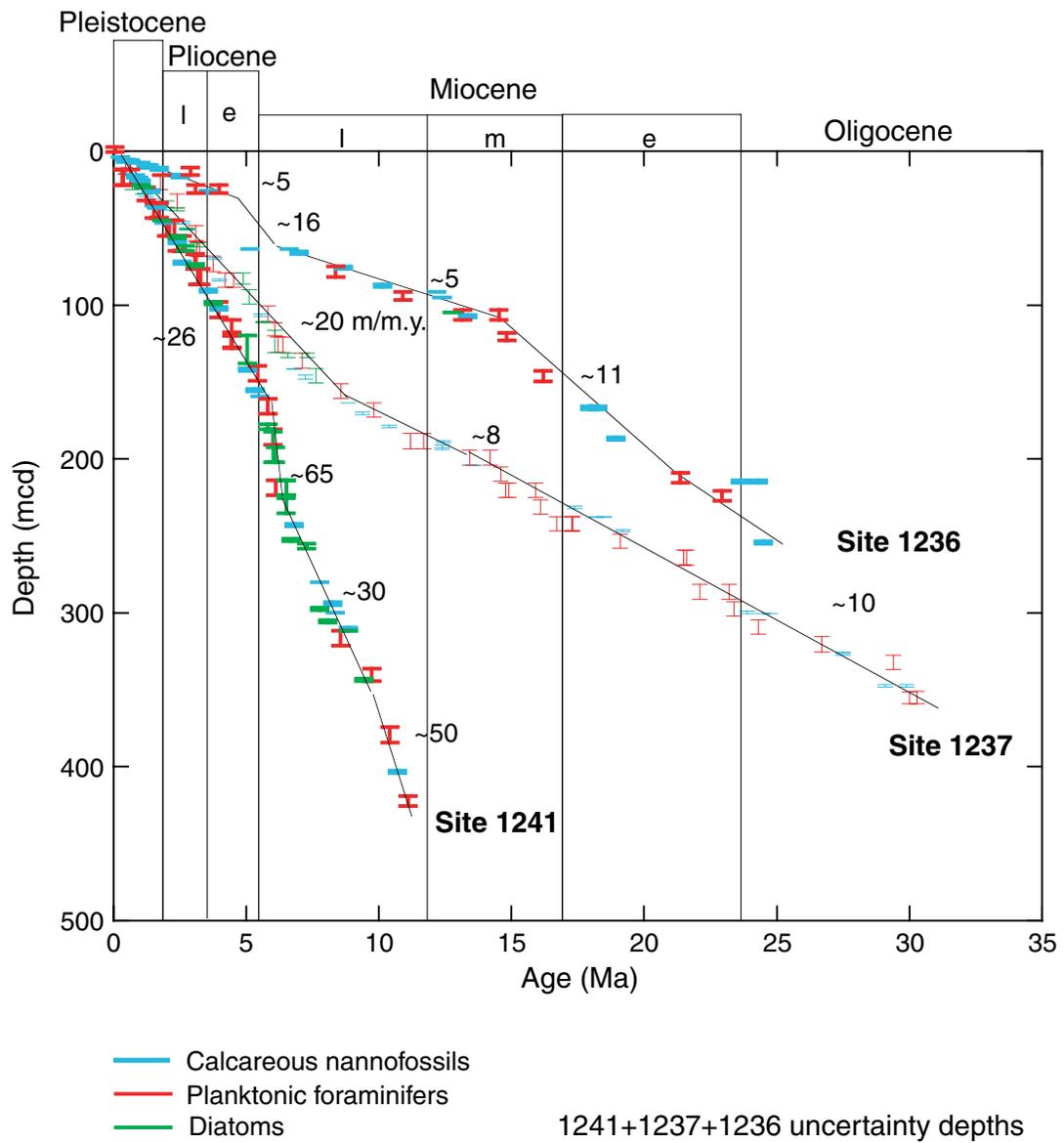
Figure F17
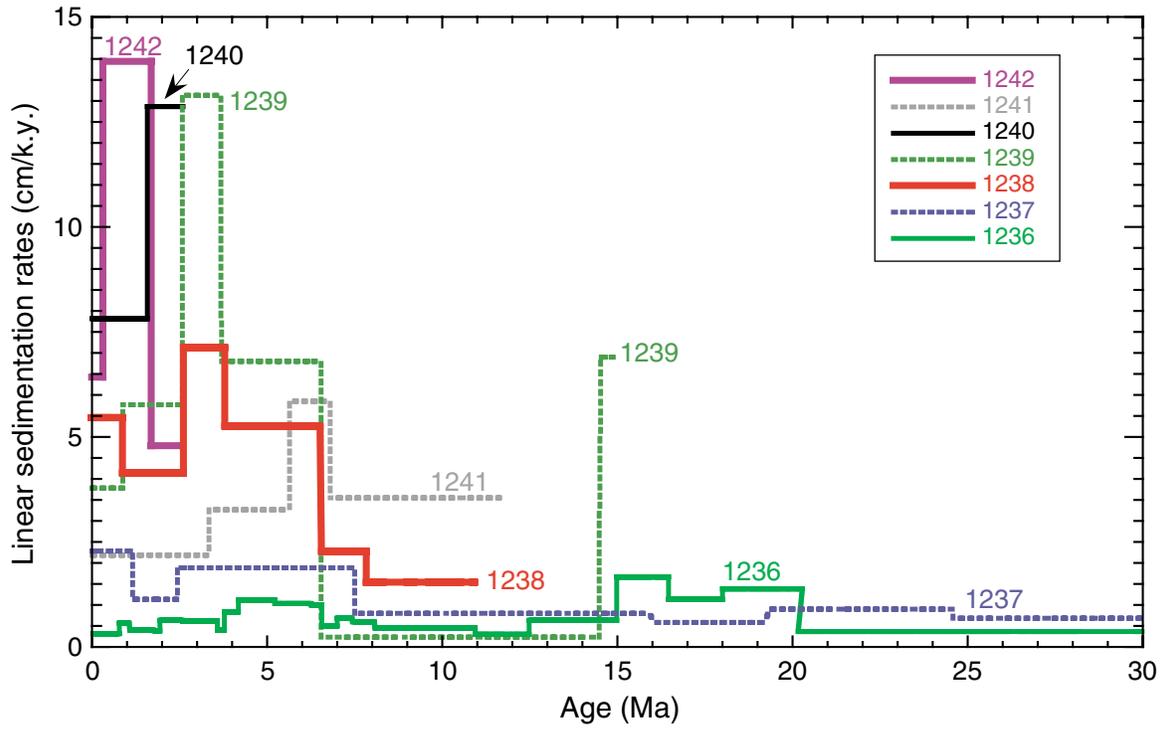
Figure F18
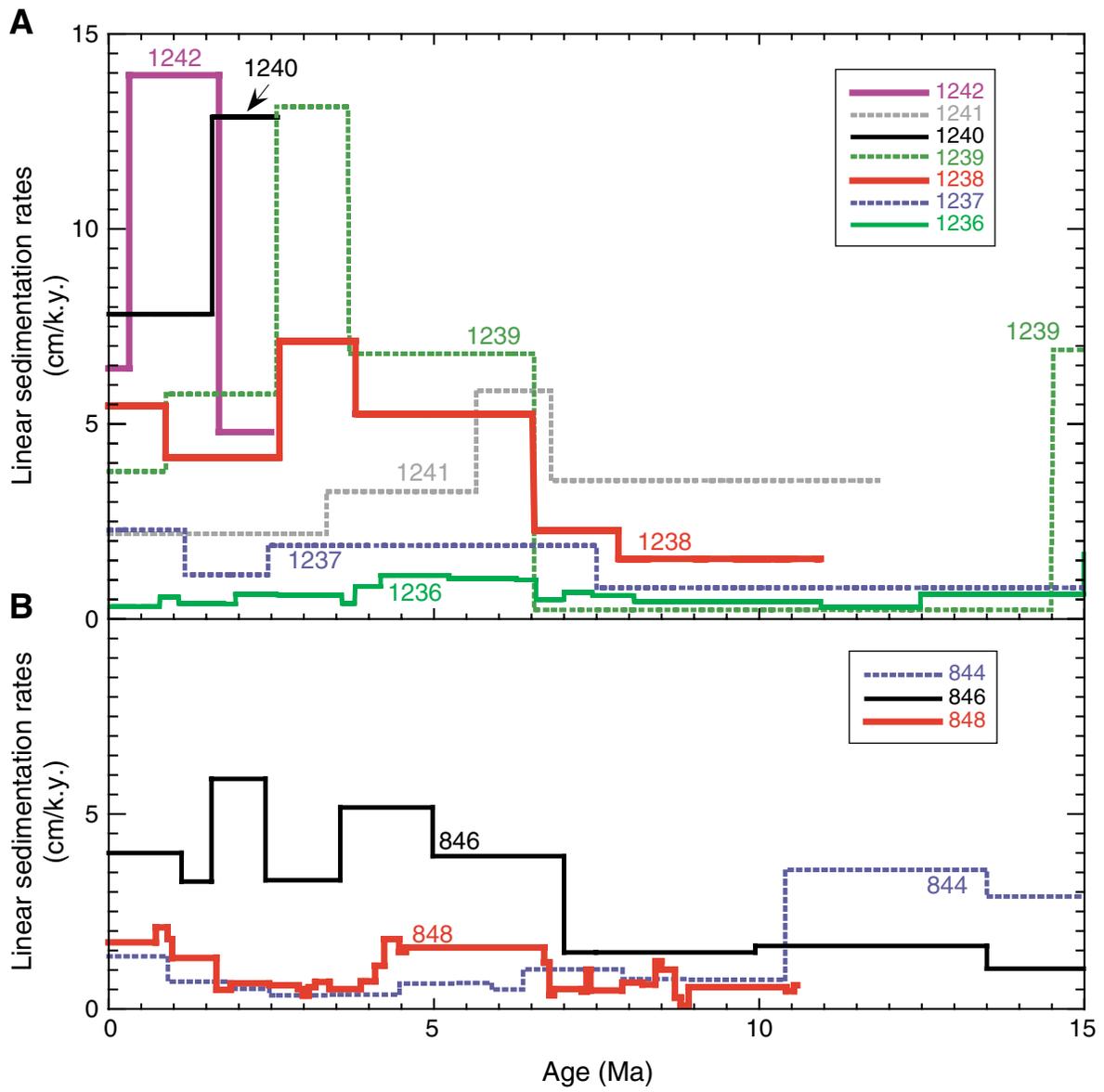
Figure F19
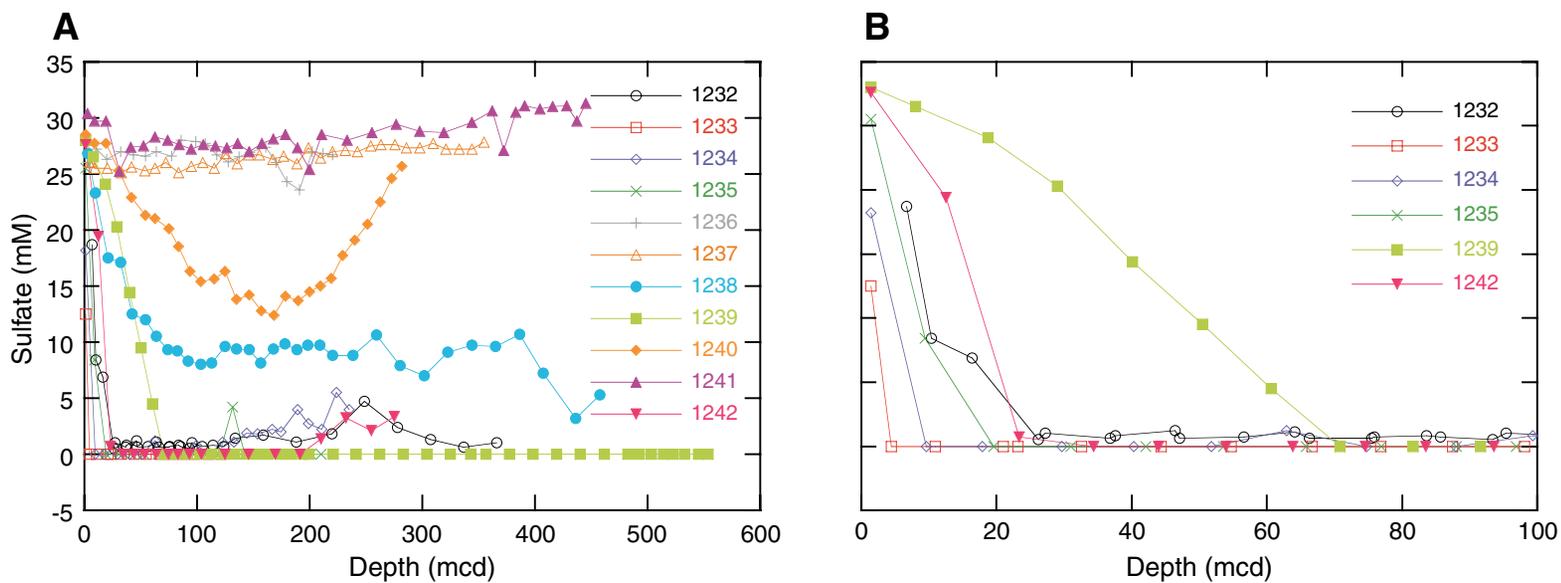
Figure F20
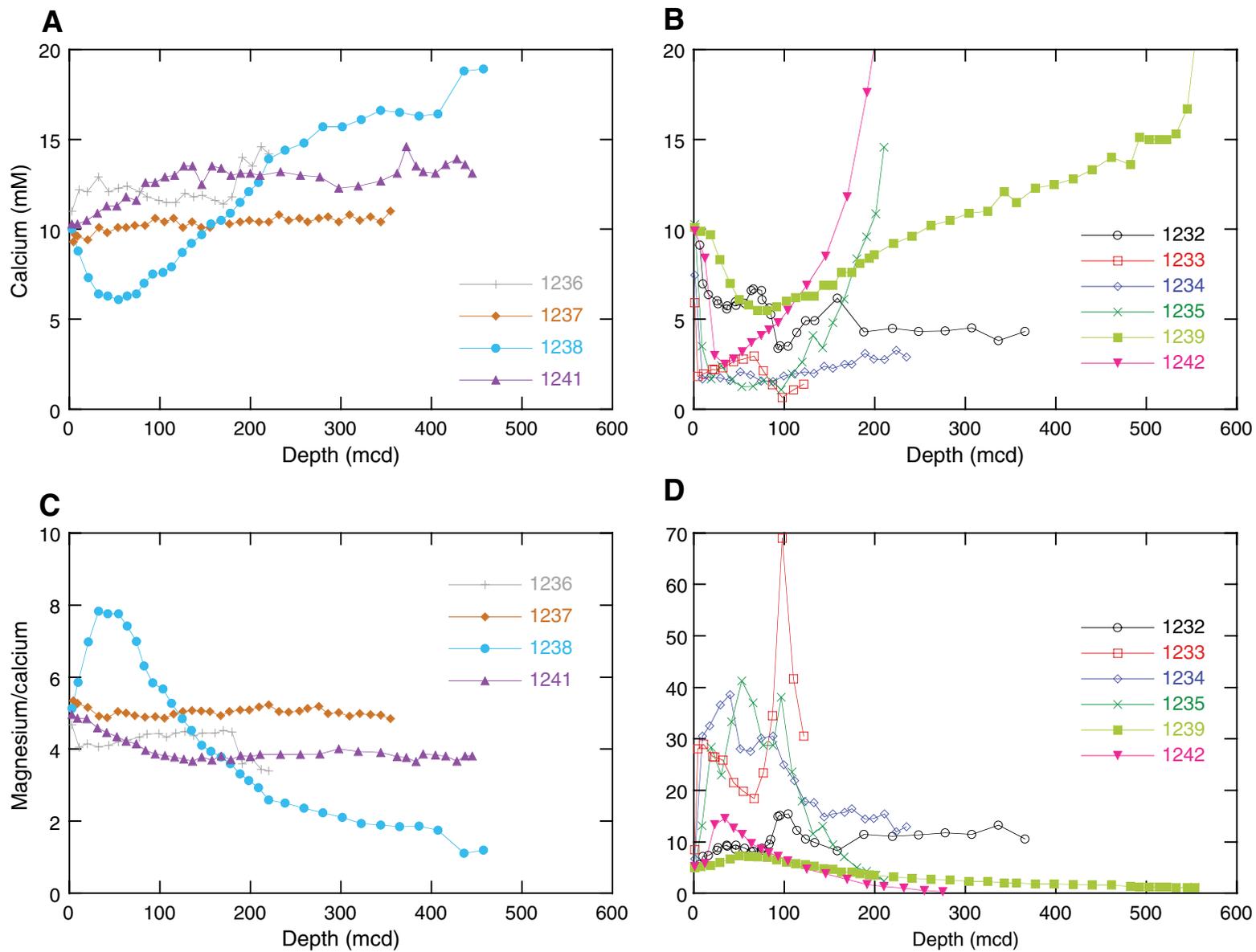
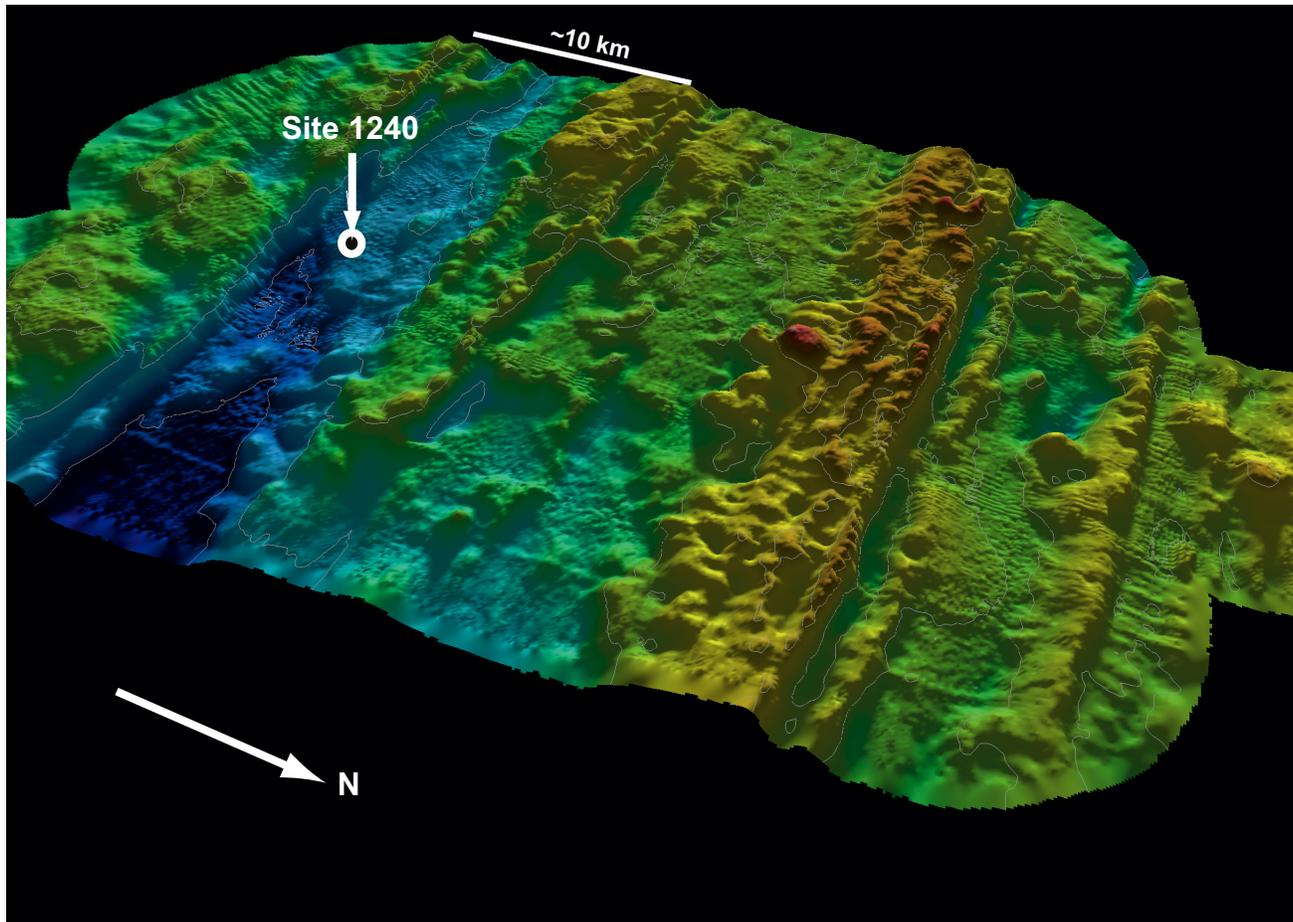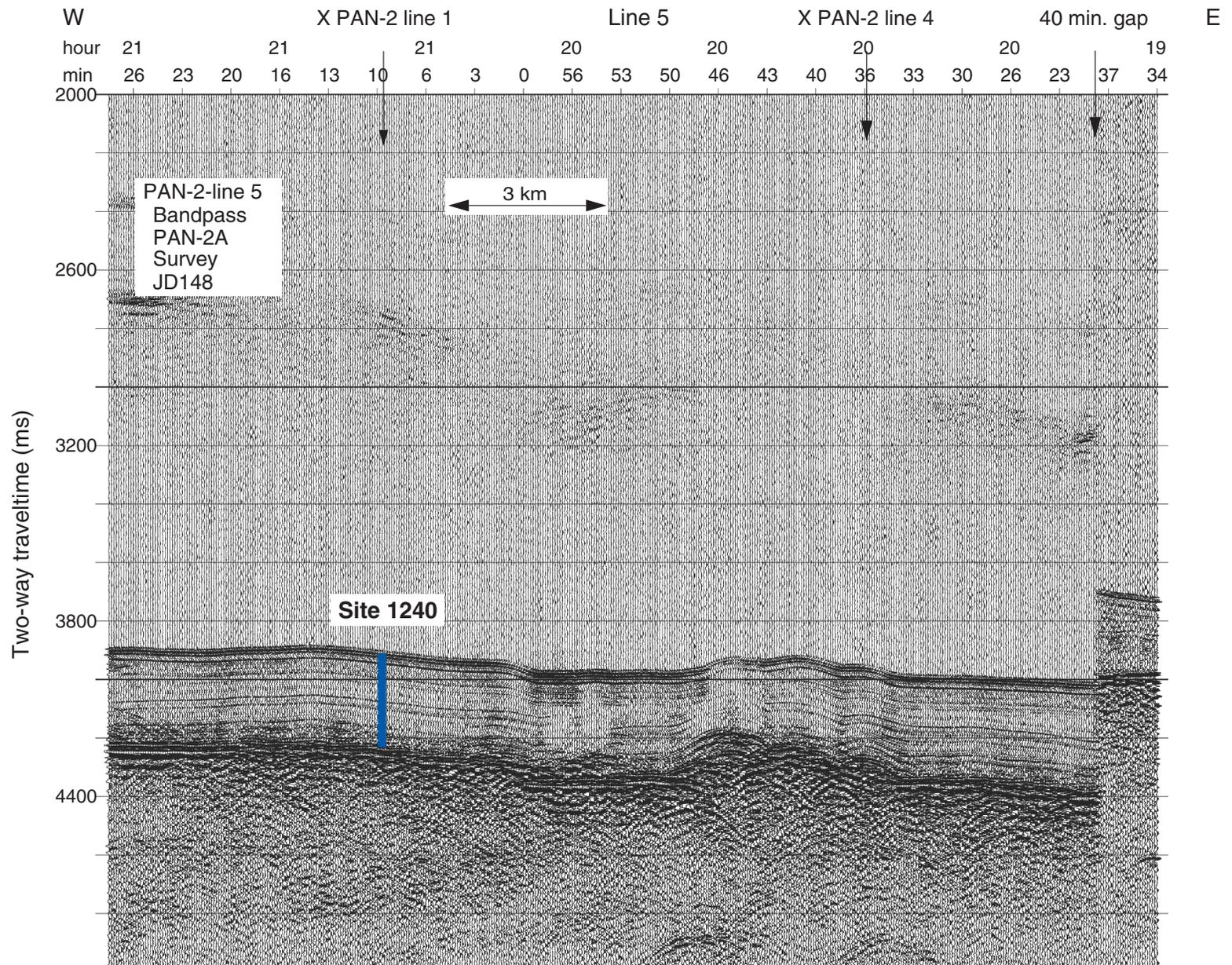Figure F21
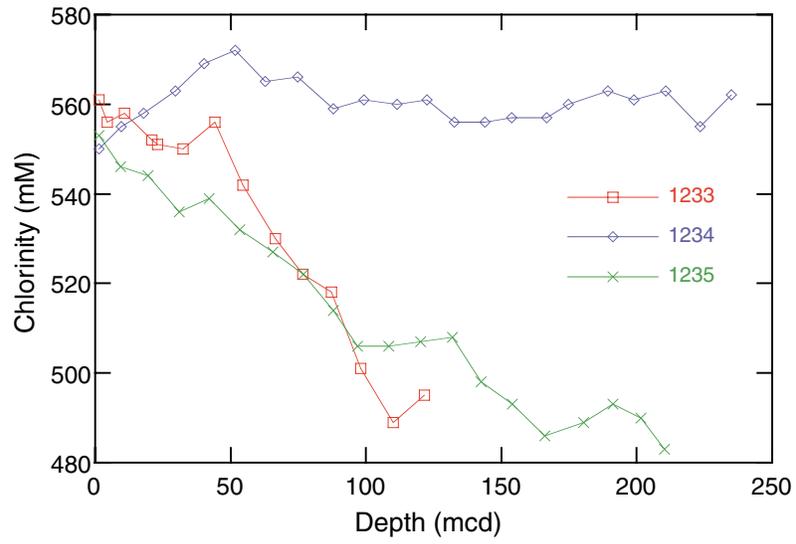
Figure F22
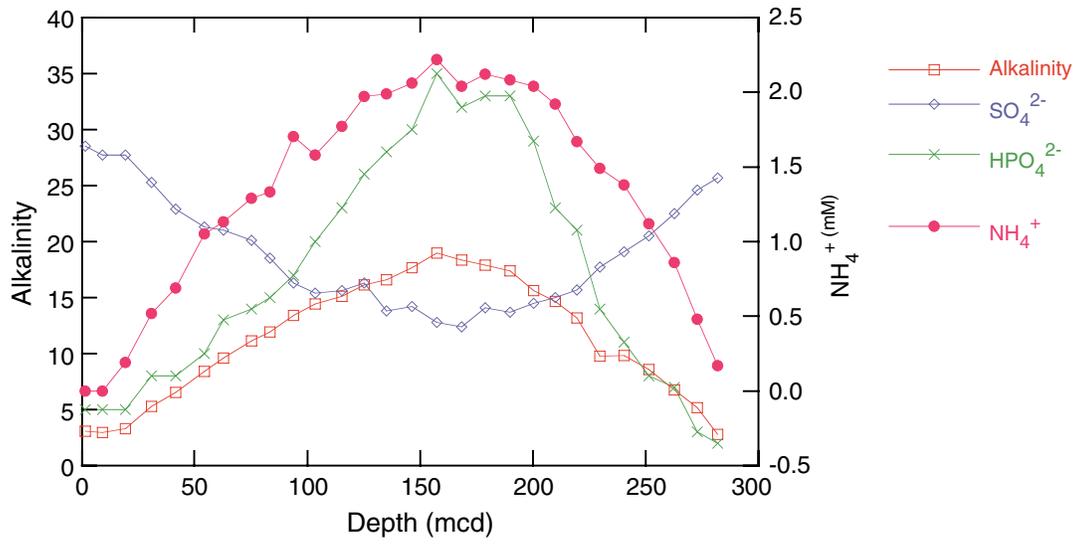
Figure F23
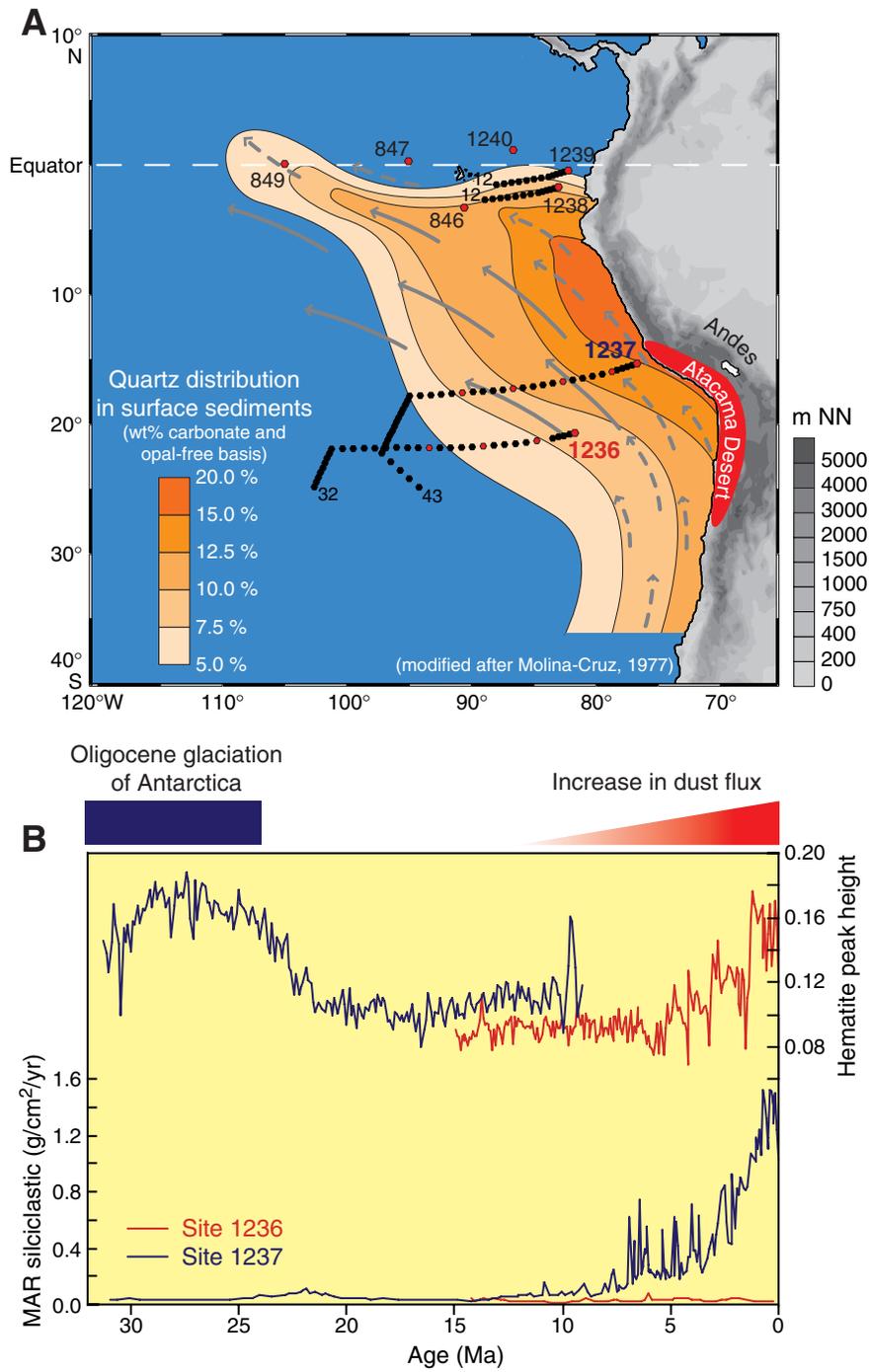
Figure F24
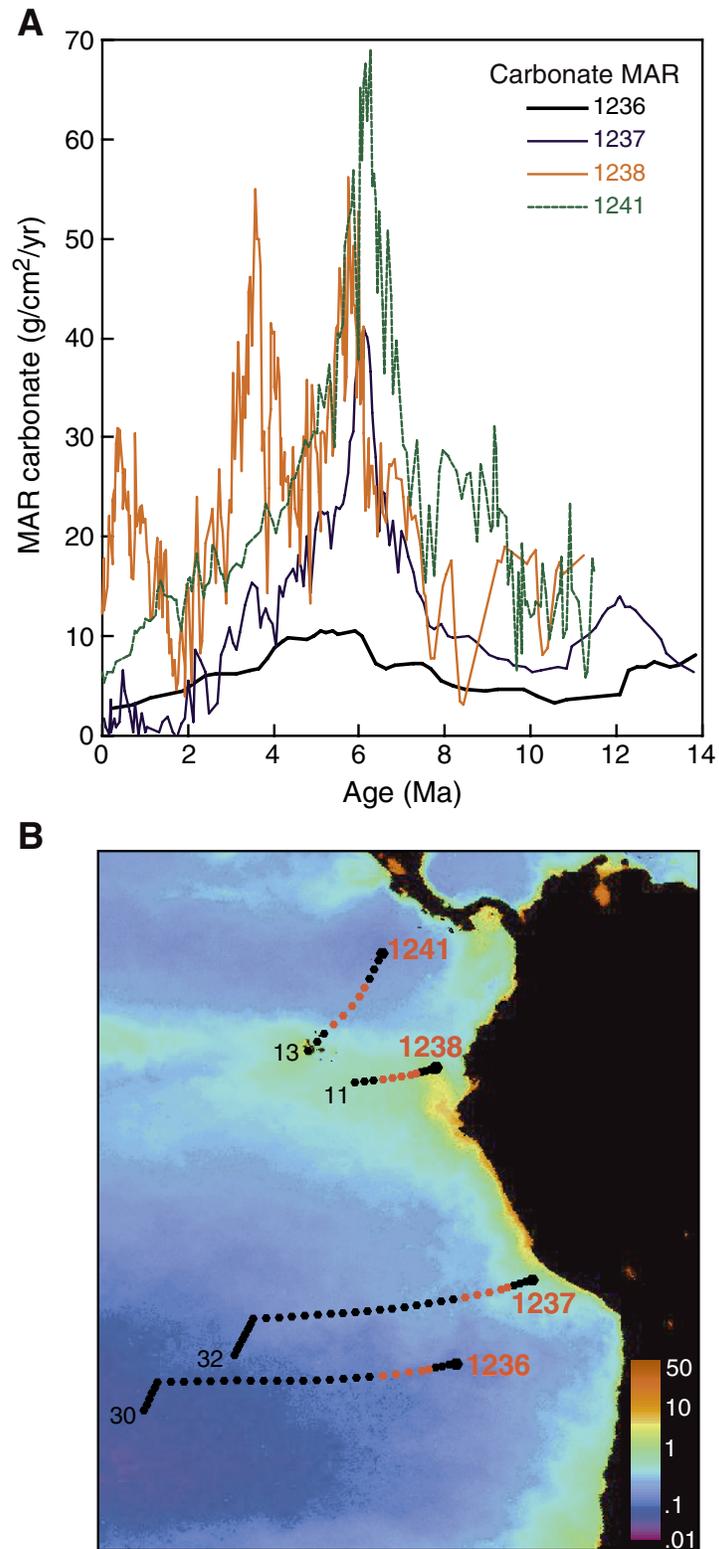
Figure F25
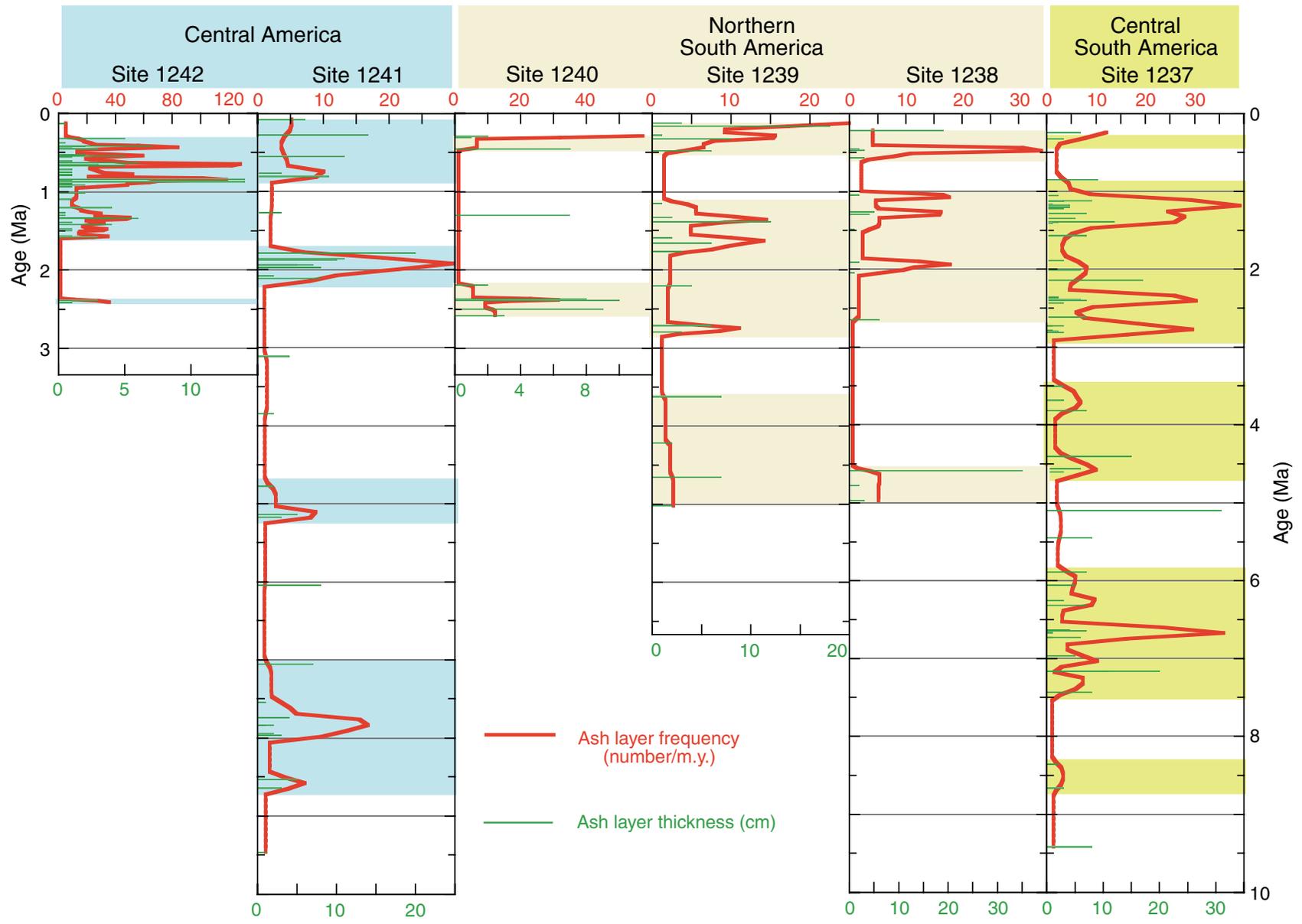
Figure F26
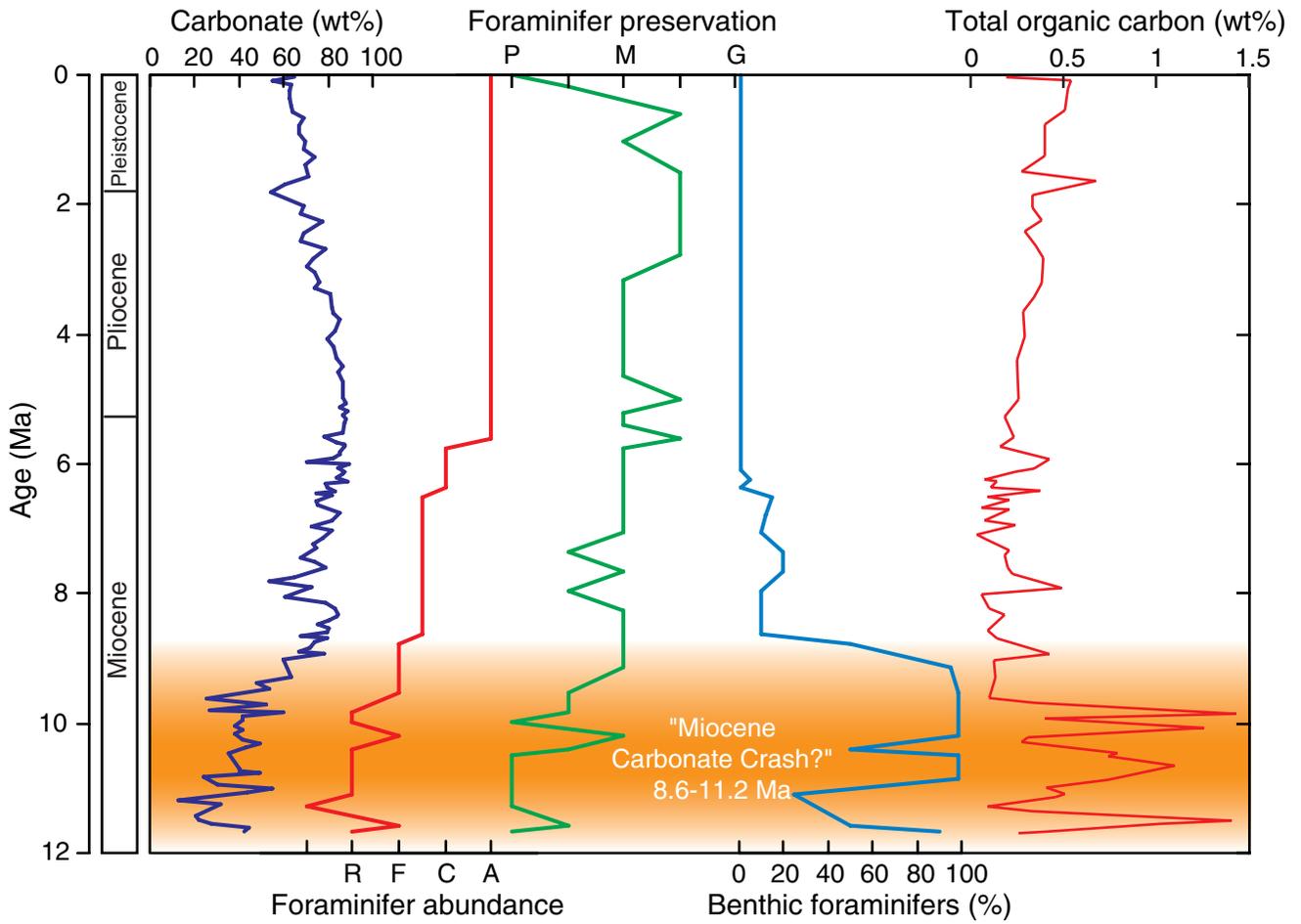
Figure F27
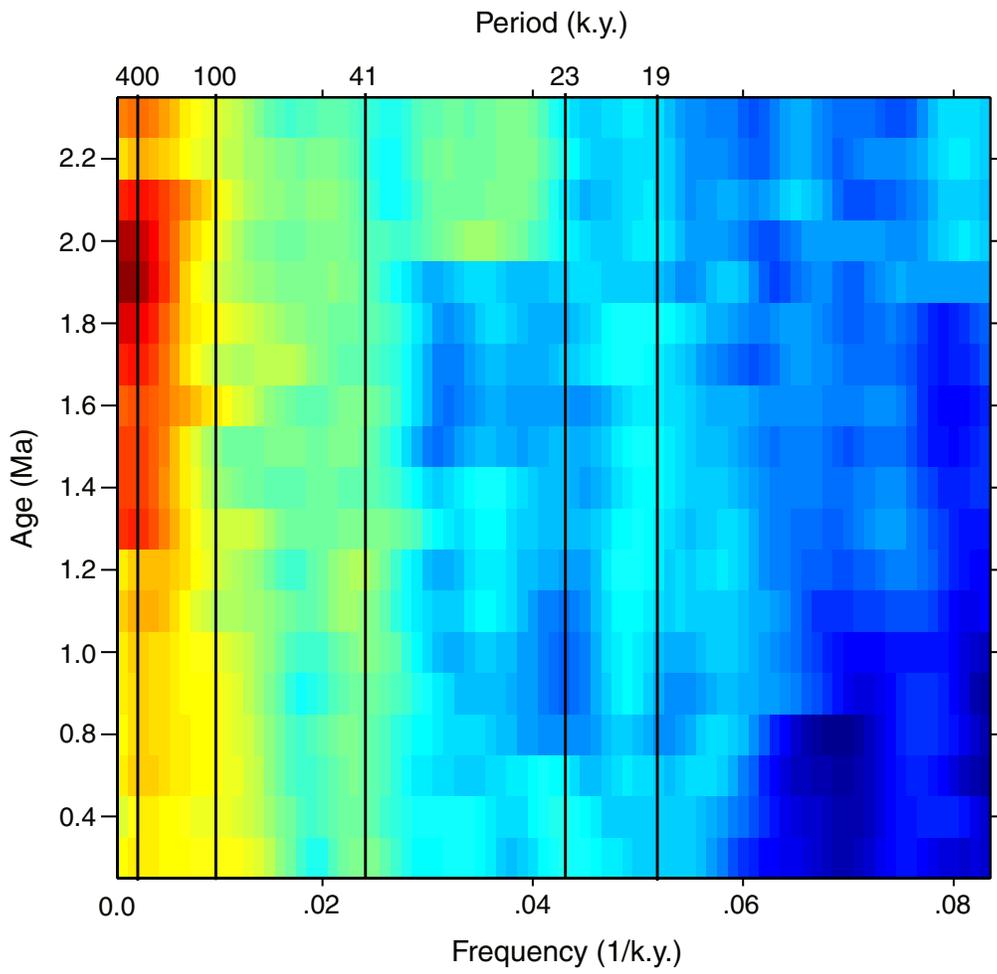
Figure F28
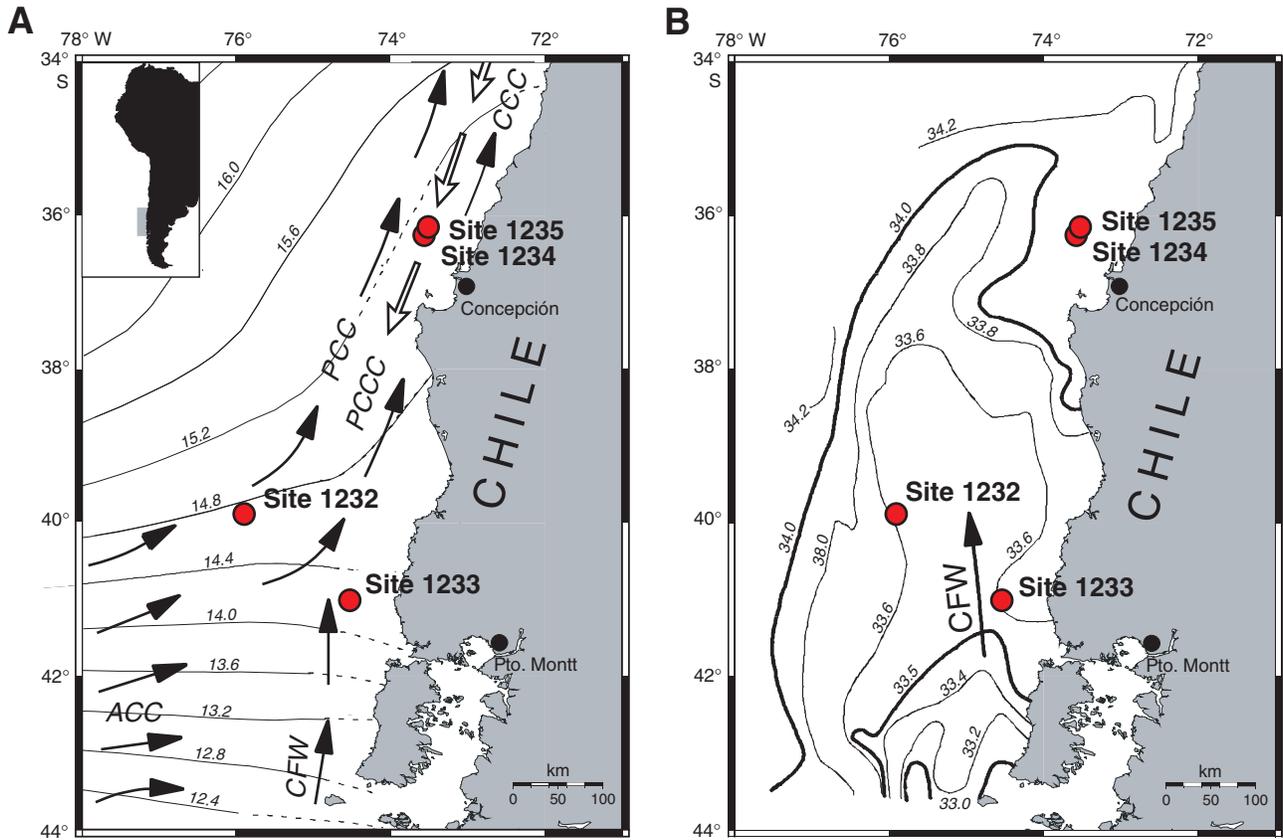
Figure F29
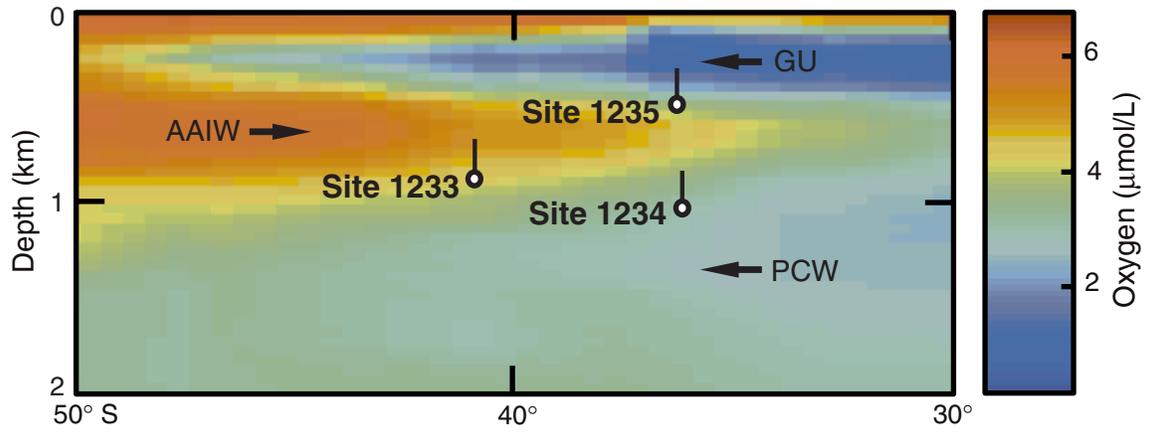
Figure F30
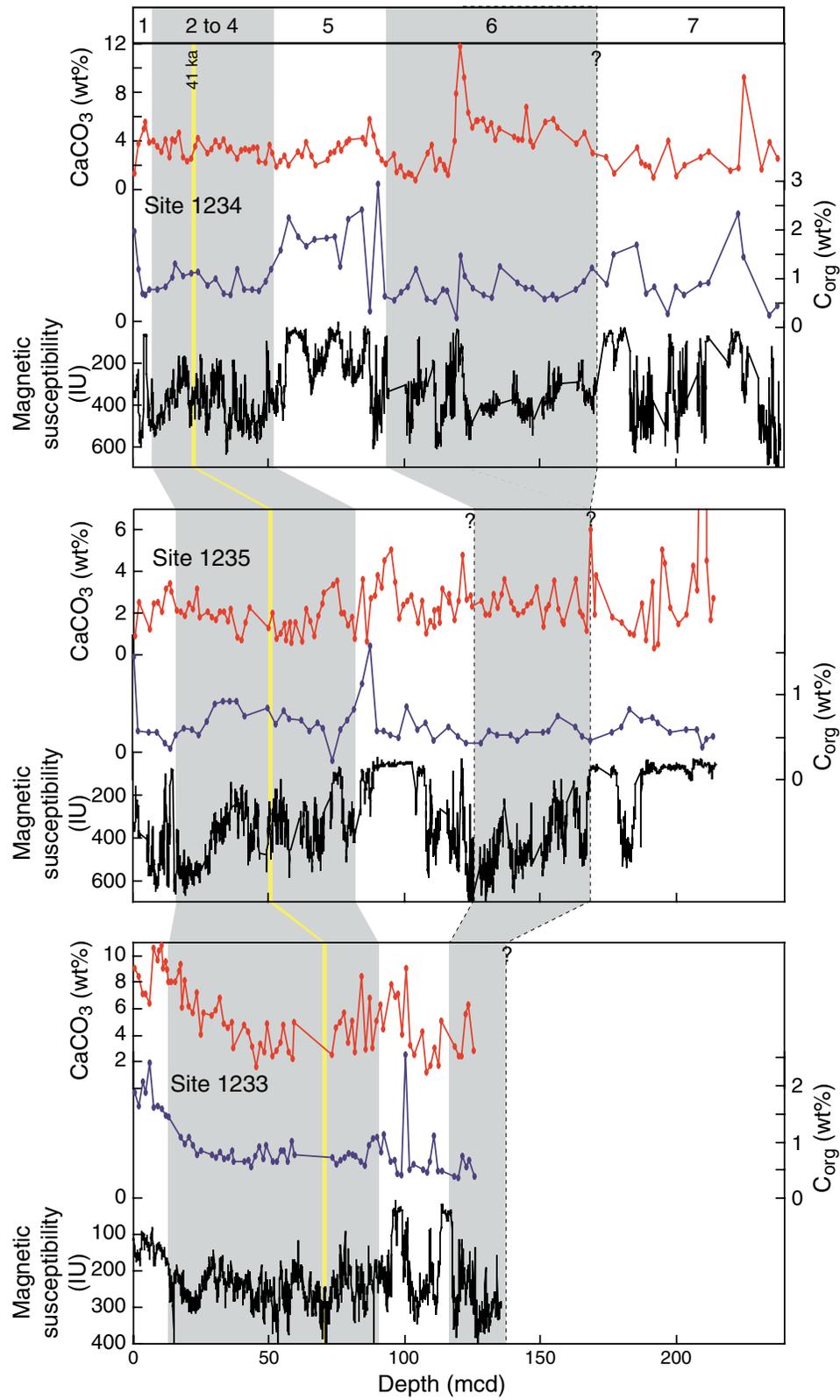
Figure F31
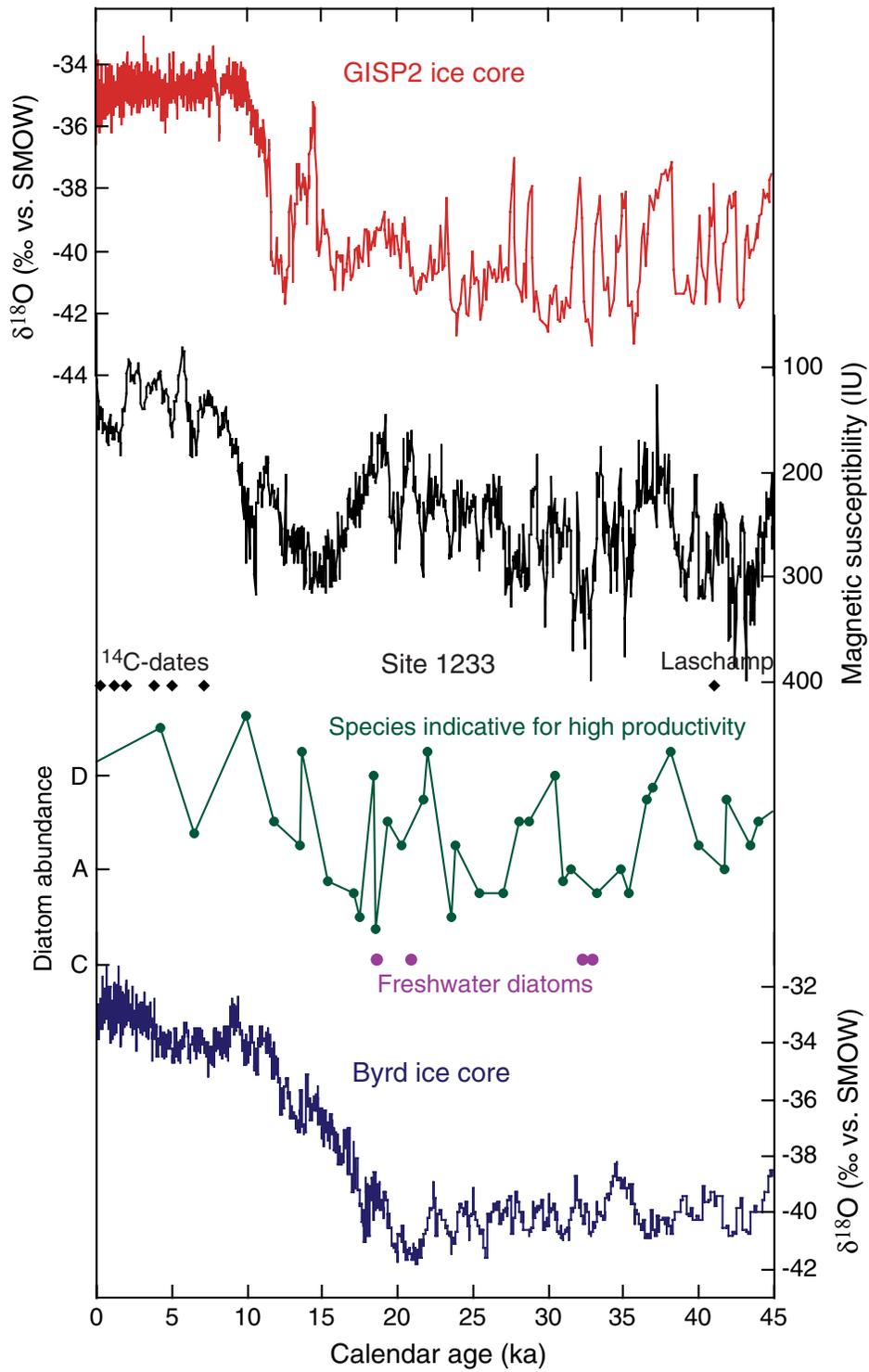
Figure F32
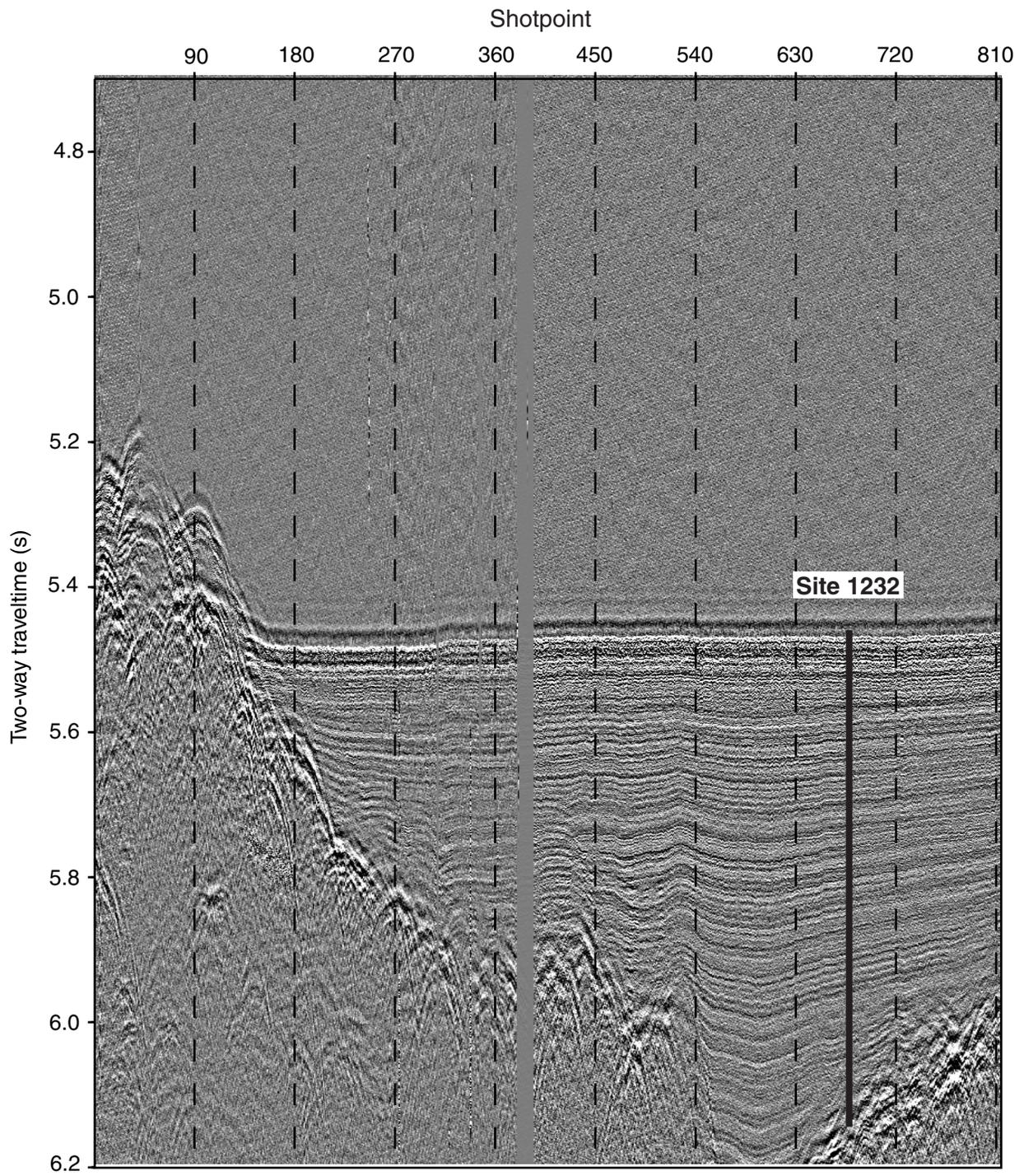
Figure F33
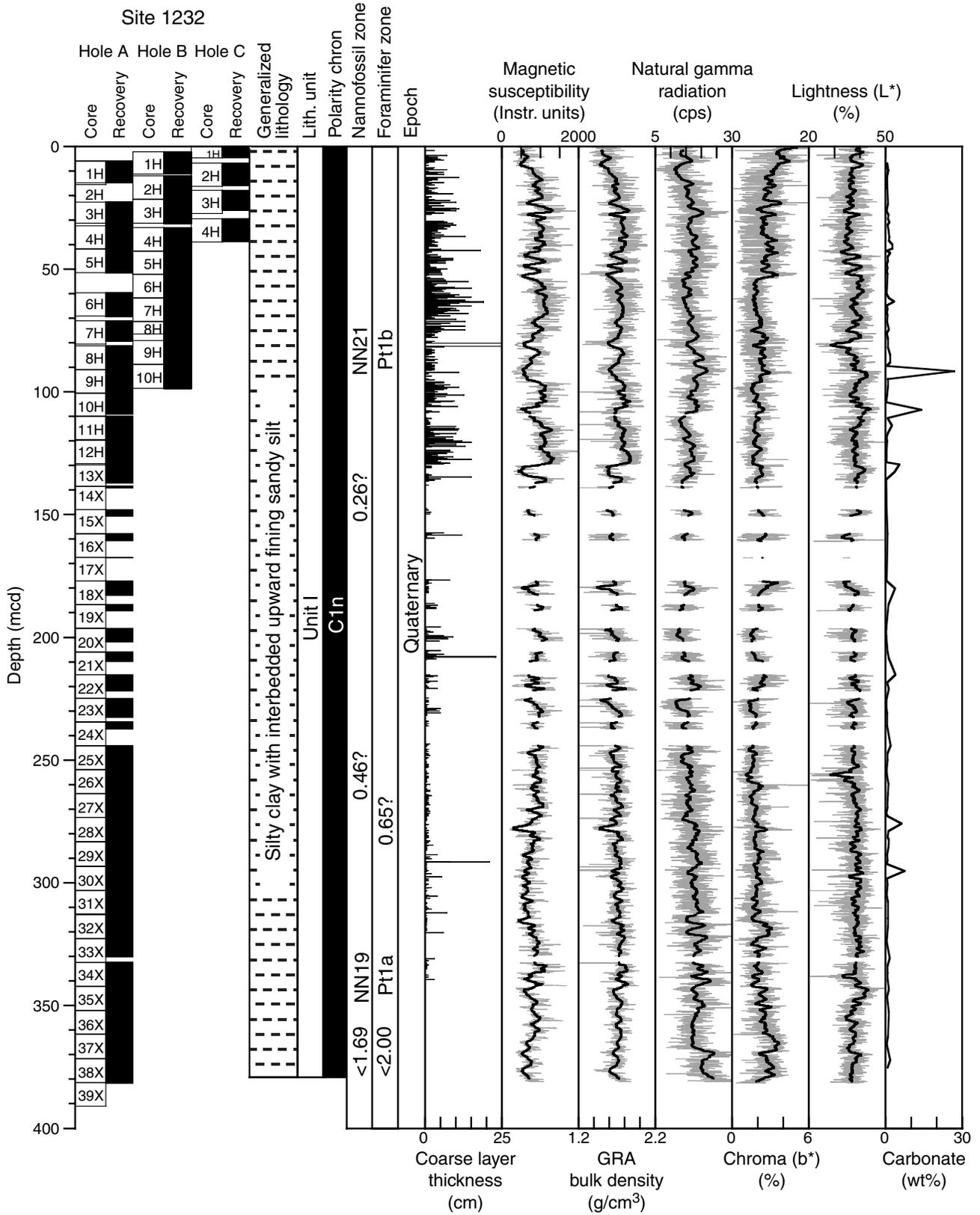
Figure F34
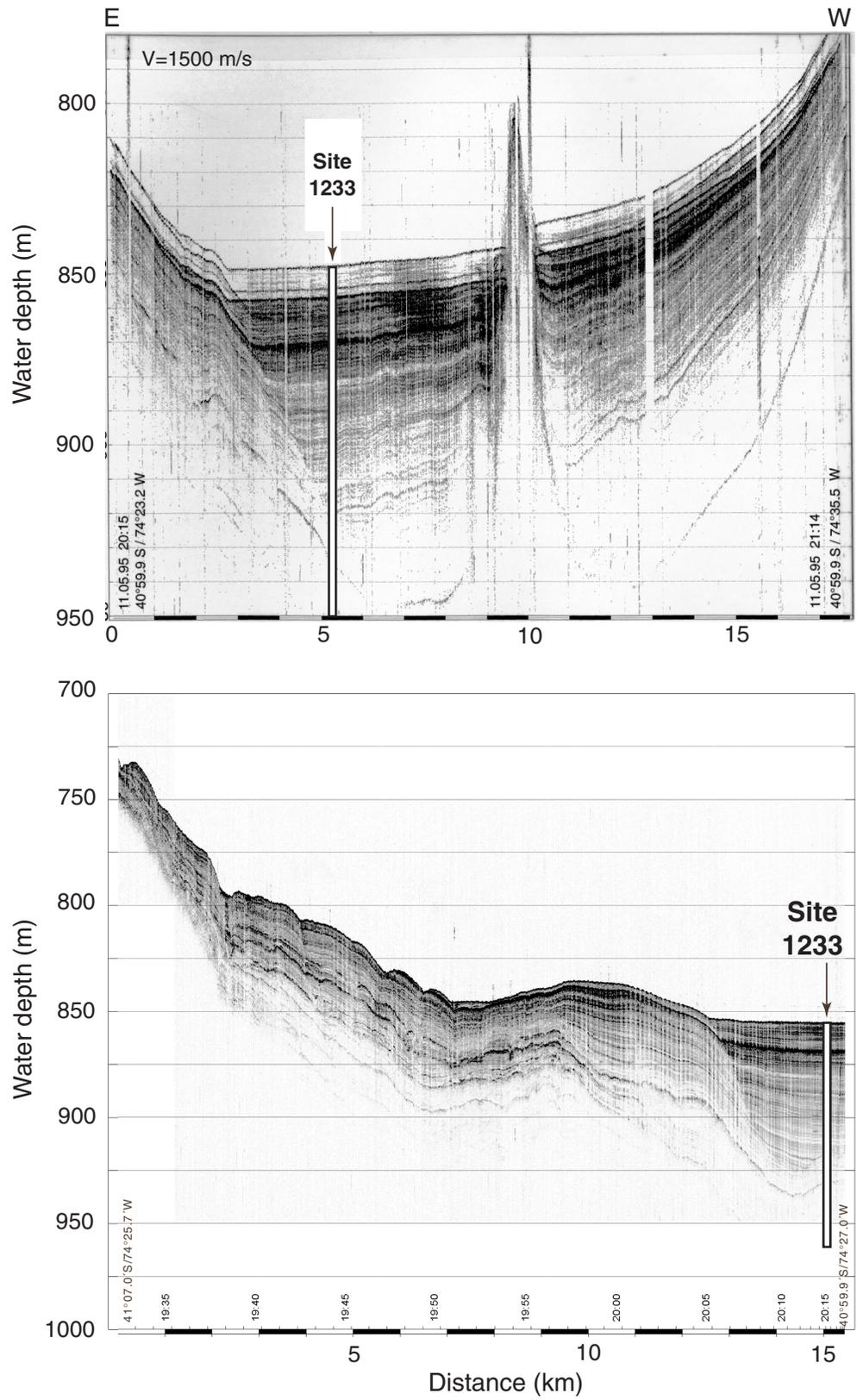
Figure F35
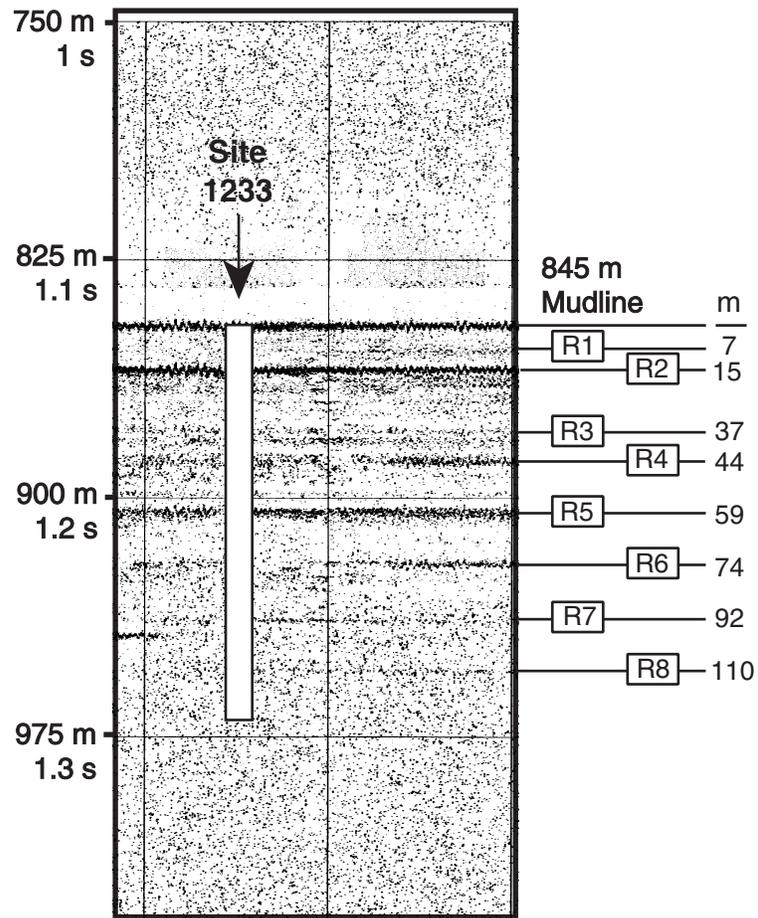
Figure F36
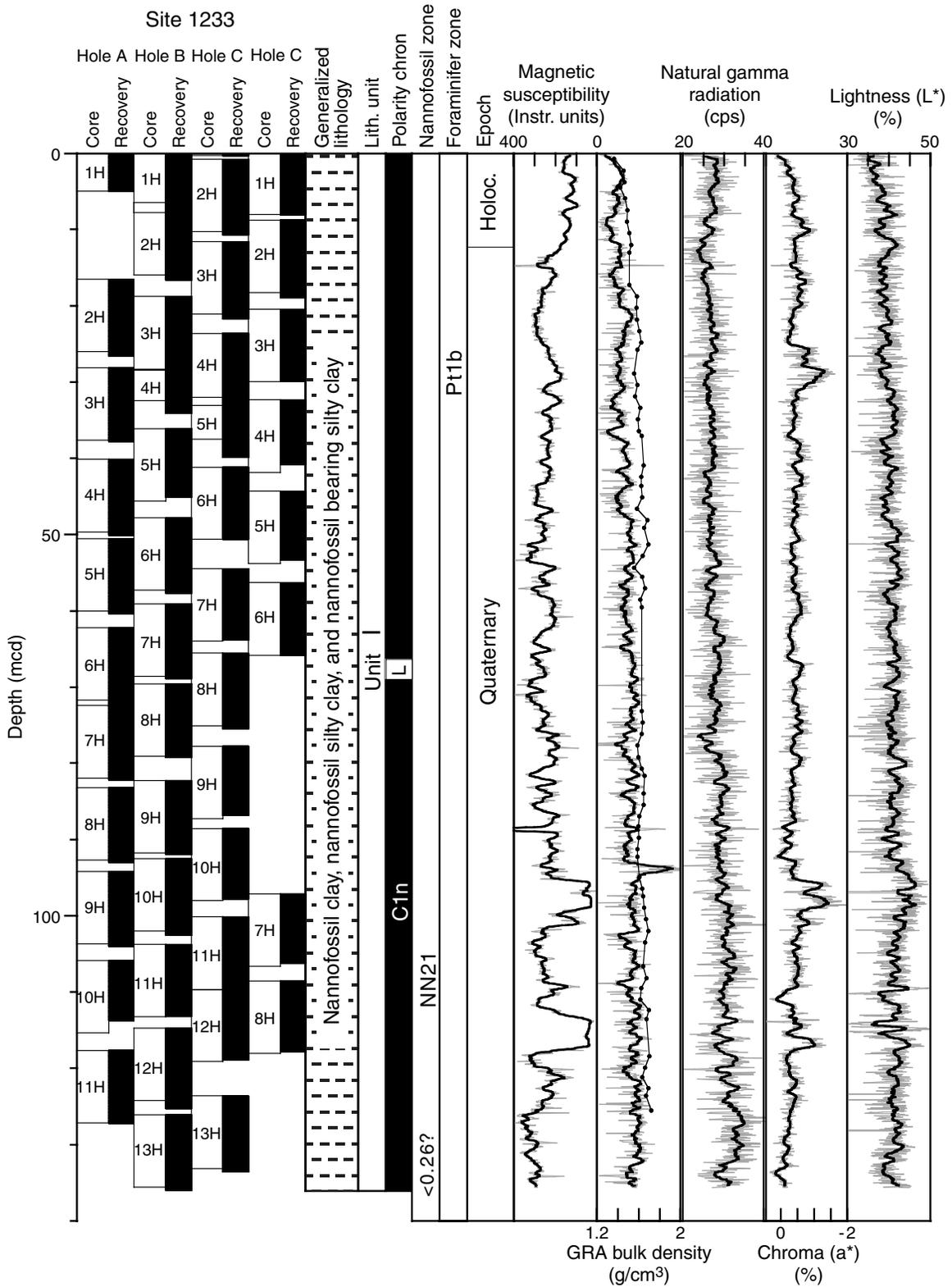
Figure F37
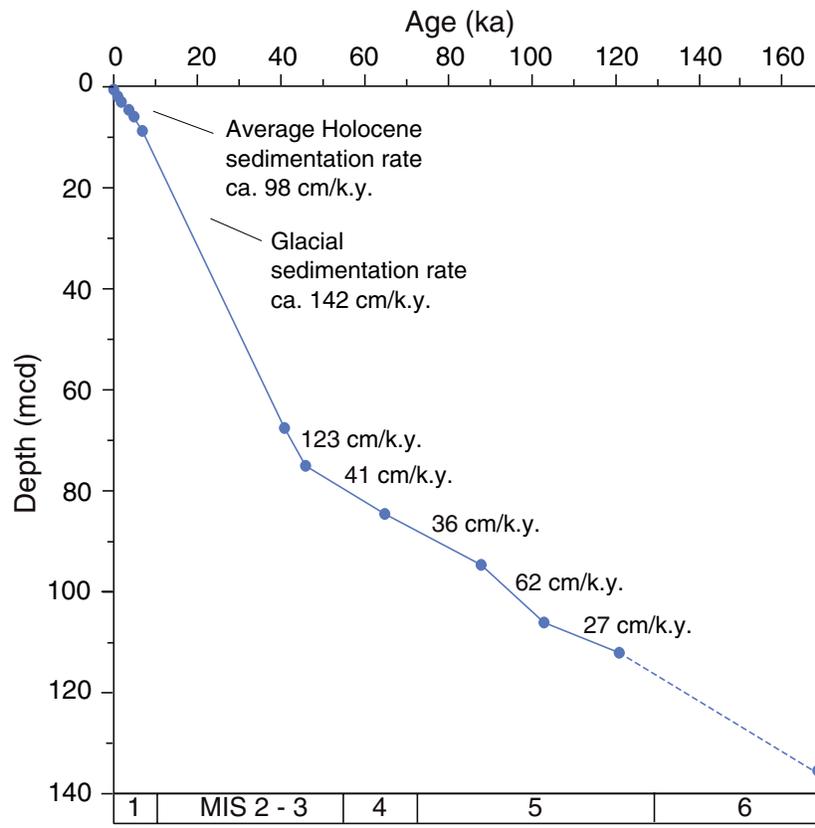
Figure F38
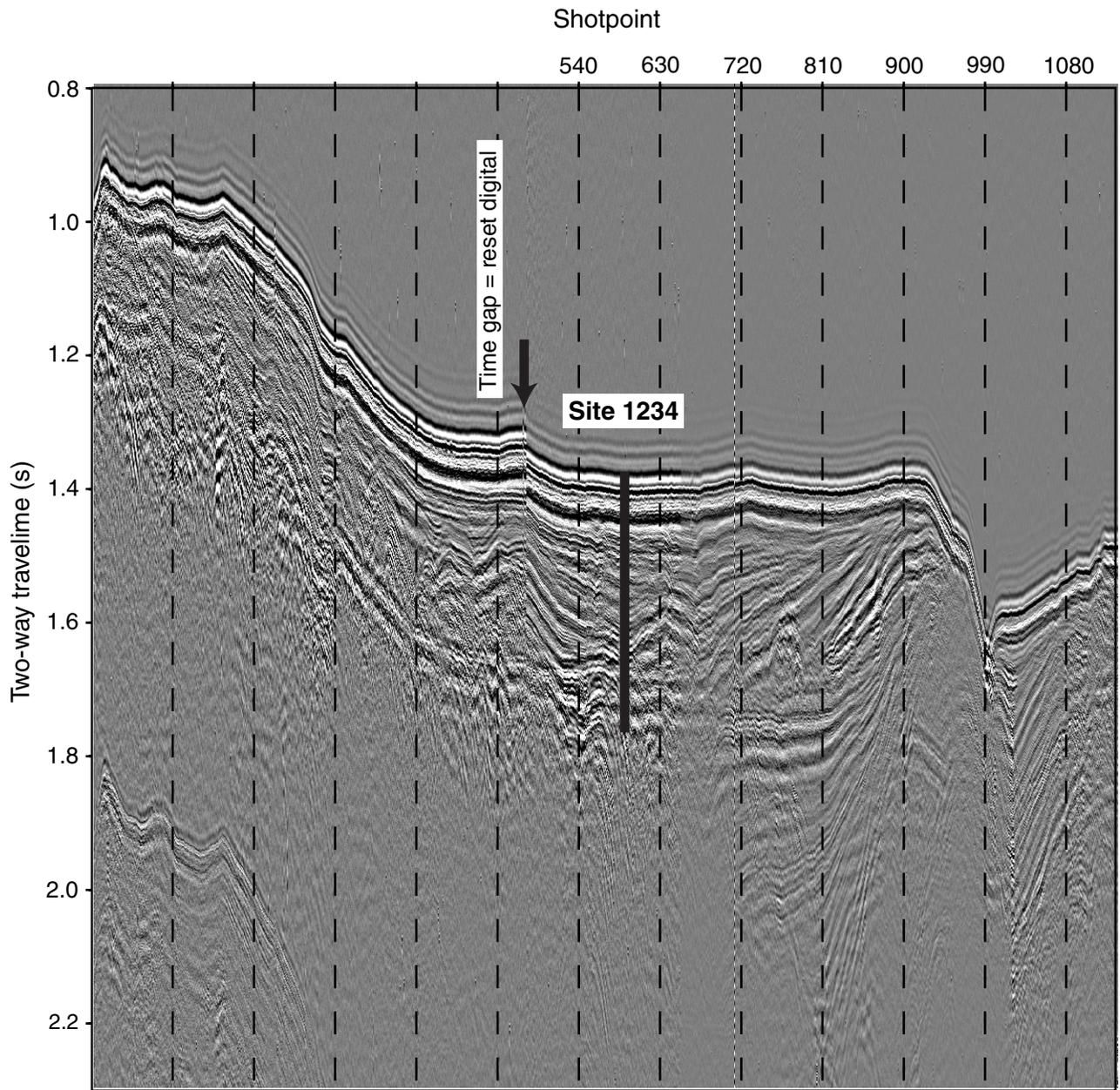
Figure F39
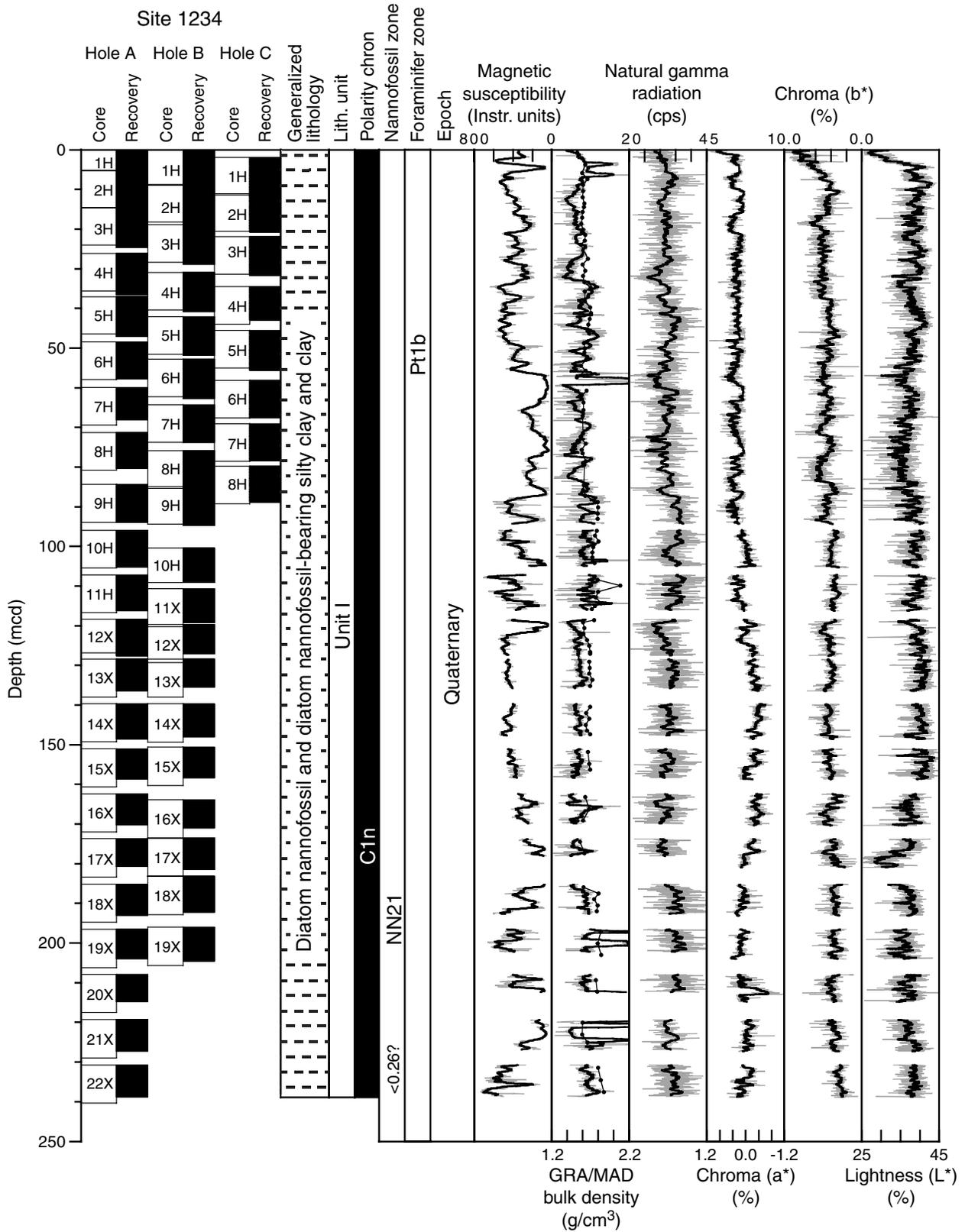
Figure F40

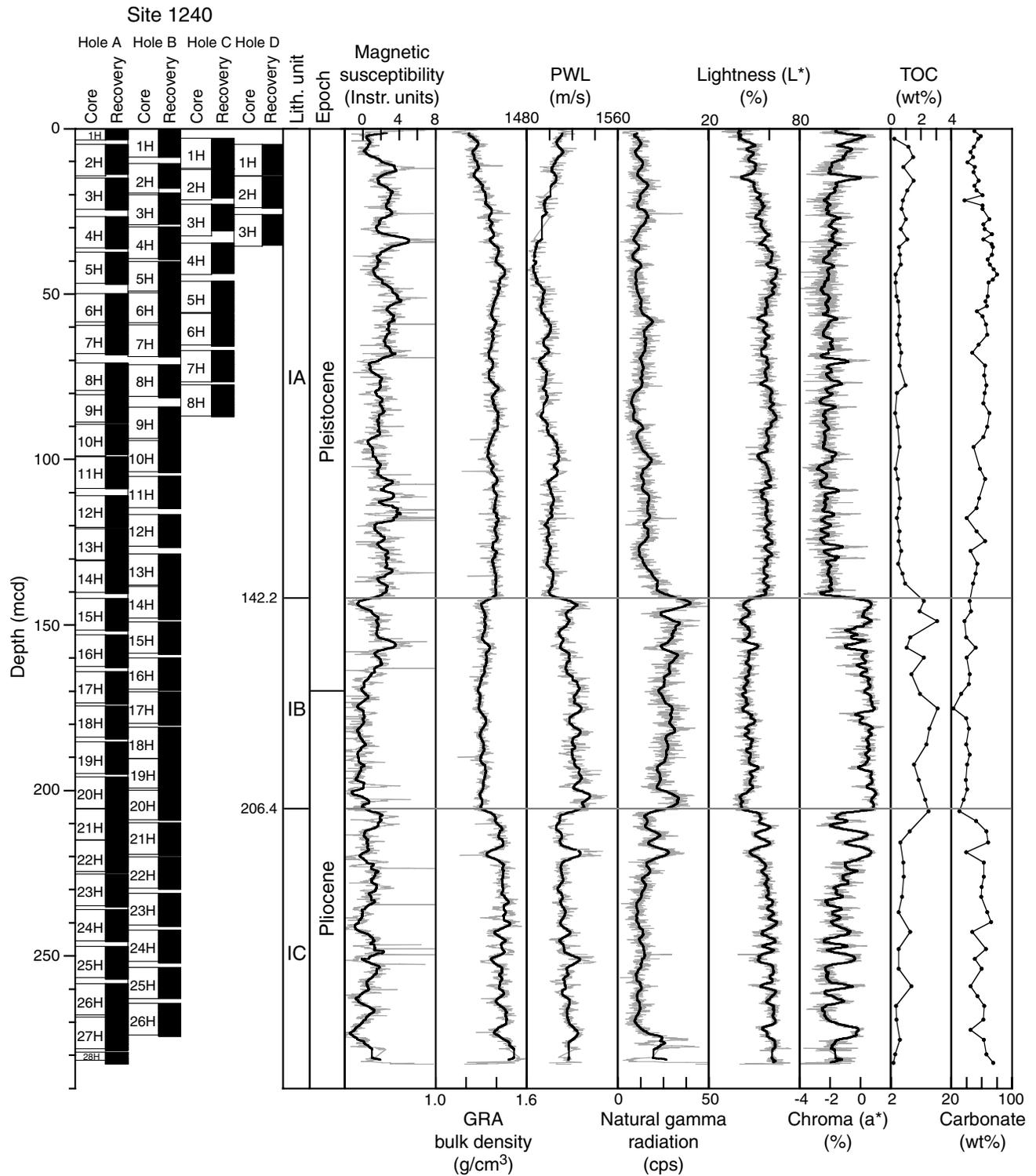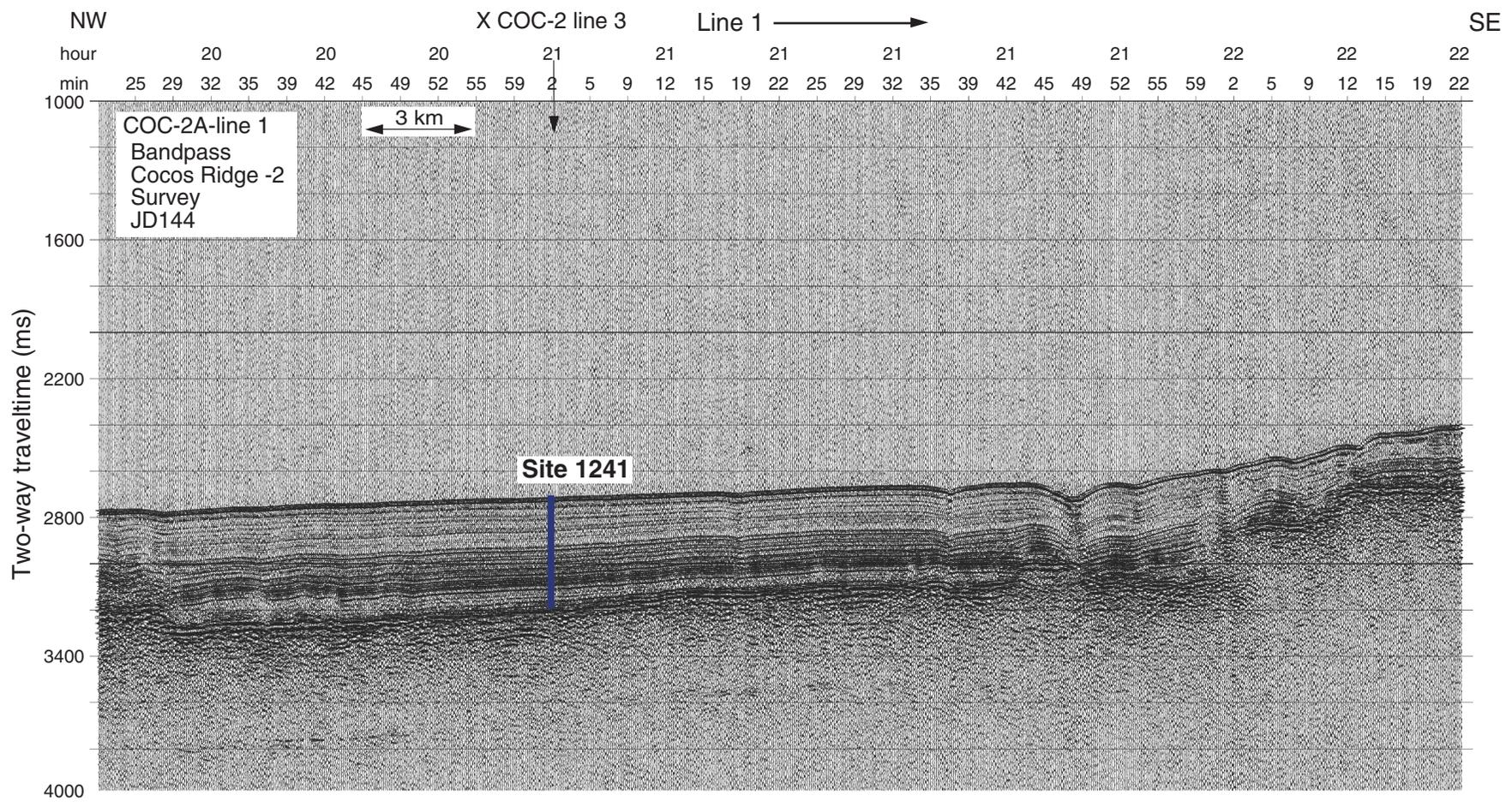Figure F41
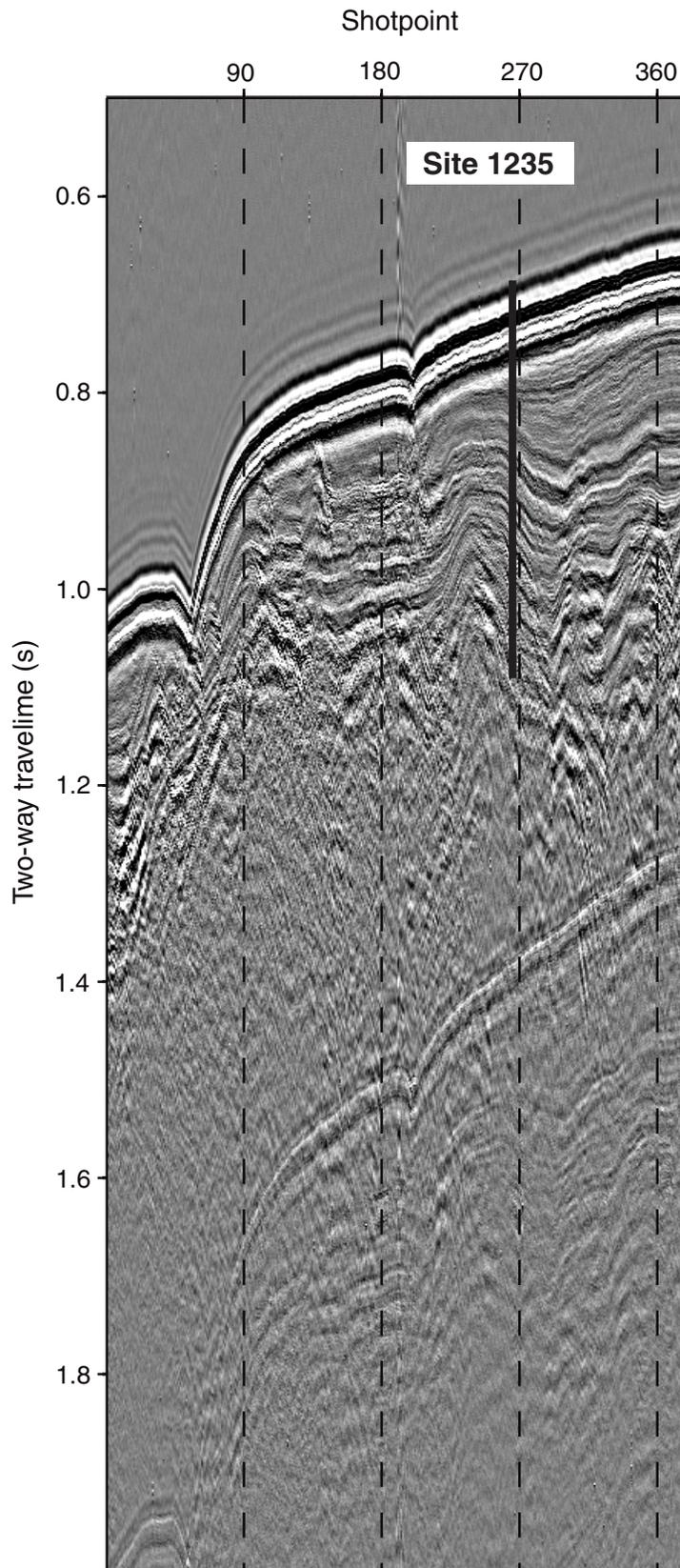
Figure F42
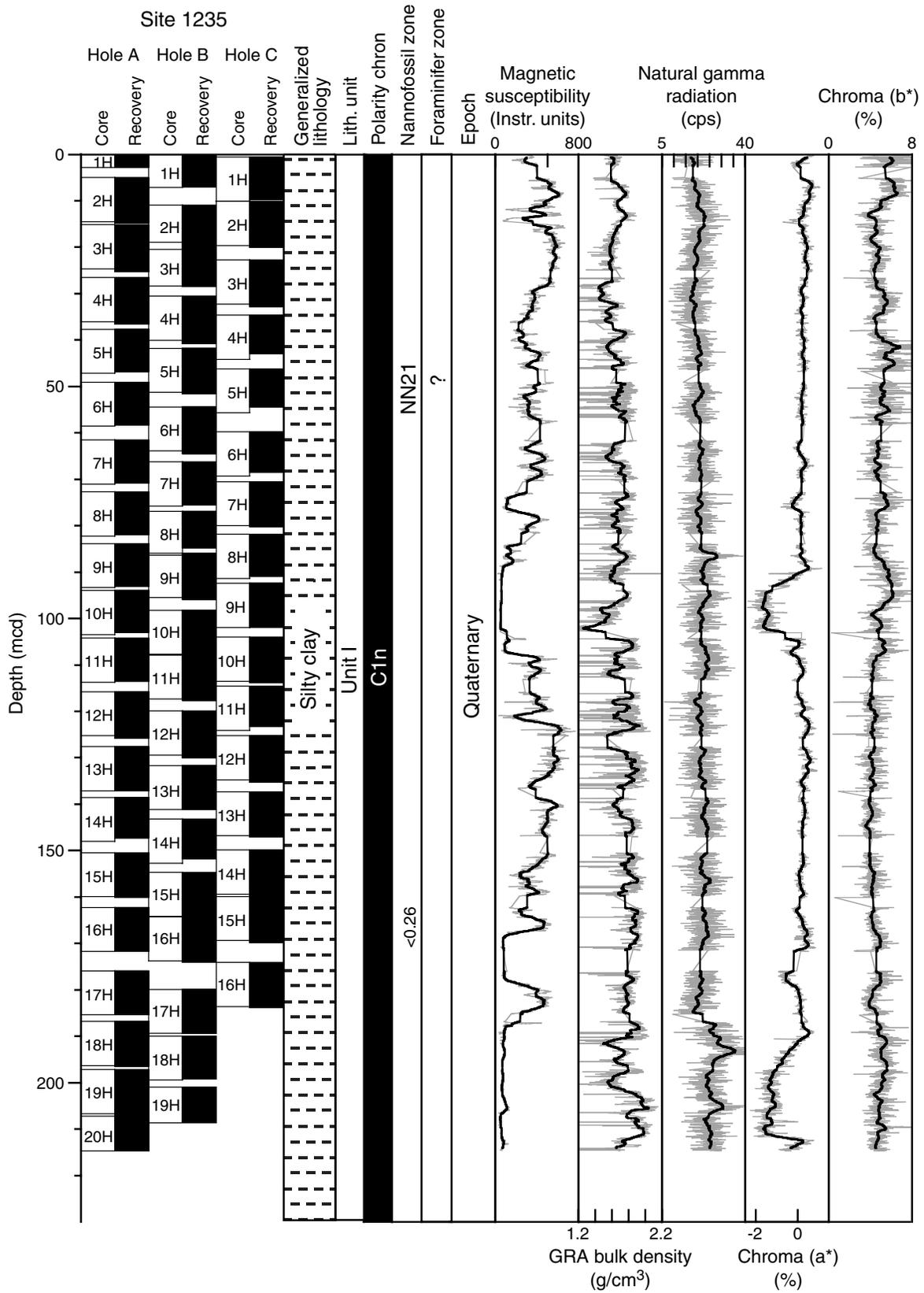
Figure F43
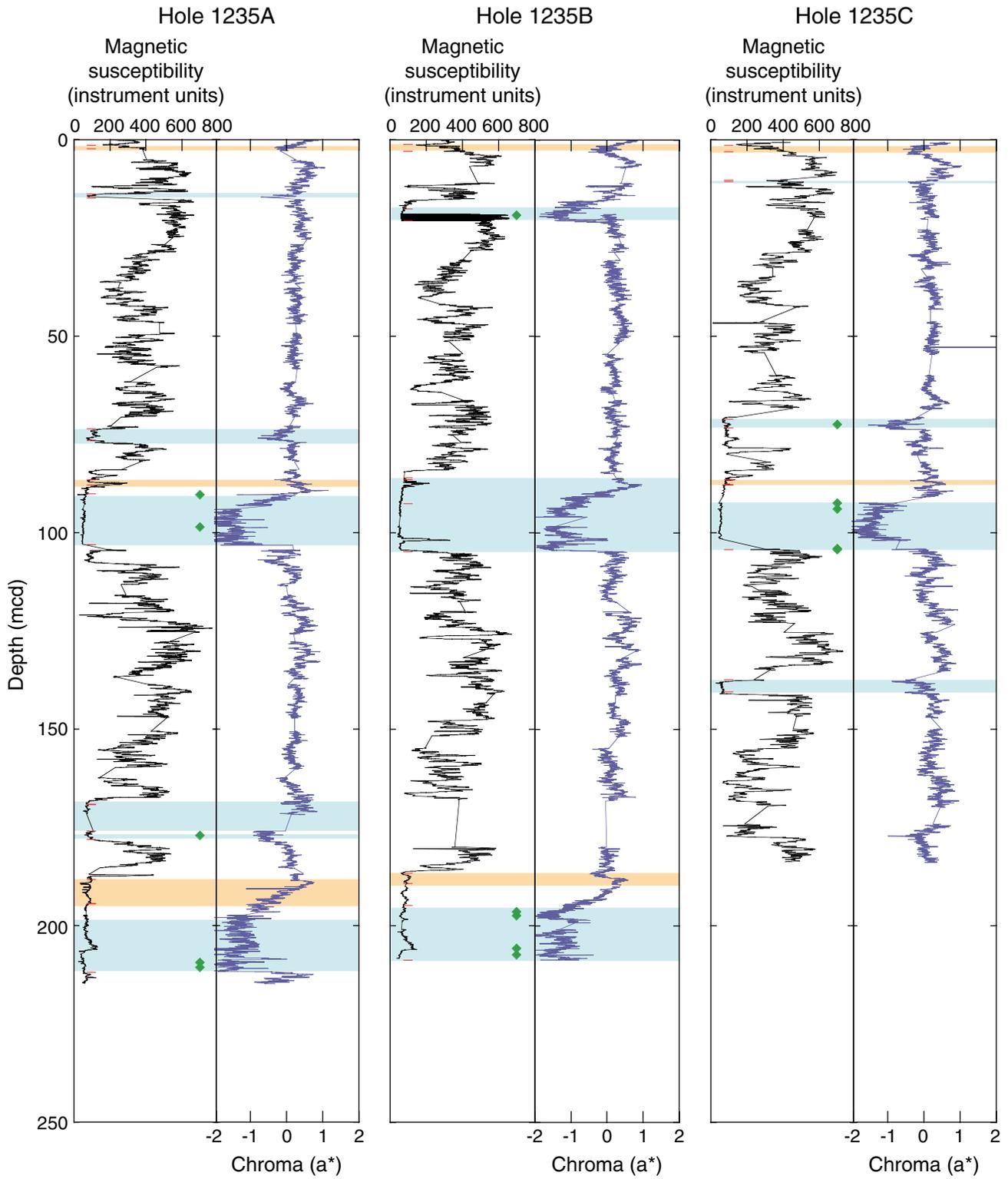
Figure F44

Figure F45

Figure F46

Figure F47
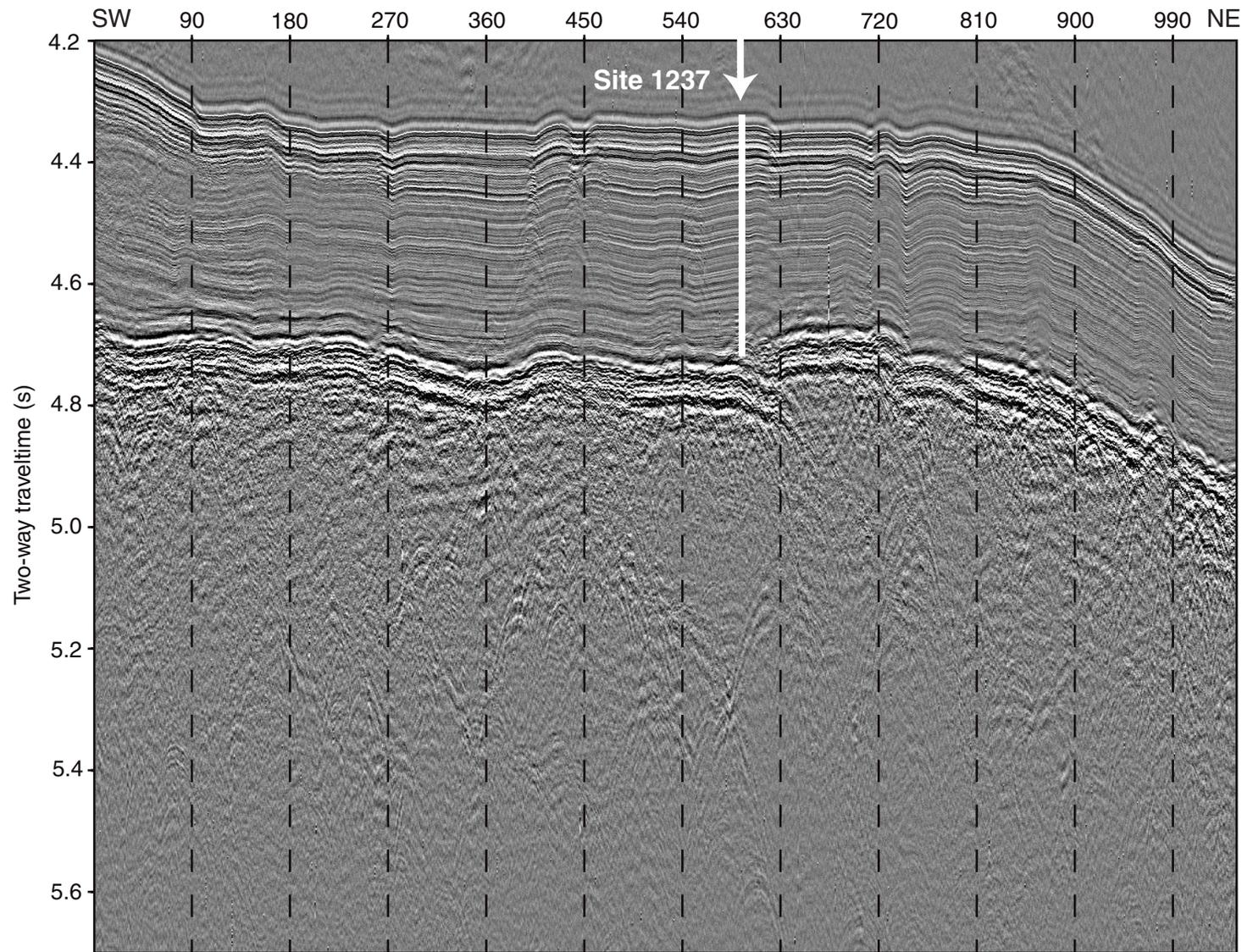
Figure F48
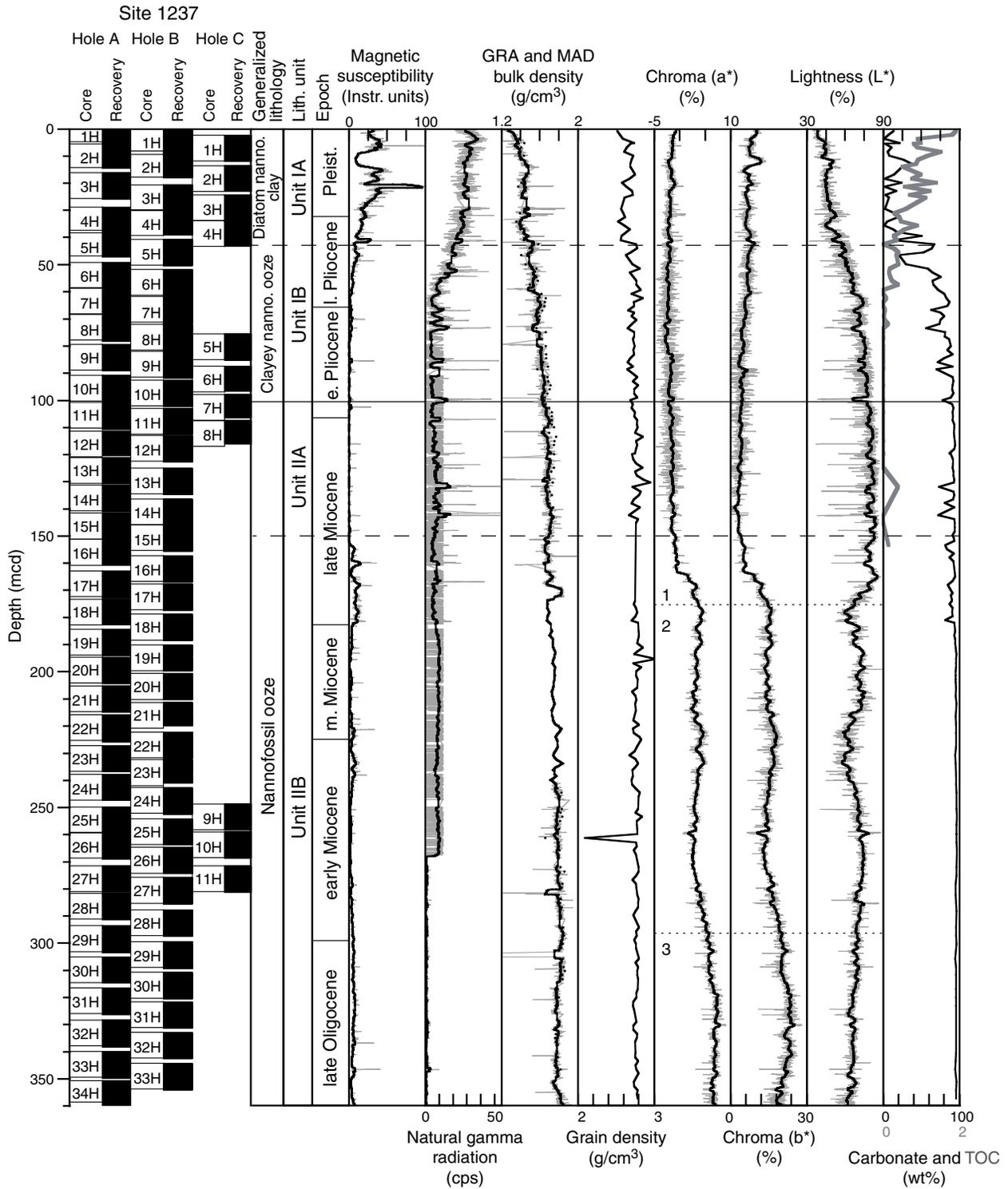
Figure F49

Figure F50

Figure F51

Figure F52

Figure F53

A

B

C

D

E

F

Figure F54

Figure F55

Figure F56

Figure F57

W   X PAN-2 line 1   Line 5   X PAN-2 line 4   40 min. gap   E

hour	21			21		21			20		20			20		20		19
min	26	23	20	16	13	10	6	3	0	56	53	50	46	43	40	36	33	30	26	23	37	34

PAN-2-line 5
Bandpass
PAN-2A
Survey
JD148

3 km

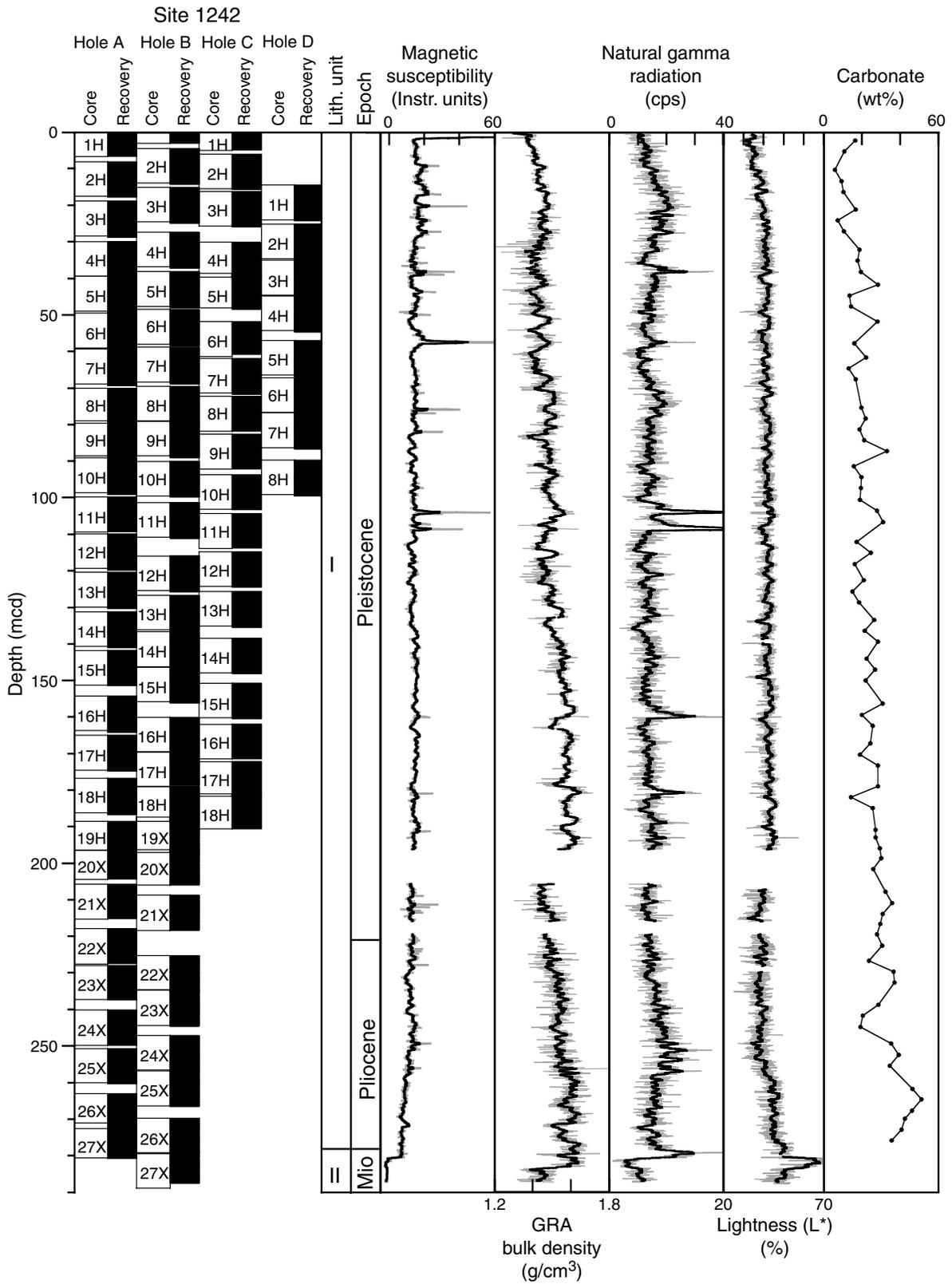Site 1240

Two-way traveltime (ms)

Figure F58

Figure F59

Figure F60

Figure F61

Figure F62

Figure F63